Inaugural dissertation

for

obtaining the doctoral degree

of the

Combined Faculty of Mathematics, Engineering and Natural Sciences

of the

Ruprecht - Karls - University

Heidelberg

Presented by

M.Sc. Damián Carvajal Ibáñez

born in: Granada, Spain

Oral examination: 21st of July 2023

Interferon modulates adult neurogenesis by regulating mRNA translation and cell cycle in neural stem cells

Referees: Prof. Dr. Ana Martin-Villalba

Dr. Michael Milsom

Science, from the Latin "*Scientia*", means knowing; observing, and understanding phenomena. When humans make science, our biggest limitation is ourselves, as observing and understanding are restrained by how our brain process information. Therefore, studying the brain is not just understanding the brain, but "*Scientia*" itself.

To my grandparents

Table of Contents

Abstract

Stem cells display intrinsic interferon signaling, which protects them from viral infections. In the aging brain, the increased presence of interferons drives a decline in function in neural stem cells, yet the role of interferon in the young brain is poorly studied. Regardless of whether in the young or old brain, how interferon regulates neural stem cells and whether the intrinsic signaling contributes to the modulation of neurogenesis also remains unknown. Here, I apply single-cell transcriptomics to mice lacking type-I and -II interferon receptors, to assess the presence of interferon regulation in the young and old brains. I find that interferons act selectively on neural stem cells, and not neural progenitors, both in the young and the old brain. This selective role of interferons contributes to shaping the intrinsic interferon signaling in neural stem cells. To unveil the molecular underpinnings of the interferon response, I profile the cell cycle progression, transcriptome, translatome, and phospho-proteome of neural stem cells exposed to interferon β. Briefly, interferon β transiently activates mTORC1 while simultaneously arresting neural stem cells in G_0, quiescence state. Importantly, the observed uncoupling of mTORC1 and cell cycle by interferon β represses the translation of the key stem cell activity factor *Sox2*. In addition, interferon β induces a late shutdown of protein synthesis in neural stem cells, mediated by the inhibition of mTORC1 and the upregulation of p-eIF2α^{S51}. This biphasic regulation of mTORC1 activity and inhibition of cell cycle promotes the exit of the activation state of neural stem cells. Last, I identify IFIT1 as a key effector of the interferon-mediated modulation of neurogenesis in neural stem cells. Unpublished results from my group indicate a novel role of IFIT1 in binding eukaryotic mRNAs in neural stem cells, which suggests a potential role of IFIT1 in neurogenesis. My results show that the absence of IFIT1 impairs the dynamics of the neurogenic niches at all ages in the adult brain, as well as their social traits, learning capacity, and memory acquisition. Overall, I profile the molecular underpinnings of the interferon response in neural stem cells and unveil the regulatory role of interferons in regulating neural stem cells in the young homeostatic brain. This regulatory role of interferons on stemness at all ages reveals novel therapeutic implications of interferons not only in neurogenesis but also in cancer and viral infections in the brain as well as neurodegenerative disorders.

Zusammenfassung

Stammzellen verfügen über eine intrinsische Interferon-Signalgebung, die sie vor Virusinfektionen schützt. Im alternden Gehirn führt das vermehrte Vorhandensein von Interferonen zu einem Funktionsrückgang der neuronalen Stammzellen. Die Rolle von Interferon im jungen Gehirn ist jedoch nur unzureichend untersucht. Sowohl im jungen als auch im alten Gehirn ist nicht bekannt, wie Interferon neuronale Stammzellen reguliert und ob die intrinsische Signalgebung zur Modulation der Neurogenese beiträgt. Hier wende ich die Einzelzell-Transkriptomik bei Mäusen an, denen Typ-I und -II Interferonrezeptoren fehlen, um die Existenz der Interferonregulation im jungen und alten Gehirn zu untersuchen. Ich zeige auf, dass Interferon gelichermaßen im jungen und alten Gehirn selektiv auf neurale Stammzellen, nicht aber auf Vorläuferzellen, wirkt. Diese selektive Rolle der Interferone trägt dazu bei, die intrinsische Interferon-Signalgebung in neuralen Stammzellen zu gestalten. Um die molekularen Grundlagen der Interferon-Antwort aufzudecken, habe ich ein Profil des Zellzyklus, Transkriptoms, Translatoms und Phospho-Proteoms von neuralen Stammzellen erstellt, die Interferon β ausgesetzt waren. Zusammenfassend ergibt sich dass Interferon β vorübergehend mTORC1 aktiviert, während es gleichzeitig die neuralen Stammzellen in G_0 (zurück)hält. Hervorzuheben ist, dass die beobachtete Entkopplung von mTORC1 und Zellzyklus durch Interferon β die Translation des wichtigen Stammzellaktivitätsfaktors *Sox2* unterdrückt. Zusätzlich induziert Interferon β eine späte Abschaltung der Proteinsynthese in neuralen Stammzellen, die durch die Hemmung von mTORC1 und die Hochregulierung von p-eIF2α^{S51} vermittelt wird. Diese biphasische Regulierung der mTORC1-Aktivität und die Hemmung des Zellzyklus fördern das Verlassen des Aktivierungszustands neuraler Stammzellen. Schließlich identifiziere ich IFIT1 als Schlüsseleffektor in der Modulation der Neurogenese durch Interferon in Stammzellen. Unveröffentlichte Ergebnisse meiner Gruppe weisen auf eine neue Rolle von IFIT1 bei der Bindung eukaryotischer mRNAs in neuralen Stammzellen hin, was auf eine mögliche Funktion von IFIT1 in der Neurogenese schließen lässt. Hier zeige ich, dass das Fehlen von IFIT1 die Dynamik der Neurogenese im erwachsenen Gehirn beeinträchtigt, sowie soziale Eigenschaften, Lernfähigkeit und Gedächtniserwerb einschränkt. Insgesamt habe ich die molekularen Grundlagen der Interferone in neuronalen Stammzellen beschrieben und die Funktion von Interferonen bei der Regulierung neuronaler Stammzellen im jungen homöostatischen Gehirn enthüllt. Diese regulierende Rolle der Interferone für Stammzellen in allen Altersstufen offenbart neue therapeutische Implikationen. Dies betrifft nicht nur die Neurogenese, sondern auch Krebs, Virusinfektionen des Gehirns sowie neurodegenerative Erkrankungen.

1. Introduction

1.1 Adult neurogenesis in humans

Neurogenesis is the process of generating new neurons. In humans, developmental neurogenesis is responsible for producing the more than 100 billion neurons that constitute the adult brain (Herculano-Houzel, 2009). In adults, despite the lower turnover of somatic cells relative to other organs, the brain is also subjected to homeostatic regeneration of neurons in certain brain areas (Bergmann *et al*, 2015).

1.1.1 Adult neurogenesis in the human hippocampus

Historically, the presence of adult neurogenesis in humans was first suggested by Eriksson *et al.* in 1998. This study, led by Fred H. Gage and colleagues, found newly-generated neurons in the brains of cancer patients that had been administered the thymidine analog bromodeoxyuridine (BrdU) for diagnostic purposes (Eriksson *et al*, 1998). 7 years later, a study led by Jonas Frisén presented a revolutionary approach to birth date cells in the adult brain (Spalding *et al*, 2005). Frisén and colleagues noticed that the atmospheric increase in ^{14}C levels after the intense nuclear bomb testing between 1955 and 1963 could be used to determine whether a neuron was generated in adulthood from those individuals born before 1950. At first, the authors did not find evidence of neurogenesis in the human brain cortex (Spalding *et al*, 2005). However, 7 years later, they confirmed the presence of abundant neurogenesis in the hippocampus of adult humans (Spalding *et al*, 2013).

Despite this elegant proof of evidence, in the last 5 years, the presence of neurogenesis in adult aged humans was again put at stake. In 2018, two follow-up studies showed contradictory findings: while Sorrells *et al*. found an absence of neural progenitors in the adult hippocampus (Sorrells *et al*, 2018), Boldrini *et al*. found stable and abundant neurogenesis in adult humans (Boldrini *et al*, 2018). Both studies employed immunostainings to assess the presence of markers used to identify neural progenitors during development or in model organisms, such as doublecortin (DCX), KI-67, or PSA-NCAM, in brain sections from post-mortem humans. The observed discrepancies were first suggested to rely on poor antigen preservation of DCX by Sorrells *et al*. 2018 due to sub-optimal fixation times and antigen retrieval during tissue processing (Kempermann *et al*, 2018; Tartt *et al*, 2018). However, Sorrells *et al*. 2018 proved no influence of fixation in the preservation of DCX, fuelling the controversy (Paredes *et al*, 2018). The later findings of an independent group supported the abundant prevalence of neural

progenitors in the healthy adult brain, also based on immunostainings (Moreno-Jiménez *et al*, 2019; Terreros-Roncal *et al*, 2021).

Although both supporters and detractors agreed on the limitations of their marker-based strategy, more recent single-cell transcriptomic approaches have only contributed further to the debate. First, single-nucleus RNA-seq (snRNA-seq) of the adult hippocampus showed a lack of adult neurogenesis in humans, as compared to mice, pigs, or macaques (Franjic *et al*, 2022). Conversely, two other snRNA-seq-based reports found the presence of immature neurons in aged humans, to comparable levels as in aged macaques (Wang *et al*, 2022; Zhou *et al*, 2022). Interestingly, one of these latest studies also re-analyzed the previous dataset from Franjic *et al*. 2022 and suggested that the lack of neural progenitors in this dataset was due to an increased inflammatory signature in these samples (Wang *et al*, 2022). More recently, Tosoni *et al*. tried to reconcile the controversies of these single-cell RNA-Seq studies. Far from closing the debate, the report concludes that as long as a consensus method for sampling and analysis of this transcriptome data is absent, these high-throughput analyses will continue leading to controversial findings (Tosoni *et al*, 2023).

Regardless of whether neural progenitors are active in the human brain, even in supporting studies, whether these immature neurons integrate and actively contribute to the human neural circuitry along the individual's lifespan remains largely unaddressed.

1.1.2 Adult neurogenesis in the human subventricular zone

Adult neurogenesis in the olfactory bulbs (OB) of the adult human brain seems to be less controversial. The generation of new neurons in the OB declines dramatically 18 months after birth in humans, with just a negligible number of immature neurons present in adults (Sanai *et al*, 2011). In line with this finding, no substantial incorporation of ^{14}C was found in the DNA of cells from the OB in humans (Bergmann *et al*, 2012). However, a follow-up study found that despite the absence of new neurons in the OB, an increased prevalence of immature neurons is present in the subventricular zone and adjacent striatum in humans (Ernst *et al*, 2014). Based on this, it is likely that the OB-fated adult neurogenesis from the subventricular, as present in most mammals, might be striatum-fated in the human brain. Interestingly, follow-up results have shown the potential of these human progenitors to also contribute to the architecture of the human frontal cortex, at least during early infancy (Paredes *et al*, 2016).

Due to the possibility of chemical, genetic, and interventional manipulation, adult neurogenesis is better described in rodents.

1.2 Adult neurogenesis in mice

The first evidence of adult neurogenesis in mammals was suggested in the brain of rats (Altman, 1962). Mice, along with rats, have historically been the preferred research model to study adult neurogenesis. The neural stem cells (NSCs) in the adult murine brain are originated from embryonic stem cells during the development of the mouse embryo. In the developing brain, neuroepithelial cells -also called neuroectodermal cells- give rise to the different neural and glial lineages in temporally-controlled waves of differentiation (reviewed in Kriegstein & Alvarez-Buylla, 2009). Right after the first waves producing neurons at embryonic day 9-10 (E9-10), neuroepithelial cells gain a glial-biased fate and start acquiring characteristics of radial glial (RG) cells. RG cells were initially thought to give rise exclusively to astrocytes and oligodendrocytes in the late developmental waves. It was not until 1990 when it was sown that RG cells retain their neurogenic potential even after birth, in this case in songbirds (Alvarez-Buylla *et al*, 1990). This finding not only showed the presence of neurogenesis in other adult individuals but also hinted at the glial origin (RG cells) of the adult newly-born neurons. Later studies confirmed the glial origin of the NSCs present both at late development and adulthood in rodents both in the ventricular-subventricular zone (vSVZ) and the subgranular zone (SGZ) (Götz *et al*, 1998; Doetsch *et al*, 1999; reviewed in Obernier & Alvarez-Buylla, 2019).

Despite the shared characteristics between NSCs and RG cells (e.g. expression of GLAST, BLBP, GFAP, etc.) the exact time of origin of NSCs during development in the mammalian brain could not be proven until much later than 1990. In 2015, two parallel studies showed that the onset of adult NSCs takes place between E13.5-15.5 in the developing brain (Fuentealba *et al*, 2015; Furutachi *et al*, 2015). While most RG cells are depleted by continuous division and differentiation, a specific subgroup of RG cells slows-down cell cycle and give rise to a reserve of NSCs serving as a life-long source of neurogenic output both in the vSVZ and the SGZ. Interestingly, Fuentealba *et al*. also showed how as early as E11.5 (before the establishment of the NSC reserve) developmental cues already determine the spatial-related potency of RG cells (Fuentealba *et al*, 2015). This potency is further maintained in NSCs in the adult and determines the different neural output produced in different adult neurogenic areas, namely the vSVZ and SGZ.

1.2.1 Adult neurogenesis in the murine ventricular-subventricular zone

The ventricular-subventricular zone (vSVZ) composes the largest neurogenic niche of the mouse brain (Lim & Alvarez-Buylla, 2016). Along the walls of the ventricles -mainly on the lateral wall-, neural stem cells (NSCs) distribute forming clusters with adult neurogenic potential. These clusters are characterized to compose a pinwheel structure where a quiescent NSC (qNSC) is surrounded by ependymal cells (Figure 1.1) (Mirzadeh *et al*, 2008). Ependymal cells coat the walls of the ventricle and physically separate the stem cell niche from the cerebrospinal fluid (CSF). Despite the physical separation, qNSCs are ciliated cells and can contact the CSF by an apical cilium. In addition, qNSCs also establish contacts with pericytes and endothelial cells from proximal blood vessels by a basal end-foot prolongation (Mirzadeh *et al*, 2008). This polarization allows qNSCs to sense stimulus from the CSF, the blood system as well as additional contacts with astrocytes, oligodendrocytes, and microglia, pointing out the complexity of the regulatory cues controlling the activation of qNSCs.

Upon exposure to the correct stimuli, qNSCs enter cell cycle and give rise to active NSCs (aNSC). Then, aNSCs divide symmetrically giving rise to either qNSCs or to downstream trans-amplifying progenitors (TAPs) (Obernier *et al*, 2018). TAPs are highly-proliferative progenitors that divide symmetrically, amplifying the neural output and finally giving rise to the migrating immature neuronal progenitors, neuroblasts (NB) (Ponti *et al*, 2013). NBs then migrate along the rostral migratory stream (RMS) to the olfactory bulb (OB), where they distribute radially and differentiate into granular cell interneurons (Figure 1.1) (Doetsch & Alvarez-Buylla, 1996). Interestingly, the high variety of subtypes of interneurons generated by the vSVZ-NSCs relies on the spatial and temporal heterogeneity of these NSCs. NSCs are intrinsically-fated to generate specific subtypes of interneurons depending not only on their location on the dorsal, medial or lateral wall but also on their anterior-posterior/dorso-ventral positioning (reviewed in Chaker *et al*, 2016; Obernier & Alvarez-Buylla, 2019). In addition, recent reports have further contributed to unveiling the heterogeneity of the vSVZ niche, identifying new subsets of NSCs or ventral subregions with specific fate for the OB (Del Águila *et al*, 2022; Cebrian-Silla *et al*, 2021; Delgado *et al*, 2021; preprint Chaker *et al*, 2021).

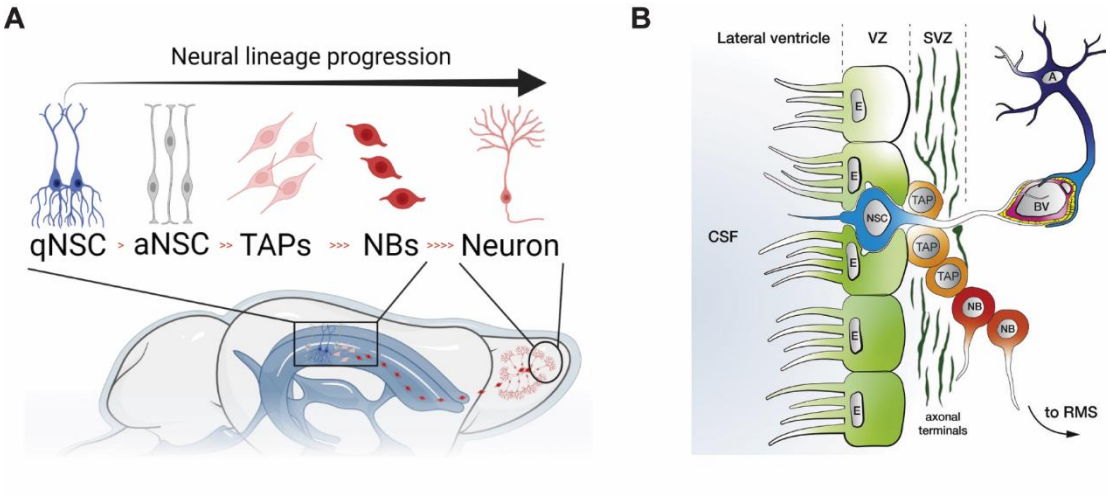

Figure 1.1: Adult neurogenesis in the ventricular-Subventricular Zone

(**A**) Schematic illustration of the neuronal lineage of the ventricular-subventricular zone (vSVZ) from quiescent neural stem cells (qNSC), active NSCs (aNSC), transit-amplifying progenitors (TAPs), migrating neuroblasts (NBs) and neurons at the olfactory bulb. (**B**) Zoom-in scheme on the lateral wall of the vSVZ. A, astrocyte; BV, blood vessel; CSF, cerebrospinal fluid; E, endothelial cell; GCL, granule cell layer; IN, interneuron; TAP, transit-amplifying progenitor; NB, neuroblast; NSC, neural stem cell; RMS, rostral migratory stream; SVZ, subventricular zone; VZ, ventricular zone. Scheme adapted from Urbán *et al*, 2019.

Upon integration in the OB, granular cell interneurons optimize olfactory function by improving olfactory discrimination (Gheusi *et al*, 2000). During mating neurogenesis in the OB and the hippocampus of females is regulated by pheromones produced by males (Mak *et al*, 2008). The production of new neurons and their synaptic integration in the OB is also enhanced during pregnancy and lactation in females (Shingo *et al*, 2003; Kopel *et al*, 2012). Interestingly, while disruption of pregnancy-induced OB-restricted neurogenesis alters only social interactions (Feierstein *et al*, 2010), complete disruption of both OB and DG neurogenesis can perturb also maternal behaviour (Sakamoto *et al*, 2011). Likewise, increased neurogenesis in males upon the birth of pups contributes to the recognition and rearing of the offspring (Mak & Weiss, 2010).

1.2.2 Adult neurogenesis in the murine hippocampus

The subgranular zone (SGZ) on the dentate gyrus (DG) of the hippocampus is the second-largest neurogenic niche in the adult mouse brain (Obernier & Alvarez-Buylla, 2019). In this region, despite the similar embryonic origin, the neuronal subtype fate, as well as the NSC dynamics, are largely different from those in the vSVZ. In contrast to the vSVZ, NSCs in the DG are located far from the ventricles, right underneath a layer of granular neurons termed the granular cell layer (GCL). This subgranular zone is not irrigated by the cerebrospinal fluid but it is highly vascularized, allowing NSCs to sense

cues from pericytes and endothelial cells (Palmer *et al*, 2000). NSCs in the SGZ not only establish contacts with this vascular plexus but also assemble a network of processes to interact with synapsis and astrocytes (Moss *et al*, 2016). Similar to the vSVZ, NSCs and their progenitor cells are also surrounded by other niche cells including oligodendrocytes and microglia in the DG (Figure 1.2).

In the SGZ, NSCs also rely on sensing different stimuli to get activated (Obernier & Alvarez-Buylla, 2019). Upon activation, aNSCs divide symmetrically or asymmetrically to give rise to qNSCs and TAPs. The generated TAPs will then divide, give rise to NBs and migrate tangentially a short distance to the GCL above the progenitor NSCs (Sun *et al*, 2015). In the GCL new-born neurons will mature into DG excitatory glutamatergic neurons that will extend mossy fiber connections to the CA3 of the hippocampus (Toda & Gage, 2018). The addition of new neurons contributes not to the replacement but to the plasticity of the hippocampal tri-synaptic network (Kempermann, 2022). The contribution of adult plasticity of this DG network has been extensively studied by chemical, radiation-based, or genetic NSC ablation (reviewed in Toda & Gage, 2018). Although different ablation methods sometimes led to conflicting interpretations, there is a consensus that DG adult neurogenesis controls spatial learning and memory (Deng *et al*, 2009; Imayoshi *et al*, 2008). Interestingly, recent reports have shown how new-born neurons in the DG promote the encoding of new memories while weakening the existing ones (Epp *et al*, 2016; Temprana *et al*, 2015; McHugh *et al*, 2022).

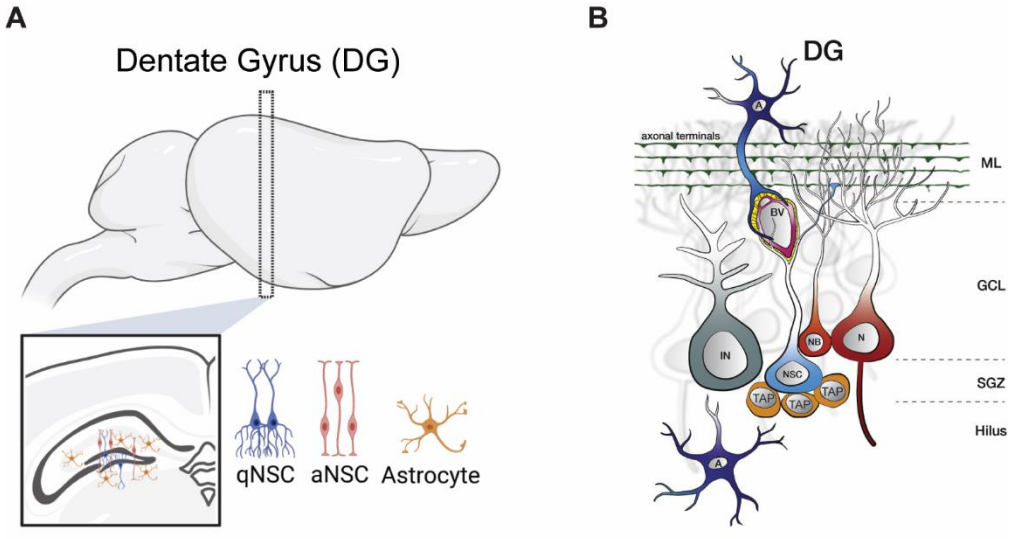

Figure 1.2: Adult neurogenesis in the Dentate Gyrus

(**A**) Schematic illustration of the neurogenic niche of the Dentate Gyrus (DG) in the hippocampus depicting quiescent neural stem cells (qNSC), active NSC (aNSC), and astrocytes. (**B**) Zoom-in scheme on the DG. A, astrocyte; BV, blood vessel; GCL, granule cell layer; IN, interneuron; TAP, transit-amplifying progenitor; ML, molecular layer; N, neuron; NB, neuroblast; SGZ. Scheme adapted from Urbán *et al*, 2019.

1.3 Homeostasis of neural stem cells

The activation of NSCs and the production of new-born neurons in the adult brain is influenced by a variety of complex stimuli. A comprehensive summary of intrinsic (Urbán *et al*, 2019; Murao *et al*, 2016) and extrinsic factors (Obernier & Alvarez-Buylla, 2019) controlling the activation of NSCs has been extensively reviewed.

Here, I summarize the cues regulating the quiescence vs. activation transition in adult NSCs with a special focus on protein translation, cell cycle, and aging. As NSCs from the vSVZ and DG share many of these features, I refer to NSCs in the generic term of the adult mammalian brain, irrespective or their location, unless specified.

1.3.1 Modulating quiescence and activation in neural stem cells

The stem cell niches in the adult brain undergo a lower turnover than those in other tissues such as the gut, skin, or bone marrow (Urbaìn *et al*, 2021). This relies on a higher prevalence of quiescence among NSCs in the brain. Cell quiescence is defined as a reversible state of cell cycle arrest (G_0 or quiescence state) in which certain cells reside for prolonged periods (Cheung & Rando, 2013). During this proliferation arrest, quiescent stem cells reduce their metabolic activity to minimize the accumulation of damage while maintaining their stemness (Cheung & Rando, 2013). As a reversible state, stem cells can exit quiescence and re-enter cell cycle in response to physiological stimuli (Urbán *et al*, 2019). Upon activation, qNSCs transient through a continuum of substages from a deeply dormant quiescent to a cycling active NSC state (Llorens-Bobadilla *et al*, 2015; Basak *et al*, 2018; Dulken *et al*, 2017; Hochgerner *et al*, 2018; Shin *et al*, 2015; Artegiani *et al*, 2017). These substages are referred to as dormant (qNSC1), primed-quiescent (qNSC2), non-mitotic active (aNSC1), and actively cycling active (aNSC2) (Figure 1.3). The progression through these substages involves a continuum of transcriptional changes boosting protein synthesis and cell cycle while promoting a shift from glial to neuronal markers and from glycolytic or fatty-acid metabolism to oxidative metabolism (Llorens-Bobadilla *et al*, 2015; Knobloch *et al*, 2017). These shifts are also promoted by additional mechanisms involving post-transcriptional (Baser *et al*, 2019), post-translational (Urbán *et al*, 2016; Blomfield *et al*, 2019), and epigenetic (preprint Kremer *et al.,* 2022; Wu *et al.,* 2010) regulation.

From those mechanisms, the tight control of protein synthesis and proliferation are key regulators of the quiescent state of stem cells across different tissues.

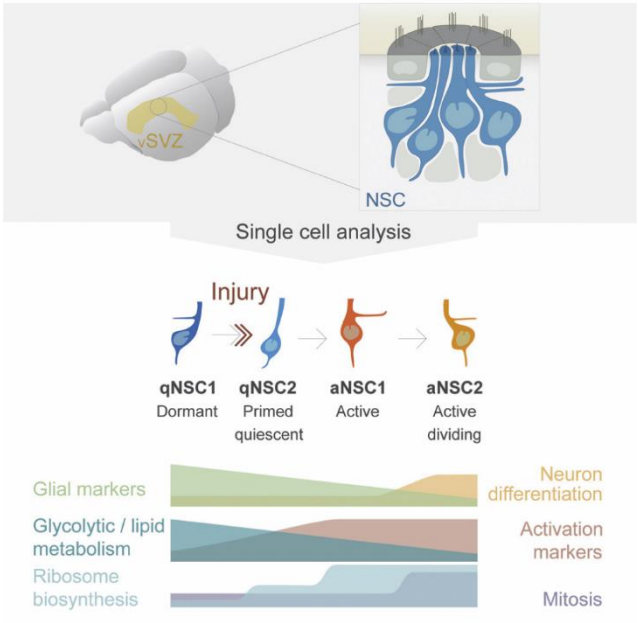

Figure 1.3: Transcriptional changes driving activation of NSCs in the vSVZ

Schematic summary of the transcriptomic transitions upon activation of quiescent neural stem cells (qNSC) in the ventricular-subventricular zone (vSVZ). Progression in the continuum of cell substages is characterized by changing gradients in the expression of the different pathways in single-cell transcriptomics. aNSC, active NSC. Adapted from Llorens-Bobadilla *et al*, 2015.

1.3.2 Protein synthesis and stem cell quiescence, role of mTOR

Translational control modulates the activity of stem cells residing in different adult tissues. Protein synthesis modulates the proliferation of adult hematopoietic stem cells (HSCs) and regulates the self-renewal and differentiation of adult hair follicle stem cells (HFSCs), muscle stem cells (MuSCs or satellite cells) and neural stem cells (NSCs) (Signer *et al*, 2014; Blanco *et al*, 2016; Zismanov *et al*, 2016b; Baser *et al*, 2019; Tahmasebi *et al*, 2019; Frye & Blanco, 2016). In particular in NSCs, modulation of mRNA translation by mTORC1 controls stem cell activation in the young and the old brain (Paliouras *et al*, 2012; Romine *et al*, 2015; Baser *et al*, 2019).

mTOR is a serine/threonine protein kinase that can be found in two different complexes in mammals, namely mTOR complex 1 (mTORC1) and mTOR complex 2 (mTORC2). mTORC1 and C2 complexes are metabolic hubs that coordinate growth, survival and proliferation in response to the presence or absence of metabolites, growth factors, inflammatory cytokines, cell-to-cell signals and stress cues (Liu & Sabatini, 2020). The distinct roles and effectors of mTORC1 and mTORC2 have been historically identified by the chemical inhibition of these complexes by Rapamycin (mTORC1 inhibitor) and Torin1 (mTORC1 and mTORC2 inhibitor) (Thoreen *et al*, 2012). mTORC1 regulates

mRNA translation, ribosome biogenesis, and autophagy as well as metabolic processes including nucleotide synthesis, lipid synthesis, and aerobic glycolysis. mTORC2 regulates cytoskeletal reorganization and cell mobility, as well as cell survival and proliferation (Liu & Sabatini, 2020).

Regarding the control of mRNA translation, mTORC1 regulates the cap-dependent initiation of translation by phosphorylating its two effector proteins 1) the p70 S6 kinase 1 (S6K) and 2) the eukaryotic initiation factor 4E-binding proteins (4E-BPs) (Liu & Sabatini, 2020). Firstly, the phosphorylation of S6K at its Thr389 leads to the sequential phosphorylation and activation of its main target protein, the ribosomal protein S6 (S6). The phosphorylation of S6, despite not having a clear function (Ruvinsky *et al*, 2005) has been associated with increased ribosome biogenesis (Chauvin *et al*, 2014). In addition to S6, activated S6K phosphorylates additional target effectors leading to increased rRNA transcription, and more efficient assembly of the mRNA translation preinitiation complex (Liu & Sabatini, 2020). Second, phosphorylation of 4E-BP1 releases this binding protein from sequestrating the eukaryotic translation initiation factor 4E (eIF4E) (Hara *et al*, 1997). eIF4E is responsible for the binding to the 5' cap of mRNAs and the recruitment of additional translation initiator factors, the RNA helicase eIF4A and the scaffolding protein eIF4G, to the mRNA. Altogether, eIF4E, eIF4A, and eIF4G constitute the eukaryotic translation initiation factor 4F complex (eIF4F), responsible for cap-mediated translation initiation in eukaryotes.

A global readout of the activation of mTORC1 is the translation efficiency of TOP-mRNAs. TOP-mRNAs are mRNAs carrying 5′ terminal oligopyrimidine motifs (TOP motif) that encode most of the ribosomal proteins in the cell (Avni *et al*, 1996). mTORC1-mediated increase in the translation of these TOP-mRNAs sustains protein synthesis upregulation. Several effectors, in addition to 4E-BP1, controlling the specific translation of TOP-mRNAs upon mTORC1 activation have been proposed (Nandagopal & Roux, 2015; Miloslavski *et al*, 2014). One example is the La-related protein 1 (LARP1) (Tcherkezian *et al*, 2014). LARP1 binds to the 5'TOP motif and represses the translation of TOP-mRNAs by hindering the 5' cap from eIF4E (Nandagopal & Roux, 2015). Upon mTORC1 activation, mTORC1-driven phosphorylation of LARP1 enables eIF4E-cap binding and translation initiation (Jia *et al*, 2021).

1.3.3 Cell cycle and stem cell quiescence

The regulation of protein synthesis is intimately ligated to the control of cell proliferation. mTOR activity controls the expression of cyclin D1 (*Ccnd1*), the regulatory partner of the

Cdk4/6 complex (Averous *et al*, 2008). During G_1, the activated CyclinD1-Cdk4/6 complex phosphorylates the retinoblastoma protein (Rb1). The phosphorylated Rb1 translocates into the nucleus and promotes transcription of S phase cell cycle genes (Topacio *et al*, 2019). Interestingly, the Cdk4/6 complex acts as a dual regulator of growth (protein synthesis) and proliferation (cell cycle) (Romero-Pozuelo *et al*, 2020). Cdk4/6 activity not only promotes G_1/S transition but also controls the activity of the Tuberous Sclerosis Complex 2 (TSC2), the main negative regulator of mTORC1 (Yang *et al*, 2017). The bidirectional regulation of proliferation by mTOR and of growth by Cdk4/6 directly impacts the activation of NSCs. Overexpression of Cdk4 and cyclin D1 in NSCs shortens G_1 and promotes progenitor proliferation at the expense of neurogenesis both in the vSVZ (Lange *et al*, 2009) and the DG (Artegiani *et al*, 2011). In addition, Cyclin D1 also inhibits the glial fate of NSCs during development (Bizen *et al*; Ma *et al*, 2010) and in NSCs *ex-vivo* through transportation in extracellular vesicles (Song *et al*, 2021).

1.3.4 Post-transcriptional regulation dictates the identity and fate of neural stem cells

The quiescence vs. differentiation commitment of NSCs is also affected by post-transcriptional and post-translational mechanisms, some of which involve directly mTOR. qNSCs enhance the degradation of the activation-related transcription factor Ascl1 by expressing the inhibitor protein Id4 or targeting Ascl1 for ubiquitin-mediated degradation (Blomfield *et al*, 2019; Urbán *et al*, 2016). Interestingly, dynamic control of mTOR activity in sVSZ-NSCs drives the exit of activation by repressing the translation of the stemness factors *Sox2* and *Pax6* (Baser *et al*, 2019). Similar to TOP-mRNAs, *Sox2* was identified to carry a TOP-like motif in its 5' UTR coined pyrimidine-rich motif (PRM motif). Interestingly, as opposed to TOP-mRNAs, the translation of *Sox2* in NSCs is only repressed when a dual control of mTOR and cell cycle is induced (Baser *et al*, 2019). This underscores the relevance of the dual regulation of protein synthesis and cell proliferation to coordinate the activation of NSCs. However, upstream homeostatic signals controlling this orchestrated regulation remain missing.

1.4 Aging impairs adult neurogenesis

The homeostatic balance of quiescent and active NSCs in the adult brain can be challenged by different conditions including disease (Kulkarni *et al*, 2016), injury (Llorens-Bobadilla *et al*, 2015), mating and pregnancy (Mak *et al*, 2008; Shingo *et al*, 2003) and aging (Dulken *et al*, 2019; Kalamakis *et al*, 2019; Baruch *et al*, 2014). From those, aging has recently been more extensively studied.

During aging, neurogenesis decreases drastically with a drop in the total number of NSCs and their ability to proliferate both in the DG (Seib & Martin-Villalba, 2014; Wu *et al*, 2023) and the vSVZ (Obernier *et al*, 2018; Kalamakis *et al*, 2019). The neurogenic niches in the old brain display age-related processes such as senescence, loss of proteostasis, and chronic inflammation, as many other aging tissues (Nicaise *et al*, 2020; Moore *et al*, 2015; Leeman *et al*, 2018). Drivers of this age-related phenotype are imbalanced levels of signaling molecules such as cytokines in the blood, cerebrospinal fluid or local niche environment (Villeda *et al*, 2011; Baruch *et al*, 2014), wnt proteins (Miranda *et al*, 2012; Seib *et al*, 2013), BMP proteins (Yousef *et al*, 2015; Silva-vargas *et al*, 2016), and growth factors (Shetty *et al*, 2005; Silva-Vargas *et al*, 2016; Katsimpardi *et al*, 2014). Given such systemic changes, it remained unclear until recently whether the age-related quiescence was extrinsically induced or was also a cell-intrinsic characteristic of exhausted stem cells. In 2019, Kalamakis *et al*. showed that young and old NSCs are transcriptionally indistinguishable, except for the upregulation of inflammatory-related genes in aging. Moreover, old NSCs retain the proliferation and differentiation capacity of young NSCs (Kalamakis *et al*, 2019). These findings confirmed the cell-extrinsic source of aging-inducing factors in the old brain (Figure 1.4). In addition, the use of high throughput sequencing techniques in this and other studies has highlighted the role of extrinsic interferons (IFN) in inducing NSC quiescence in the old brain (Baruch *et al*, 2014; Kalamakis *et al*, 2019; Dulken *et al*, 2019).

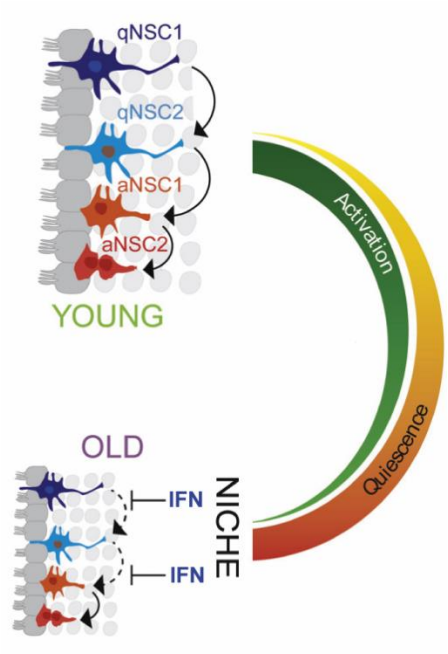

Figure 1.4: Effect of aging in the vSVZ neurogenic niche

Schematic representation of the age-related changes exerted by interferon (IFN) in the ventricular-subventricular zone inducing quiescence in neural stem cells (NSC). Adapted from Kalamakis *et al*, 2019.

1.4.1 Interferons drive quiescence in the aging brain

Upon aging, the chronic increase in type-I IFN signaling decreases neurogenesis in the SGZ and the vSVZ (Baruch *et al*, 2014; Kalamakis *et al*, 2019). Blockade of type-I IFN response or its downstream component, CXCL10, in an aged brain restores the young choroid plexus properties, as well as the neurogenic capacity and the cognitive functions (Baruch *et al*, 2014; Kalamakis *et al*, 2019). The source of origin of IFN in the aging brain remains controversial. scRNA-Seq of the vSVZ niche and neighboring cells showed that endothelial cells display the strongest IFN signature in the nice (Kalamakis *et al*, 2019). Interestingly, although systemic IFN-β is not able to cross the blood-brain barrier, it can induce the production of CXCL10 from endothelial cells (Blank & Prinz, 2017; Blank *et al*, 2016). Kalamakis *et al*. suggested that endothelial cells could be translating systemic signals to the niche, which was supported by a later study reporting that endothelial cells react to pro-aging factors such as cytokines in the blood and drive the aging phenotype in the old DG (Yousef *et al*, 2019). Similarly, a subset of T cells clonally expands in the vSVZ and contributes to the age-related decline of neurogenesis by chronically secreting IFN-γ (Dulken *et al*, 2019). Intriguingly, chronic interferon signaling is one of the key factors inducing senescence across tissues (Glück & Ablasser, 2019). Interestingly in the DG, age-related increased senescence of NBs induces an expansion of natural killer cells that impairs neurogenesis (Jin *et al*, 2021).

Overall, recent research efforts point to the relevant role of interferon signaling in promoting aging in NSCs and their niche (Dulken *et al*, 2019; Kalamakis *et al*, 2019; Baruch *et al*, 2014). Understanding how NSCs enter quiescence -and not senescence- upon exposure to interferons in the old brain is key to harnessing the regenerative capacity of NSCs in aging.

1.4.2 Interferons in the old brain: Quiescence or senescence?

In addition to interferons, the higher prevalence of senescent cells in the vSVZ and DG upon aging (Molofsky *et al*, 2006; Jin *et al*, 2021) is directly related to the decrease in neurogenesis in the old brain (Deana M. Apple *et al*, 2019; Ogrodnik *et al*, 2019). Key factors differentiate the dormant (qNSC) vs. exhausted nature of senescent cells. Identification of senescent cells is based on a panel of different biomarkers including the expression of a senescence-associated secretory phenotype (SASP) -including IFNs-, and the expression of the cell cycle inhibitor p16INK4A, among others (Di Micco *et al*, 2021; Frisch & MacFawn, 2020). The secretion of matrix metalloproteases, as a major component of the SASP, alters the properties of the ECM (Di Micco *et al*, 2021). During aging, increased stiffness of the niche leads to a functional decline of oligodendrocyte

progenitors (Segel *et al*, 2019). In addition, increased expression of p16INK4A in the aged DG hinders the activation of NSCs (Micheli *et al*, 2019). Interestingly, decreased expression of Sox2 correlates with the enrichment of p16INK4A-expressing cells in the old DG, which triggers an increase in type-I IFN (Nicaise *et al*, 2020; Carrasco-Garcia *et al*, 2019; De Cecco *et al*, 2019). IFNs play a key role in inducing and intensifying senescence in an auto- and paracrine manner (Frisch & MacFawn, 2020; Glück & Ablasser, 2019).

Similar to quiescence, protein synthesis is downregulated in senescent cells. Yet, senescent cells hyperactivate mTORC1 to sustain the SASP (Payea *et al*, 2021). This hyperactivation of mTORC1 is critical to maintaining senescence (Demidenko *et al*, 2009). Notably, while quiescent stem cells reduce protein synthesis via modulation of mTORC1, senescent cells suppress global protein synthesis by several mechanisms including the inhibition of mRNA translation initiation by phosphorylation of eIF2α (Payea *et al*, 2021; Eiermann *et al*, 2020). The phosphorylation of eIF2α is a hallmark of the integrated stress response that is generated upon viral infection, ER stress, nutrient stress, or ROS sensing (Eiermann *et al*, 2020). These stressors activate eIF2α-kinases such as the Pkr kinase, in the case of dsRNA viral infections, which phosphorylate eIF2α at Ser51 (Gal-Ben-Ari *et al*, 2019). Phosphorylation of eIF2α by Pkr sequesters the translation initiation factor eIF2B, slowing down the regeneration of the ternary complex and impairing the homeostatic rate of translation initiation (Pavitt, 2018). Despite the global shutdown of protein synthesis by p-eIF2α^{S51}, the scarcity of ternary complex can benefit a subset of transcripts harboring upstream open reading frames (uORFs) (Young & Wek, 2016). These transcripts, such as *Atf4*, are involved in the ISR and involved in quiescence maintenance in adult stem cells in the muscle (Zismanov *et al*, 2016b).

Albeit the higher prevalence of senescent somatic cells in the vSVZ and DG in the old brain (Molofsky *et al*, 2006; Ogrodnik *et al*, 2019; Jin *et al*, 2021), it is unclear how qNSCs are selectively safeguarded from senescence. The potential implication of interferons, mTORC1, and phosphorylation of eIF2α in discerning quiescence and senescence remains unexplored in NSCs.

1.5 Interferons and inflammation in stem cell biology

Interferons (IFN) are cytokines originally describe to restrict viral infections (Isaacs *et al*, 1957a, 1957b). The cytostatic and pro-inflammatory functions of interferons make them highly relevant for stem cell biology not only in the immune system but also in adult stem

cells across different tissues (Kalamakis *et al*, 2019; Demerdash *et al*, 2021; Sato *et al*, 2020; Wu *et al*, 2018).

1.5.1 Interferons and receptors

The interferon family is composed of type-I, -II, and -III IFNs, each signaling through different receptors that induce different functions in their target cells.

Type-I IFNs consist of 13 (human) and 14 (murine) subtypes of IFN-α, along with IFN-β, IFN-ε, IFN-κ, IFN-ω (human and mice), IFN-ζ (mice), IFN-δ (pigs) and IFN-τ (cattle) (Pestka *et al*, 2004; Platanias, 2005; Ivashkiv, 2018; Wack *et al*, 2015). Among all, IFN-α and IFN-β are the most predominantly-studied subtypes of type-I IFNs. Type-I IFNs are mainly produced after pattern-recognition receptor (PRR) activation but also upon recognition of host factors and cytokines. Recognition of these signals leads to the phosphorylation and dimerization of interferon regulatory 3/7 (IRF3/7) proteins, which upregulates the transcription of type-I IFNs (Stanifer *et al*, 2020). IFN-β is ubiquitously produced and secreted exerting its function in an auto- and paracrine manner (Mazewski *et al*, 2020). Type-I IFNs are recognized by the interferon α/β receptor (IFNAR), a heterodimeric receptor composed of the IFNAR1 and IFNAR2 subunits, expressed in all nucleated cells (Schreiber, 2017). Type-I IFNs first bind IFNAR2 with high affinity, which then recruits and dimerizes with the low-affinity subunit IFNAR1. Upon IFNAR dimerization, the receptor activates its downstream kinases TYK2 and JAK1, associated with IFNAR1 and IFNAR2, respectively (Lee & Ashkar, 2018; Stanifer *et al*, 2020).

The type-II IFN family consists only of IFN-γ, which is mainly produced by natural killer and natural killer T cells (Alspach *et al*, 2019). Despite this restrictive production, IFN-γ is recognized by the interferon γ receptor (IFNGR), which is expressed in nearly every cell type. IFNGR is composed of two subunits, IFNGR1 and IFNGR2, each of them associated with its downstream target kinases JAK1 and JAK2, respectively. Upon IFN-γ binding, conformational changes in IFNGR activate its associated JAKs, which trigger the IFN-γ signaling cascade (Alspach *et al*, 2019).

The type-III IFN or IFN-λ family comprises four members: IFN-λ1, λ2, λ3 (IL29, IL28A, and IL28B, respectively), and IFN-λ4, which are widely expressed in the body (Stanifer *et al*, 2020). Similar to type-I IFNs, recognition of pathogen-associated molecular patterns (PAMPs) by PRRs activates IRF3/7 and initiates transcription of IFN-λ. Type-III IFNs are recognized by a heterodimeric receptor composed of the interferon λ receptor (IFNLR1; IL-28Rα) and the interleukin 10 receptor 2 (IL-10R2). While IL-10R2 is ubiquitously expressed, IFNLR1 is expressed only in epithelial and immune cells,

restricting IFN-λ response mainly to barrier surfaces (Stanifer *et al*, 2020). Similar to type-I IFNs, binding of IFN-λ to its receptor causes receptor dimerization and activation of its associated kinases JAK1 and TYK2, associated with IFNLR1 and IL-10R2, respectively (Stanifer *et al*, 2020).

1.5.2 Canonical interferon signaling

Upon receptor binding, different IFNs trigger similar but nonidentical signaling pathways that fine-tune the antiviral, proliferation, and survival response in the target cells (Mazewski *et al*, 2020; Stanifer *et al*, 2020; Ivashkiv & Donlin, 2014).

In the type-I and -III IFN canonical JAK/STAT signaling pathway (Figure 1.5), activated Tyk2 and Jak1 tyrosine-phosphorylate the signal transducer and activator of transcription (STAT) 1-5 and STAT6 (type-I IFN-specific) (Mazewski *et al*, 2020; Stanifer *et al*, 2020). Phospho-STAT1-6 dimerize and shapes the transcriptome of the cell to promote an antiviral and anti-proliferative state ubiquitously (STAT1-3) or in a cell type-specific manner (STAT4-6) (Stanifer *et al*, 2020). The STAT1/STAT2 heterodimer, the most prominent complex resulting from type-I and -III IFN response, associates with IRF9 to constitute the interferon-stimulated gene factor 3 (ISGF3) complex (Mazewski *et al*, 2020). ISGF3 recognizes and binds the IFN-stimulated response elements (ISREs; AGTTTCNNTTTCN) present at the regulatory region of a subset of interferon-stimulated genes (ISGs) (Mazewski *et al*, 2020; Michalska *et al*, 2018). Activated TYK2 and JAK1 kinases can also promote the formation of phosphorylated STAT1 or STAT3 homodimer complexes but in a reduced proportion than STAT1/STAT2 (Michalska *et al*, 2018; Stewart *et al*, 2002).

Distinctively, in the type-II IFN canonical JAK/STAT signaling pathway (Figure 1.5), activated JAK1/2 phosphorylate only STAT1 (Alspach *et al*, 2019). Phosphorylated STAT1 homodimers, known as γ-activated factor (GAF), bind and activate transcription of ISGs containing the γ-activated sequence (GAS; $TTCN^{(2-4)}GAA$) in their upstream promoters (Michalska *et al*, 2018; Alspach *et al*, 2019). Although GAS-mediated expression of ISGs can be partially triggered by type-I IFN, it is largely associated with the IFN-γ.

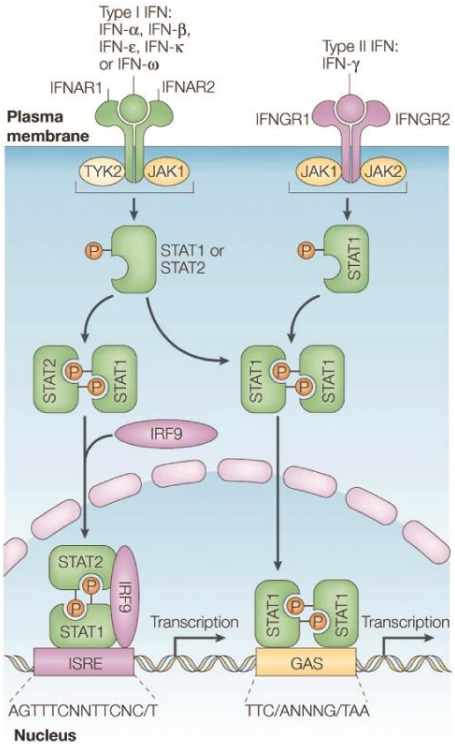

Figure 1.5: Canonical signaling pathway of type-I and -II interferons

Adapted from Platanias, 2005.

Functionally, the IFN canonical JAK/STAT pathway upregulates the expression of different subsets of ISGs that establish a cellular antiviral state (Ivashkiv & Donlin, 2014). ISRE-ISGs (ISGF3-controlled) largely contribute to the viral-restricting response, GAS-related ISGs induce a pro-inflammatory signature and STAT3 homodimer-related ISGs indirectly inhibit the expression of pro-inflammatory genes (Mazewski *et al*, 2020). The IFN response is, however, cell type- and context-dependent, leading to a specific expression of different subsets and an abundance of ISGs (Mazewski *et al*, 2020; Stanifer *et al*, 2020; Ivashkiv & Donlin, 2014). Interestingly, even among the same cell types, a heterogenous response to IFNs has been reported with cells that respond and cells that are refractory to IFN (Rand *et al*, 2012; Stanifer *et al*, 2020). This stochastic responsiveness to IFNs has been associated with a differential basal expression of IRF9 (Maiwald *et al*, 2010; Stanifer *et al*, 2020).

1.5.3 Non-canonical interferon signaling – protein synthesis control

In the case of type-I IFNs, binding to IFNARs also triggers non-canonical signaling pathways, that can signal through the p38 MAPK pathway, protein kinase C-delta (PKCδ), phosphoinositide 3-kinase (PI3K), TNK1, calmodulin-dependent kinase II

(CamKII), mammalian target of rapamycin (mTOR), cyclin-dependent kinase 8 (CDK8), and CDK9 downstream of sirtuin 2 (SIRT2) deacetylation, independently of STATs (Saleiro & Platanias, 2019; Mazewski *et al*, 2020). PKC, PI3K/mTOR, TNK1, CamKII, CDK8, and SIRT2 pathways are implicated in a Jak2-independent activation of STAT1, which augments the canonical upregulation of ISGs (Saleiro & Platanias, 2019). However, these non-canonical pathways also contribute to the establishment of an antiviral state of the cell in different ways.

The PI3K/Akt/mTOR pathway controls among others growth, proliferation, differentiation, and survival (Jean & Kiger, 2014). In the interferon response, activation of mTOR promotes optimal translation of ISGs, in addition to the mTOR-related target TOP-mRNAs (Figure 1.6) (Thoreen *et al*, 2012; Mazewski *et al*, 2020). Type-I, -II, and -III IFNs have been reported to activate the PI3K/mTOR pathway in different cell types (Lekmine *et al*, 2003, 2004; Ivashkiv & Donlin, 2014; Syedbasha *et al*, 2020). Type-I IFNs induce tyrosine phosphorylation of IRS1 in a JAK-dependent but STAT-independent manner that induces the activation of PI3K (Platanias, 2005; Uddin *et al*, 1995). Similarly, type-III IFNs also trigger the activation of PI3K by JAKs (Syedbasha *et al*, 2020), probably involving IRS1. Differently, type-II IFNs activate PI3K in an IRS1/2-independent manner (Alsayed *et al*, 2000). Despite the activatory role of IFNs on mTOR activity, IFN-β, and IFN-γ can also inhibit mTOR, suggesting that the effect of IFN on PI3K/mTOR signaling might be cell-type specific (Su *et al*, 2015; Vigo *et al*, 2019).

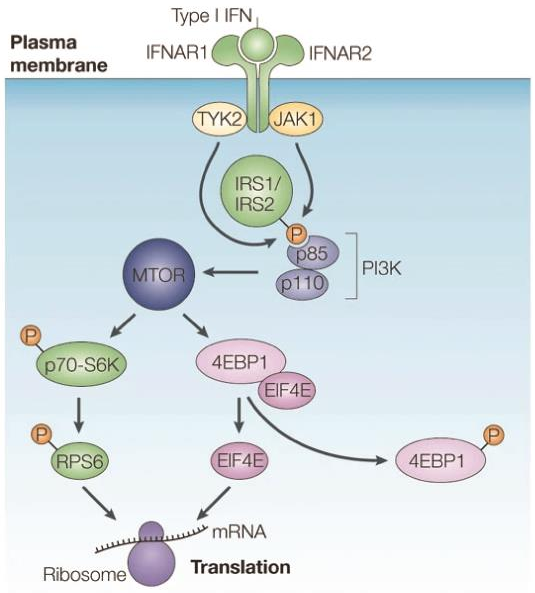

Figure 1.6: Non-canonical signaling pathway of type-I interferon

Adapted from Platanias, 2005.

Both the canonical and the non-canonical IFN signaling pathways trigger changes in mRNA translation efficiency, which affect cellular mRNAs beyond ISGs (Mazewski *et al*, 2020; Ivashkiv & Donlin, 2014). For instance, in addition to the effect on translation by modulating mTOR, the canonical JAK/STAT pathway upregulates the expression of protein kinase R (PKR; *Eif2ak2*), an ISG that restricts mRNA translation initiation (Ivashkiv & Donlin, 2014). PKR is activated by dsRNA and phosphorylates the translation initiation factor eIF2α at Ser51, resulting in a global inhibition of mRNA translation initiation (see section 1.4.2 for more details about p-eIF2α^{S51}).

1.5.4 Interferons in stem cells – Intrinsic or extrinsic response?

Despite the traditional dogma that interferon responses are built upon viral exposure, recent findings show that interferon signaling can occur in the absence of pathogens and intrinsically protect stem cells even before the onset of infection (Figure 1.7).

In a study led by Charles Rice, Wu *et al*. found that stem cells (mainly embryonic stem cells -ESCs- but also adult stem cells) intrinsically express a subset of ISGs in the absence of viruses (Wu *et al*, 2018). This intrinsic expression of ISGs, which does not occur in differentiated cells, protects stem cells from infection. Despite the mostly *in-vitro* nature of the study by Wu *et al*., more recent findings also support the presence of this intrinsic response in intestinal stem cells *ex-vivo* (preprint Funk *et al*, 2021). Interestingly, Wu *et al*. also found that stem cells from different tissues display distinct patterns of ISGs, which also differs from those ISGs expressed by differentiated cells upon infection (Wu *et al*, 2018). Controversially, Wu *et al*. also propose that stem cells are refractory to external interferons nor viral infections and fail to build an interferon response, as compared to their differentiated progeny (Wu *et al*, 2018). This agrees with previous reports showing an attenuated response of ESCs to interferons (Burke *et al*, 1978; Muckenhuber *et al*, 2023) but clashes with the consistent responsiveness of adult stem cells across different tissues (Essers *et al*, 2009; Baldridge *et al*, 2010; Baruch *et al*, 2014; Takashima *et al*, 2019).

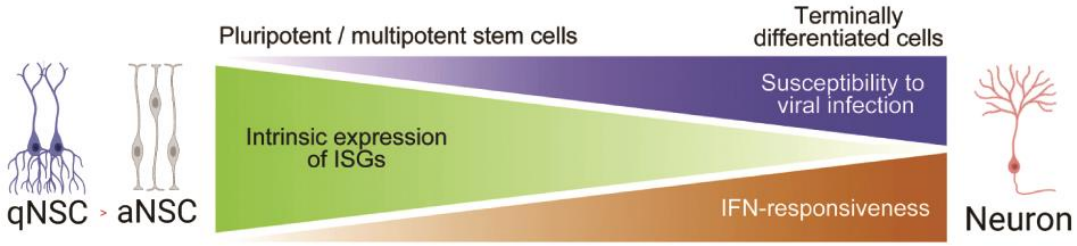

Figure 1.7: Intrinsic interferon signature of stem cells

qNSC, quiescent neural stem cell; aNSC, active neural stem cell. Adapted from Wu *et al*, 2018.

How stem cells maintain an intrinsic expression of ISGs in the absence of inducers is unclear. Two potential non-exclusive mechanisms might be responsible for maintaining the intrinsic interferon response in stem cells. First, Wu *et al*. pointed out epigenetic modifications, as ESCs have enriched H3K4me3 and H3K27ac modifications around ISGs such as IFITM3, correlating with their upregulation (Wu *et al*, 2018). Follow-up studies have supported the role of epigenetic modifications in regulating the expression of ISGs in ESCs (Muckenhuber *et al*, 2023), as well as of chromatin accessibility in intestinal stem cells (preprint Funk *et al*, 2021). Second, the basal expression of endogenous retroviruses could also sustain an interferon response in stem cells (Grow *et al*, 2015). The expression of these recognition patterns can be sensed by the cytosolic dsDNA sensor cGAS, expressed in stem cells in the absence of infections (Yang *et al*, 2015). Activation of the cGAS-STING pathway triggers the interferon response in an auto- and paracrine manner (Naik *et al*, 2018). Interestingly, quiescent hematopoietic stem cells express circular RNAs that avoid cGAS activation, preventing the induction of an interferon response (Xia *et al*, 2018).

Last, the heterogeneity and prevalence of the intrinsic and extrinsic interferon response in the stem cell niches have however not been studied at the single-cell resolution. Only an American Society of Hematology Meeting abstract by Haas *et al*. highlighted the heterogeneous distribution of interferon positive and negative cells in the hematopoietic niche (meeting abstract Haas *et al*, 2017). Interestingly, interferon-reporter-positive cells would retain their IFN response even after transplantation, supporting the epigenetic-related long-term memory of the interferon signature in stem cells (meeting abstract Haas *et al*, 2017). More recently, it was shown how stem cells in the bone marrow respond heterogeneously to inflammation (Bogeska *et al*, 2022) and more specifically to interferons (preprint Bouman *et al*, 2023). However, none of these reports discerned the extrinsic or intrinsic nature of the interferon response in stem cells.

1.5.5 Interferons in NSCs in health and disease

In addition to the prevalence and role of interferon in the aging brain (See section 1.4), interferon also regulates NSCs under different conditions.

During development, JAK/STAT signaling regulates the glial differentiation of NSCs through activation of STAT1 and STAT3 (He *et al*, 2005). However, IFNs have not yet been proved to participate in this mechanism, which is regulated by a number of other cytokines such as the leukemia inhibitory factor (LIF) (Kulkarni *et al*, 2016).

In healthy adults, interferons can also modulate the activation of adult NSCs. The absence of basal IFN-β signaling is detrimental to the survival of neurons in different brain areas including the vSVZ, the OB, and the DG (Ejlerskov *et al*, 2015; Blank & Prinz, 2017). In addition, IFN-γ exerts anti-proliferative effects on NSCs *in-vitro* by activation of STAT1 and STAT3 (Kulkarni *et al*, 2016). IFN-γ also exerts anti-proliferative effects on NSCs *in-vivo* but simultaneously increases the number of NBs in the vSVZ without an absolute increase in OB neurogenesis (Pereira *et al*, 2015). Conversely, IFN-γ has also been proposed to induce the proliferation of neural progenitors *in-vitro* by inducing the expression of sonic hedgehog (Shh) (Sun *et al*, 2010). Interestingly, in the SGZ, IFN-γ induces NSC proliferation and enhances neurogenesis both in young and aged mice (Baron *et al*, 2008).

During brain injury and inflammation, IFN-γ in the choroid plexus modulates and recruits immune cells, which influence NSCs among other cells (Kunis *et al*, 2013; Kulkarni *et al*, 2016). This acute increase of IFN-γ also primes the activation of the deep qNSCs in the vSVZ (Llorens-Bobadilla *et al*, 2015). Interestingly, although activation of neurogenesis after injury improves recovery, increased neurogenesis in the hippocampus after stroke is suggested to be detrimental to the cognitive recovery of mice (Cuartero *et al*, 2019).

During disease, chronic secretion of cytokines including IFN-α by microglia inhibits neurogenesis in the DG, driving depression-like behaviours in mice (Zheng *et al*, 2015). In Alzheimer's disease (AD), the expression of type-I and -II IFNs is impaired in the choroid plexus and the hippocampus in mouse models (Mesquita *et al*, 2015). Furthermore, IFN-γ induces the production of β-amyloid (Aβ) peptides from astrocytes (Blasko *et al*, 2000; Hong *et al*, 2003), increases death in primary neurons in the presence of Aβ peptides (Bate *et al*, 2006) and is associated to a worse prognosis of AD (Huberman *et al*, 1994; Kulkarni *et al*, 2016; Asselineau *et al*, 2015). In line with these findings, the absence of type-I IFN reduced the secretion of pro-inflammatory cytokines and ameliorated some treats of AD in mouse models (Minter *et al*, 2016). In multiple sclerosis (MS), high expression of IFN-γ contributes to a worse outcome (Kulkarni *et al*, 2016). Interestingly, While IFN-γ proceeds to MS relapse; IFN-α was associated with MS clinical remission (Dettke *et al*, 1997). Mouse models of MS show that type-I IFN signaling in astrocytes reduces inflammation and stops the progression of MS (Teige *et al*, 2003; Rothhammer *et al*, 2016).

Despite these described roles of interferon, it is still not clear whether interferon regulates stem cells also during homeostasis or exerts a role only upon disease or aging.

1.5.6 Interferons in stem cells across different tissues in health and disease

Beyond NSCs, interferons regulate the activation and differentiation of stem cells not only in the hematopoietic system but also in the skeletal muscle, intestine, skin, and adipose tissue.

In the hematopoietic system, IFNs regulate hematopoietic stem cells (HSCs) and their offspring (Demerdash *et al*, 2021). IFN-γ controls HSC emergence and IFN-α promotes functional maturation and expansion of HSCs during development (Zhang *et al*, 2020; Sawamiphak *et al*, 2014; Kim *et al*, 2016). In adulthood, IFNs induce cell division of HSCs while impairing their self-renewal and reducing their long-term function (Demerdash *et al*, 2021). While IFN-α and IFN-γ inhibit cell division in HSCs *in-vitro*, they induce cell cycle entry of quiescent HSCs and expansion of their downstream myeloid and lymphoid progenitors *in-vivo* (G R Klimpel, W R Fleischmann, 1982; Yang *et al*, 2005; Baldridge *et al*, 2010; Essers *et al*, 2009; Pietras *et al*, 2014). This activation of quiescent HSCs is mediated by canonical, noncanonical -in the case of IFN-α- signaling, and by altering the physical localization of HSCs in the niche -in the case of IFN-γ (Essers *et al*, 2009; Florez *et al*, 2020). Despite this activation of HSCs by both type-I and -II IFNs *in-vivo*, the total pool of HSCs remains stable (Baldridge *et al*, 2010; Essers *et al*, 2009). For type-I IFN, the uniform number of HSCs is explained by IFN-α inducing only a transient activation of HSCs that rapidly return to a quiescent state upon chronic sensing of IFN (Pietras *et al*, 2014). Differently, type-II IFNs also compensate for their activation of HSCs by impairing self-renewal and promoting differentiation (Matatall *et al*, 2014; de Bruin *et al*, 2013). Recently a more-detailed analysis of the effect of interferon on HSCs *in-vivo* with single-cell resolution has shown heterogeneity in this response (preprint Bouman *et al*, 2023). In addition, IFNs can influence HSCs indirectly by altering their bone marrow niche acting on mesenchymal stromal cells (MSCs) and macrophages (McCabe *et al*, 2015; Schürch *et al*, 2014; Umemoto *et al*, 2017) or on the vasculature and ECM (Prendergast *et al*, 2017; Negrotto *et al*, 2011; Uckelmann *et al*, 2016). During infection, the acute secretion of IFNs activates HSCs to differentiate and battle the pathogen. However, despite the beneficial component of the defense, this interferon response compromises the functional potency of HSCs, leading to accelerated aging (Matatall *et al*, 2016; Demerdash *et al*, 2021; Bogeska *et al*, 2022). Interestingly, a recent study proposes that although HSCs respond to infection, it is the progenitors and not the HSCs who are involved in the differentiation wave upon infection (Fanti *et al*, 2023). During aging, the number of HSCs in the bone marrow increases but aged HSCs have a lower regenerative capacity, display a disproportional clonal distribution of their blood progeny

and a myeloid-fated bias (Pang *et al*, 2011; Akunuru & Geiger, 2016; Mejia-Ramirez & Florian, 2020). Similarly, chronic inflammation in aging (Zhu *et al*, 2021) is also accompanied by extended exposure to IFN-α or IFN-γ which compromises the life-long persistence of HSCs (Matatall *et al*, 2016; Demerdash *et al*, 2021; Pietras *et al*, 2014).

In the muscle, IFN-γ is required for efficient regeneration both in young and aged individuals (Cheng *et al*, 2008; Zhang *et al*, 2020). In response to injury, IFN-γ fine-tunes the secretory phenotype of macrophages that regulate the activity of muscle stem cells (MuSCs) (Zhang *et al*, 2020). Conversely, a recent report showed the opposite effect for type-I IFN, which prevents MuSC expansion and compromised regeneration (Gallay *et al*, 2022). During aging, MuSCs reduce their regenerative capacity and are more susceptible to senescence and apoptosis (Sousa-Victor *et al*, 2014; Jejurikar *et al*, 2006). Chronic inflammation and cumulative DNA damage are some of the main drivers of this age-related loss of function on MuSCs, which relies on Notch and Wnt signaling, among others (Yamakawa *et al*, 2020; Brack *et al*, 2007; Carlson *et al*, 2008).

Mesenchymal stem cells (MSCs) also are influenced by aging, albeit the cues involved are not fully described (Beane *et al*, 2014). Nevertheless, type-I and -II IFNs enhance the immunomodulatory function of MSCs both by canonical and noncanonical IFN signaling (Vigo *et al*, 2019; Guan *et al*, 2017).

In the gut, JAK/STAT-mediated signaling also controls the proliferation of intestinal stem cells (ISCs) (Jasper, 2020; Hou *et al*, 2021). Chronic interferon stimulation leads to the functional decline of ISCs (Sato *et al*, 2020) or even apoptosis in the case of IFN-γ (Takashima *et al*, 2019). In aging, old ISCs display an inflammatory signature that is stably maintained also *ex-vivo* (preprint Funk *et al*, 2021). Interestingly, in response to interferons, ISCs actively downregulate their interferon response to preserve stemness via the negative regulator of IFN, IRF2 (Sato *et al*, 2020).

In the skin, expression of IRF2 antagonizes the correct functioning of adult epidermal stem cells (EpdSC) (Mercado *et al*, 2019). Also, in the context of skin disorders, chronic interferon signaling has been associated with a loss of quiescent hair follicle stem cells (HFSCs) and an increase in skin progenitor cells (Orvain *et al*, 2020).

1.6 IFIT1, an ISG to selectively modulate mRNA translation

IFIT1 (*P56* or *Isg56*) belongs to a large family of proteins known as interferon-inducible proteins with tetratricopeptide repeats (IFIT) (Fensterl & Sen, 2015). The human IFIT

family is composed of four well-characterized -*IFIT1* (*ISG56*), *IFIT2* (*ISG54*), *IFIT3* (*ISG60* or *IFIT4*), and *IFIT5* (*ISG58*)- and two less well-characterized -*IFIT1B* and *IFIT1P1*- members. Similarly, the murine IFIT family is composed of three well-characterized -*Ifit1* (*Isg56*), *Ifit2* (*Isg54*), and *Ifit3* (*Isg49*)- and two less well-characterized -*Ifit1b* (*2010002M12Rik*) and *Ifit3b* (*I830012O16Rik*)- members (Fensterl & Sen, 2015). The expression of IFIT genes is controlled by type-I interferon through ISRE elements, except for human *IFIT1B* (Fensterl & Sen, 2011). Despite the high inter-species sequence similarity of IFIT members, several structural differences exist between human and mouse IFIT members -including IFIT1-, which also affects their function (Daugherty *et al*, 2016).

1.6.1 RNA-binding properties of IFIT members and IFIT1

IFIT1 interacts directly with the 5' termini of certain viral RNAs to restrict viral replication (Fensterl & Sen, 2015). Effective binding of IFIT1 to the 5'-termini of viral RNAs blocks their translation initiation by out-competing eIF4E (Figure 1.8) (Kumar *et al*, 2014). Although both human and murine IFIT1 proteins can sequester 5'-triphosphate (5'-ppp) viral RNAs (Pichlmair *et al*, 2011), the affinity for 5'-ppp is not strong enough to efficiently block viral replication (Pinto *et al*, 2015). The RNA binding affinity is however higher for certain capped RNAs, albeit human and murine IFIT1 differ in their 5'-cap-binding properties (Daugherty *et al*, 2016). Murine IFIT1 alone can selectively capture and inhibit the translation of capped viral RNAs lacking 2'-O-methylation -cap0 or m7GpppNN-, but not RNAs containing a methylated cap -cap1 or m7GpppNmN- (Habjan *et al*, 2013; Daffis *et al*, 2010). Differently, human IFIT1 alone cannot discriminate between cap0 and cap1 as efficiently as its mouse paralogue (Daugherty *et al*, 2016; Abbas *et al*, 2017). This basal lack of discrimination relies on the dependency of human IFIT1 on interacting with human IFIT3. Human IFIT3 binds and regulates IFIT1's 5' RNA ligand binding specificity and protein half-life (Johnson *et al*, 2018). Mouse IFIT3, however, lacks the C-terminal domain responsible for the IFIT1-IFIT3 interaction in humans, constituting another dissimilarity between species (Johnson *et al*, 2018). Interestingly, binding of IFIT members to RNA is not only dictated by the 5'cap. The secondary structure of the 5'UTR is relevant for the binding of mouse IFIT1 (Hyde *et al*, 2014) and IFIT2 was reported to bind selectively AU-rich RNAs (Yang *et al*, 2012). Differently to IFIT1 and IFIT2, binding to RNA by IFIT3 has not been described.

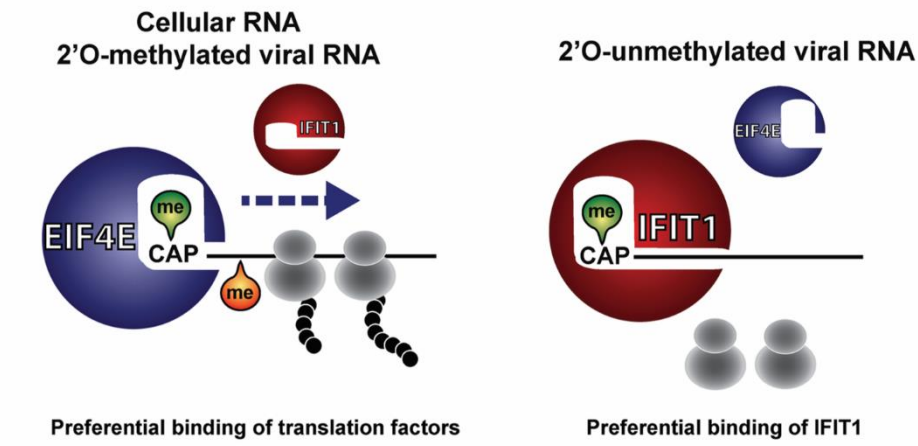

Figure 1.8: Selective inhibition of mRNA translation by IFIT1-RNA binding
Adapted from Habjan *et al*, 2013.

1.6.2 Protein-binding properties of IFIT members and IFIT1

In addition to RNA, IFIT members also interact with other proteins. IFIT1, IFIT2, and IFIT3 cross-interact and form a super complex containing many other RNA-binding proteins as well as proteins involved in mRNA translation regulation (Pichlmair *et al*, 2011; Johnson *et al*, 2018). The removal of any of these three IFIT members results in an impaired antiviral response to different viruses (Fensterl *et al*, 2012; Schmeisser *et al*, 2010). In addition, IFIT proteins were originally suggested to inhibit global protein synthesis by direct interaction with the eukaryotic initiation factor 3 (eIF3) (Guo *et al*, 2000; Terenzi *et al*, 2005). Although later studies could not reproduce the changes in global protein synthesis (Pichlmair *et al*, 2011), the binding of IFIT1 to eIF3 inhibits cap-independent translation initiation in viruses carrying internal ribosome entry sites such as the hepatitis C virus (Wang *et al*, 2003; Raychoudhuri *et al*, 2011). The later-on described RNA-binding properties of IFIT1 were accepted as its preferential mechanism of action, albeit the IFIT1/2-eIF3 interaction has not been formally refuted. Of note, the two mechanisms are not exclusive, as different regions of the IFIT1 proteins are involved in the selective binding of RNA or eIF3 (Fensterl & Sen, 2015). Another example of protein-protein interaction is the binding of IFIT1 with the human papillomavirus (HPV) E1 helicase protein. Sequestering of E1 by IFIT1 effectively restricts HPV viral replication (Terenzi *et al*, 2008).

In addition, several studies have also shown that IFIT1/IFIT2 can bind STING and interfere with the cGAS signaling pathway (Li *et al*, 2009). By blocking the cGAS pathway, IFIT members would act as negative feedback regulators of the interferon response, repressing the expression of IFN-β mRNA. Follow-up studies neglected

(Pichlmair *et al*, 2011) or confirmed (John *et al*, 2018) these findings, making the potential function of IFIT1 in regulating the IFN response controversial. Last, IFIT1 and IFIT3 have been recently proposed to interact with ANXA2, involved in the endosomal recycling of EGFR. This interaction enhances the recycling of p-EGFR and increases signaling in the cells, with significant relevance for IFIT1-overexpressed cancers (Pidugu *et al*, 2019).

Aim of the study

Current findings show that interferons are responsible for the decline in neurogenesis in the aging brain, yet it is poorly described whether such interferon response relies on the recently-reported intrinsic interferon signature of stem cells. Whether intrinsic or extrinsic interferon responses modulate neurogenesis also in the young homeostatic brain, as well as which are the molecular underpinnings downstream of interferon in neural stem cells have not been sufficiently investigated. Thus, my research aims to:

- Investigate the relevance of interferons in modulating neurogenesis in the young adult brain.
- Elucidate the contribution of intrinsic vs. extrinsic interferon response in the neural lineage and their biological relevance.
- Describe the molecular underpinnings of the interferon response in neural stem cells with a focus on the post-transcriptional regulation of mRNA translation.

2. Materials and methods

2.1 Mouse models and animal welfare

C57BL/6 male mice were purchased from Janvier or bred in-house at the DKFZ Center for Preclinical Research. Male *Ifnagr*^{KO} (IFNAR$^{-/-}$IFNGR$^{-/-}$; Huang *et al*, 1993; Müller *et al*, 1994) were backcrossed with a C57BL6 background. Male TiCY mice (Tlx-CreERT2-YFP; (Liu *et al*, 2008); TiCY$^{B6\text{-}Tg(Nr2e1\text{-}Cre/ERT2)1GscGt(ROSA)26Sortm1(EYFP)CosFastm1Cgn/Amv}$ were crossed with *Ifnagr*^{KO} mice in-house to generate TiCY-IFNAGRKO$^{B6\text{-}Tg(Nr2e1\text{-}Cre/ERT2)1GscGt(ROSA)26Sortm1(EYFP)CosFastm1CgnIfnar1tm1AgtIfngr1tmAgt/Amv}$ mice. ISRE-eGFP$^{B6\text{-}Tg(Isre\text{-}eGFP)}$ mice were kindly provided by Dr. Marieke Essers from DKFZ (Tovey *et al*, 2006). IFIT1KO$^{B6\text{-}Ifit1tm1Vlcg}$ mice were a kind gift from Prof. Giulio Superti-Furga from the CeMM Research Center (Fensterl *et al*, 2012). Animals were housed under standard conditions and fed ad libitum. All procedures were approved by the Regierungpräsidium Karlsruhe.

For 5-Bromo-2´-Deoxyuridine (BrdU) *in-vivo* experiments, BrdU (Sigma-Aldrich) was administered intraperitoneally for 6 consecutive days with 50 mg BrdU/kg body weight/day. BrdU was dissolved in 0.9% NaCl (Berlin-Chemie). Treated individuals were closely supervised daily for the following 3 weeks (21 days). At the collection time-point, mice were anesthetized by intraperitoneal injection of 300 µl Perfusion Solution containing 0.286% Rompun (Bayer), 142.9 mg/ml Ketamizol (WDT) in 0.9% NaCl (Berlin-Chemie) prior to animal perfusion.

2.2 Cell culture and treatments

The description of cell culture experiments is partially adapted from my already documented protocols in Carvajal Ibañez *et al*, 2023 as:

For NSC isolation, 8 to 12 weeks old male mice were sacrificed by cervical dislocation, and the brains were transferred to a plate on ice containing Hanks' Balanced Salt solution (HBSS, Life Technologies) supplemented with 2.5 mM HEPES (ThermoFisher), 0.65% D-Glucose and 1% Penicillin-Streptomycin (Invitrogen). The vSVZ was dissected as described (Mirzadeh *et al*, 2010) and the extracted tissues were digested with papain using the Neural Tissue Dissociation kit (Miltenyi Biotec). NSCs were isolated by culturing the resulting cell-rich solution in Neurobasal A Medium supplemented with 2% B27 Supplement serum-free, 1% L-Glutamine (all from ThermoFisher), 2 µg/ml of heparin, 20 ng/ml of human basic FGF (ReliaTech) and 20 ng/ml of human EGF (Promokine). Prior to use in experiments, isolated NSCs were checked for neurosphere-like growth and were treated with accutase (ThermoFisher) and transferred to a new

flask after 5-7 days of stable culture. Cells were maintained in a 37°C, 5% CO2 incubator and were splitted every 3-4 days.

The different treatments with recombinant proteins or chemical inhibitors were performed by incubating the NSCs for different times -indicated in the figure captions- as follows: For interferon treatments, mouse recombinant IFN-β (Millipore; #IF011), previously dissolved in DPBS with 0.1% bovine serum albumin BSA (Roche), was added to the cell medium at final concentration 40 µ/ml for the indicated times. Control samples were subjected to an equal volume of 0.1% BSA in PBS (vehicle). For the Torin1 treatment (Cay10997), Torin1 was dissolved in 100% DMSO and added to cells at a final concentration of 250 nM for the indicated times. Control cells were treated with the same volume of 100% DMSO (vehicle). For the Rapamycin treatment (Cay13346), Rapamycin was dissolved in 100% DMSO and added to cells at a final concentration of 100 nM for the indicated times. Control cells were treated with the same volume of 100% DMSO (vehicle). For the ISRIB treatment (Sigma), ISRIB (Sidrauski *et al*, 2015) was dissolved in 100% DMSO and added to the cell medium at a final concentration of 500 nM for the indicated times. Control cells were treated with the same volume of 100% DMSO (vehicle).

2.3 Generation of mutant neural stem cell lines by CRISPR/Cas9

2.3.1 $TSC2^{mut}$ and $TSC2^{cntrl}$ NSCs

The description of the generation of $TSC2^{mut}$ NSCs is partially adapted from my already documented protocols in Carvajal Ibañez *et al*, 2023 as: CRISPR-Cas9 gRNAs targeting exon 2 of *Tsc2* (ENSMUSG00000002496) were designed using the CCTop target online predictor (Stemmer *et al*, 2015). The cutting efficiency of three different gRNAs was evaluated by T7EI Assay using T7 Endonuclease I (NEB). From those, the TSC2Ex2-gRNA (TGTTGGGATTGGGAACATCGAGG) was selected and cloned into the Cas9-containing plasmid pSpCas9(BB)-2A-GFP (Addgene) as described (Ran *et al*, 2013). For nucleofection, $1x10^6$ NSCs were incubated with 2,5 µg of the Cas9 and gRNA-containing plasmid with the Amaxa P4 Primary Cell 4D-Nucleofector X Kit S (Lonza) using the CA137 program in a 4D-Nucleofector X Unit (Lonza). Cells were left to recover for 1 day at 37°C and 5% CO_2. Cells were then collected, accutased, and resuspended in PBS/10% B27 using at all steps mild centrifuging conditions of 300 x g, 5 min at 4C.

NSCs with high expression of GFP were single-cell sorted by FACS in 96-well round-bottom plates containing 100µL of Neurobasal A Medium supplemented with 2% B27 Supplement serum-free, 1% L-Glutamine (all from ThermoFisher), 2 µg/ml of heparin,

1% Penicillin-Streptomycin (Invitrogen), and three times the usual amount of growth factors, namely a final 60 ng/ml of human basic FGF (ReliaTech), 60 ng/ml of human EGF (Promokine). One week after sorting, 50 µL of the above-described medium was added to every well, and extra 25 µL to the corner wells if the volume if those was especially reduced. Then, 20-25 µL of the above-described medium was added every 5 days, if needed. Single NSC colonies were expanded and every well was checked every 5 days looking for growing neurospheres. When neurospheres were found, they were collected, accutased, and expanded in normal culture medium without extra growth factors or antibiotics, as described in section 2.2. TSC2 abundancy was checked by western blot (see section 2.11). NSC clones were named with a serial number consisting of their plate number and well position (Plate#, Well#; eg. 3H12) to allow correlation of different TSC2 levels and response in the data.

Table 2.1: Oligonucleotides used for luciferase cloning of constructs

Oligo name	Sequence (**PAM Sequence**)	Description
TSC2Ex2-gRNA	TGTTGGGATTGGGAACATCG**AGG**	CRISPR/Cas9 TSC2 gRNA
TSC2Ex2-F	CACCTGTTGGGATTGGGAACATCG	CRISPR-mediated cloning
TSC2Ex2-R	AAACCGATGTTCCCAATCCCAACA	CRISPR -mediated cloning
pSCas9_gRNA Seq	AAGTTGATAACGGACTAGC	gRNA plasmid sequencing primer
T7EI_Ex2-F	CCTCTTCTGGTGTGTCATCTAC	T7EI Assay primer
T7EI_Ex2-R	CCTAGGGAGAACTAATGGCAATC	T7EI Assay primer

Table adapted from Carvajal Ibañez *et al*, 2023.

2.3.2 IFIT1-myc NSCs

The genetically modified myc-tagged IFIT1 line was created by Dr. Maxim Skabkin in the lab of Prof. Dr. Ana Martin-Villalba by CRISPR/Cas9 knock-in of a myc tag sequence to the CDS of *Ifit1* right after the second aminoacid codon. This was performed as documented by Dr. Skabkin: “Two guide RNAs were designed to introduce a myc-tag sequence just downstream of the second Gly codon in the open reading frame for the mouse IFIT1 gene (Gene ID: 15957). For the selection of optimal guide sequences, the guide RNA design tool by ATUM (formerly DNA 2.0) was used to choose the sequences providing the highest score for KnockIn efficiency with minimal off-targets. The guide

sequences were 5'-TTACCCCATGGTTGCTGTAA-3' and 5'-TCTCCACTCTGAGGGAACCC-3'. Both gRNA sequences as well as the sequence of nickase Cas9-D10A under chicken beta actin promoter were assembled in pD1421 by ATUM (formerly DNA 2.0) giving rise to pCRIS1 plasmid, which was used for Cas9-mediated knock-in in NSCs. A 200-nt myc oligonucleotide carrying the myc-tag sequence (5'-GAGCAGAAGCTGATCTCCGAGGAAGACCTG-3') flanked by 84-nt and 86-nt fragments of the mouse IFIT1 was from IDT. 1x106 NSCs (p5) isolated from the SVZ of two C57BL/6N male mice (age 8 weeks) were mixed with 2.5 µg of pCRIS1 and 50 pmol of myc-oligo in 100 µl of P4 transfection solution prepared with the Amaxa P4 Primary Cell 4D-Nucleofection X Kit (Lonza, #V4XP-4024). The cells were subjected to nucleofection using CA137 program in a 4D-Nucleofector X Unit (Lonza). To allow cells to recover and perform Cas9-mediated KnockIn, they grew in NBM media 46 hrs post-nucleofection. Cells were sorted as single cells at the Flow Cytometry Core facility (DKFZ) into two 96-well plates for each replicate. Dr. Maxim Skabkin sorted cells from the 5% most intensively expressing DasherGFP encoded in pCRIS1. Collected single NSC were growing for the first week in 1:1 fresh/conditioned NBM media supplied with 3X-to-normal concentration of FGF and EGF. During next two weeks, the growth factors concentration in the media was decreased till 2X-to-normal. Sorted single NSCs gave rise to fast growing colonies in 3-6 weeks. A part of cells from each colony was used to extract the genomic DNA with the QuickExtract DNA Extraction Solution (Epicentre, #QE09050) and 1 µl of the final genomic DNA extract was used for colony PCR with a myc-Fw primer corresponding the inserted myc-tag sequence and IFIT1-R primer located 340 nt downstream from the site of myc-tag insertion. For each replicate one clone was found generating a PCR product with expected length. Following sequencing showed the both clones were heterozygous carrying one wt and one myc-tagged *Ifit1* allele."

2.4 Flow cytometry Analysis

For the flow cytometry analysis, vSVZ single cell suspensions were generated and stained as described (Llorens-Bobadilla *et al*, 2015). Briefly, vSVZ was microdissected using the Neural Tissue Dissociation kit with Trypsin and gentleMACS Octo dissociator (Miltenyi). Cells were stained with the antibodies summarized in Table 2.2 and were added Sytoxblue (Thermo; 1:500) right before acquisition.

Table 2.2: Antibodies used for FACS

Reagent	Manufacturer	Catalog number; ID	Dilution
Anti-CD45-APC-Cy7	BD	#557659; RRID:AB_396774	1:200
Anti-O4-APC-Vio770	Miltenyi Biotec	Custom, based on #130119981	1:100
Anti-Ter119 APC-Cy7	BioLegend	# 116223; RRID:AB_2137788	1:100
Alexa Fluor 488 EGF complex	Life Technologies	#E-13345	1:100
Anti-Prominin1-APC	Thermo Fisher	# 17-1331-81, RRID:AB_823120	1:75
Anti-GLAST-PE (ACSA-1)	Miltenyi Biotec	#130098804; RRID:AB_10829184	1:50
Anti-PSA-NCAM-PE-Vio770	Miltenyi Biotec	#130-095-212	1:50

Table adapted from Carvajal Ibañez *et al*, 2023.

The flow cytometry results were analyzed using FlowJo v.10. I size-selected the vSVZ cells of interest and excluded doublets, dead cells (Sytoxblue$^+$) and myeloid cells (CD45$^+$), erythrocytes (Ter119$^+$) and oligodendrocytes (O4$^+$) cells as recently described (Kalamakis *et al*, 2019) (See gating in Appendix). Signal acquirement was performed on a BD FACSCanto II and BD FACSFortessa at the DKFZ Flow Cytometry Facility.

2.5 Cycleflow: Cell cycle analysis tool

The cycleflow methodology is partially adapted from my already documented protocol in Carvajal Ibañez *et al*, 2023 as: Cell cycle progression was assessed using CycleFlow as described (Jolly *et al*, 2022) with some modifications. CycleFlow was applied to NSCs with a pre-treatment of IFN-β. 24 hours after cell seeding, either vehicle or IFN-β was added to NSCs for 17 h. Then, EdU from the Click-iT Plus EdU Flow Cytometry Assay Kit (ThermoFisher) was added at a final concentration of 10 µM. Cells were incubated for 1 hour. Cells were collected, washed with DPBS, and resuspended in a pre-warmed medium containing either vehicle or IFN-β. Cells were then divided into different wells to be incubated and collected at the indicated incubation times (Figure 3.2A). At the specified time, cells were collected, dissociated with Accutase® (Sigma), and stained for viability with Zombie Red (Bioleged) following the manufacturer's recommendations.

After that, cells were washed and PFA-fixed using the Click-iT Plus EdU Flow Cytometry Assay Kit (ThermoFisher). Fixed cells were kept in 90% methanol DPBS at −20°C until completion of the time-course. After completing all sample collections, the Click-iT reaction was performed following the manufacturer's recommendations in combination with final staining with the DNA dye FxCycle Violet reagent (ThermoFisher; 1:1,000). Signal acquirement was performed on a BD LSRFortessa Flow Cytometer and results were analyzed using FlowJo v.10. Doublets and non-viable cells -Zombie Red^+ (Bioleged)- were excluded from the analysis. Doublets were discriminated using the signal of DNA area versus width and gates were established based on fluorescence-minus-one (FMO) controls. Cell-cycle progression mathematical inference was performed using uniform priors as already described (Jolly *et al*, 2022).

2.6 O-propargyl-puromycin (OPP) assay

The description of the OPP experiments is partially adapted from my already documented protocols in Carvajal Ibañez *et al*, 2023 as: Poly-D-lysine (Gibco) was used to pre-coat eight-well glass chambers (lab-tek) overnight. This was followed by an additional coating with laminin (Sigma). Cells were plated and then treated with IFN-β (Millipore) or ISRIB (Sigma) after 2 days for the specified times. OPP (Thermo) was dissolved in DMSO and added to all conditions at a final concentration of 50 µM, incubating the cells for 1 hour prior to collection. The Click-iT Plus OPP Alexa Fluor 488 Protein Synthesis Assay Kit (Thermo) was used to process the cells following the manufacturer's instructions, excluding the DNA staining step. Cells were mounted with fluoromount-G containing DAPI (ebioscience). Using a Leica TCS SP5 II confocal microscope with 40× magnification, five representative images were captured per sample. Fiji was used to quantify the OPP intensity, which was then normalized to the vehicle-treated samples. Control treatments, including no-OPP (negative control), N2 supplement (Gibco; positive control), and cycloheximide (CHX; Sigma; negative control), were always processed in parallel.

2.7 Fractionation of polysome profiles

The description of polysome experiments is partially adapted from my already documented protocols in Carvajal Ibañez *et al*, 2023 as: NSCs were treated with either vehicle or IFN-β as described previously (see section 2.2). Just before cell collection, cells were treated with 100 µg/ml cycloheximide (CHX, EDM Millipore) dissolved in H_2O and incubated for 5 minutes at 37°C with 25% CO_2. The cells were collected by centrifugation, washed with ice-cold DPBS containing 100 µg/ml CHX, and then lysed using polysomal lysis buffer [20 mM Tris–HCl, pH 7.4, 120 mM KCl, 5 mM MgCl2, 14 mM

β-mercaptoethanol, 1% NP-40, 100 µg/ml CHX, 1x complete protease inhibitor cocktail (Roche), 100 µ/ml RNase Inhibitor (Thermo Fisher)]. The lysates from differently treated NSCs were loaded onto a preformed 17.5–50% sucrose gradient in 20 mM Tris–HCl pH 7.4, 120 mM KCl, 5 mM $MgCl_2$, 2 mM DTT, and 100 µg/ml CHX. Free mRNPs, ribosome subunits, and polysome complexes were separated by centrifugation for 2.5 hours at 210,000 x g using an SW41 rotor (Beckman Ultracentrifuge L8M). The ~12ml content of the centrifuged tubes was fractionated using the Foxy R1 Density Gradient Fractionation System (Teledyne-ISCO) and the absorbance at 254 nm was recorded. 12x 1 ml fractions were collected and stored at -80°C.

2.8 RT-qPCR

When RNA was isolated for RT-qPCR (not ribosome/polysome profiling, nor RIP), NSCs were lysed and subjected to the RNeasy Plus Mini kit (Qiagen) using the 20-gauge needle homogenization step according to the manufacturer's instructions.

From every fraction, 300 µl were taken for RNA extraction and pre-treated with proteinase K (80 µg/ml, Qiagen) for 1 hour at 50ºC. RNA was then purified by phenol/chloroform extraction following the method described in Faye *et al*, 2014. Up to 2.5 µg of isolated RNA were used for cDNA synthesis with the SuperScrptTM VILOTM cDNA synthesis kit (Thermo Fisher). All RNA samples were measured using NanoDrop2000 (ThermoScientific) before cDNA synthesis. qPCR was performed with the Power SYBR® Green PCR Master Mix (Thermo Fisher) using the CFX384 Touch™ Real-Time PCR Detection System (Bio-Rad). Data analysis is based on the $\Delta\Delta C_t$ method with normalization of the raw data to input genes for bulk-RNA-qPCR. For polysome fractions, the ΔC_t method was used to calculate relative gene expression. The percentage of the total amount of mRNAs for all fractions was used to present the distribution of analyzed mRNAs across polysome fractions.

Table 2.3: Oligonucleotide primers used for RT-qPCR

Gene Target	Manufacturer	Catalog number
Actb	Qiagen	Mm_Actb_2_SG
Ifit3	Qiagen	Mm_Ifit3_1_SG
Irf9	Qiagen	Mm_Irf9_1_SG
Trex1	Qiagen	Mm_Trex1_1_SG
Ifit2	Qiagen	Mm_Ifit2_1_SG
Slfn9	Qiagen	Mm_Slfn9_1_SG
Rbms2	Qiagen	Mm_Rbms2_vb.1_SG

Sox2	Qiagen	Mm_Sox2_1_SG
Rps17	Qiagen	Mm_Rps17_1_SG
Rpl34	Qiagen	Mm_Rpl34_1_SG
Smad6	Qiagen	Mm_Smad6_1_SG
Gadd45g	Qiagen	Mm_Gadd45g_1_SG
Hist4h4	Qiagen	Mm_Hist4h4_1_SG
Gbx1	Qiagen	Mm_Gbx1_1_SG
Rgs8	Qiagen	Mm_Rgs8_2_SG
Neurog2	Qiagen	Mm_Neurog2_1_SG

Table adapted from Carvajal Ibañez *et al*, 2023.

2.9 Ribosome Sequencing (Ribo-Seq)

The description of Ribo-Seq experiments in section 2.9 is partially adapted from my already documented protocols in Carvajal Ibañez *et al*, 2023.

2.9.1 Cell lysates preparation and RNase digestion

Cells were treated with vehicle or IFN-β 48 h after seeding and incubated at 37°C 25% CO2 for the corresponding incubation times. After the corresponding incubation time, NSCs were incubated with 100 µg/ml CHX at 37°C 25% CO2 for 5 minutes. The cells were then collected, washed with DPBS supplemented with 100 µg/ml CHX, and lysed in 150 µl of the polysomal lysis buffer (see section 2.7). Cells were incubated for lysis for 10 minutes on ice. Then, lysates were cleared by centrifugation, and supernatants were collected. One aliquot of 50 µl from each condition was taken and kept at -80ºC as the input for RNA sequencing (RNA-Seq). OD260 was measured in every sample using NanoDrop2000 (ThermoScientific) and the corresponding volumes for 40 µg of total RNA were used for the subsequent RNase digestion. Each sample volume was increased up to final 200 µl with RNase buffer (20 mM Tris-HCl pH 7.4, 5 mM MgCl2, 150 mM NaCl, 1 mM DTT, and 100 µg/ml CHX) following published recommendations (McGlincy & Ingolia, 2017) supplied with 2,5 U/µg of RNA of Ambion™ RNase I (Sendoel *et al*, 2017) and incubating at 25ºC for 45 minutes. The reactions were then immediately stopped by the addition of a 2.5 µl SuperaseInTM RNase inhibitor (Ambion, 20 U/µL). Digested lysates were directly loaded on top of an 800 µL 25% sucrose cushion prepared in 50 mM HEPES pH 7.4 (ThermoFisher), 200 mM NaCl, 10 mM MgCl2, 100 µg/ml CHX and cOmplete™ EDTA-free Protease Inhibitor Cocktail (Roche). Samples were centrifuged at 100,000 rpm for 1 hour in a TLA100.2 rotor (Beckman Coulter Optima TL 100). Pelleted footprints were then dissolved in 300 µl TRIzol (Ambion) and RNA was extracted

with the Direct-Zol RNA Miniprep kit (Zymo Research) in a final volume of 40 µl of water. Recovered footprints were then quantified again and 4 µg of RNA was subjected to depletion with the Gold Ribo-Zero kit (Illumina), following the manufacturer's instructions. RNA finally recovered in 11 µl H_2O. Samples were then measured in Qubit 2.0 using the Qubit™ RNA HS Assay Kit (Thermo Fisher).

2.9.2 Footprint purification and library preparation

Footprint-containing RNA samples were resolved by electrophoresis in a 15% NOVEX TBE-Urea gel (Thermo Fisher). For this, RNA samples were mixed with an equal volume of the 2x NovexTM TBE-Urea Sample buffer (Invitrogen) and were denatured at 80ºC for 2 minutes. A 28-nucleotide oligonucleotide (o28-P) phosphorylated at 3' end (AUUGUUUAGACUAGCUGACUGACGUACA/3Phos/, IDT) was used as a size control and was also diluted with the 2x NovexTM TBE-Urea Sample buffer and denatured similarly. 15% TBE-Urea polyacrylamide gels (ThermoScientific) were pre-run at 200 V for 30 minutes and then run at 200 V for 70 minutes together with the o28-P oligo and the GeneRuler ultra-low range DNA ladder (ThermoScientific). Gels were stained with SYBRTM Gold (1:10,000 dilution in 1xTBE, ThermoScientific) for 12 minutes and visualized with a DarkReader transilluminator (Clare Chemical Research). Regions on the lane of each sample were restricted within the position of the o28-P marker and the 35-nt DNA ladder band was excised and transferred to gel-breaker tubes (Istbiotech) which were centrifuged twice at 14,000 rpm for 5 minutes at 4ºC. Gel fragments were incubated in 500 µl 10 mM Tris-HCl pH 7 at 70ºC for 15 minutes with 14,000 rpm shaking. The grinded suspension was then spun at 16,000 g for 3 minutes at 4ºC in Spin-X cellulose acetate columns (Sigma-Aldrich) and RNA was isolated by sodium acetate-isopropanol precipitation as previously reported (Faye *et al*, 2014) and finally resuspended in 15 µl 10 mM Tris-HCl pH 7. Recovered RNA was dephosphorylated with T4 PNK (NEB) in the absence of ATP.at 37ºC for 2 hours supplemented with Recombinant RNase inhibitor (Takara). T4 PNK was heat-inactivated and RNA was precipitated as in Faye *et al*, 2014 and dissolved in 10 mM Tris-HCl pH7. Indexed libraries were generated using the SMARTer smRNA-Seq kit for Illumina (Takara) following the manufacturer's instructions and performing the size selection (inserts <150 bp) using Agencourt AMPure XP Beads (BeckmanCoulter). Prior to library preparation, all samples were analyzed by Bioanalyzer using the Small RNA Analysis kit (Agilent). Libraries were sequenced in HiSeq 2000 v4 at the DKFZ Genomics and Proteomics Core Facility.

2.9.3 Total RNA library preparation

For the parallel total RNA sequencing, the same NSC lysates were used as described above (section 2.9.1). Differently from the footprints, 20 µg of total RNA was used for library preparation. RNA was extracted with phenol/chloroform as described in Faye *et al*, 2014. Then DNA was depleted by incubating the RNA samples with 3U of TURBO DNase (Ambion) for 15 min at 37°C., treated with TURBO DNase. RNA was again extracted with phenol/chloroform as in Faye *et al*, 2014. Ribosomal RNA was depleted with the Gold Ribo-Zero kit (Illumina), and 80 ng of each RNA sample was used to synthesize cDNA and make a library using the NEBNext Ultra Directional RNA library kit for Illumina (NEB). Libraries were assessed for quality using the Bioanalyzer 2100 and sequenced in HiSeq 2000 v4 at the DKFZ Genomics and Proteomics Core Facility.

2.9.4 Ribo-Seq Analysis

The analysis applied by Manuel Goepferich trimmed the reads by applying the tool TrimGalore version 0.4.4_dev. The adaptor sequence “AGATCGGAAGAGC” (Illumina TruSeq, Sanger iPCR; auto-detected), as well as 3 bp from the 5′-end and 15 bp from the 3′-end, were removed. As a sanity check, sequences that, after the trimming, were shorter than 18 bp were removed using TrimGalore's default settings. After these two steps reads had an average length of 33 bp. Next, reads were mapped to the mm10 transcriptome build GRC38.93 from ENSEMBL using boWTie version 0.12.7 with its standard options. Reads falling into genes were counted from BAM files applying a suited R/Bioconductor workflow (function SummarizeOverlaps with mode “Union”). Duplicated reads were removed. For ribosomal footprinting samples, reads in the whole gene body or the CDS were quantified separately. For total RNA samples, only reads in the whole gene body were counted. Subsequently, to estimate the translation efficiency (TE), log-fold changes between ribosome-protected reads from the CDS and total RNA samples were computed by applying DESeq2. DESeq2 was chosen as it is considered a standard tool for modeling negative-binomial distributions arising in sequencing experiments. The likelihood ratio test (LRT) was applied to the TE analysis upon IFN-β treatment or upon IFN-β treatment and the genotype (WT or $IFIT1^{KO}$). GSEA was performed using the clusterProfiler tool from Bioconductor using fold-changes for all expressed genes. Gene ontology terms related to “biological process” with an FDR < 0.05 and the highest significance were selected for the plots. TOP-mRNAs (Table 3.1) were defined as in Thoreen *et al*, 2012.

2.10 Proteome and phosphoproteome

Dr. Maxim Skabkin performed the proteome and phosphoproteome treatments as he documented and adapted from Carvajal Ibañez *et al*, 2023: “Cells were treated with vehicle or IFN-β and incubated at 37°C 25% CO2 for the time specified in the figures by. Cell lysates for the proteome and phosphoproteome analysis were prepared as described (Potel *et al*, 2018) with some modifications. Briefly, cells were collected, washed, and weighted to determine the pellets‘ mass. The pellets were resuspended in six times the mass of a lysis buffer [100 mM Tris–HCl pH 8.5, 7 M Urea, 1 mM $MgCl_2$, 1 mM sodium orthovanadate, 1% Trition X-100, 1× PhosphoSTOP inhibitor (Roche), 1× Complete EDTA free protease inhibitor (Roche)]. To assure effective lysis, the resuspended pellets were subjected to sonication 3x 10 s (1 s on, 1 s off) with 30 s pause at 40% output using the Fisherbrand Model 120 Sonic Dismembrator (Fisher Scientific). Lysates were then centrifuged at 21,000 x g, for 1 h at 4°C and only the supernatant was recovered. The resulting clarified lysates were incubated for 2 h at RT. The total protein content was quantified with the Pierce BCA Protein Assay Kit (Thermo Fisher). For all samples, 400 µg protein was aliquoted and submitted to metal-affinity enrichment and mass spectrometry at the DKFZ Genomics and Proteomics Facility. Proteins and phospho-peptides were quantified and analyzed for differential abundance using Perseus45.”

2.11 WB Analysis

The description of W experiments is partially adapted from my already documented protocols in Carvajal Ibañez *et al*, 2023 as: Protein concentration was determined with the PierceTM BCA Protein Assay kit (Thermo Fisher). 20 µg of total protein was used per sample. 4x loading buffer (BioRad) was added and samples were boiled at 95ºC for 4 minutes. Then, the total volume was loaded into each well of an 8-16% MiniProtean TGS Stain-Free gel (BioRad). Samples were run for 30 minutes at 200 V. Proteins were transferred onto nitrocellulose membrane 0.45 µm (BioRAd) using the Trans-Blot® Turbo™ Transfer System (BioRad). Membranes were blocked for 1 hour in 5% BSA in TBS buffer with 0.1% Tween®20 (Sigma-Andrich). Membranes were then incubated with primary antibodies diluted in 5% BSA in TBS buffer with 0.1% Tween®20 overnight at 4ºC under gentle rotation. A list of used antibodies is found in Table 2.4. Membranes were washed four times in 1x TBS with 0.1% Tween®20 and incubated with either goat α-mouse (Dianova; 115-035-003) or α-rabbit (Dianova; 111-035-003) HRP-conjugated secondary antibodies (diluted 1:5000) diluted in blocking buffer for 1 hour at RT. Membranes were washed again and developed with the Western Lighting® Plus ECL

solution (GE). Membranes were immediately exposed in the ChemiDoc™ MP Imaging System (BioRad).

Table 2. 4: Antibodies used for Western Blot

Reagent	Manufacturer	Catalog number; ID	Dilution
Rabbit anti-Akt	Cell Signaling	#9272; RRID: AB_329827	1:1000
Rabbit anti-4E-BP1 (53H11)	Cell Signaling	#9644; RRID:AB_2097841	1:1000
Rabbit anti-eIF2α (D7D3)	Cell Signaling	#5324S	1:1000
Rabbit anti-Rb1 (D20)	Cell Signaling	#9313; RRID:AB_1904119	1:1000
Rabbit anti-S6	Abcam	#ab2217	1:1000
Rabbit anti-p70 S6 kinase (49D7)	Cell Signaling	#2708; RRID:AB_390722	1:1000
Rabbit anti-TSC2 (D93F12)	Cell Signaling	#4308; RRID:AB_10547134	1:1000
Rabbit anti-LARP1	Cell Signaling	#14763	1:1000
Mouse anti-myc tag (9B11)	Cell Signaling	#2276	1:5000
Rabbit anti-GAPDH	Cell Signaling	#2118	1:1000
Rabbit anti-actin (I-19)	Santa Cruz	sc-1616-R	1:3000
Rabbit anti-vinculin (EPR8185)	Abcam	ab129002; RRID:AB_11144129	1:5000
Mouse anti-phospho-Akt (T308)	US Biological	A1124-07R	1:1000
Rabbit anti-phospho-Akt (S473)	Cell Signaling	9271L	1:1000
Rabbit anti-phospho-4E-BP1 (S65)	Cell Signaling	#9451; RRID:AB_330947	1:1000
Rabbit anti-phospho-eIF2α (S51; 119A11)	Cell Signaling	#3398	1:1000
Rabbit anti-phospho-Rb (S780; D59B7)	Cell Signaling	#8180; RRID:AB_10950972	1:1000
Rabbit anti-phospho-p70 S6 kinase (T389; 108D2)	Cell signaling	#9234; RRID:AB_2269803	1:1000

Rabbit anti-phospho-S6 (S235/236; 91B2)	Cell Signaling	#4857; RRID:AB_2181035	1:1000
Rabbit anti-phospho-S6 (S240/244)	Cell Signaling	#2215; RRID:AB_331682	1:1000
Rabbit anti-phospho-TSC2 (T1462; 5B12)	Cell Signaling	#3617; RRID:AB_490956	1:1000
Rabbit anti-phospho-TSC2 (S1452)	Custom	Provided by Romero-Pozuelo *et al*, 2020	1:250

Table adapted from Carvajal Ibañez *et al*, 2023.

2.12 Luciferase reporter assay

2.12.1 Luciferase plasmid construction

Dr. Maxim Skabkin generated the luciferase plasmids as he documented and adapted from Carvajal Ibañez *et al*, 2023: ”DNA constructs with WT or mutated 5'UTRs of mouse *Sox2* mRNA were assembled into the psiCheck-2 vector (Promega) together with synthetic Renilla luciferase gene (hRluc) driven by SV40 early enhancer/promoter and synthetic Firefly luciferase gene (hluc+) under HSV-TK promoter by. The UTRs flank hRluc open reading frame. The full-length 5'UTRs of mouse *Sox2* (NM_011443.4) and *Rps21* (variant2, NM_025587.2), as well as their mutated variants carrying the deletions of PRM in Sox2 (5UTRmut Sox2; CTCTT deleted), PRM in Rps21 (5UTRmut Rps21; TCCTTTC deleted), were synthesized and inserted into pEX-K4 (*Sox2*) or pEX-A2 (*Rps21*) by Eurofins. The cloned UTRs were amplified using the Phusion High-Fidelity DNA polymerase (NEB) using primers carrying SfiI and NheI sites and inserted in-frame between the SV40 promoter and the CDS of *hRluc*. The used primers are listed in Table 2.5. The full-length 5'UTR of mouse beta-actin (*Actb*) mRNA (NM_007393.5) was generated by amplification of the cDNA library prepared from NSCs isolated from C57BL/6 mice. Then, the 5’UTR of *Actb* was amplified and cloned similarly to *Sox2* and *Rps21* in the psiCheck-2 vector (Promega). Successful cloning and lack of undesired mutations were checked by sequencing all plasmids.”

Table 2.5: Oligonucleotide used for luciferase cloning of constructs

Oligo name	Sequence (amplified gene sequence)	Description
5UTR-Sox2-F	ATGCAGAGGCCGAGGCCGCCTCGGCCTCTGGATGGTTGTCTATTAACTTGTTC	full-length 5'UTR of mouse *Sox2*
5UTR-Sox2-R	ATGGTGGCTAGCGGGCGCTGGGCGGGCG	full-length 5'UTR of mouse *Sox2*

5UTR-Rps21-F	ATGCAGAGGCCGAGGCCGCCTCGGCCTCTCCTCCTGCCCAATAGTGCTGC	full-length 5'UTR of mouse *Rps21*
5UTR-Rps21-R	ATGGTGGCTAGCCTGAGGCCGTCCCTGCTC	full-length 5'UTR of mouse *Rps21*
5UTR-Actb-F	GGCCGAGGCCGCCTCGGCCTCTTATAAAACCCGGCGGCGC	full-length 5'UTR of mouse *Actb*
5UTR-Actb-R	ATGGTGGCTAGCGGCGAACTGGTGGCGGGTG	full-length 5'UTR of mouse *Actb*

Table adapted from Carvajal Ibañez *et al*, 2023.

2.12.2 Nucleofection of NSCs and luciferase assay

Per condition, I nucleofected 5 µg of the corresponding DNA using the Amaxa P4 Primary Cell 4D-Nucleofector X Kit S (Lonza) into 3 million NSCs per condition employing the CA137 program in a 4D-Nucleofector X Unit (Lonza). Afterward, the cells were washed, separated in three technical replicates, and plated in 96-well plates with Neurobasal A Medium supplemented with 2% B27 Supplement serum-free, 1% L-Glutamine (all from ThermoFisher), 2 µg/ml of heparin, 20 ng/ml of human basic FGF (ReliaTech) and 20 ng/ml of human EGF (Promokine). After a recovery period of 18-24 hours, cells were treated with IFN-β, Torin1, Rapamycin, ISRIB, or a combination of them as stated in the captions and described in section 2.2. After incubation, NSCs were washed with DPBS and lysed in 1× Passive Lysis buffer from the Dual-Luciferase Reporter Assay System (Promega). Plates were then incubated at RT for 15 min on an orbital shaker for complete lysate. Afterward, plates were sealed with Parafilm and stored at -20°C until development. To develop the assay, luciferase assay reagent was added to each well, mixed, and all volume was transferred into a new White Cliniplate (Thermo Fisher). First, the firefly activity was measured in the white plate, as acquired by Synergy LX multi-mode reader (BioTek). Then, 100 µl of Stop&Glo reagent was added and the plate was scanned again for Renilla luciferase using the same instrument. Using three technical replicates, Renilla luminescence was normalized to Firefly luminescence, and the treatments were then normalized to the vehicle samples, resulting in the fold change effect.

2.13 Immunoprecipitation of IFIT1 (IFIT1-IP)

2.13.1 Immunoprecipitation Assay and Library preparation

Immunoprecipitation of IFIT1 and library preparation was performed by Dr. Maxim Skabkin as he described in the documentation of his protocol: “To perform RNA-IP from

NSCs carrying myc+/-IFIT1 gene, Dr. Maxim Skabkin used the Magna RIP Kit (EMD Millipore, #17-700). 1.8x106 NSCs, wild-type (p6) and of both myc+/-IFIT1 replicates (p4) were seeded in 150 cm2 flasks in NBM media. Three days later, 40 U/ml of mouse recombinant IFNβ (EMD Millipore, #IF011) was added to the cells for another 14 hrs. Afterward, cells were collected and washed twice with ice-cold PBS. The final cells' pellet was weighted, resuspended in an equal volume of complete RIP Lysis Buffer from the Magna Kit, and put at -800 C to improve lysis. The next day, the lysates were quickly thawed in a water bath at 300C and clarified by c/f at 14000 rpm for 10 min at 40C. 5 µl of each lysate were taken for direct RNA extraction and used as 'input' for library generation (see below). The flowing steps were exactly performed as described in the Magna kit manual. For immunoprecipitation of myc-IFIT1, Dr. Maxim Skabkin used 5 µg of custom-ordered mouse anti-myc antibody (clone 9B11) prepared by Cell Signaling per 100 µl of cell lysate. Total RNA from the input and RIP fractions was treated with 2 U of TURBO DNAse (ThermoFisher Scientific, #AM2238) for 15 min at 370C. After the treatment, RNA was extracted with phenol/chloroform and recovered via ethanol precipitation. Before proceeding to library preparation, ribosomal RNA was removed from one-tenth of the extracted input RNA and total RIP RNA fractions with the Ribo-Zero GOLD rRNA Removal Kit (Illumina, #RZHM11106). To identify RNAs bound to myc-tag IFIT1 Dr. Maxim Skabkin repeated the RIP assay three times and used the final RNA samples to generate libraries for three different types of RNA: tRNA and short RNA fragments, short mRNAs, and long mRNAs. To make libraries for tRNA and RNA fragments Dr. Maxim Skabkin first treated the rRNA-depleted RNA samples with T4 PNK (Takara) without ATP and then with 1 mM ATP to introduce phospho group at the 5' ends. The final end-repaired RNAs were used to make indexed libraries with the NEBNext Multiplex Small RNA Library Prep Set for Illumina (NEB, #E7300S) exactly as described in the kit's manual. Finally, libraries were amplified using index oligos from the NEBNext Multiplex Oligos for Illumina (NEB, #E7335S). To prepare libraries for short and long RNAs, input and RIP RNA samples after rRNA depletion were fragmented, correspondingly, for 11 and 15 min at 940C using the NEBNext Magnesium RNA Fragmentation Module (NEB, #E6150S). The final fragmented RNAs were used to make indexed libraries for NGS with the NEBNext Ultra Directional RNA Library Prep Kit for Illumina (NEB, #E7420S). Indexed libraries were generated via PCR amplification using index oligos from the NEBNext Multiplex Oligos for Illumina (NEB, #E7335S) and mixed at equal amounts to make a multiplex of all analyzed samples. The average library size was estimated using the Bioanalyzer 2100 Agilent and DNA concentration was measured using the NanoDrop One (Thermo Scientific). The final libraries were sequenced with HiSeq 2000 v4 SE 50 bp at DKFZ core facility."

2.13.2 Immunoprecipitation Analysis

Analysis of the RIP Assay was performed by Manuel Goepfereich as documented: “Reads were mapped to the mm10 genome using bowtie (Version 0.12.7-2) with its default settings. Reads counting was performed utilizing the Bioconductor pipeline, specifically the function summarizeOverlaps from the R package GenomicAlignments. Enrichment in the IP-fraction was computed by fitting the DESeq2 model on the count data with the design RIP-IP ~ (RIP-WT & Input). The identity of sequencing libraries - medium and large- was treated as an additional confounder. Genes showing an enrichment greater than 1 log2(FC) and a p-value smaller than 0.1 after FDR correction were selected as a set of Ifit1-targets.” Manuel Goepfereich also performed the integration of the IFIT1-IP and Ribo-Seq results by computing a score of the p-value from the IFIT1-IP and the effect size of the translation efficiency changes from the Ribo-Seq.

2.14 Immunofluorescence stainings

Brains were extracted and incubated for 16h in 4% paraformaldehyde under rotation at 4ºC. The next day, the brains were washed twice for 5 minutes each using DPBS and transferred to 10 ml of pre-filtered 30% sucrose PBS for 3-4 days at 4ºC. After this period, brains sank in the sucrose solution and were snap-frozen and submerged in OCT (Tissue-Tek) using dry ice. Samples were then cut into 15 µm-thick coronal sections using the LeicaCM1950 cryo-microtome. The sections were placed on Superfrost Plus™ Adhesion Microscope Slides (ThermoScientific), kept at -20ºC overnight, and transferred then to -80ºC for long-term storage.

2.14.1 Immunofluorescence of the vSVZ

For immunofluorescence of the vSVZ, the slides were immersed in 2 N HCl solution at 37ºC for 30 minutes. Then, they were rinsed in 0.1 M Borate buffer pH 8.5 for 10 minutes at RT. Then, slides were washed 6 times with PBS for 15 minutes before being blocked with PBS 3% Horse Serum (Biochrom) and 0.25% Triton X-100 (Thermo Fisher) at RT for 60 minutes. After blocking, the glass slides were incubated overnight at 4ºC with primary antibodies diluted in the same blocking solution as indicated (See Table 2.6). Excess antibody was washed by a quick immersion of the sections into room-temperature PBS and then washed again twice in PBS for 25 minutes each. The sections were then blocked again for 15 minutes. Then, samples were incubated for 2 hours at room temperature in the dark with secondary antibodies diluted in the blocking solution as indicated (See Table 2.7). Finally, slides were washed three times with PBS and mounted using Fluoromont GTM (ThermoScientific) without DAPI. Images were acquired using a Leica TCS SP5 II confocal microscope at the DKFZ Light Microscopy Facility.

2.14.2 Immunofluorescence of the dentate gyrus (DG)

For immunofluorescence of the DG, the slides were immersed in HIER Antigen retrieval buffer (10 mM Sodium citrate, 0.05% Tween 20, pH 6.0) at 95ºC for 20 minutes. Then, the slides were rinsed in RT water for 1 minute and directly transferred to cold water for 10 minutes. Then, slides were rinsed for 1 minute in PBS before blocking them with PBS 3% Horse Serum (Biochrom) and 0.25% Triton X-100 (Thermo Fisher) at RT for 60 minutes. After blocking, the glass slides were incubated overnight at 4ºC with primary antibodies diluted in the same blocking solution as indicated (See Table 2.6). Excess antibody was washed by a quick immersion of the sections into room-temperature PBS and then washed again twice in PBS for 25 minutes each. The sections were then blocked again for 15 minutes. Then, samples were incubated for 2 hours at room temperature in the dark with secondary antibodies diluted in the blocking solution as indicated (See Table 2.7). Finally, slides were washed three times with PBS and mounted using Fluoromont GTM (ThermoScientific) without DAPI. Images were acquired using a Leica TCS SP5 II confocal microscope at the DKFZ Light Microscopy Facility.

Table 2.6: Primary antibodies used for immunofluorescence

Antibody	Manufacturer	ID	Dilution
Rat anti-BrdU	Abcam	Ab6326	1:100
Rabbit anti-DCX	Cell Signaling	#4604	1:500
Chicken anti-KI-67	LSBio	LS-C772946-100	1:1000
Goat anti-Sox2	R&D	AF2018	1:200
Rat anti-GFAP	Invitrogen	130300	1:1000
Mouse anti-S100b	Atlas antibodies	AMAb91038	1:100

Table 2.7: Secondary antibodies used for immunofluorescence

Antibody	Manufacturer	ID	Dilution
Donkey anti-rat Alexa405	Abcam	ab175670	1:500
Donkey anti-rabbit Alexa 555	Invitrogen	A-31572	1:1000
Donkey anti-chicken Alexa488	Jackson ImmunoResearch	703-545-155	1:1000
Donkey anti-chicken Alexa555	Dianova	703-545-155	1:1000

Donkey anti-goat Alexa647	Invitrogen	A-21447	1:1000
Donkey anti-mouse Alexa 488	Invitrogen	A21202	1:1000

2.14.3 Spatial analysis of cell distances

The spatial analysis of the IF sections from the vSVZ was performed in collaboration with Roman Remme from Fred Hamprecht's lab, at Heidelberg University. I manually annotated all the images for active label-retaining cells -LRCs- ($BrdU^+Sox2^+KI\text{-}67^+DCX^-$) and non-active LRCs ($BrdU^+Sox2^+KI\text{-}67^-DCX^-$) using Fiji. Then, I also annotated the spatial corners of the ventricles, namely the ventral, medial, and dorsolateral corners manually using Fiji. In addition, to avoid the faulty use of $BrdU^+Sox2^+KI\text{-}67^+DCX^-$ cells located far from the ventricle, I manually draw a 100µm mask (from the ventricle to the striatum) for every image. Using these annotations, Roman Remme computed the Euclidean distances between the annotated points. Roman Remme also computed a "randomized value" distance evaluation by assigning "active" or "non-active" labels stochastically to my manually-identified cells of the vSVZ sections.

2.15 Behavioural studies of mice

The behavioural studies were carried out at the Interdisciplinary Neurobehavioral Core Department at the University of Heidelberg, in coordination with Dr. Claudia Pitzer.

They were performed in two batches, with two years of difference between them. The first batch consisted of 16 male 2 months-old $IFIT1^{WT}$ and 18 male 2 months-old $IFIT1^{KO}$ animals and was conducted by Dr. Santiago Cerrizuela. The second batch consisted of 9 male 30 months-old $IFIT1^{WT}$ and 9 male 30 months-old $IFIT1^{KO}$ animals and was conducted by me, Damian Carvajal Ibanez. All ages refer to the age of the animals at the beginning of the study period. The animals were subjected to the elevated plus maze test, the three-chamber sociability and social novelty test, and the active-place avoidance test, in that order. All tests were separated by 1-3 days, all animals were handled 1 week before the start of the experiment, and were single-housed in the behavioural facilities for a total duration of 1-2 months. For both batches, when more than one mouse was tested on the same day, $IFIT1^{WT}$ and $IFIT1^{KO}$ genotypes were used in parallel

2.15.1 Elevated Plus Maze Test (EPM)

I assessed the anxiety-like behaviour traits of our cohort mice by the elevated plus maze test, as in Krieger *et al*, 2012. In this test, the anxiety-like behaviour is evaluated as the conflict of the mice between their intrinsic interest in exploring a new area and the

dangerous properties of an open environment. As described by Krieger *et al*, 2012 “The maze is a crossed-shaped platform (grey opaque plastic material) with equally sized arms (8×30 cm^2) and a central intersection (8×8 cm^2), allowing mice to move freely into each zone of the maze. Two of the arms (opposing each other) were flanked by 17 cm high opaque walls (closed arms); the remaining two arms are without walls (open arms). The maze is elevated 70 cm above the floor.”. Similar to Krieger *et al*, 2012, tested mice were allowed to become familiar with the EPM arena for 10 minutes. Then, the tested individuals were introduced into the maze in the central intersection and the motion of the mice is recorded by a camera and tracked with the SYGNIS tracker software (SYGNIS). The time spent in each arm is then quantified. I then computed the percentage of time spent with open arms as an indicative of the anxiety-like behaviour. Statistical tests were applied as described in the figure captions.

2.15.2 Active Place Avoidance Test (APA)

I assessed the learning process and the spatial memory acquisition of our cohort mice by the APA test, similar to Krieger *et al*, 2012 and Seib *et al*, 2013. The active place avoidance platform (Serrano *et al*, 2008) consisted of a rotating (1rpm, clockwise) circular platform (r=43cm), with a 60 degrees non-moving region as a shock zone (Figure 3.32A) and was surrounded by a transparent wall. The show zone is imaginarily delimited by visual cues placed on the walls around the test platform. In this memory test, subject mice are placed on the platform and are allowed to freely walk on the rotating platform. As soon as the subject mouse enters the shock zone, an electric shock is given to the mouse (500 ms, 60Hz, 0.4mA). This shock is repeatedly given to the subject mouse every 1,5 seconds as long as the mouse is inside the shock area. Due to the active rotation of the circular platform, static mice are passively introduced into the shock area in the course of the test and they learn to actively avoid the designated shock area. The APA test consists of a total of 10 trials. In trial 1, the subject animal is placed on the platform and is allowed to walk freely for 10 min without the thread of the electric shock. Sequentially, in trials 2-9 (both included) the subject animal is placed on the platform and is allowed to walk freely for 10 min with the thread of the electric shock active in the shock area. Trials 1-9 were conducted with intervals of 10 min in-between. This phase defines the learning phase of the experiment. 24 hours after trial 9, trial 10 is conducted. In trial 10, the subject animal is placed on the platform and is allowed to walk freely for 10 min without the thread of the electric shock. Despite the absence of shock, the subject animals actively avoid the shock area based on their spatial memory. The time to the first entry to the shock area (latency to first) was recorded for all samples. Animals that did not enter the shock zone at any time during the duration of the experiment were

automatically assigned a latency to first of 600 seconds. The first batch (2 months-old animals) was recorded using the SYGNIS TRACKER V4.1.14, while the second batch (30 months-old animals) was recorded using the EthoVision XT 17 (Noldus). Statistics were applied as described in the figure captions.

2.15.3 Three-Chamber Sociability and Social Novelty Test

I assessed the social interaction of our cohort mice by the three-chamber sociability and social novelty test, as in Eltokhi *et al*, 2020. In this test, a walled platform consists of three chambers (40×40×40cm^3) communicated by a hole (Figure 3.33A and Figure 3.34A). In the lateral chambers, a small chamber is placed in the middle to host either nothing (empty cage), a littermate individual to the test animal (littermate), or a CD1-background animal that never interacted with either the littermate or the tested animal before (intruder). The social and social novelty tests consist of a total of 3 trials: In trial 1, the subject mouse is placed in the middle of an empty 3-chamber arena and is allowed to explore the area for 5 min (habituation trial). In trial 2, the same subject mouse is placed in the middle of the 3 chambers, in which one of the cages is occupied by a littermate mouse and the second cage is empty. This trial 2 will measure the sociability of the subject mouse for 5 min. In trial 3, the same subject mouse is placed in the middle of the 3 chambers, in which one of the cages is occupied by the same littermate as in trial 2 and the second cage is occupied by a CD1-background intruder mouse. This trial 3 will measure the social novelty traits of the subject mouse for 5 min. Each trial is separated by a 15 min break, where the subject mouse is placed back in its original cage. The motion of the mouse is tracked during the 5 min of each trial using the EthoVision XT software (Noldus). Depending on the availability of the device, 2-3 mice were tested simultaneously, always balancing the different genotypes homogeneously. The time recorded with each of the two lateral cages was recorded and computed. I also computed the sociability index ((time littermate – time empty cage)/(time littermate + time empty cage)x100) and the social novelty index ((time intruder – time littermate)/(time intruder + time littermate)x100). Statistics were applied as described in the figure captions.

2.16 vSVZ single-cell transcriptomics

2.16.1 vSVZ single-cell transcriptomics of IFNAGR^{WT} and IFNAGR^{KO} mice

Single-cell transcriptomics experiments were performed by Dr. Santiago Cerrizuela and the bioinformatical and statistical analysis was performed by Jooa Hooli exactly as reported in Carvajal Ibañez *et al*, 2023.

2.16.2 vSVZ single-cell transcriptomics of IFIT1^{WT} and IFIT1^{KO} mice

To characterize the transcriptome and the 5'UTR changes in the transcripts of neural lineage cells in aging, I conducted a 10x experiment using the Chromium Single Cell V(D)J Reagent Kits v1.1 (10x Genomics), which captures the 5'-termini of the sequenced mRNAs. The experiment was performed in two different batches: Batch 1 consisted of 3 male 2,5 months-old IFIT1^{KO} and 4 male 17 months-old IFIT1^{KO} mice. Batch 2 consisted of 3 male 2,25 months-old IFIT1^{WT} and 8 male 22 months-old IFIT1^{WT} mice (22 months-old IFIT1^{WT} mice were pooled in groups of two to compose a final 4-replicate cohort). See details of the mouse lines in section 2.1.

After sacrificing the animals, the vSVZ and the OB of the sample mice were isolated as previously described (Kremer *et al*, 2021) and sorted in a BD FACSAria II (OB samples) and a BD FACSFusion I (vSVZ samples) simultaneously at the DKFZ Flow Cytometry Facility. The FACS-sorting strategy collected neural lineage cells from two brain regions: 1) GLAST^{+} lineage cells from the vSVZ and 2) PSA-NCAM^{+} late neural progenitors from the rostral migratory stream (RMS) and the olfactory bulb (OB). I size-selected the cells of interest and excluded doublets, dead cells (Sytoxblue^{+}) and myeloid cells (CD45^{+}), erythrocytes (Ter119^{+}), and oligodendrocytes (O4^{+}) cells as recently described (Kalamakis *et al*, 2019), see gatings in the Appendix. Right before the 20 min antibody staining incubation time, Hashtag-oligos (HTO) antibodies TotalSeq-C (Biolegend) were added to the antibody mix 1:100 and were incubated with the cells as any other staining antibody. Each biological replicate was labeled with a different HTO, as summarized in table 2.8. All sorted cells were pooled into 4 groups: IFIT1^{WT} young, IFIT1^{WT} old, IFIT1^{KO} young, and IFIT1^{KO} old, and each group was processed in a separate 10x reaction using the Chromium Next GEM Chip G using Chromium Next GEM Single Cell 5' Library & Gel Bead Kit v1.1 without the Chromium Single Cell V(D)J Enrichment Kit (all from 10x Genomics).

Libraries were prepared following 10x Genomic's protocols by the members of the Single-cell open lab at the DKFZ. The four gene expression libraries were sequenced separately on a NovaSeq 6K S1 PE 100bp at the Sequencing facility from the DKFZ Genomics and Proteomics Core Facility. The four hashtag libraries were pooled by genotype (2 final libraries) and were sequenced separately on a NextSeq MidOutput 550 PE 75bp at the Sequencing open lab provided by the DKFZ Genomics and Proteomics Core Facility.

Table 2. 8: Hashtag-oligos (HTOs) used for sample discrimination in 5'UTR 10x

Barcode ID (TotalSeq™C)	Sequence	Sample	10x Reaction
0302	GGTCGAGAGCATTCA	IFIT1 vSVZ Young_1	1 (Day 1)
		IFIT1 vSVZ Old_1	2 (Day 1)
		WT vSVZ Young_1	3 (Day 2)
		WT vSVZ Old_1	4 (Day 2)
0303	CTTGCCGCATGTCAT	IFIT1 vSVZ Young_2	1 (Day 1)
		IFIT1 vSVZ Old_2	2 (Day 1)
		WT vSVZ Young_2	3 (Day 2)
		WT vSVZ Old_2	4 (Day 2)
0304	AAAGCATTCTTCACG	IFIT1 vSVZ Young_3	1 (Day 1)
		IFIT1 vSVZ Old_3	2 (Day 1)
		WT vSVZ Young_3	3 (Day 2)
		WT vSVZ Old_3	4 (Day 2)
0306	TATGCTGCCACGGTA	IFIT1 vSVZ Old_4	2 (Day 1)
		WT vSVZ Old_4	4 (Day 2)
0307	GAGTCTGCCAGTATC	IFIT1 OB Young_1	1 (Day 1)
		IFIT1 OB Old_1	2 (Day 1)
		WT OB Young_1	3 (Day 2)
		WT OB Old_1	4 (Day 2)
0308	TATAGAACGCCAGGC	IFIT1 OB Young_2	1 (Day 1)
		IFIT1 OB Old_2	2 (Day 1)
		WT OB Young_2	3 (Day 2)
		WT OB Old_2	4 (Day 2)
0309	TGCCTATGAAACAAG	IFIT1 OB Young_3	1 (Day 1)
		IFIT1 OB Old_3	2 (Day 1)
		WT OB Young_3	3 (Day 2)
		WT OB Old_3	4 (Day 2)
0310	CCGATTGTAACAGAC	IFIT1 OB Old_4	2 (Day 1)
		WT OB Old_4	4 (Day 2)

2.17 Statistical analysis

Statistical analysis was adapted from Carvajal Ibañez *et al*, 2023: Biological replicates are plotted in the figures and denoted as “n”. These biological replicates refer to either different murine individuals or different colonies of NSCs extracted from different mice. The biological sample size (n) is denoted in the figures or the figure caption for every experiment. Bars represent mean ± SD unless differently specified. Only biological replicates were considered for statistical analyses. Statistical tests were performed in GraphPad Prism7 (unless otherwise indicated) as indicated in each figure legend with a significance level of $\alpha = 0.05$. To test for biphasic response in WB, Jooa Hooli applied linear models explaining log2 FC were fitted with a single explanatory variable of time being greater than a change time. To find this change time, models were fitted for varying change times and the model with the lowest AIC was chosen. To determine the significance of this biphasic response, one-way ANOVA was performed on this model. For all sequencing-related data, statistical analyses were performed by Manuel Goepferich or Jooa Hooli.

2.18 Illustrations

Illustrations and schemes were designed in Adobe Illustrator 26.0.1 and biorender.com.

3. Results

Some of the results hereby reported in sections 3.1, 3.2, and 3.3 were published in the publication “Interferon regulates neural stem cell function at all ages by orchestrating mTOR and cell cycle” at EMBO Mol. Medicine on 13th of January 2023. Parts of the text adapted from the published manuscript are pertinently cited. In brief, investigation and validation were performed by me, Dr. Maxim Skabkin, Dr. Santiago Cerrizuela, and Marc Zumwinkel, and data analyses/curation were performed by Jooa Hooli and Manuel Goepferich. The contributions to the published data, as well as additional contributions to the results by Dr. Maxim Skabkin (sections 3.4 and 3.5) and Dr. Santiago Cerrizuela (section 3.5.4) are specified in each section.

3.1 Interferons as a homeostatic regulator of stem cells in the young and old brain

I first aimed to investigate the potential role of interferons in stem cell homeostasis. Despite previous results showing the role of interferons in the aged brain (Kalamakis *et al*, 2019; Baruch *et al*, 2014), I hypothesized that interferons could mediate NSC activation already in the young brain. To address this hypothesis, I combined single-cell transcriptome and bulk translatome analysis in transgenic animals including models lacking extrinsic type-I and type-II interferon responses, as well as type-I interferon-reporter mice.

3.1.1 Profiling the interferon response in neural stem cells and their progeny in-vivo in IFNAGR^{WT} and IFNAGR^{KO} mice.

To explore the presence of interferon in the neurogenic niche, I made use of a dataset created by Dr. Santiago Cerrizuela. Dr. Santiago Cerrizuela used type-I and -II interferon receptor wildtype (IFNAGR^{WT}) or knockout (IFNAGR^{KO}) TiCY (Tlx-CreERT2-YFP) mice of different ages. TiCY-background mice express cre-ERT2 recombinase in neural stem cells, as controlled by the Tlx regulatory element. Upon tamoxifen injection, cre-ERT2 recombines eYFP and activates its expression, stably labeling NSCs and their resulting offspring (FIG). Dr. Santiago Cerrizuela injected young (7-10 weeks old) and old (71-98 weeks old) IFNAGR^{WT} or IFNAGR^{KO} TiCY mice with tamoxifen (TAM) and FACS-sorted the neurogenic lineage cells 6-9 weeks after TAM injection (Figure 3.1A, upper panel). The FACS-sorting strategy collected cells from two brain regions: 1) Lineage cells (GLAST^{+}eYFP$^{-/+}$) from the vSVZ; 2) Labelled offspring (eYFP^{+}) and late neural progenitors (PSA-NCAM^{+}eYFP$^{-/+}$) from the adjacent striatum (Str), the rostral migratory

stream (RMS) and the olfactory bulb (OB) (Figure 3.1A-B). After quality processing, the dataset collected 15,548 cells consisting of NSCs, their offspring, and adjacent cells including microglia and endothelial cells. Using previously-characterized markers (Llorens-Bobadilla *et al*, 2015; Kalamakis *et al*, 2019) the different lineage cell subtypes were profiled spanning from quiescent NSC (qNSC1) to primed-quiescent NSC (qNSC2), activated NSC (aNSC), transit-amplifying progenitor (TAP), and neuroblast (NB) (Figure 3.1C-D). In addition, additional neuronal markers were employed to identify late pseudotime cells as neurons (Figure 3.1D).

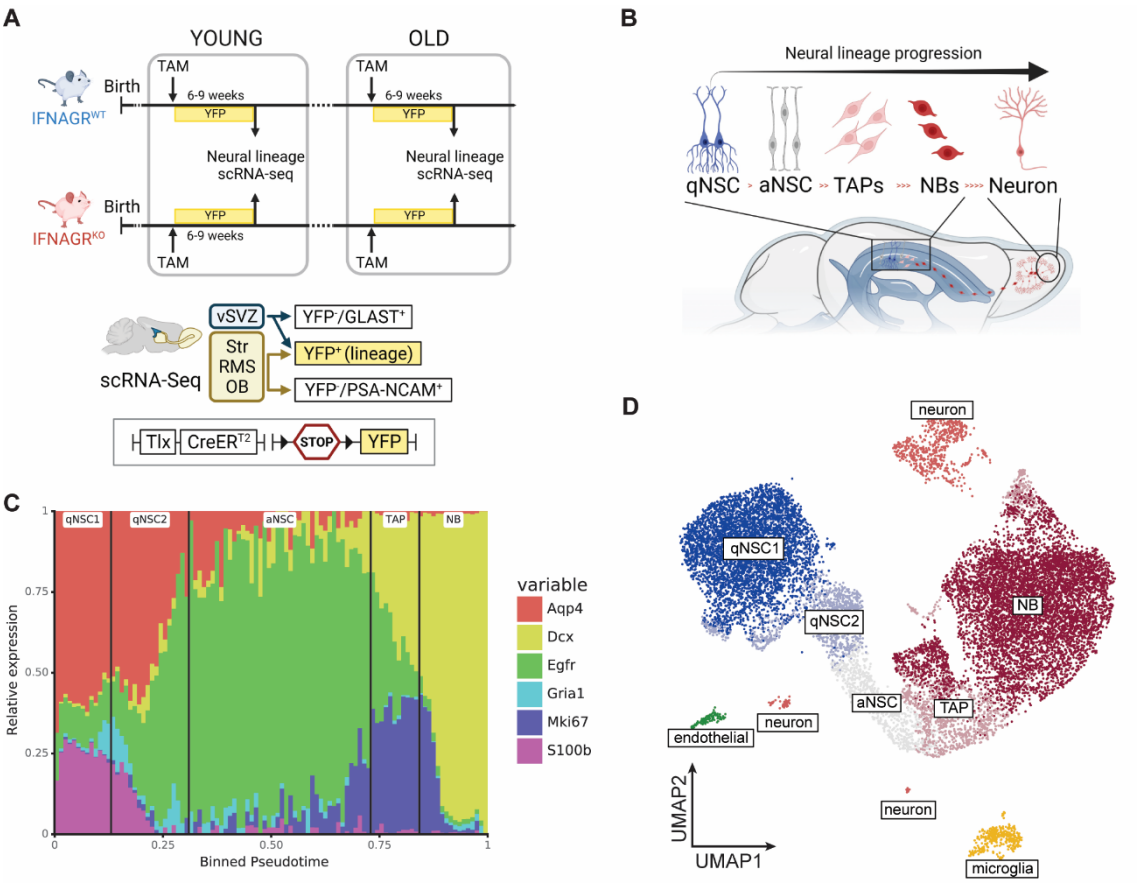

Figure 3.1: Inference of IFN signatures in the vSVZ niche

Figure and caption adapted from Carvajal Ibañez *et al*, 2023. "(**A**) Experimental layout for scRNA-Seq in young and old mice lacking interferon receptors. All mice represent TiCY (Tlx reporter, see Materials and Methods) that are either IFNAGR^{WT} or ^{KO}. vSVZ (Ventricular Subventricular Zone), RMS (Rostral Migratory Stream), OB (Olfactory Bulb), TAM (Tamoxifen)." (**B**) Schematic illustration of the neuronal lineage of the ventricular-subventricular zone (vSVZ) from quiescent neural stem cells (qNSC), active NSCs (aNSC), transit-amplifying progenitors (TAPs), migrating neuroblasts (NBs) and neurons at the olfactory bulb. "(**C**) Relative gene expression of relevant markers for cell types along pseudotime. Black lines denote cuts between cell types. (**D**) UMAP embedding shows the 15,548 single cells in this analysis with their cell types. n = 2 biological replicates per age and genotype."

To study the response to interferon of the lineage dataset, I aimed to assess the transcriptional enrichment of interferon-stimulated genes (ISGs) in our dataset. Previous reports have shown that scRNA-seq methods successfully identified an increased interferon response in the aged brain, but were underpowered to assess a basal interferon response at gene resolution (Kalamakis *et al*, 2019). Thus, to increase the resolution of the analysis, I aimed to develop a reliable interferon response signature based on the response of NSCs to interferon beta (IFN-β) *ex-vivo*.

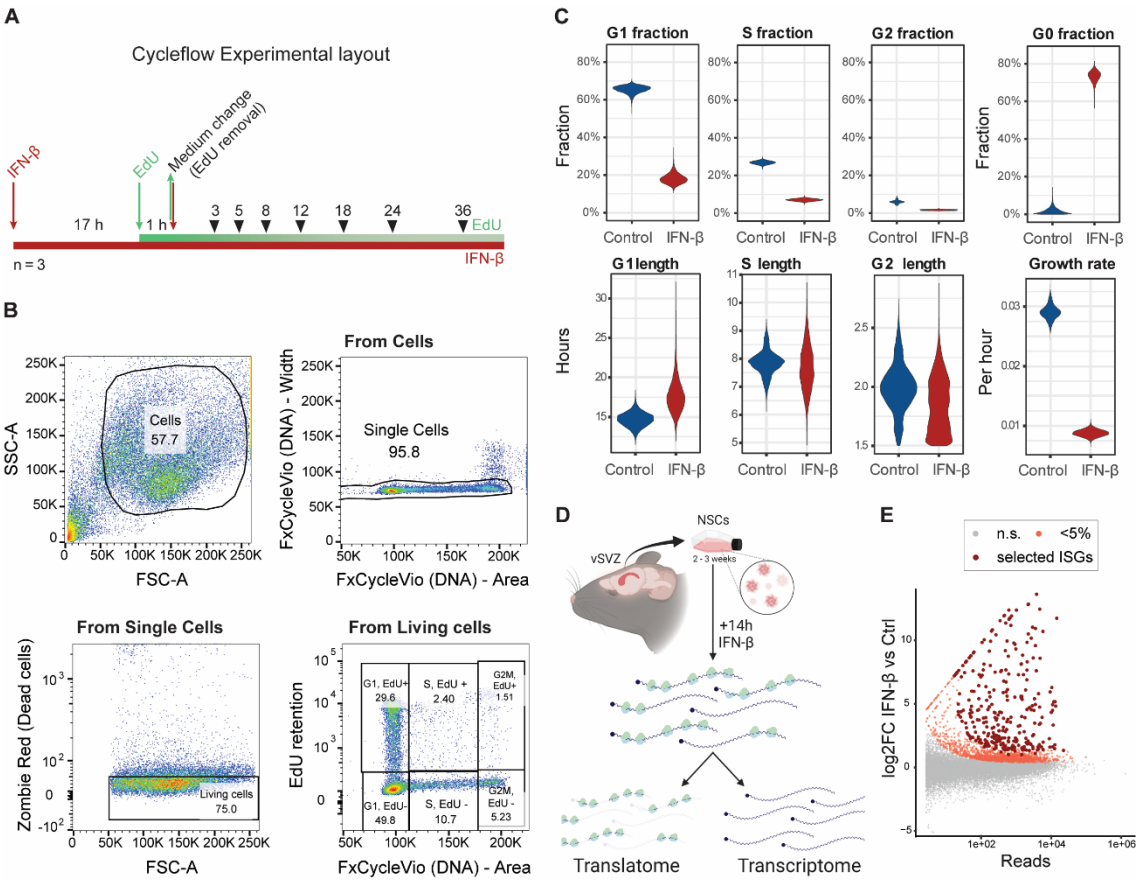

Figure 3.2: Assessment of the interferon response in NSCs by cycleflow and Ribo-Seq

Figure and caption adapted from Carvajal Ibañez *et al*, 2023. "(**A**) Scheme of experimental timeline for EdU and IFN-β exposure for Cycleflow. (**B**) Gating strategy for quantification of cell cycle states for Cycleflow. (**C**) Cell cycle fractions inferred from Cycleflow in IFN-β-treated NSCs. n = 3 biological replicates. (**D**) Schematic representation of Ribo-Seq pipeline in NSCs. (**E**) MA plot of differential expression between IFN-β 16 h treated bulk cells and control cells. Light red dots are significantly upregulated (one-sided Wald test), and dark red dots are the top 300 genes selected as the "NSC Type-I Interferon Response". n = 4 biological replicates."

First, to assess whether the response to IFN-β of *ex-vivo* NSCs recapitulates the *in-vivo* phenotype, I subjected NSCs cultured *ex-vivo* in the absence or presence of IFN-β to Cycleflow (Jolly *et al*, 2022)(Figure 3.2A). Cycleflow is a cell cycle inference method that

1) assesses the fraction of cells at different cell cycle stages including the quiescence stage (G_0), 2) models the length of each cell cycle stage and 3) measures global proliferation, of a given cell population upon different conditions (Jolly *et al*, 2022). To output these three parameters, Cycleflow combines a simultaneous assessment of the cell cycle stage (DNA amount) and dilution of the thymidine analog EdU (5-ethynyl-2′-deoxyuridine), during several time points after EdU incubation. I recorded all the cell stages and EdU incorporation state of the cells over 7 time points in NSCs and Jooa Hooli analyzed and modeled the data as in Jolly *et al*, 2022 (Figure 3.2A-B), assisted by Adrien Jolly, from Prof. Thomas Höfer's lab. Similarly to previous reports (Kalamakis *et al*, 2019), NSCs stop cycling upon exposure to interferon (Figure 3.2C, growth rate). Cycleflow analysis unveiled that interferon did not just keep NSCs at G_1, but retained almost 80% of the NSCs in the G_0 quiescent stage (Figure 3.2C). The remaining 20% maintained their cycling properties but stayed significantly longer in G_1. This shows that *ex-vivo* treatment of NSCs with interferons recapitulates the response to interferon that is observed *in-vivo* (Kalamakis *et al*, 2019).

Next, to generate the interferon signature, I treated NSCs for 14h with IFN-β and performed Ribosomal Sequencing (Ribo-Seq) together with Dr. Maxim Skabkin (Figure 3.2D). This Ribo-Seq data was analyzed by Jooa Hooli and Manuel Goepferich (see more Ribo-Seq details in section 3.2.2, page 71). Using only the transcriptome of the NSC Ribo-Seq dataset, Jooa Hooli selected the 300 highest upregulated genes to score a type-I interferon signaling in the homeostatic brain (Figure 3.2E, Table Supl. 1). These 300 genes were coined the "NSC Type-I Interferon Response" signature.

3.1.2 Interferons target NSCs specifically both in the young and the old brain

Next, Jooa Hooli applied the "NSC Type-I Interferon Response" (Figure 3.2) to our $IFNAGR^{WT}$ and $IFNAGR^{KO}$ scRNAseq dataset (Figure 3.1D, R3A). Our NSC Type-I Interferon Response geneset unveiled a novel basal interferon response in the young brain (Figure 3.3B). This response was absent when applying available interferon alpha gene-sets (Figure 3.3C). This shows that available genesets are underpowered to find a basal interferon response in neural lineage, as they only capture such response in highly-responsive microglia and endothelial cells (Figure 3.3C). Of note, also in our "NSC Type-I Interferon Response" microglia and endothelial cells scored the highest interferon score. This confirms the reliability and sensibility of our "NSC Type-I Interferon Response" signature to score basal and prominent responses across all cell types in the vSVZ.

Within this interferon basal response, it was surprising to find heterogeneity in the response to interferon in different cell subtypes along the neural lineage, both in the young and the old brain (Figure 3.3B, right panel). NSCs, both quiescent and active, express the highest interferon response score, which drops dramatically in their offspring early (TAPs) and late (NB) progenitors. This interferon response was then slightly increased again in the neurons produced in the olfactory bulbs. Upon aging, the interferon score increased as expected in IFNAGR^{WT} mice (Kalamakis *et al*, 2019; Baruch *et al*, 2014) but maintained the heterogeneity of the response among NSCs, progenitors, and neurons (Figure 3.3B, right panel). Surprisingly, neural progenitors remained irresponsive to external interferons at all ages (Figure 3.3B, right panel). This non-responsiveness was not due to the lack of expression of interferon receptors, as they were expressed equally at all ages and across all cell types along the neural lineage (Figure 3.3D).

In the absence of interferon sensing (IFNAGR^{KO}), NSCs retained an intrinsic high expression of the interferon score, which also dropped dramatically in their neural progenitors (Figure 3.3B, right panel). Surprisingly, this intrinsic basal level did not change in aged animals, proving the role of extrinsic interferons in the age-dependent increased interferon response. Additionally, the basal response in IFNAGR^{KO} mice was slightly different from that of IFNAGR^{WT} mice, suggesting that extrinsic interferons or expression of the interferon receptors might have a role in an early fine-tuning of the intrinsic interferon response (Figure 3.3B, right panel). The presence and role of such intrinsic interferon response in stem cells were recently described (Wu *et al*, 2018). Applying the Wu *et al*. “Intrinsic IFN Response” to our dataset largely agrees with our findings (Figure 3.3E). The Wu *et al.* response confirms the basal interferon score in IFNAGR^{WT} mice, which is increased upon aging. It also confirms that in the absence of interferon sensing (IFNAGR^{KO}), the interferon intrinsic signature is retained at all ages. The Wu *et al.* response signature peaks however at the active NSCs and progenitor stages, different from our “NSC Type-I Interferon response”. As the Wu *et al.* signature was built from *in-vitro* progenitor lines from different tissues, this suggests that the intrinsic signature from Wu *et al.* might be more indicative of the progenitor’s than the stem cell’s intrinsic response.

Altogether, I conclude that interferon targets neural stem cells preferentially, as compared to other neural progenitors both in the young and the old brain. This sensing of interferons modulates and contributes to the stem cell intrinsic interferon response, resulting in an increased response in aging.

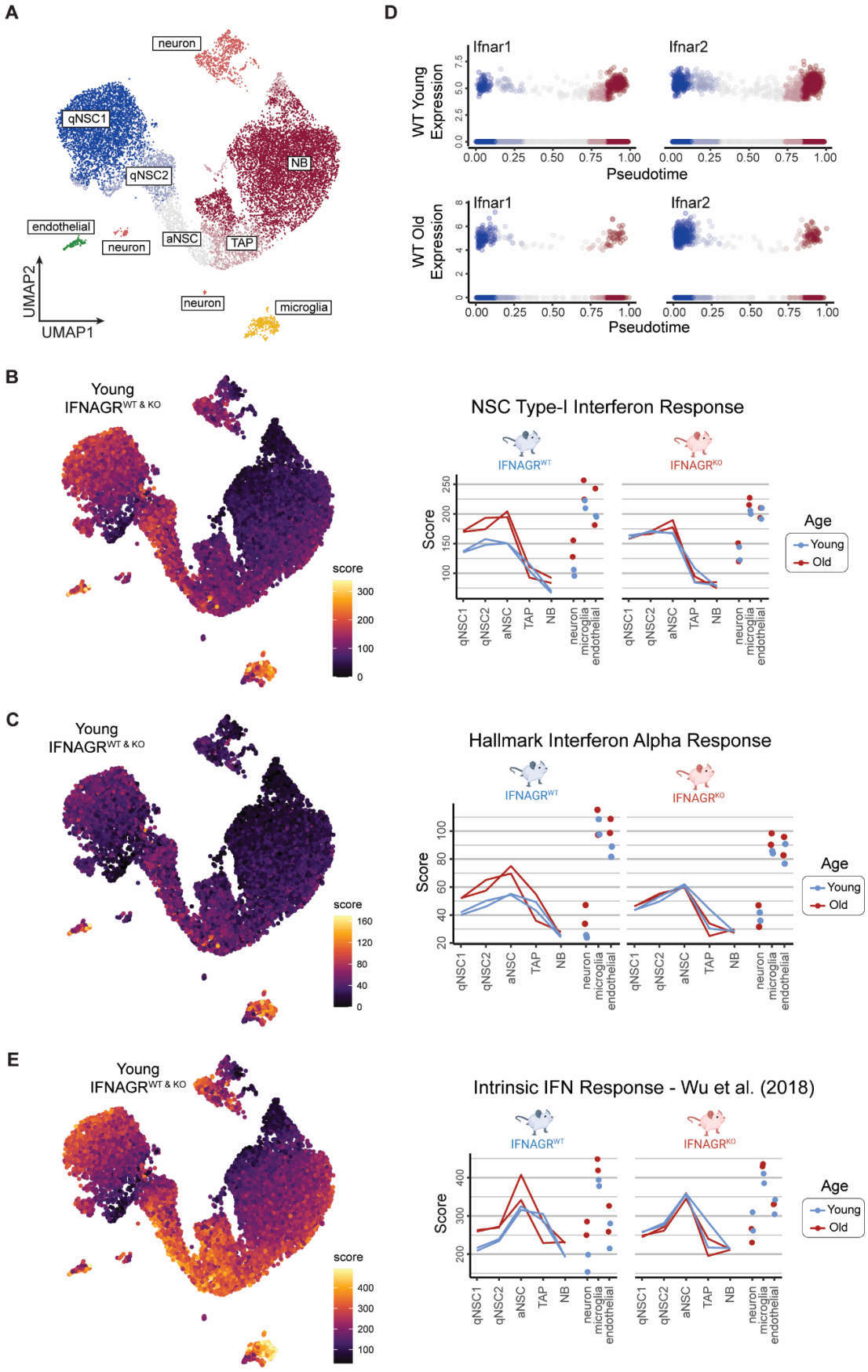

Figure 3.3: Interferons target NSCs selectively in the brain at all ages

(Figure caption located on the next page)

3.1.3 Interferon-reporter mice confirm that NSCs are preferentially targeted by interferons in the young and old brain

To validate the scRNAseq results, I made use of the type-I interferon-reporter mouse line (ISRE-eGFP), which was a kind gift from Dr. Marieke Essers (DKFZ, Germany). ISRE-eGFP mice express the fluorescent protein eGFP upon stimulation of their upstream interferon-sensitive response element (ISRE). Upon type-I interferon binding, phosphorylated dimers of STAT1-STAT2 bind to ISRE elements and activate the transcription of their associated ISGs, including the eGFP reporter gene (Platanias, 2005) (Figure 1.5). I first assessed the number of interferon-responsive cells along the neural lineage in young (2 months old), middle (6 months old), and aged (16 months old) mice. For this, I FACS-analyzed the brains of these mice to quantify for eGFP cells excluding debris, doublets, dead cells (Sytox blue), leucocytes (CD45+), oligodendrocytes (O4+), and erythrocytes (Ter119+) from the analysis (Figure Supl.1). Based on previous publications (Llorens-Bobadilla *et al*, 2015; Baser *et al*, 2019), I identified NSCs ($GLAST^+CD133^+$) and NBs ($PSA\text{-}NCAM^+$) from the vSVZ (Figure Supl.1A), as well as late NBs/immature neurons ($PSA\text{-}NCAM^+$) from the olfactory bulbs (Figure Supl.1B).

Similar to the observation using the NSC Type-I Interferon Response in scRNA-Seq data, I found an average of 39,2% of $eGFP^+$ NSCs already in the young brain (2 MO), with an increased prevalence to 48-53% of $eGFP^+$ NSCs in aging (Figure 3.4A-B). This increase is present already at 6 months-old animals and is maintained in older individuals, in line with the observed reduction of total NSCs in the vSVZ of 6 months old mice (Kalamakis *et al*, 2019). Along the neural lineage, NSCs showed the highest interferon response, with a drastic decrease in their vSVZ NB progenitors, and a final increase in immature neurons (Figure 3.4B). Similarly, the age-dependent increase in interferon responsiveness was more prominent in NSCs and late NBs/immature neurons than in early neural progenitors. This confirms the role of interferons in regulating neural stem cells in young and old animals and confirms the non-responsiveness of neural progenitors to external interferons.

Related to Figure 3.3:

Figure and caption adapted from Carvajal Ibañez *et al*, 2023 "(**A**) UMAP embedding shows the 15,548 single cells with their cell types. Scores computed for the NSC Type-I Interferon Response signature (**B**), the Hallmark Interferon Alpha Response signature (**C**), and the Wu *et al* (2018) intrinsic interferon response gene set (**E**) displayed in the UMAP embedding for young cells (colors clipped to the range seen in the lineage cells) and averaged for the cell types in our analysis at varying ages in $IFNAGR^{WT}$ and ^{KO} cells. n = 2 biological replicates per age and genotype. (**D**) Relative expression of type-I IFN receptors in young and old wildtype cells over pseudotime colored by lineage cell types."

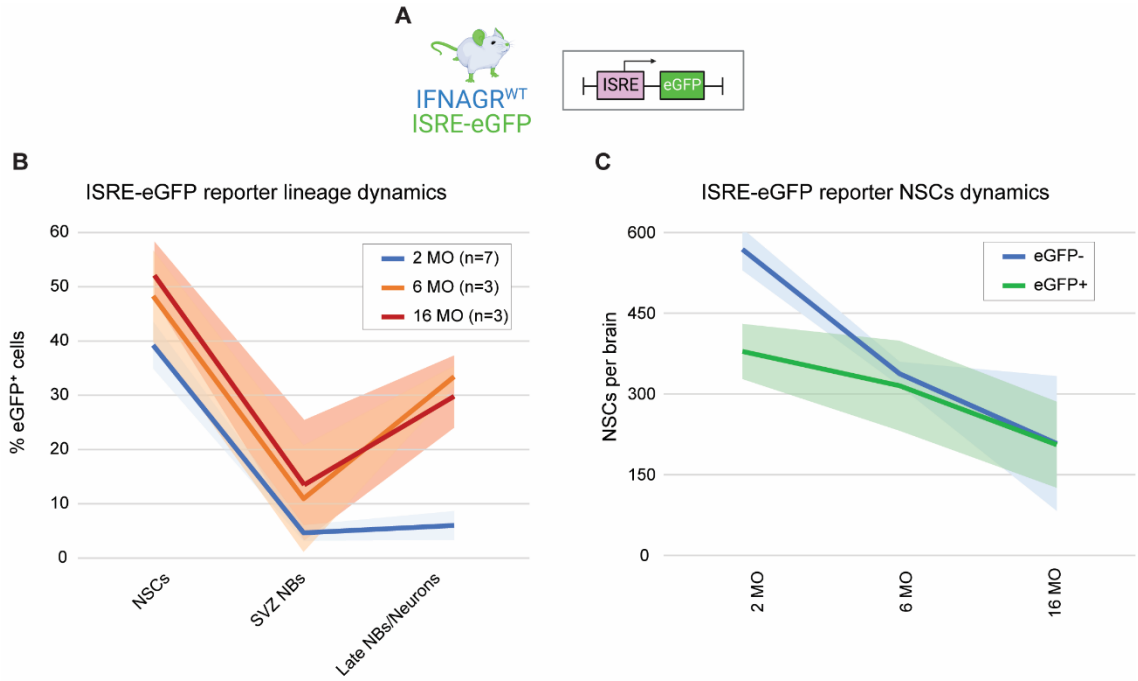

Figure 3.4: NSCs respond selectively to interferons at all ages in the brain

(**A**) Schematic representation of the type-I interferon reporter ISRE-eGFP mouse. (**B, C**) FACS quantification of eGFP+ cells across different ages in the type-I interferon reporter mouse (ISRE-eGFP) within the different lineage populations: NSCs (Glast+CD133+), SVZ NBs (SVZ Glast-CD133-PSA-NCAM+) and late NB/Neurons (OB Glast-CD133-PSA-NCAM+). Lines depict mean average and shadow depicts SD of a given cell population/time point. n = 3-7 biological replicates per age and genotype.

The increase in the percentage of eGFP$^+$ NSCs indicates that the relative abundance of eGFP$^+$ and eGFP$^-$ NSCs changes over time. I decided to further explore the effect of time on the total abundance of these cells in the vSVZ. In this FACS-analysis, the vSVZ tissue is dissociated, stained, and acquired entirely, which allows an accurate estimation of the total numbers of NSCs in these brains. I observed that, despite the higher prevalence of interferons in aging, the eGFP$^+$ NSCs reduced their numbers slower than eGFP$^-$ NSCs (Figure 3.4C). While eGFP$^-$ NSCs are almost halved from 2 MO (Av. 569 NSCs) to 6 MO (Av.338 NSCs) individuals, eGFP+ NSCs were hardly reduced from 2 MO (Av. 379 NSCs) to 6 MO (Av. 315 NSCs) individuals. This underscores the importance of interferons in regulating the dynamics of the neural stem cell pool at all ages and unveils an additional layer of regulation that can be integrated into the current models of NSC dynamics (Carvajal Ibañez *et al*, 2023; Kalamakis *et al*, 2019).

3.2 Balancing canonical and non-canonical interferon signaling to uncouple growth and proliferation in NSCs

The molecular underpinnings of the interferon response in NSCs are poorly studied, albeit the role of interferons in modulating NSCs in aging, and now also in the young brain. To describe how downstream effectors of the interferon response modulate NSCs, I focused on the post-transcriptional modulation that interferons exert. Interferons modulate mRNA translation in terminally-differentiated cells, in addition to their canonical transcriptional ISG response (Mazewski *et al*, 2020). I thus hypothesized that IFN-β could also affect mRNA translation in NSCs, leading to the induction of quiescence and arrest at the G_0 quiescent state (Figure 3.2).

3.2.1 Interferon induces a biphasic regulation of global protein synthesis in NSCs that does not affect the translation of ISGs.

To address whether IFN treatment influences mRNA translation in NSCs, I first examined the global protein synthesis levels upon exposure to IFN-β. I treated NSCs with IFN-β for short (2 hours) and long incubations (16 hours) and assessed global protein synthesis by the incorporation of O-propargyl-puromycin (OPP) into newly-synthesized proteins (Figure 3.5A). In the presence of interferon, NSCs showed an early transient increase of protein synthesis followed by a profound protein synthesis shutdown (Figure 3.5B-C). Of note, NSCs grew optimally in growth factor- and metabolite-rich medium in this experimental set-up. Therefore, the early increase in protein synthesis, despite mild, might be biologically significant, as these cells are already synthesizing proteins at their optimal rate. In support of this, increasing insulin concentration in the cells (N2 supplement) did as well not increase especially their translation levels (Figure 3.5B).

To understand the major components driving this biphasic regulation of protein synthesis, I next profiled the translatome of these NSCs. Supervised by Dr. Maxim Skabkin, I established and performed ribosomal sequencing (Ribo-Seq) on NSCs treated with IFN-β for short and long periods (Figure 3.6A). This Ribo-Seq data, already mentioned in section 3.1.1, page 60, was initially analyzed by Dr. Manuel Goepferich and later quality-curated by Jooa Hooli. The-quality correlation both in the transcriptome and translatome libraries of this data showed a high quality of the sample and library preparation (Figure Supl.2A-B).

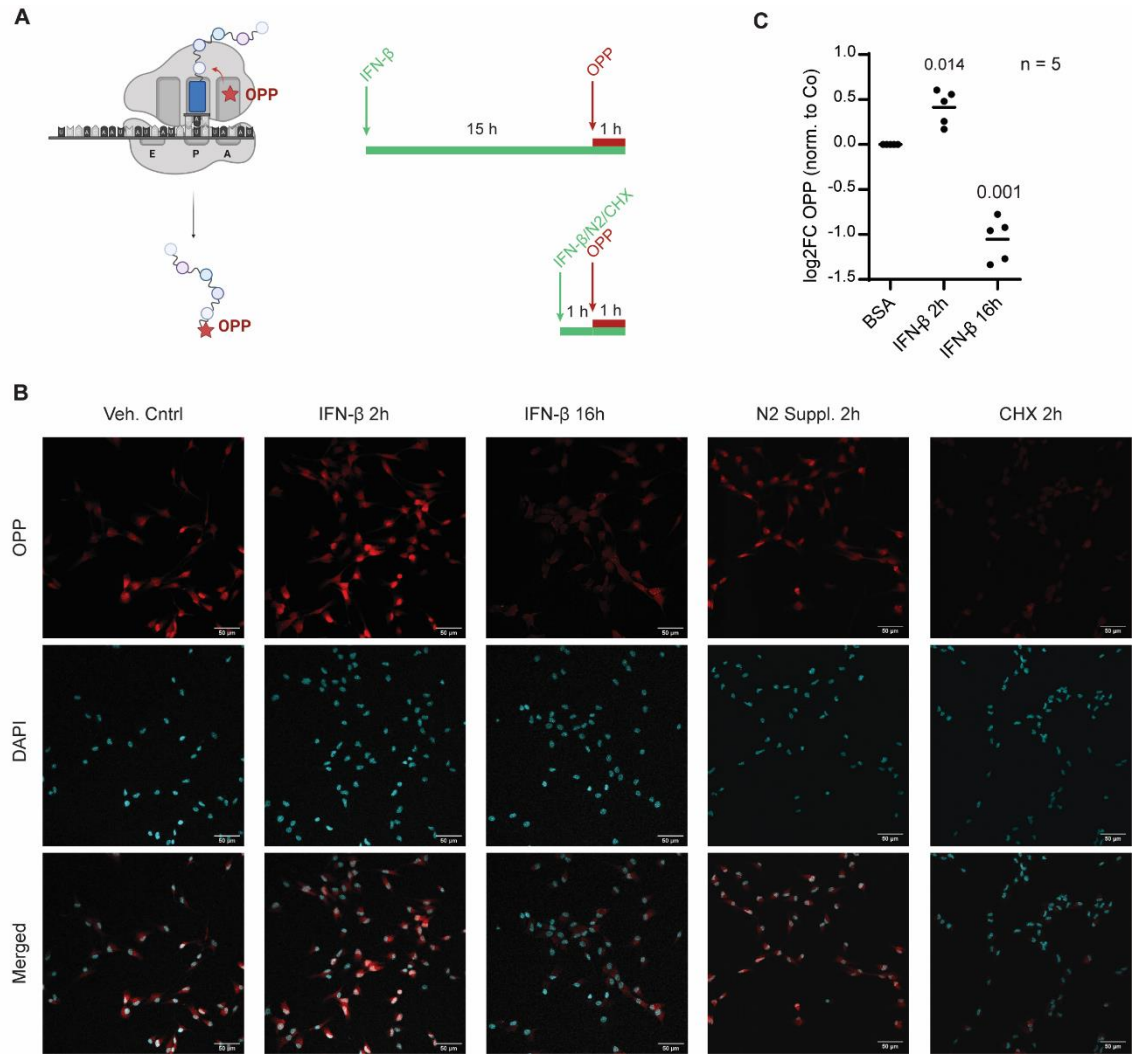

Figure 3.5: Interferon exerts a biphasic control on protein synthesis response in NSCs

Figure and caption adapted from Carvajal Ibañez *et al*, 2023 (**A**) Schematic representation of the mechanism of action of OPP (O-propargyl-puromycin) and the experimental setup. "(**B**) Representative images of the OPP assay in WT NSCs treated with IFN-β at 2 and 16 h. N2 supplement or Cycloheximide (CHX) where added as controls. Bar scale represents 50 µm. (**C**) Quantification of the OPP assay in WT NSCs treated with IFN-β at 2 and 16 h. n = 5 biological replicates. One-way ANOVA with Dunnett's multiple comparison test was computed (p-values specified) using vehicle-treated NSCs as the control group."

The analysis of the translation efficiency (TE) in these NSCs reveals a subset of genes being differentially translated at the assessed time points (Figure 3.6B-C). The translation efficiency and gene ontology (GO) analysis of this data confirms that NSCs are highly responsive to interferon and consistently upregulate the translation of ISGs and inhibit the translation of cell-cycle-related genes (Figure 3.6B-E). Interestingly, interferon inhibits the translation of cell-cycle-related genes already at 2 hours of incubation (Figure 3.6D), while global protein synthesis is upregulated (Figure 3.5). Regardless of this uncoupling of growth and proliferation, the consistent inhibition of cell-

cycle-related genes (Figure 3.6D-E) agrees with my evidence that interferon induces cell-cycle exit in NSCs (Figure 3.2C).

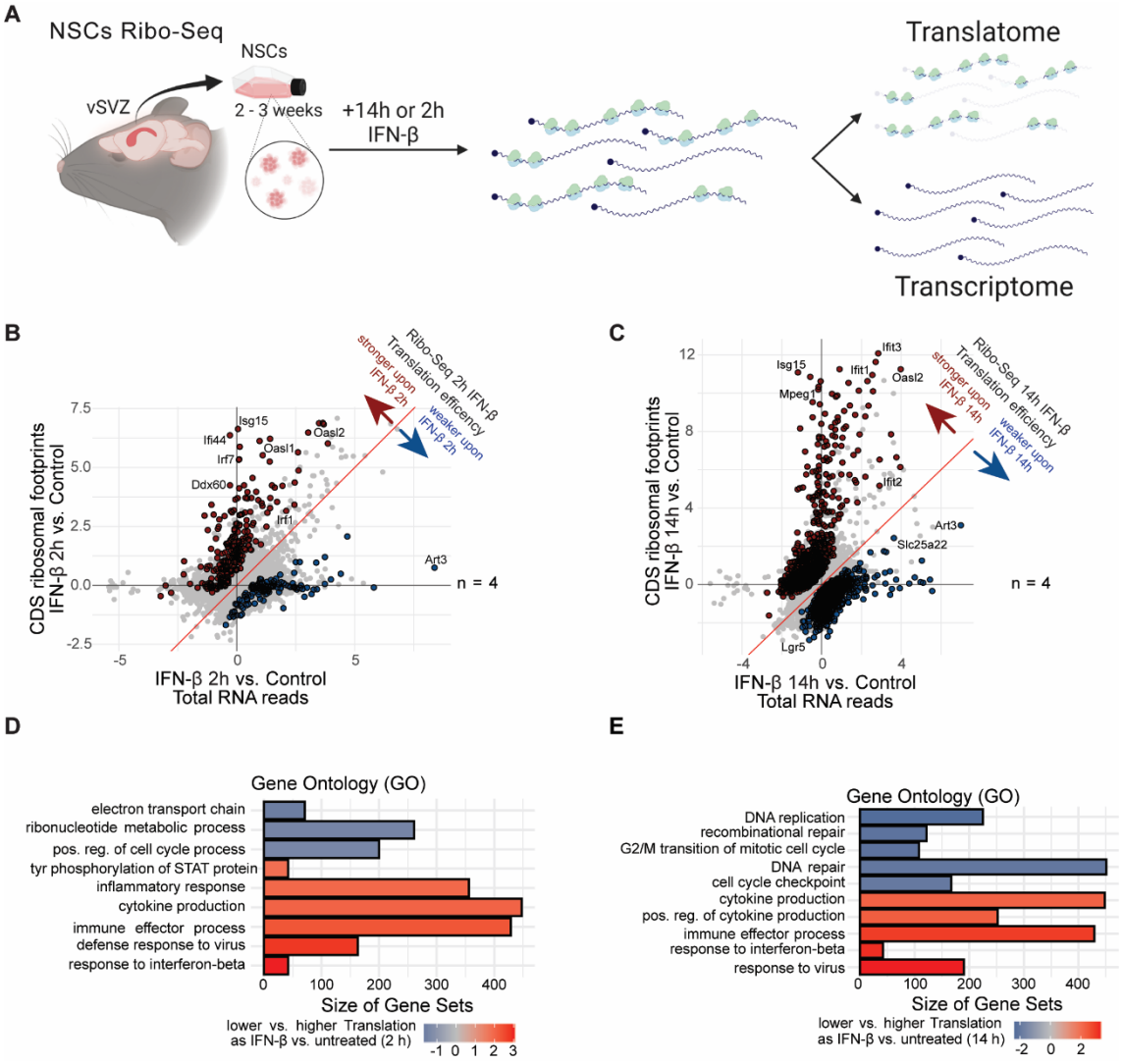

Figure 3.6: Interferon upregulates the translation of ISGs despite the biphasic control on protein synthesis in NSCs

Figure and caption adapted from Carvajal Ibañez *et al*, 2023. (**A**) Schematic representation of the Ribo-Seq experiment on *ex-vivo* NSCs. "(**B, C**) Ribo-Seq results depicting translation efficiency as the interaction of log2 fold changes (LFC) between footprints mapped to the CDS, referred to as "CDS counts", and total RNA after 2 or 14 h IFN-β treatment. FDR < 10%, LR-Test in DESeq2. Genes with a P value < 0.1 after FDR correction are highlighted. n = 4 biological replicates. (**D, E**) Associated GO-terms to panels B and C. n = 4 biological replicates."

Conversely, the translation efficiency of ISGs is at its highest upon 14 hours of interferon incubation (Figure 3.6C, E), while global protein synthesis is strongly inhibited (Figure 3.5). This uncovers a disconnection between global mRNA translation and ISG translation regulation. This consistent upregulation of ISGs in translation at both time

points was further confirmed by RT-qPCR from *Ifit3* and *Irf9* in the polysome profile extraction of NSCs (Figure Supl.3).

3.2.2 mTOR mediates the biphasic control of protein synthesis induced by interferon.

Given the drastic effect of interferon treatment on global protein synthesis in NSCs (Figure 3.5), I hypothesized that interferon might be controlling some major effectors of mRNA translation in NSCs. One of the major components of mRNA translation control is the mammalian Target of Rapamycin (mTOR) complex. mTOR regulates global translation in the cell and strongly targets a subset of mRNAs called TOP-mRNAs (Thoreen *et al*, 2012). The translation efficiency of these TOP-mRNAs can thus serve as a readout of mTOR activity. Our NSC Ribo-Seq dataset revealed that the translation of TOP-mRNAs was controlled biphasically in NSCs by interferon, similar to global protein synthesis (Figure 3.7A-B). This biphasic control of translation is also observed in the metagene profile of the footprints (ribosome-bound mRNA fragments) of these TOPmRNAs (Figure 3.7C-D).

After 2 hours of interferon treatment, the translation of TOP-mRNAs was slightly increased, despite not being significant (Figure 3.7A, Table R1). Further validation on the distribution of these mRNAs on the polysome profiles of NSCs treated with interferon confirmed this mild upregulation, with a significant increase in the heavy polysomes for *Rpl34* (Figure Supl.4). Conversely, after 14 hours of IFN treatment, the translation of TOP-mRNAs was significantly reduced (Figure 3.7B, Table R1). This late downregulation was highly significant also in the polysome distribution of the TOP-mRNAs *Rps17* and *Rpl34* (Figure Supl.4).

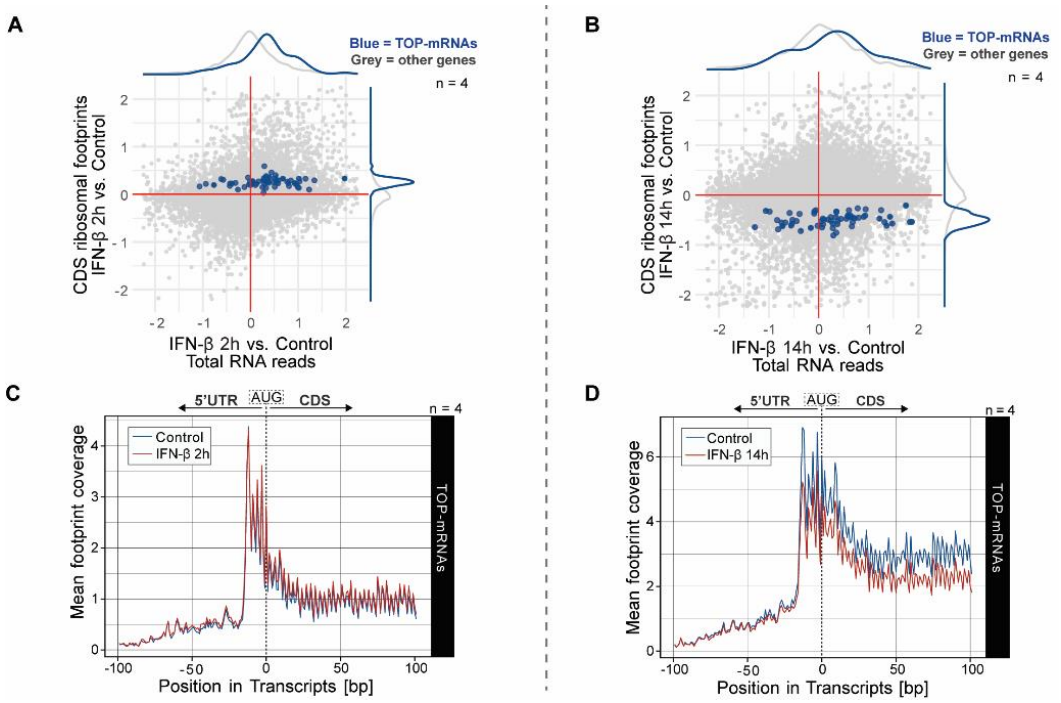

Figure 3.7: Translation of TOP-mRNAs in NSCs is biphasically regulated upon interferon treatment

Figure and caption adapted from Carvajal Ibañez *et al*, 2023 "(**A, B**) Ribo-Seq results of 2 and 14 h IFN-β treatments. 5′ terminal oligopyrimidine motif-containing mRNAs (TOP-mRNAs) highlighted in blue. n = 4 biological replicates. (**C, D**) Coverage profile of ribosome-protected reads (footprints) of TOP-mRNAs in 2 and 14 h IFN-β treatment. Nucleotide 0 depicts the start codon (AUG) marking the interface between 5′ untranslated region (5' UTR) and coding sequence (CDS)."

Table 3. 1: Translation Efficiency TOP-mRNAs in Ribo-Seq of NSCs treated with IFN-β

Gene	pvalue 2h IFN-β	padj 2h IFN-β	pvalue 14h IFN-β	padj 14h IFN-β
Eef1a1	0,9707	1,0000	0,4244	0,7382
Eef1b2	0,9503	1,0000	0,0144	0,1124
Eef1d	0,0758	0,6036	0,5592	0,8202
Eef1e1	0,9465	1,0000	0,2019	0,5225
Eef1g	0,7570	0,9950	0,4007	0,7207
Eef2	0,9478	1,0000	0,2566	0,5872
Eif3e	0,0684	0,5801	0,6437	0,8635
Eif3f	0,5879	0,9759	0,4837	0,7793
Eif3h	0,0339	0,4331	0,1840	0,5000
Fau	0,8256	0,9971	0,0004	0,0074
Hnrnpa1	0,7319	0,9946	0,2411	0,5694
Npm1	0,8806	0,9998	0,4608	0,7631
Pabpc1	0,5259	0,9669	0,0612	0,2770
Rpl10a	0,0518	0,5186	0,0948	0,3543
Rpl12	0,8400	0,9977	0,3181	0,6483
Rpl13a	0,9430	1,0000	0,3590	0,6843
Rpl14	0,9468	1,0000	0,0582	0,2699
Rpl18	0,5634	0,9719	0,0000	0,0000
Rpl18a	0,5351	0,9697	0,1422	0,4349
Rpl19	0,1047	0,6674	0,3980	0,7189
Rpl21	0,3969	0,9327	0,5925	0,8381
Rpl22	0,8403	0,9977	0,5236	0,8003
Rpl23	0,8592	0,9988	0,7902	0,9322
Rpl23a	0,3247	0,9067	0,0033	0,0387
Rpl30	0,7681	0,9950	0,0422	0,2223
Rpl32	0,4070	0,9377	0,1299	0,4154
Rpl34	0,6179	0,9792	0,5647	0,8234
Rpl35	0,1675	0,7855	0,0172	0,1274
Rpl36a	0,7614	0,9950	0,0060	0,0601
Rpl37	0,6247	0,9806	0,3041	0,6342
Rpl37a	0,0053	0,1667	0,4965	0,7865
Rpl38	0,4079	0,9378	0,4651	0,7659
Rpl39	0,7738	0,9950	0,2402	0,5689
Rpl4	0,3839	0,9297	0,2127	0,5358
Rpl41	0,6992	0,9923	0,0436	0,2272
Rpl5	0,9551	1,0000	0,7510	0,9160
Rpl6	0,7574	0,9950	0,0689	0,2960
Rpl7	0,2636	0,8751	0,6870	0,8860
Rpl7a	0,7070	0,9937	0,0004	0,0074
Rpl8	0,1208	0,7005	0,0002	0,0049
Rpl9	0,7043	0,9935	0,0947	0,3542
Rplp0	0,5531	0,9719	0,1081	0,3789
Rplp1	0,2059	0,8339	0,8846	0,9684
Rplp2	0,1226	0,7017	0,0248	0,1600
Rps10	0,8258	0,9971	0,1591	0,4624
Rps11	0,5425	0,9699	0,7492	0,9156
Rps14	0,5421	0,9699	0,1125	0,3872
Rps15	0,8273	0,9971	0,9561	0,9973
Rps15a	0,9839	1,0000	0,8928	0,9719
Rps16	0,1695	0,7896	0,0000	0,0000
Rps18	0,6066	0,9785	0,0000	0,0004
Rps19	0,9741	1,0000	0,8892	0,9702
Rps20	0,7230	0,9944	0,2560	0,5870
Rps21	0,6831	0,9910	0,2367	0,5647
Rps24	0,3496	0,9181	0,0761	0,3132
Rps25	0,8568	0,9988	0,0002	0,0049
Rps26	0,2463	0,8658	0,3072	0,6369
Rps27a	0,0829	0,6229	0,7408	0,9118
Rps3	0,2692	0,8795	0,0837	0,3306
Rps4x	0,3932	0,9325	0,0249	0,1600
Rps5	0,2414	0,8615	0,0129	0,1041
Rps9	0,6441	0,9826	0,0569	0,2660
Tpt1	0,9624	1,0000	0,0403	0,2157

Table adapted from Carvajal Ibañez *et al*, 2023. p-values <0.05 are highlighted in blue.

The biphasic control of translation of TOP-mRNAs correlates with the biphasic control of total protein synthesis, suggesting mTOR as a major component driving this post-transcriptional regulation in NSCs. To validate whether interferon controls mTOR activity dynamically in NSCs, Dr. Skabkin assessed the activation status of the downstream effectors of mTOR, 4EBP1, and S6K. Indeed, interferon treatment affected the phosphorylation level of these two effectors dynamically in NSCs. The phosphorylation of the eukaryotic translation initiation factor 4E-binding protein 1 (4EBP1) was strongly inhibited upon long interferon treatment, but not in early incubation periods (Figure 3.8A). Similarly, interferon treatment led to a biphasic regulation of the phosphorylation of protein S6 kinase (S6K) at Thr389, a mTORC1-specific phosphosite (Figure 3.8A; Ma & Blenis, 2009). The downstream target of S6K, protein S6 (S6) followed the same biphasic regulation at Ser235/236 and Ser240/244 (Figure 3.8A). Altogether, this indicates that interferon induces an early up- followed by a late down-regulation of mTORC1 activity in NSCs.

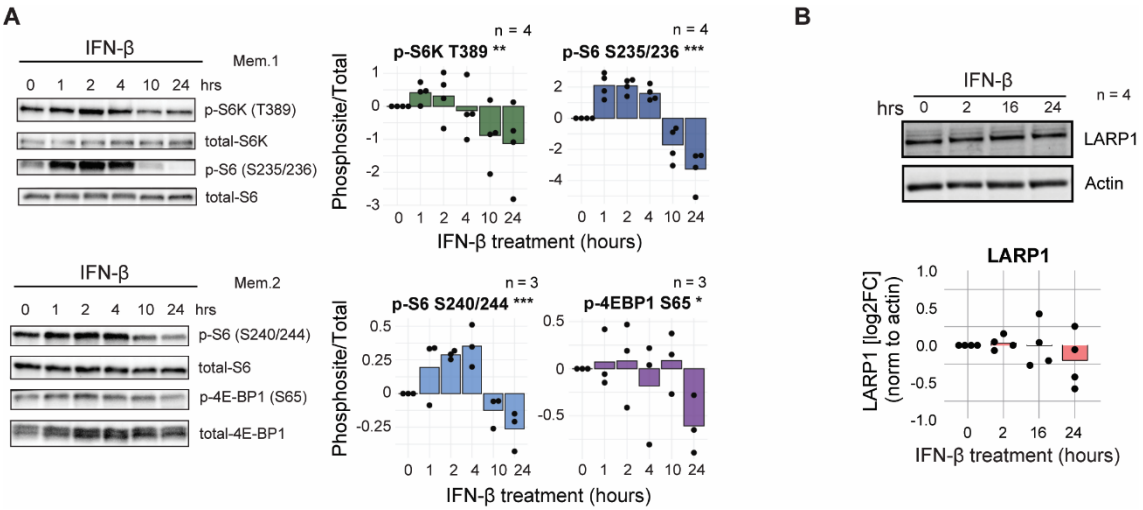

Figure 3.8: Interferon controls mTORC1 activity bipashically in NSCs

Figure and caption adapted from Carvajal Ibañez *et al*, 2023 "(**A**) Representative WB and phosphorylation levels quantification (log2FC) of the mTOR-related proteins ribosomal protein S6 kinase (S6K), ribosomal protein S6 (S6) and eIF4E-binding protein 1 (4E-BP1) from NSCs treated with IFN-β and normalized to control (t = 0 h). Bars represent the mean value. One-way ANOVA for the biphasic response test. p-4 E-BP1^{S65} * (P = 0.021), p-S6$^{S235/236}$ & p-S6$^{S240/244}$ ***(P < 0.001), p-S6K^{T389} **(P = 0.004). (**B**) Representative WB image and quantification (log2FC) of LARP1 from IFN-β-treated NSCs normalized to control (t = 0 h). Bars represent the mean value. n = 4 biological replicates."

I then hypothesized that LARP1 could be the downstream effector of mTORC1 driving the biphasic control of TOP-mRNAs in NSCs. I explored a phosphoproteomic dataset generated by Dr. Maxim Skabkin. This dataset contains differentially phosphorylated phosphosites from NSCs treated with interferon β at short (2 hours) and long (16 hours)

treatments. Two phosphosites were significantly upregulated upon extended incubation with interferon (Table Supl. 2). These phosphosites, p-LARP1^{S498} and p-LARP1^{T492} (human S521 and T515, respectively) have been previously reported but lack any functional relevance (Jia *et al*, 2021). In addition to the phosphorylation status, total LARP1 was not affected by interferon (Figure 3.8B).

Overall, this indicates that interferon causes a biphasic control of mTORC1 activity in NSCs, causing a transient up- followed by the profound down-regulation of mRNA translation.

3.2.3 The biphasic regulation of mTOR activity is mediated by a JAK/STAT-PI3K crosstalk

Such a biphasic control of mTORC1 activity by interferon was not previously described. Thus, I next ought to investigate the molecular underpinnings driving this biphasic response.

Interferons can modulate mTOR activity by the interferon non-canonical signaling pathway (Mazewski *et al*, 2020). In brief, interferon receptors crosstalk with PI3K-Akt-TSC2 modulating the activity of mTOR (Figure 3.9A). Interestingly, interferon lead to a transient increase in phosphorylation of p-Akt^{T308} and p-TSC2^{T1462} phosphosites, followed by a profound decrease of the phosphorylation levels of these both in later time points (Figure 3.9B). This biphasic regulation correlates with the biphasic mode of regulation of mTOR and uncovers the JAK/STAT-PI3K crosstalk as a major effector of interferon signaling in NSCs. Phosphorylation of Akt at Thr308 is the best, but not the only, predictor of Akt activity (Vincent *et al*, 2011). Phosphorylation at p-Akt^{S473}, directly controlled by mTORC2, can also modulate the activity of Akt (Figure 3.9A) (Breuleux *et al*, 2009). I, therefore, checked the phosphorylation levels of p-Akt^{S473} in NSCs treated with interferon and found no significant change in any of the time points assessed (Figure 3.9C). This indicates that the regulation of Akt at its residue Thr308 is responsible for its dynamic activation level and rules out the implication of mTORC2 in the biphasic regulation of mTOR activity.

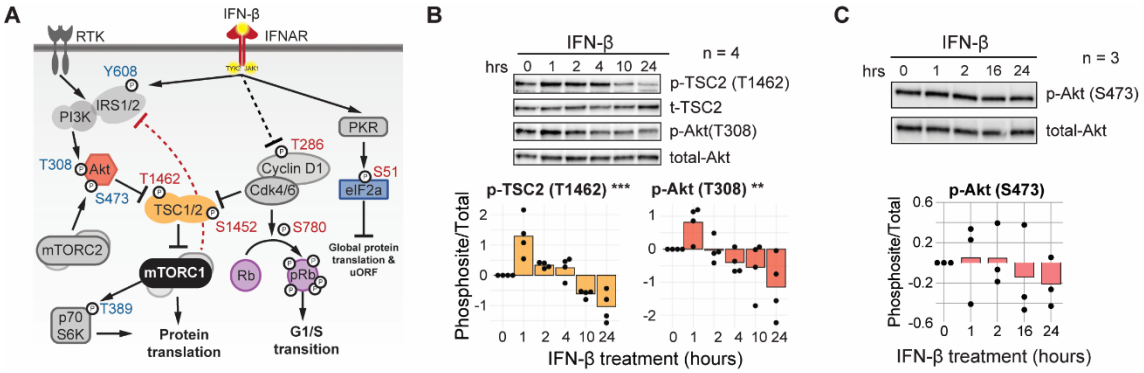

Figure 3.9: Interferon crosstalks with PI3K to modulate mTORC1 activity in NSCs

Figure and caption adapted from Carvajal Ibañez *et al*, 2023 "(**A**) Schematic representation of the type-I interferon signaling pathway and its crosstalk with the receptor tyrosine kinase (RTK) pathway. Activatory (blue) and inhibitory (red) phosphosites are depicted. Red inhibitory lines depict late mTORC1-derived inhibitory feedback loops. (**B**) Representative WB image and quantification (log2FC) of p-TSC2^{Thr1462} & p-Akt^{Thr308} from IFNβ-treated NSCs normalized to control. Bars represent the mean value. One-way ANOVA for the biphasic response test. p-TSC2^{T1462} ***($P < 0.001$), p-Akt^{T308} **($P = 0.003$). n = 4 biological replicates. (**C**) Representative WB image and quantification (log2FC) of p-Akt^{Ser473} from IFN-β-treated NSCs normalized to control (t = 0 h). Bars represent the mean value. One sample t-test was computed, with no significant results. n = 3 biological replicates."

3.2.4 The biphasic regulation of protein synthesis by interferon is dependent on but not exclusive to mTORC1 activity

The JAK/STAT-PI3K crosstalk signaling converges to the main regulator of mTOR activity, TSC1/2 (Figure 3.9A). To validate our findings, I generated TSC2 knockout NSCs and evaluated their response to interferon β. For this, Marc Zumwinkel designed and evaluated the targeting efficiency of gRNAs targeting exons 2,3, 4, and 5 of TSC2 under my supervision. He concluded that the gRNA targeting exon 2 was the most efficient (not shown). I then nucleofected NSCs with a plasmid containing both the gRNA and SpCas9 and sorted individual NSCs for single colony growth. The assessment of TSC2 expression by western blot lead us to classify our resulting clones in two different groups: 1) NSCs that did not change their TSC2 expression levels compared to wt NSCs -TSC2^{cntrl}-, and 2) NSCs that reduced their TSC2 expression levels to at least half of the wt levels -TSC2^{mut}-. I included TSC2^{cntrl} NSCs as an additional control to the nucleofection, FACS-sorting, and single-growth manipulations, in case this could compromise the response of these NSCs to interferons. Overall, given the low efficiency of nucleofection and survival, I obtained two TSC2^{cntrl} and four TSC2^{mut} NSC clones (Figure 3.10A). Of note, I could never find a full knockout of TSC2 in none of our screenings. This might be due to the low efficiency of nucleofection and clone expansion rather than the potential lethality of this genotype in NSCs as different groups have

generated similar knockouts in the past (Costa *et al*, 2016; Grabole *et al*, 2016; Blair *et al*, 2018).

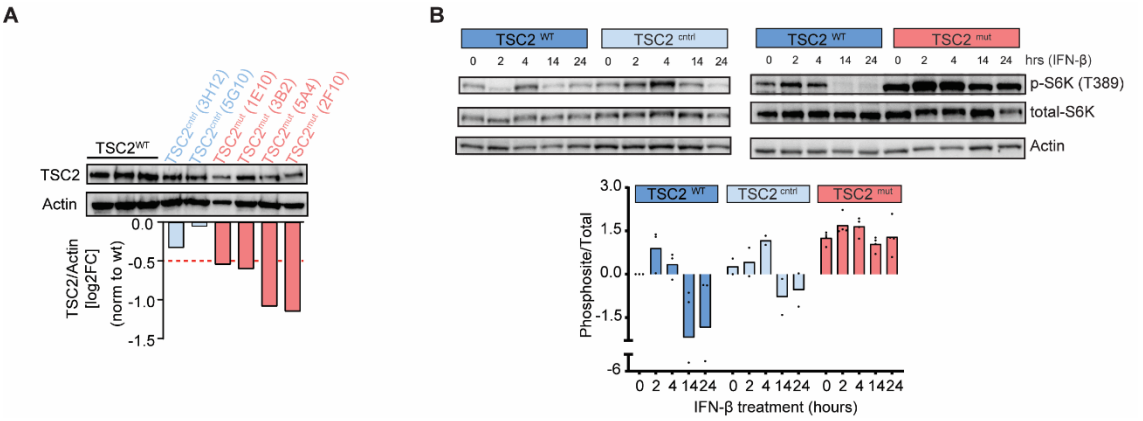

Figure 3.10: TSC2^{mut} NSCs confirm the role of mTORC1 in the biphasic control of mRNA translation

Figure and caption adapted from Carvajal Ibañez *et al*, 2023 "(**A**) WB images and quantifications of TSC2 relative to actin beta and normalized to TSC2WT NSCs in different CRISPR-mutated (TSC2^{mut}) or CRSPR-non-mutated (TSC2^{cntrl}) NSC clones. (**B**) Representative WB images and quantifications (log2FC) of p-p70S6K^{Thr389} in TSC2^{WT}, TSC2^{cntrl} & TSC2^{mut} NSCs treated with IFN-β and normalized to vehicle TSC2^{WT}. Bars represent the mean value. n = 2–4 clonal replicates."

I then exposed these TSC2^{WT}, TSC2^{cntrl,} and TSC2^{mut} NSCs to interferon β and assessed their mTOR activity using p-S6K^{Thr398} as a readout (Figure 3.10B). TSC2^{WT} and TSC2^{cntrl} displayed a similar biphasic regulation of p-S6K^{Thr398}. Differently, TSC2^{mut} NSCs displayed a strong basal upregulation of mTOR activity, that remained oblivious to the interferon treatment. This underscored the relevance of TSC2 in regulating both the early and late modulation of mTORC1 activity.

To address whether the lack of mTORC1 modulation would also lead to an absence of changes in global mRNA translation, I analyzed the distribution of cellular mRNAs along the polysome profiles in these NSCs. Upon 14 hours of interferon treatment, TSC2^{WT} and TSC2^{cntrl} NSCs displayed a strong depletion of mRNAs in the heavy polysomal fractions and a significant increase of mRNA-free 60S ribosomal complexes (Figure 3.11A-B). Conversely, TSC2^{mut} NSCs displayed a less drastic reduction of mRNA abundance in heavy polysomes, but maintained an increase in 60S ribosomal complexes, suggesting a non-complete regression of the global mRNA translation shutdown (Figure 3.11C).

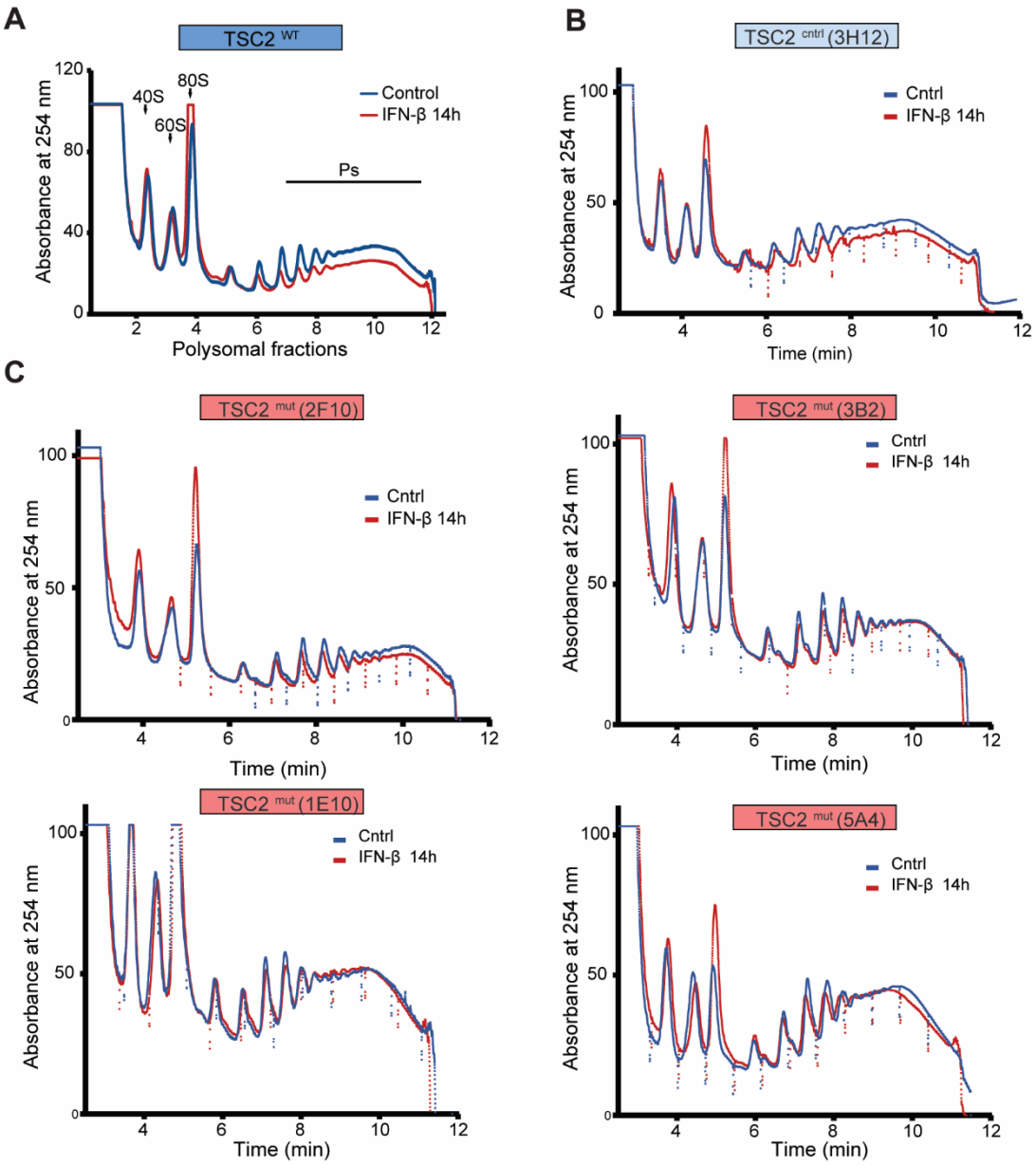

Figure 3.11: TSC2^{mut} NSCs maintain a mild downregulation of global mRNA translation upon IFN treatment

Figure and caption adapted from Carvajal Ibañez *et al*, 2023. "Representative polysome profiles of TSC2^{WT} (**A**), TSC2^{cntrl} (**B**) and TSC2^{mut} (**C**) NSCs treated with IFN-β for 14 h."

To validate whether the knockdown of TSC2 would effectively rescue the downregulation of mRNA translation, I assessed global protein synthesis by OPP incorporation in the TSC2^{mut} NSCs (Figure 3.12A). In line with the polysome profiles, TSC2^{mut} NSCs failed to completely regress the late downregulation of protein synthesis, even in the absence of mTORC1 downregulation (Figure 3.12). This remaining inhibition of protein synthesis indicates that mTORC1 contributes but is not solely responsible for the global mRNA translation shutdown induced by interferon. This data also shows that mTORC1 is

responsible for the transient upregulation of protein synthesis, as deregulation of mTORC1 in TSC2^{mut} NSCs completely rescues this transient increase in OPP incorporation.

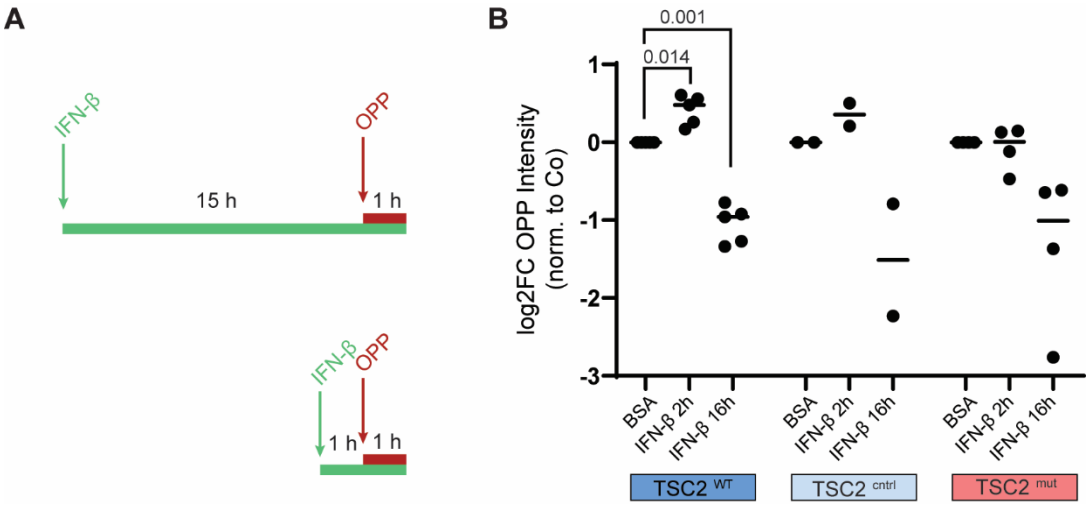

Figure 3.12: Late downregulation of protein synthesis does not rely exclusively on mTORC1 activity

Figure and caption adapted from Carvajal Ibañez *et al*, 2023 "(**A**) Schematic representation of the OPP (O-propargyl-puromycin) experimental setup. (**B**) Quantification of the OPP assay in WT, TSC2^{cntrl} & TSC2^{mut} NSCs treated with IFN-β at 2 and 16 h. Two-way ANOVA with Dunnett's multiple comparison tests was computed (P-values specified). n = 5 biological replicates for WT NSCs and 2–3 clonal replicates for TSC2cntrl & TSC2mut NSCs, respectively."

3.2.5 Phosphorylation of eIF2α drives the late shutdown of protein synthesis by interferon.

As the lack of regulation of mTORC1 in TSC2^{mut} NSCs failed to rescue the late shutdown of protein synthesis, interferon β might induce additional mechanisms shaping this late response. In addition to the non-canonical signaling pathway, the canonical signaling of interferon induces the expression of ISGs that interfere with mRNA translation (Ivashkiv & Donlin, 2014). One of these ISGs is the protein kinase R (Pkr; *Eif2ak2*). Pkr inhibits global eukaryotic mRNA translation by phosphorylating the alpha subunit of the translation initiation factor eIF2 (p-eIF2α^{S51}) (Gal-Ben-Ari *et al*, 2019). Interestingly, although Pkr expression is highly induced upon interferon binding, the activation of Pkr requires the presence of dsRNA, which typically indicated the presence of a viral infection (Gal-Ben-Ari *et al*, 2019).

I hypothesized that, given the particular intrinsic properties of interferon response in NSCs, sensing of extrinsic interferons might be sufficient to also activate the antiviral function of Pkr. I first confirmed that NSCs upregulated the expression of Pkr in the

phosphoproteome dataset introduced in section 3.2.2, page 71 (Figure 3.13A-B). Surprisingly, NSCs did not only increase Pkr protein levels but also displayed increased phosphorylation of p-eIF2αS51 (Figure 3.13C). Phosphorylation of p-eIF2α^{S51} upon interferon treatment also led to increased use of uORFs in a subset of genes in NSCs, as shown by our Ribo-Seq results (Figure 3.13D). Importantly, the upregulation of p-eIF2α^{S51} takes place only upon extended incubation with interferon β indicating 1) that phosphorylation of eIF2α is only relevant for the late component of the biphasic regulation of protein synthesis and 2) that phosphorylation of eIF2α requires transcriptional upregulation of Pkr.

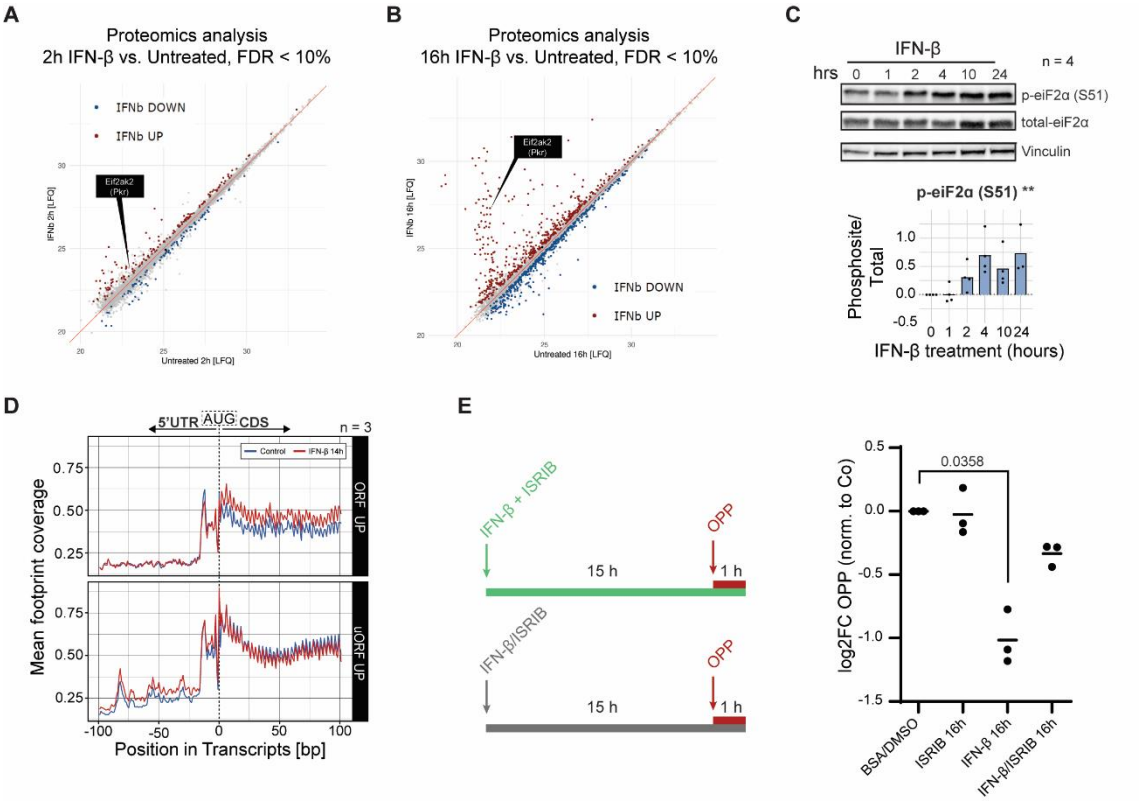

Figure 3.13: The Phosphorylation of eIF2α drives the late shutdown of protein synthesis caused by interferon β

Figure and caption adapted from Carvajal Ibañez *et al*, 2023 "Relate label-free quantification (LFQ) of proteomics from WT NSCs untreated or treated with IFN-β for 2h (**A**) or 16h (**B**). n = 5 biological replicates. (**C**) Representative WB images and quantifications (log2FC) of p-eIF2α^{S51} in IFN-β-treated NSCs normalized to control (t = 0 h). Bars represent the mean value. Spearman's rank correlation test. p-eIF2α^{S51} **(P = 0.003724). n = 4 biological replicates. (**D**) Coverage profile of ribosome-protected reads (footprints) in genes with upregulated canonical (upper) or alternative upstream (lower) ORFs upon extended IFN-β treatment. Nucleotide 0 depicts the start codon (AUG) marking the interface between the 5′ untranslated region (5' UTR) and coding sequence (CDS). (**E**) Schematic representation of the OPP (O-propargyl-puromycin) experimental setup in the presence or absence of the integrated stress response inhibitor (ISRIB). One-way ANOVA with Tukey's multiple comparison test was computed (P-values specified). n = 3 biological replicates."

To finally confirm the causality between the phosphorylation of eIF2α and the late shutdown of global protein synthesis, I blocked the effect of p-eIF2α^{S51} with the Intrinsic Stress Response Inhibitor (ISRIB; Sidrauski *et al*, 2015) and assessed protein synthesis by OPP incorporation (Figure 3.13E, left panel). ISRIB treatment blocks the effects of eIF2α phosphorylation by binding to the translation initiation factor 2B (eIF2B) and allosterically preventing the binding and resulting inhibition caused by p-eIF2αS51 (Sidrauski *et al*, 2015). As a result, the combination of ISRIB and interferon β successfully reversed the late global inhibition of protein synthesis (Figure 3.13E, right panel). This underscores the major role of Pkr and p-eIF2α^{S51} in the late shutdown of protein synthesis exerted by interferon.

3.2.6 Interferon uncouples mTOR activity to the cell cycle in NSCs

Stepping away from the complexity of the signaling pathways into the global picture of the interferon response, it did not escape my attention that interferon induced a transient activation of mTOR while simultaneously promoting the exit of cell cycle (see section 3.1.1, page 60; and section 3.2.1, page 68).

To validate whether cell cycle was indeed repressed already in the early interferon response, I assessed, together with Dr. Maxim Skabkin, the regulation of the cell cycle by interferon in the G_1-S cell cycle checkpoint. I decided to focus on this cell stage checkpoint as I previously observed that interferon does not only push most of the cells out of the cell cycle (G_0) but also increases the length of G_1 significantly (see section 3.1.1, page 60; Figure 3.2C). One major regulator at the cell cycle G_1-S checkpoint is the cyclin-dependent kinase complex Cdk4/6. Interestingly, Cdk4/6 was recently appointed as a dual regulator of mTOR activity and cell cycle, underscoring its potential role in the interferon response in NSCs (Romero-Pozuelo *et al*, 2020). When active, the Cdk4/6 complex phosphorylates Rb1 and licenses transcription of S phase cell cycle genes (Topacio *et al*, 2019). Indeed, phosphorylation of Rb1 at Ser780 was gradually reduced upon interferon treatment in NSCs (Figure 3.14A). This gradual inhibition indicates that interferon represses Cdk4/6 activity already at early incubation times, disconnecting cell proliferation and growth transiently in NSCs. As the activity of Cdk4/6 is largely regulated by its regulatory partner, cyclinD1 (*Ccnd1*) (Topacio *et al*, 2019), I explored the differential regulation of CyclinD1 in the phosphoproteome dataset introduced in section 3.2.2, page 71. I found that interferon treatment increased the phosphorylation levels of p-CyclinD1^{T286} (Table Supl. 2). Phosphorylation at Thr286 prevents Cdk4/6 activation by inducing nuclear export of CyclinD1 and promoting CyclinD1 degradation in the cytosol

(Guo *et al*, 2005). This suggests that CyclinD1 is an additional target of regulation by interferons in NSCs.

Interestingly, Romero-Pozuelo *et al*. described that Cdk4/6 coordinates cell cycle and mTOR by targeting the phosphorylation of p-TSC2^{Ser1452} (Romero-Pozuelo *et al*, 2020). I found that interferon was also reducing phosphorylation of p-TSC2^{S1452} slightly in NSCs, in line with the findings of Romero-Pozuelo *et al*. Decreased p-TSC2^{S1452} should cause an early downregulation of mTOR activity, which I do not observe in NSCs (see section 3.2.1). However, this mild decrease in p-TSC2^{S1452} is blunted by a strong upregulation of p-TSC2^{T1462}, caused by simultaneous PI3K-Akt-crosstalk (Figure 3.9B), resulting in the early upregulation of mTORC1 (Figure 3.14C).

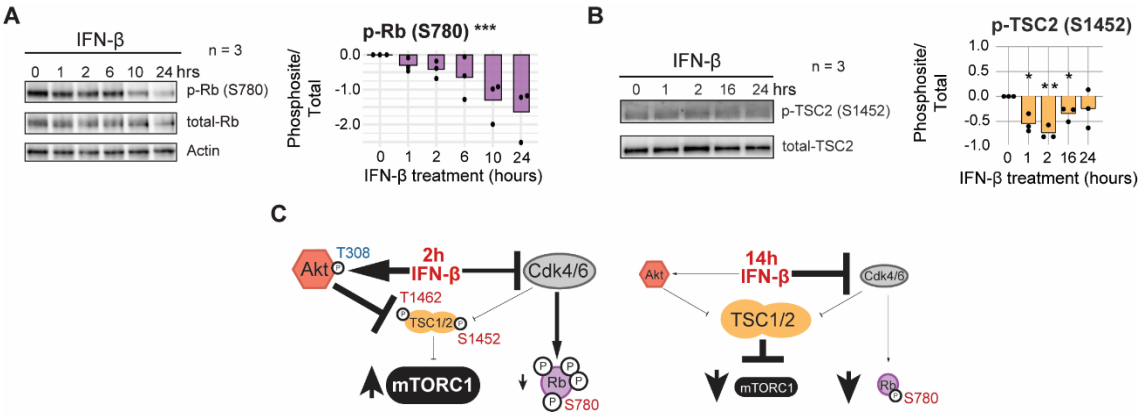

Figure 3.14: Interferon uncouples mTOR activity to the cell cycle in NSCs

Figure and caption adapted from Carvajal Ibañez *et al*, 2023. "(**A**) Representative WB image and quantifications (log2FC) of p-Rb1^{Ser780} from IFN-β-treated NSCs normalised to control (t = 0 h). Bars represent the mean value. Spearman's rank correlation test. p-Rb1^{S780} ***(P = 5.37e-06). (**B**) Representative WB image and quantification (log2FC) of p-TSC2^{Ser1452} from IFN-β-treated NSCs normalized to control (t = 0 h). Bars represent the mean. One sample t-test was computed. One hour *(P = 0.017), 2 h **(P = 0.00565), 16 h *(P = 0.0268). (**C**) Schematic representation of the prevailing signaling pathways driving the early inhibition and late activation of mTORC1."

3.3 The interferon-driven transient activation of mTOR inhibits the translation of Sox2 via its 5'PRM motif

Concomitant inhibition of cell cycle and protein translation was shown to reduce Sox2 translation on the onset of differentiation on NSCs (Baser *et al*, 2019). Baser *et al*. also showed that inhibition of protein synthesis alone failed to repress Sox2. Now, I find that interferon simultaneously induces a biphasic control of mTOR activity and an inhibition of the cell cycle, which leads to the late repression of both pathways. I, therefore,

hypothesized that interferon could be the driver regulator of Sox2 translation in NSCs, influencing their bias towards differentiation or quiescence.

3.3.1 Interferon represses Sox2 translation in NSCs.

To prove whether interferon would downregulate the translation of Sox2, Dr. Maxim Skabkin performed polysome profile RT-qPCR of NSCs treated with interferon β at early and late incubation times. He found that interferon was indeed influencing the translation efficiency of Sox2, inducing a relocation of Sox2's mRNAs from heavy polysomal to ribosome-free fractions, especially upon extended incubation (Figure 3.15A). I confirmed that interferon treatment also reduced Sox2 protein levels slightly upon extended incubation (Figure 3.15B). This underscores the relevance of interferon as a key regulator of stemness.

Interestingly, the repression of Sox2 did not follow a biphasic regulation. Whilst global mRNA translation was upregulated at 2 hours (Figure 3.5), Sox2 mRNA started being simultaneously depleted from heavy polysome fractions in this early incubation (Figure 3.15A, left panel). This suggests an unexpected and more complex regulation of Sox2 translation by interferon.

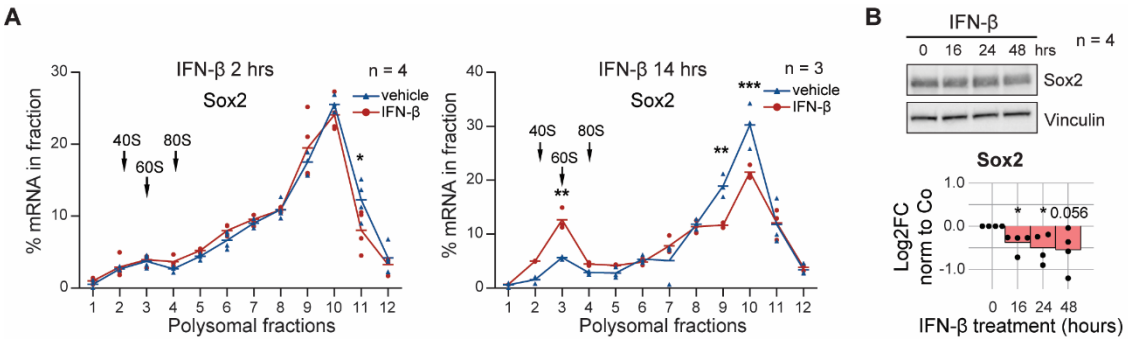

Figure 3.15: Interferon represses translation of *Sox2* in NSCs

Figure and caption adapted from Carvajal Ibañez *et al*, 2023. "(**A**) Polysome profiling (RT-qPCR) of *Sox2* mRNA upon 2 and 14 h IFN-β treatment. Hyphens represent the mean of biological replicates. Arrows represent the 40S, 60S, and 80S subunits of the ribosome. Two-way ANOVA with Šídák's multiple comparison test was computed. 2 h: fraction 11 * (P = 0.0206); 14 h: fraction 3 **(P = 0.0042), fraction 9 **(P = 0.0028), fraction 10 ***(P = 0.0003). n = 4 (2 h) or 3 (14 h) biological replicates. (**B**) Representative WB image and quantification (log2FC) of *Sox2* from IFN-β-treated NSCs normalized to control (t = 0 h). Bars represent the mean value. One sample t-test was computed. 16 h *(P = 0.0219), 24 h **(P = 0.03), 48 h (P = 0.056). n = 4 biological replicates."

3.3.2 The interferon-mediated transient activation of mTORC1 drives the repression of Sox2 translation in NSCs

Next, I aimed to uncover the nature of this complex repression of *Sox2* translation induced by interferon treatment. Given the mild repression of *Sox2* early in the interferon response, I hypothesized that the transient activation of mTOR could be driving the inhibition of *Sox2*. To validate this hypothesis, I employed a luciferase-reporter system that assesses the translation efficiency of different mRNAs upon interferon treatment. Dr. Maxim Skabkin created luciferase reporter constructs with the 5' UTR fragments of *Sox2*, *Rps21* (TOP-mRNA), and *Actb* (Figure 3.16A). Using this luciferase system, I aimed to: 1) assess whether the transient activation of mTOR drives repression of *Sox2*, 2) confirm that *Sox2* inhibition is mediated by mTORC1, and not mTORC2, and 3) assess whether the late increase in p-eIF2α^{S51} is involved in controlling the translation of *Sox2*.

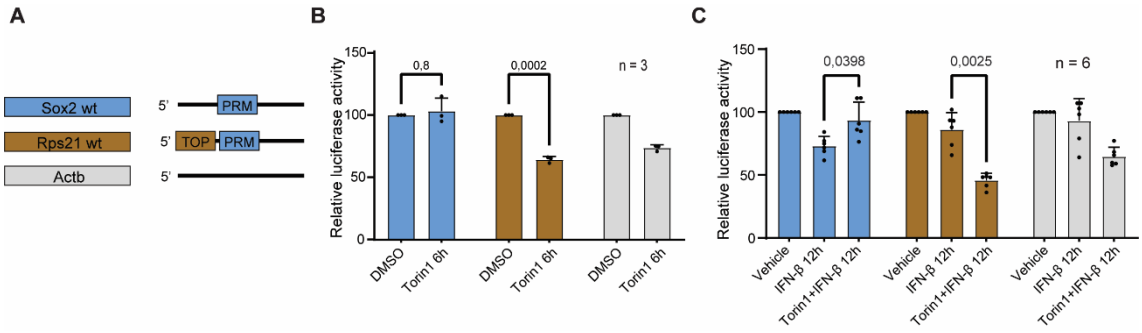

Figure 3.16: Repression of *Sox2* translation by interferon relies on the transient activation of mTOR

Figure and caption adapted from Carvajal Ibañez *et al*, 2023. "(**A**) 5'UTR constructs priming renilla luciferase controlled by the upstream 5'UTR fragment from *Sox2*, *Rps21* and *Actb*. TOP = 5'Terminal Oligopyrimidine motif; PRM = 5' Pyrimidine Rich Motif. (**B**) Luciferase activity assay in NSCs treated with Torin1. Data are normalized to vehicle and are represented as mean ± SD. n = 3 biological replicates. Two-way ANOVA test with Ŝídák's multiple comparison test (P-values specified). (**C**) Luciferase activity controlled by the upstream 5'UTR fragment from *Sox2*, *Rps21,* and Actb. Data are normalized to vehicle and are represented as mean ± SD. n = 6 biological replicates. Two-way ANOVA with Tukey's multiple comparisons test (P-value specified)."

First, to assess whether the transient activation of mTOR drives repression of Sox2, I blocked this transient activation by Torin1 treatment. Torin1 treatment alone failed to repress *Sox2* translation, as previously reported (Baser *et al*, 2019), but effectively reduced the expression of TOP-mRNAs such as *Rps21* (Figure 3.16B). As expected, interferon β treatment alone successfully repressed both *Sox2* and *Rps21* translation in NSCs (Figure 3.16B). Interestingly, the absence of the transient activation of mTOR by combined torin1+interferon β treatment failed to downregulate *Sox2* translation whilst

deepening the translation inhibition of *Rps21* (Figure 3.16C). This unveils the importance of the transient upregulation of mTORC1 and the uncoupling of cell cycle and protein synthesis as the trigger of *Sox2* repression in NSCs.

Second, I aimed to confirm the selective role of mTORC1, over mTORC2, in repressing the translation of *Sox2*. I chose to block mTOR activity with Torin1 because, despite its promiscuous effect on both mTORC1 and mTORC2 (Thoreen *et al*, 2009), Torin1 blocks mTORC1 activity completely, different from other inhibitors (Thoreen *et al*, 2012). To effectively confirm the selective causality of mTORC1 and not mTORC2, I blocked the early mTOR upregulation by Rapamycin treatment. Rapamycin inhibits mTORC1 selectively, albeit not to such an extent as Torin1 (Thoreen *et al*, 2012). As expected, rapamycin treatment recapitulated the effects of Torin1 both alone or in combination with interferon β (Figure Supl.5A-B). This confirms the selective role of mTORC1 in the interferon response in NSCs and agrees with the absence of differential p-AktSer473 phospho levels in these NSCs (Figure 3.9).

Third, to assess whether the late phosphorylation of eIF2α also drives the translation repression of Sox2, I blocked the effect of increased p-eIF2α^{S51} with the intrinsic stress response inhibitor (ISRIB). The combined treatment of ISRIB and interferon β reversed the repression of *Rps21* but not *Sox2* translation (Figure 3.17). This underscores the relevance of mTORC1 activity on the translation of Sox2, regardless of the global protein synthesis levels exerted by p-eIF2α^{S51}.

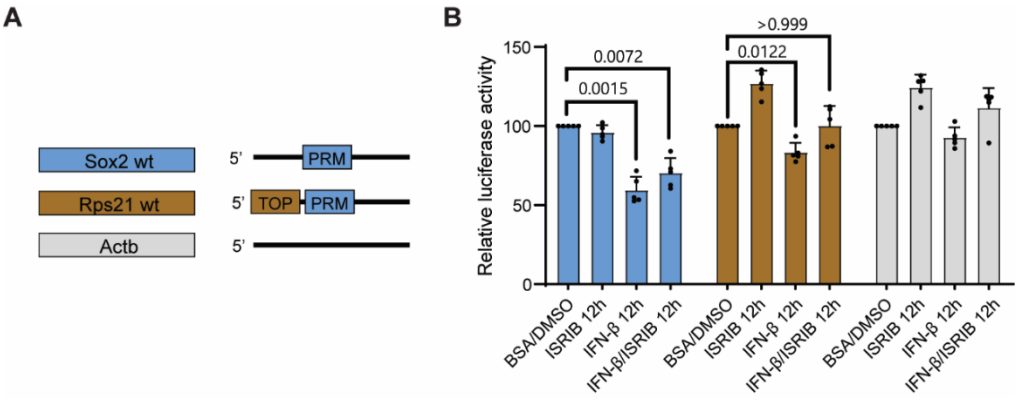

Figure 3.17: Global protein synthesis shutdown by p-eIF2 α^{S51} does not drive repression of *Sox2*

Figure and caption adapted from Carvajal Ibañez *et al*, 2023. "(**A**) 5'UTR constructs priming renilla luciferase controlled by the upstream 5'UTR fragment from Sox2, Rps21 and Actb. TOP = 5'Terminal Oligopyrimidine motif; PRM = 5' Pyrimidine Rich Motif. (**B**) Luciferase activity assay in NSCs treated with the integrated stress response inhibitor (ISRIB) and IFN-β. Data are normalized to vehicle and are represented as mean ± SD. n = 5 biological replicates. Two-way ANOVA test with Ŝídák's multiple comparison test (P-values specified)."

3.3.3 Repression of Sox2 translation relies on its 5'UTR PRM motif

I then set my focus on deciphering how the transient activation of mTORC1 was driving the selective inhibition of *Sox2* and not other mTORC1-sensitive mRNAs like *Rps21*. Previous results pointed out the presence of a 5'UTR motif in mRNAs that were post-transcriptionally downregulated in the exit of stem cell activation, including *Sox2* (Baser *et al*, 2019) (Figure 3.18A). This motif coined pyrimidine-rich motif (PRM) consists of a stretch of 6 pyrimidine bases located in the 5'UTR of the mRNAs (Baser *et al*, 2019). However, different from the 5'UTR start position of the TOP motif, PRM is located downstream, inside the 5'UTR (Figure 3.18A). Together with Dr. Maxim Skabkin, I decided to study the implication of the PRM motif in the repression of *Sox2*. Dr. Maxim Skabkin cloned mutated versions of the 5'UTR constructs of *Sox2* and *Rps21* to assess their translation efficiency in the luciferase assay (Figure 3.18B). As a control, the mutant *Rps21* with its natural TOP motif, remained susceptible to mTOR. I then assessed the translation efficiency of these targets and found that the 5'PRM motif in *Sox2* is necessary for the effective repression of *Sox2* translation (Figure 3.18C). Differently, the PRM motif did not affect the translation of *Rps21*, whose inhibition was mainly driven by its TOP motif.

Overall, the post-transcriptional repression of *Sox2* underscores the relevance of yet overlooked mechanisms selectively targeting its 5'UTR PRM motif.

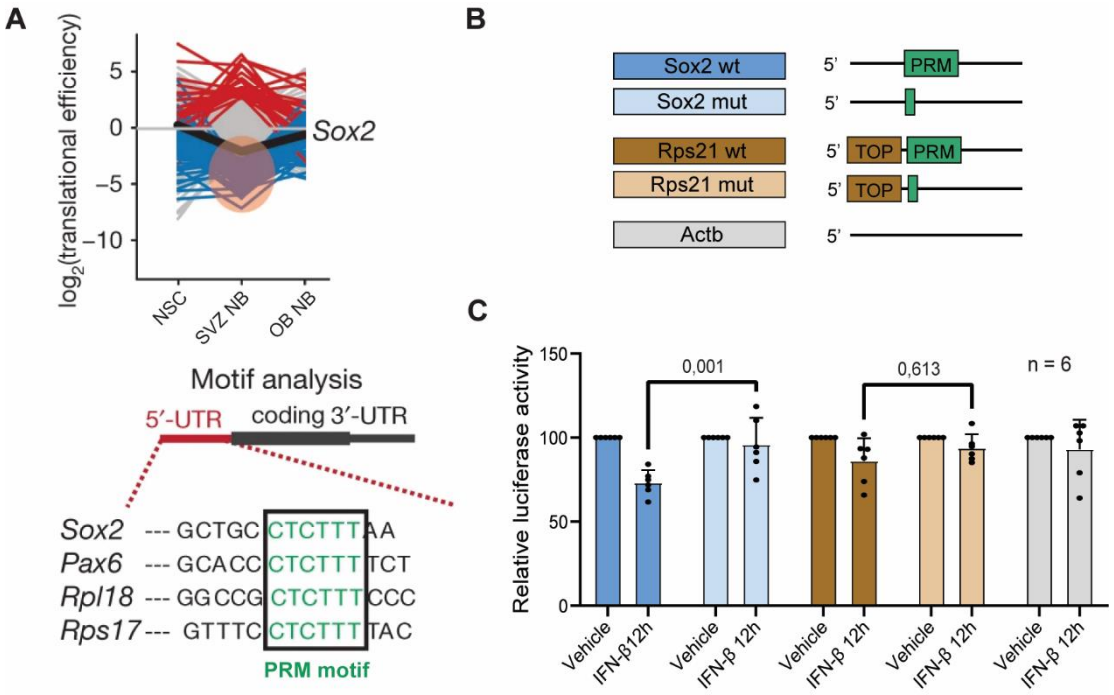

Figure 3.18: The 5'PRM motif drives the IFN-mediated repression of *Sox2* translation

(Figure caption located on the next page)

3.4 IFIT1 influences translation efficiency and mRNA abundance in NSCs

I have so far described how interferons target NSCs at all ages and regulate protein synthesis and the translation of Sox2 in NSCs. Despite my focus on how interferon regulates mRNA translation by the PI3K-crosstalk, I also observed that the transcriptional upregulation of ISGs, such as Pkr, also influenced protein synthesis in NSCs (see section 3.2.5, page 79) (Mazewski *et al*, 2020; Platanias, 2005).

Another example of these ISGs is IFIT1, which is upregulated in the vSVZ in aging (Baruch *et al*, 2014). IFIT1 is an RNA-binding ISG that prevents translation initiation of its target RNAs (Habjan *et al*, 2013). However, IFIT1 does not typically target eukaryotic mRNAs. As an antiviral effector, IFIT1 binds capped lowly-2′-O-methylated mRNAs (cap0), typical of viral RNAs (Abbas *et al*, 2017) (Figure 1.8). I hypothesized that different from its classic antiviral function, IFIT1 could be targeting eukaryotic mRNAs and modulating protein translation in NSCs.

3.4.1 IFIT1 binds eukaryotic mRNAs involved in neural stem cell activation and differentiation

To first evaluate whether IFIT1 was also targeting eukaryotic mRNAs in NSCs, Dr. Maxim Skabkin implemented an IFIT1-IP RNA sequencing to analyze the mRNAs bound to IFIT1 in NSCs. Dr. Maxim Skabkin generated CRISPR-mediated IFIT1-myc knock-in NSCs, and immunoprecipitated IFIT1-myc in NSCs treated with interferon β (Figure 3.19A-C). The immunoprecipitation revealed a range of different sizes of RNA molecules associated with IFIT1 (Figure 3.19D). Samples were divided into three fractions (small, medium, and large) using the first for tRNA- and the two later for mRNA-analysis (Figure 3.19D). The IFIT1-IP dataset was analyzed by Manuel Goepferich, who found 248 eukaryotic mRNAs significantly enriched in the medium and large IFIT1-IP fractions (Figure 3.19E) (See top 100 in Table Supl. 3). Of note, the gene set enrichment analysis (GSEA) of the IFIT1 targeted mRNAs showed enrichment of mRNAs involved in stem

Related to Figure 3.18:

Figure and caption adapted from Carvajal Ibañez *et al*, 2023. (**A**) Post-transcriptional downregulation of PRM-containing mRNAs in the NSC-to-NB transition as adapted from Baser *et al*, 2019. "(**B**) Schematic representation of the 5'UTR constructs priming the renilla luciferase. TOP = 5'Terminal Oligopyrimidine motif; PRM = 5' Pyrimidine Rich Motif. (C) Luciferase activity is controlled by the upstream 5'UTR fragment from *Sox2* (WT and mutant), *Rps21* (WT and mutant), and *Actb*. Data are normalized to vehicle and are represented as mean ± SD. n = 6 biological replicates. Two-way ANOVA with Tukey's multiple comparisons test (P-value specified)."

cell homeostasis processes such us “cell differentiation in spinal cord”, “neuron fate commitment”, and “BMP signaling pathway” (Figure 3.19F). BMP signaling is highly related to the quiescence induction of NSCs, suggesting a link between IFIT1 and the regulation of stem cell activation (Mira *et al*, 2010).

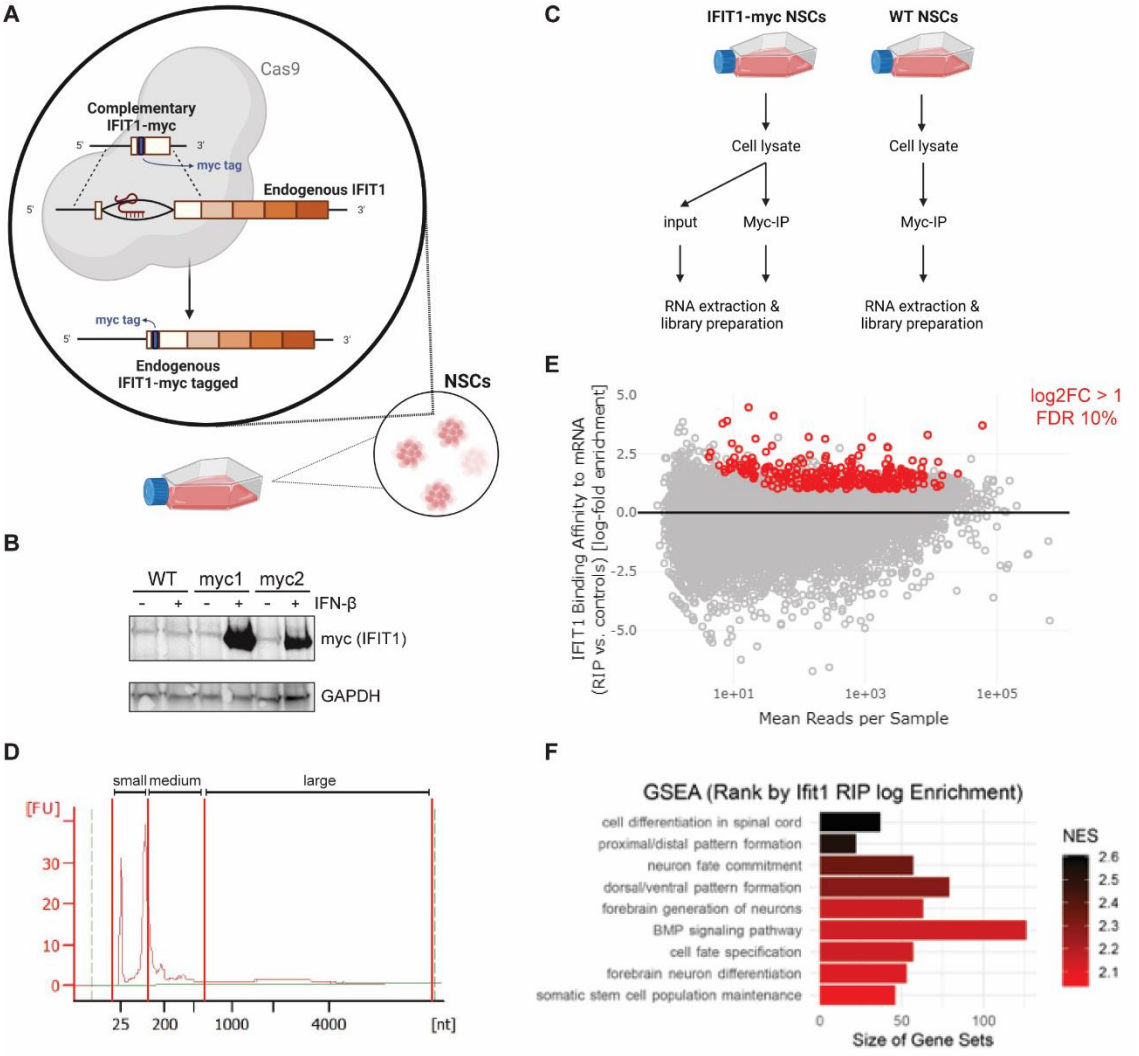

Figure 3.19: IFIT1 binds mRNAs relevant for stemness in NSCs

(**A**) Illustrative representation of the CRISPR/Cas9-mediated knock-in of myc into *Ifit1* in NSCs. (**B**) Representative WB of myc and GAPH in control WT or myc-tagged NSC clones. (**C**) Schematic representation of the experimental set-up for the IFIT1-IP experiment. (**D**) Representative plot of the size distribution of the IFIT1-IP-recovered RNA. (**E**) MA plot of differential enrichment of RNA-immunoprecipitation (RIP) in the IFIT1-myc tagged NSCs as compared to control NSCs computed with a DESeq2 model. Highlighted red dots display an enrichment higher than a log2FC=1 and a p-value smaller than 0.1 after FDR correction. n = 3 biological replicates. (**F**) Associated GO-terms to panel E.

3.4.2 IFIT1 influences translation efficiency and abundance of its target mRNAs in NSCs

IFIT1 binding at the 5'UTR end of mRNAs outcompetes eukaryotic translation initiator factors, blocking the initiation of translation (Habjan *et al*, 2013). To address whether IFIT1 binding was also affecting the translation efficiency of its target mRNAs in NSCs, I performed Ribo-Seq to NSCs from IFIT1^{WT} or IFIT1^{KO} mice treated with interferon β, together with Dr. Maxim Skabkin. This dataset was analyzed by Manuel Goepferich, calculating the effect of the genotype on translation efficiency (Figure 3.20A). In total, 187 genes displaying a differential translation efficiency (TE) upon interferon treatment in IFIT1^{KO} vs. IFIT1^{WT} were found. Gene ontology (GO) analysis of these differentially-translated genes revealed an enrichment of genes involved in cell-cycle control (Figure 3.20B).

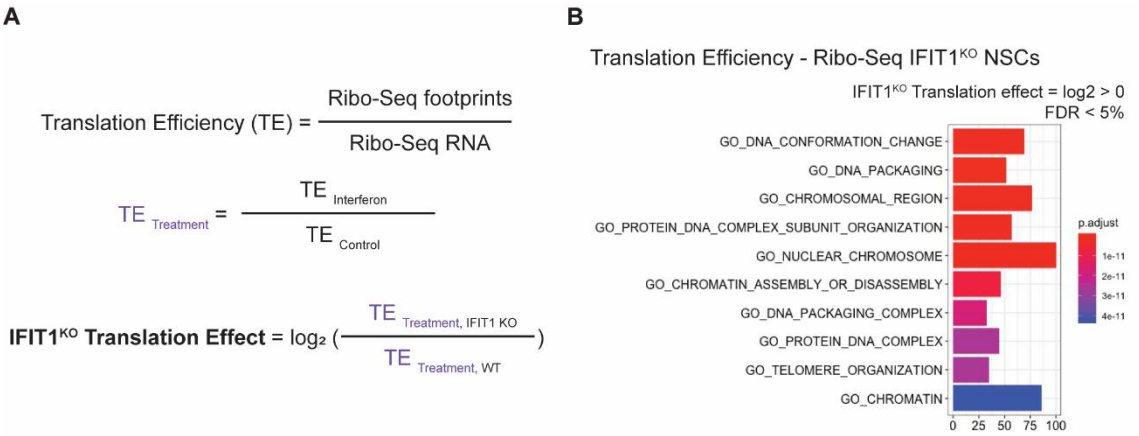

Figure 3.20: Binding of IFIT1 perturbs the efficiency of translation in eukaryotic mRNAs in NSCs

Summary of the scored translation efficiency in the IFIT1^{WT} and IFIT1^{KO} Ribo-Seq dataset (A) and the associated GO-term analysis (B) computed with FDR < 10%, LR-Test in DESeq2. Genes with a P value < 0.1 after FDR correction are used in the analysis. n = 4 biological replicates.

The intersection of the significantly differentially-translated mRNAs with the IFIT1-IP analysis further revealed 99 differentially-translated, IFIT1-binding mRNAs (Table Supl. 4). From those, the focus was set on *Smad6* and *Gadd45g*, genes involved in bone-morphogenic signaling and cell-cycle control, respectively (Mira *et al*, 2010; Zhang *et al*, 2021). As an illustrative example, the Ribo-Seq analysis reveals how in the presence of IFIT1, the translation of *Gadd45g* does not correlate with the interferon-mediated increase in total RNA (Figure 3.21). This underscores the role of IFIT1 in blocking the translation of *Gadd45g*, even in the event of transcriptional upregulation of this gene.

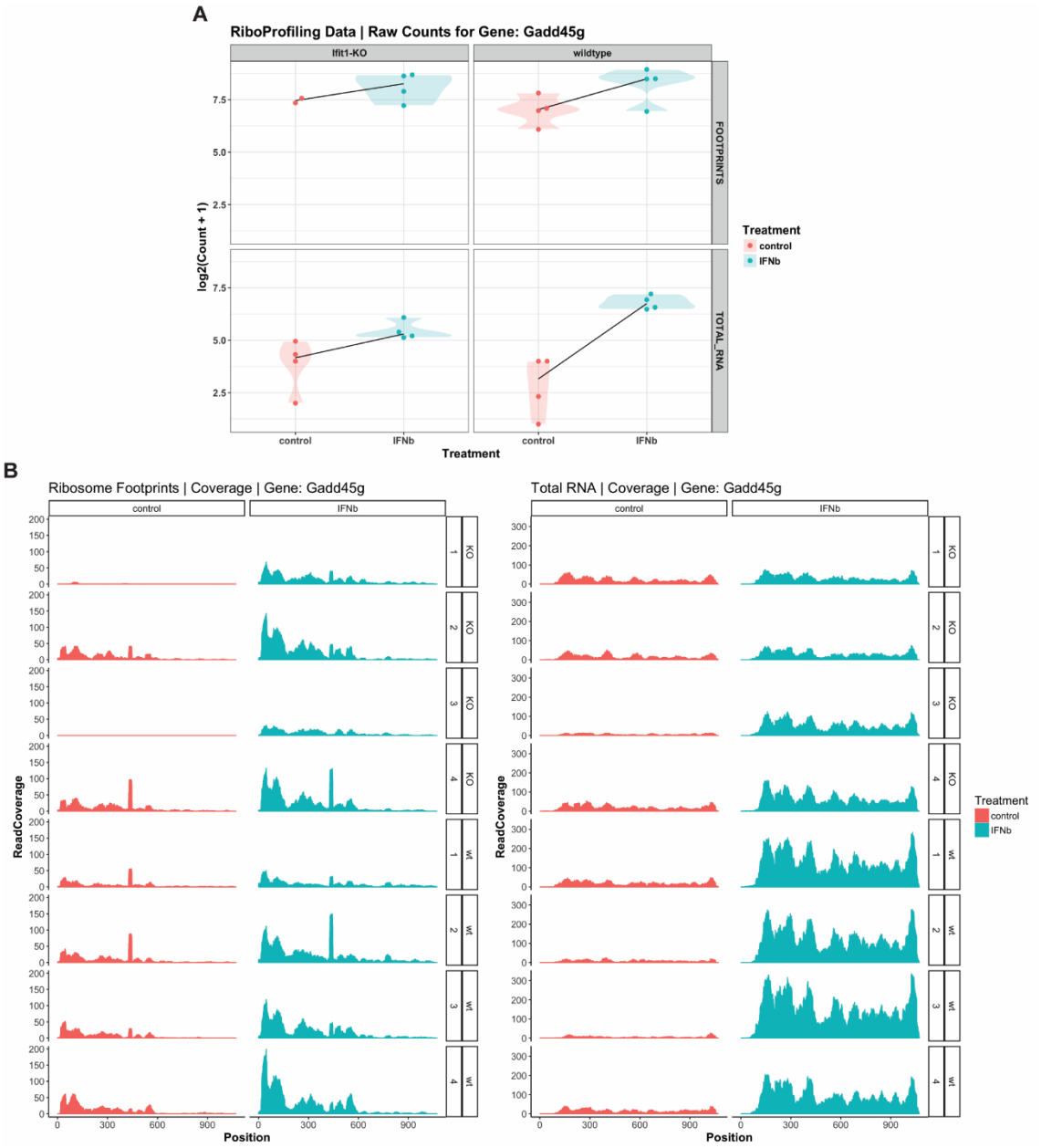

Figure 3.21: IFIT1 restricts translation of *Gadd45g* in NSCs upon interferon treatment

Visualization of the Ribo-Seq results for *Gadd45g* of IFIT1^{WT} and IFIT1^{KO} NSCs treated with interferon β as the combined log2 of the counts of footprints and RNA (**A**) or as the individual gene profile density (**B**). n = 4 biological replicates.

I then aimed to validate the differential translation efficiency of the IFIT1 binders, Gadd45g and Smad6, by polysome profile RT-qPCR (Figure 3.22). Strikingly, the two genes were regulated differentially in opposite directions in WT NSCs. While the translation of Gadd45g was repressed upon interferon treatment, Smad6 showed a tendency to upregulation (Figure 3.22A). In both cases, the absence of IFIT1 prevented the changes in their differential translation, compared to WT (Figure 3.22B). This underscores the relevance of IFIT1 in regulating the translation of eukaryotic mRNAs

such as Gadd45g and Smad6. However, these different modes of regulation also unveil that IFIT1 exerts a more complex role not just repressing mRNA translation, as initially hypothesized.

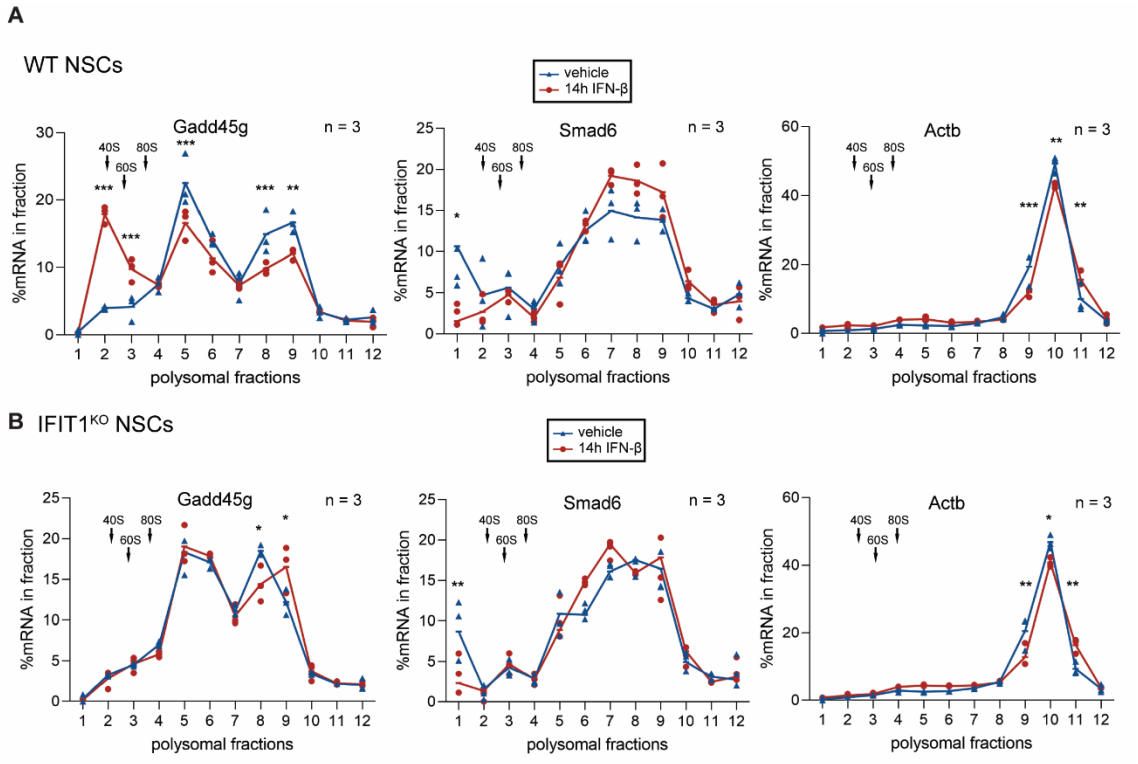

Figure 3.22: IFIT1 restricts translation of Gadd45g but not Smad6 in NSCs upon interferon treatment

Polysome profiling (RT-qPCR) of *Actb*, *Gadd45g,* and *Smad6* from WT (**A**) or IFIT1KO (**B**) NSCs treated for 14 h with IFN-β. Hyphens represent mean of biological replicates. Arrows indicate the 40S, 60S, and 80S subunits of the ribosome. Two-way ANOVA with Šídák's multiple comparison test was computed. WT *Actb*: fraction 9 ***(P = 0.0004), fraction 10 **(P = 0.0028), fraction 11 **(P = 0.0068); WT *Gadd45g*: fraction 2 ***(P < 0.0001), fraction 3 ***(P = 0.0002), fraction 5 ***(P = 0.0001), fraction 8 ***(P = 0.0008), fraction 9 **(P = 0.0024); WT *Smad6* fraction 1 *(P = 0.0393). IFIT1^{KO} *Actb*: fraction 9 **(P = 0.0016), fraction 10 *(P = 0.0213), fraction 11 **(P = 0.0051); IFIT1^{KO} *Gadd45g*: fraction 8 *(P = 0.0285), fraction 9 *(P = 0.0176); IFIT1^{KO} *Smad6* fraction 1 **(P = 0.0023). n = 3 biological replicates.

As IFIT1 binds the 5’ end of mRNAs, I hypothesized that IFIT1 could also be stabilizing mRNAs and protecting them from degradation. I, therefore, assessed the effect of the absence of IFIT1 on the abundance of IFIT1 mRNA binders in NSCs by qPCR. I found that there was heterogeneity in the differential abundance of mRNAs caused by IFIT1 among IFIT1 binders (Figure 3.23). In the absence of interferon, the expression of *Hist4h4* was downregulated while the expression of *Gbx1* was upregulated in IFIT1^{KO} NSCs (Figure 3.23). In the presence of interferon, the expression of *Gadd45g* was downregulated while the expression of *Neurog2* was upregulated in IFIT1^{KO} NSCs

(Figure 3.23). This might suggest a protective role of IFIT1 on mRNA stability during the interferon response in targets like *Gadd45g*. However, the heterogeneity of the response and the opposite trends of mRNA abundance of different targets unveils a more complex regulation.

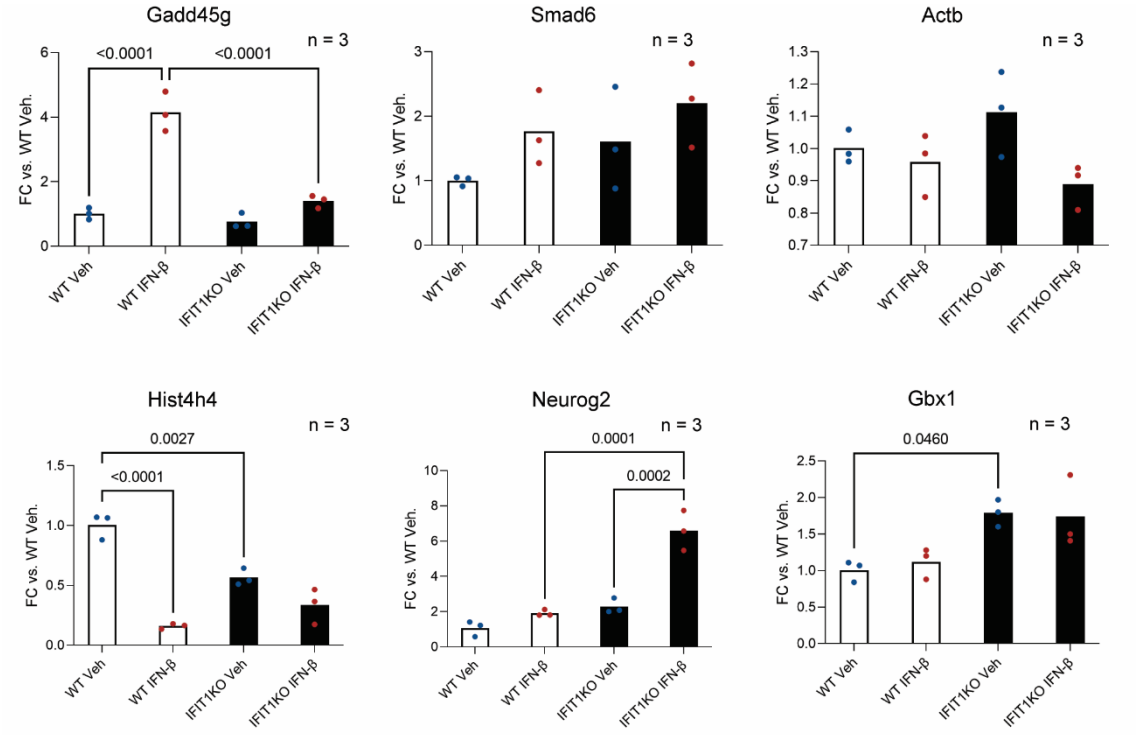

Figure 3.23: Absence of IFIT1 changes the mRNA abundance of a subset of target genes

Bulk RNA rt-qPCR analysis of the specified genes from WT or IFIT1^{KO} NSCs treated with IFN-β or vehicle for 16h. Bars represent mean average of biological replicates. One-Way ANOVA with Tukey's multiple comparison test (p-values specified). n = 3 biological replicates.

3.5 IFIT1 largely recapitulates the effect of interferon in neurogenic dynamics in aging

I showed that IFIT1 binds eukaryotic mRNAs in NSCs and modulates the translation efficiency of relevant stem cell-related mRNAs such as Gadd45g (see section 3.4, page 87). I recently reported that, in animals lacking interferon receptors (IFNAGR^{KO}), the vSVZ-NSC pool is less populated and displays a milder response to aging (Carvajal Ibañez *et al*, 2023). As IFIT1 is a major component of the interferon response, I ought to investigate to which extent is IFIT1 responsible for the effect observed in IFNAGR^{KO} animals. Thus, I hypothesized that by modulating the translation efficiency of specific mRNAs, IFIT1 would also trigger changes in the activation and neural output of NSCs in the brain.

3.5.1 The absence of IFIT1 recapitulates the absence of aging in the vSVZ observed in IFNAGR^{KO} animals

To study the potential role of IFIT1 in adult neurogenesis, I characterized changes in the NSC lineage population dynamics in mice lacking IFIT1 (IFIT1^{KO}). I dissected both the neurogenic origin, the vSVZ, and the destination, OBs, of IFIT1^{WT} and IFIT1^{KO} mice throughout their whole lifespan from 2 to 30 months of age. I excluded debris, doublets, dead cells (sytox blue), leucocytes (CD45+), oligodendrocytes (O4+), and erythrocytes (Ter119+) from the analysis (Figure Supl.6, Figure Supl.7). Similarly to the ISRE-eGFP analysis and based on previous publications (Llorens-Bobadilla *et al*, 2015; Kalamakis *et al*, 2019), I identified NSCs (GLAST^{+}CD133^{+}), aNSCs (GLAST^{+}CD133^{+}EGFR^{+}), qNSCs (GLAST^{+}CD133^{+}EGFR^{-}), TAPs (GLAST^{-}CD133^{-}EGFR^{+}), and vSVZ NBs (GLAST^{-}CD133^{-}PSA-NCAM^{+}) in the vSVZ (Figure Supl.6). In addition, I also FACS-identified OB NBs (PSA-NCAM^{+}) from the dissected OBs (Figure Supl.7).

In the vSVZ, IFIT1^{KO} animals displayed a lower number of NSCs, mainly qNSCs, than IFIT1^{WT} animals at young stages (Figure 3.24A-D). Notably, the abundance of NSCs remained stable throughout the lifespan of the animal, in contrast with the fast decline of IFIT1^{WT} mice (Figure 3.24B). These dynamics largely mimic the changes observed in IFNAGR^{KO} animals (Carvajal Ibañez *et al*, 2023), underscoring the relevant role of IFIT1 in the interferon response. Furthermore, and despite the lower number of total NSCs, IFIT1^{KO} animals produced more neural progenitors (TAPs) and NBs than IFIT1^{WT} animals (Figure 3.24E-F). This increased fraction of TAPs in the absence of IFIT1 suggests that these animals might compensate for the loss of NSCs by regulating the proliferation of TAP progenitors, resulting as a consequence in a bigger NB pool.

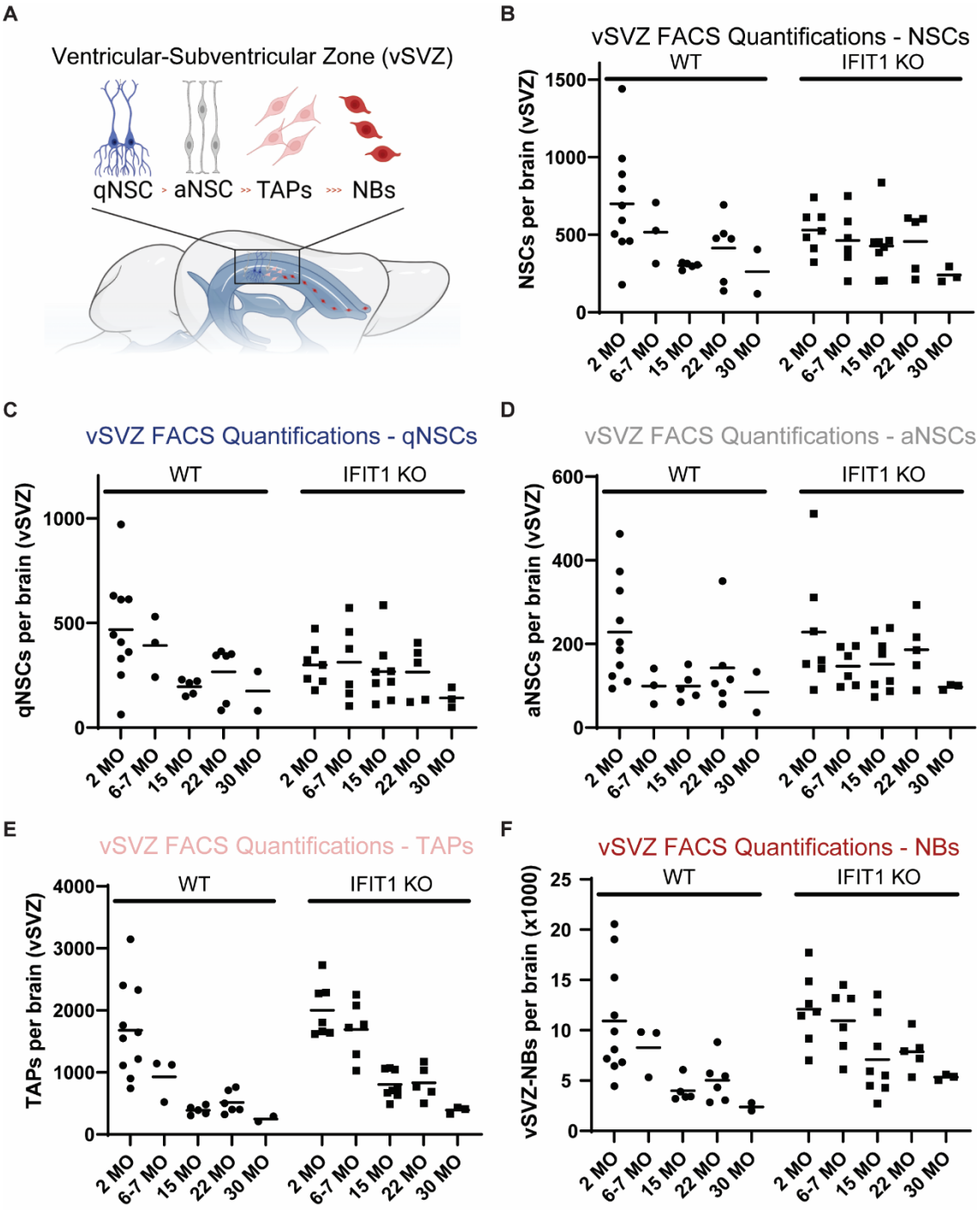

Figure 3. 24: The absence of IFIT1 largely recapitulates the neural lineage dynamics observed in the absence of interferon receptors in the vSVZ

(**A**) Schematic illustration of the neuronal lineage of the ventricular-subventricular zone (vSVZ) from quiescent neural stem cells (qNSC), active NSCs (aNSC), transit-amplifying progenitors (TAPs), migrating neuroblasts (NBs) and neurons at the olfactory bulb. FACS quantifications of NSCs (GLAST^{+}CD133^{+}) (**B**), qNSCs (GLAST^{+}CD133^{+}EGFR^{-}) (**C**), aNSCs (GLAST^{+}CD133^{+}EGFR^{+}) (**D**), TAPs (GLAST^{-}CD133^{-}EGFR^{+}) (**E**), and NBs (GLAST^{-}CD133^{-}PSA-NCAM^{+}) (**F**) of the vSVZ per brain of WT or IFIT1^{KO} animals at different ages. n = 3-10 biological replicates per age and genotype. Hyphens represent mean average of the biological replicates. MO = Months old.

In the OB, the relative increase of neurogenic output observed in the vSVZ was only consistently observed in the middle ages (6-7 and 15 MO) (Figure 3.25). In the young animals (2 MO) this might indicate that despite the higher TAP/NSC ratio observed in these animals (Figure 3.24), the final neurogenic output of NSCs might be decreased in IFIT1^{KO} animals. Conversely, with the progression of age, the absence of IFIT1 seems to be beneficial for the final neurogenic output at the OB at 6 to 15-month-old individuals (Figure 3.25B). In the very old animals, changes in the final neural output seem not to be relevant anymore. The lower production of neural output in young recapitulates the stem cell dynamics observed in IFNAGR^{KO} animals (Carvajal Ibañez *et al*, 2023), underscoring the relevance of IFIT1 as a major component of the interferon response in NSCs.

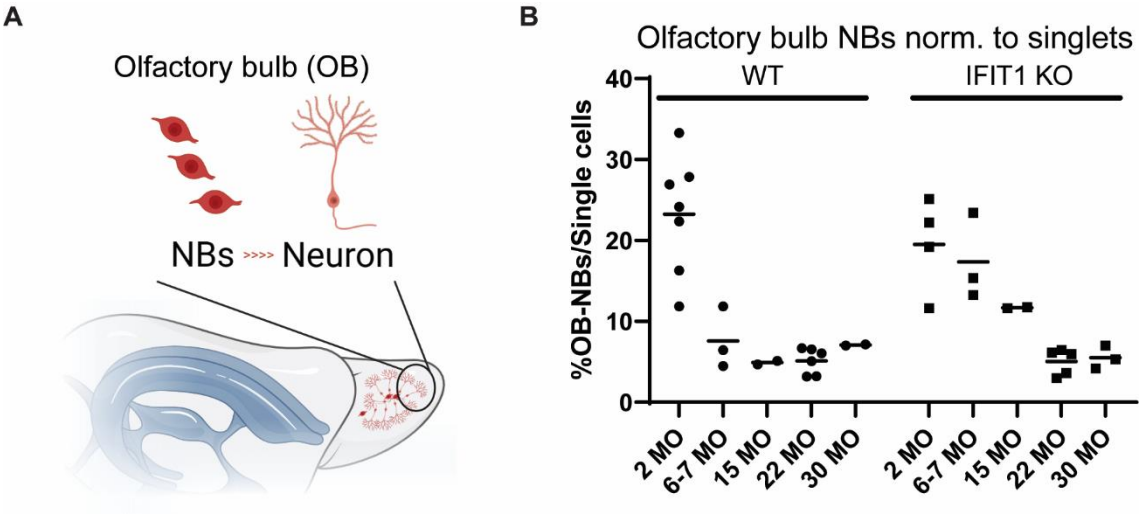

Figure 3.25: The absence of IFIT1 largely recapitulates the neural lineage dynamics observed in the absence of interferon receptors in the OB

(**A**) Schematic illustration of the late neuronal lineage located in the olfactory bulb (OB) including migrating neuroblasts (NBs) and neurons. (**B**) FACS quantifications of NBs (PSA-NCAM^{+}) normalized to single cells of the OB per brain of WT or IFIT1^{KO} animals at different ages. n = 2-7 biological replicates per age and genotype. Hyphens represent mean average of the biological replicates. MO = Months old.

Complementary to the assessment of global changes of NSCs and progenitors in the vSVZ of IFIT1^{WT} and IFIT1^{KO} mice, I aimed to validate the changes in the frequency of activation of NSCs in these animals. I administered BrdU intraperitoneally to young (2 MO) and old (22 MO) IFIT1^{WT} and IFIT1^{KO} animals and sacrificed them after 3 weeks of chase time, as previously described (Figure 3.26) (Kalamakis *et al*, 2019). Cells retaining the BrdU after this 3-week chase period would be considered label-retaining cells (LRC) that were actively dividing during the BrdU treatment and returned to a non-dividing quiescence state afterward. At the sacrificing time, I assessed the fraction of active cells among LRCs, obtaining a better readout of the activation rate of qNSCs at different ages.

I, therefore, quantified the fraction of active LRCs ($BrdU^+Sox2^+KI\text{-}67^+DCX^-$) overall LRCs ($BrdU^+Sox2^+DCX^-$) NSCs (Figure 3.26). I excluded doublecortin (DCX) positive cells to exclude cells that could retain Sox2 protein and remnants of BrdU despite having progressed to a neuroblast stage.

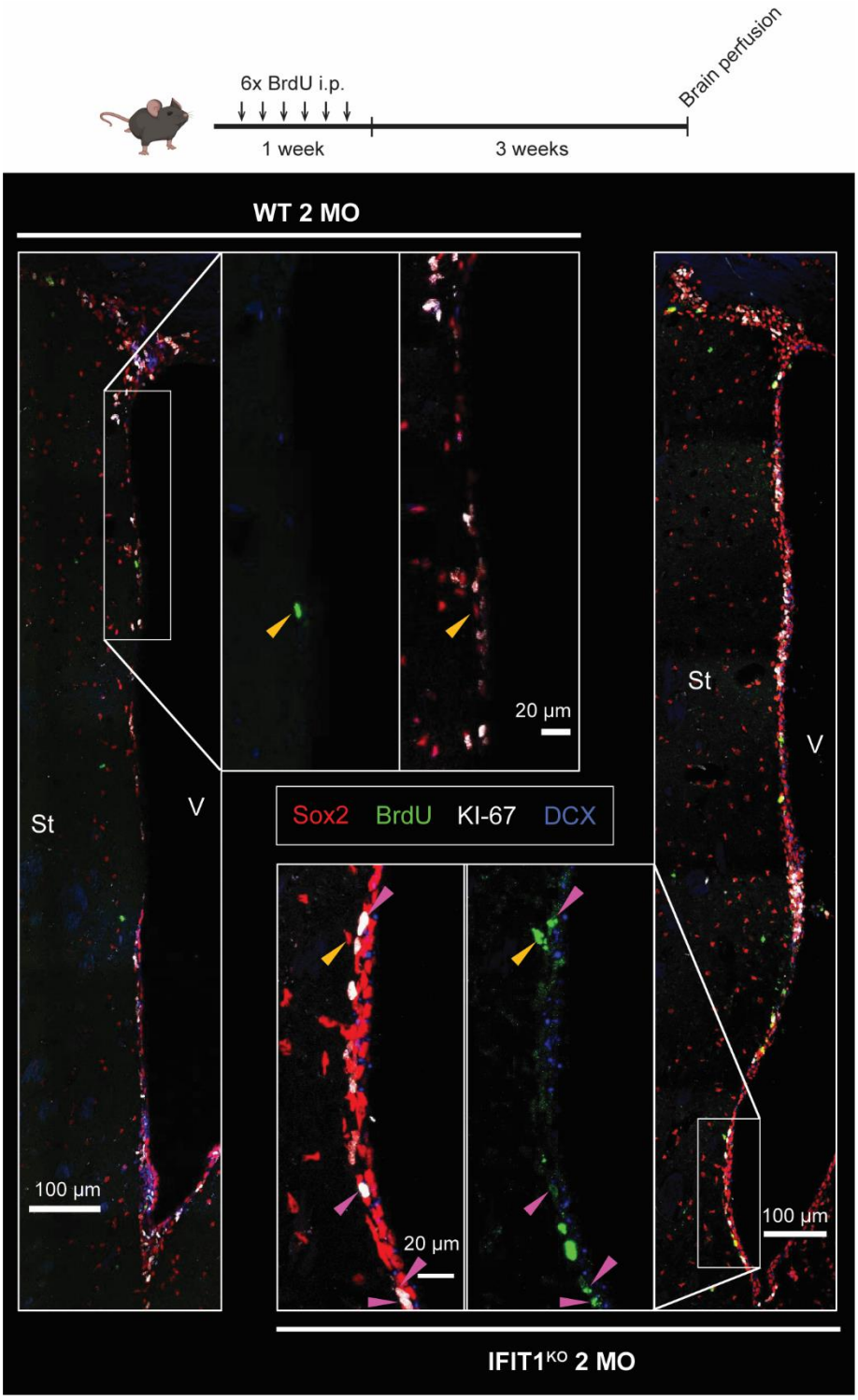

Figure 3.26: Assessment of the activation of BrdU label-retaining NSCs in the vSVZ

(Figure caption located on the next page)

Related to Figure 3.26:

Schematic representation of the BrdU incorporation in the mice (upper panel). Representative images of young IFIT1^{WT} and IFIT1^{KO} vSVZ stained by immunofluorescence (IF). Yellow arrows depict non-active label-retaining cells (non-active LRC; SOX2^{+}BrdU^{+}KI-67^{-}DCX^{-}) and purple arrows depict active LRCs (SOX2^{+}BrdU^{+}KI-67^{+}DCX^{-}). V = Ventricle; St = Striatum. MO = Months old.

Interestingly, IFIT1^{KO} individuals display a higher ratio of active LR-NSCs, more prominent in young ages, as compared to IFIT1^{WT} animals (Figure 3.27). This overall higher activation rate agrees with our FACS-analysis of the vSVZ: Despite the decrease in total numbers of NSCs in IFIT1^{WT} animals, I observe a relative increase in aNSCs vs. qNSCs in 2 MO and 22 MO individuals in comparison to WT (Figure 3.24C-D, Figure 3.27). Of note, this approach normalizes the activation rate to the number of LRCs, and cannot find global differences as observed by FACS-analysis. Overall, the higher NSCs ratio of activation as well as the total increased pool of TAPs and NBs in the absence of IFIT1, suggest IFIT1 as a negative regulator of NSC activation in the young and the old vSVZ.

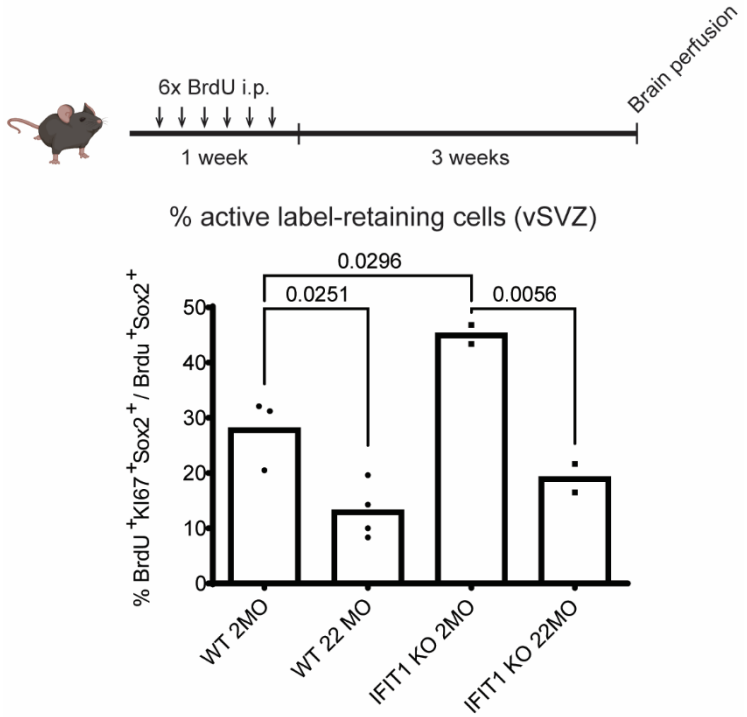

Figure 3.27: Quantification of the activation of BrdU label-retaining NSCs in the vSVZ

Schematic representation of the BrdU incorporation in the mice (upper panel). Quantification of the IF stainings of young IFIT1^{WT} and IFIT1^{KO} vSVZ. All quantified cells were DCX^{-}. One-Way ANOVA with Tukey's multiple comparison test (p-values specified). n = 2-5 biological replicates.

3.5.2 Spatial modeling of the vSVZ suggests age-related dynamics in the neurogenic niche

I next aimed to exploit the spatial information of the distribution of active and non-active LRCs in the vSVZ. For this, I established a collaboration with Roman Remme, Ph.D. Student from Fred Hamprecht's Image Analysis and Learning lab at the University of Heidelberg. Roman Remme and I aimed to deploy the 2D information of the vSVZ slides to address the following hypotheses: 1) Do active and non-active LRCs distribute stochastically along the vSVZ wall, or do these cells cluster? 2) Are there changes in the distribution of active and non-active LRCs along the vSVZ in aging and/or IFIT1^{KO} animals?

First, to address the distribution patterns of active and non-active LRCs, using my manual annotations, Roman Remme computed the distances between the different cell types. Of note, the higher abundance of non-active LRCs vs. active LRCs in this dataset would generate a bias towards lower distances between non-active LRCs. To control for this differential abundance of cell types, Roman Remme computed a randomized distance evaluation by assigning “active” or “non-active” labels stochastically to my manually-annotated cells of the vSVZ sections. The result of this control is the “randomized value”. When compared to the test value (distance), active LRCs tend to be the closest to each other (active to active), as their distance to non-active LRCs is almost three times bigger (active to non-active) (Table R2). Similarly, non-active LRCs tend to also aggregate closer to each other than to active LRCs (Table R2). This indicates that active and non-active cells are not equally distributed along the vSVZ and suggests a bias towards the presence of fully-active or fully-non-active NSC clusters. In addition, despite the closer distribution of active-active and non-active-to-non-active NSCs, non-active LRCs were located much more sparsely than their active counterparts.

Table 3.2: vSVZ cell distance between active and non-active LR cells

Statistic (median of min distance)	Value	Std	Randomized value
active to active LR	39,25	13,65	116,40
active to non-active LR	110,16	10,73	97,35
non-active to active LR	282,37	23,71	226,52
non-active to non-active LR	139,30	9,84	121,57

These results underscore the clustering potential of active LRCs but are underpowered to elucidate the mechanisms driving this active LRC clustering potential. Clusters constituted only by active LRCs can be plausible in two scenarios: A) LRCs divide and

drive full cluster activation of nearby LRCs, or B) LRCs in single-LRC clusters divide symmetrically and give rise to a fully-active LRC cluster. The current dataset is underpowered to claim the validity of one over the other with clear certainty.

Second, Roman Remme and I aimed to investigate the patterns of distribution of cells along the ventricle and the potential effect of aging and the absence of IFIT1. For this, I manually annotated the coordinates of the anatomical corners of the vSVZ ventricle in our sections, namely the ventral corner, the dorsolateral corner, and the medial corner (Figure 3.28).

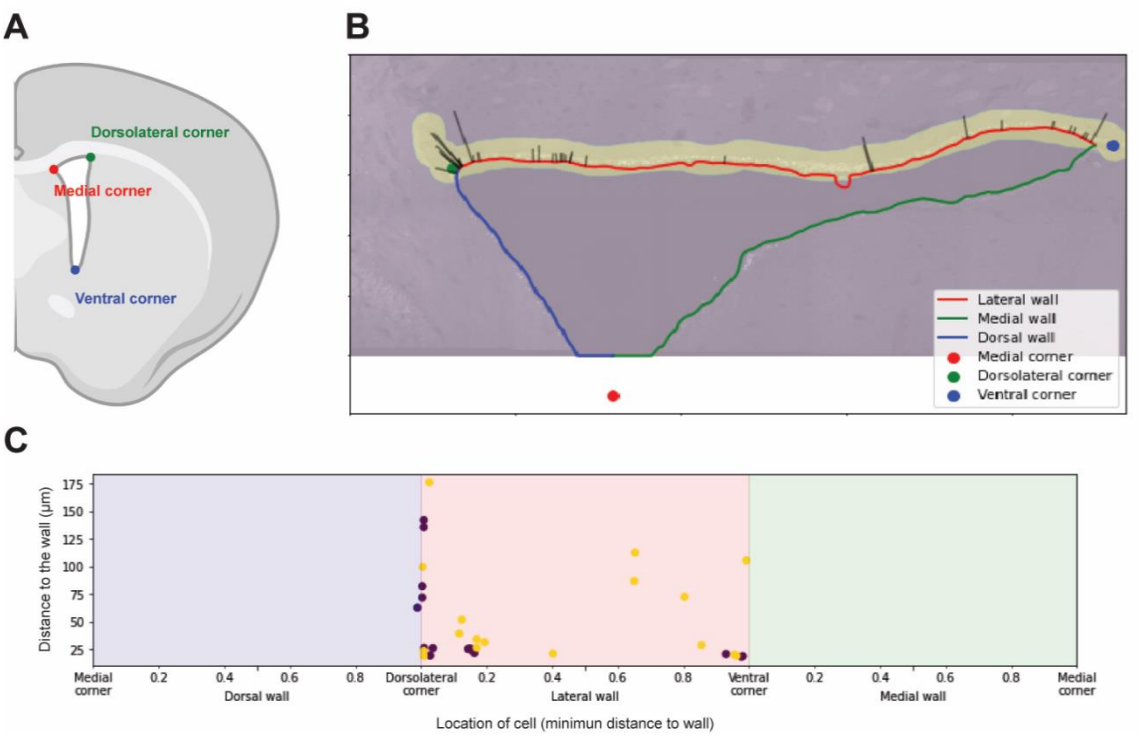

Figure 3.28: Method development to assess the distribution of active and non-active LRCs along the vSVZ

(**A**) Schematic representation of a coronal cut of the vSVZ depicting the ventral (blue), medial (red), and dorsolateral (green) corners of the ventricle. (**B**) Representative illustration depicting the integration of the computed distances from quantified cells to the wall (thin black lines), the surface of the three walls (blue, red, and green), and the manually-annotated mask of the area of interest (yellow shadow). (**C**) Representative example of the quantification displayed in (B). Purple dots represent active LRCs and yellow dots represent non-active LRCs.

Roman Remme then computed the distribution of cells in all conditions (genotypes and ages) of all my manually-annotated sections (Figure 3.29). Interestingly, non-active LRCs from IFIT1^{KO} animals recapitulate the distribution of inactive LRCs in the aged brain already in young individuals (Figure 3.29). However, given the exploratory scope

of these experiments, the small sample size does not allow us to confidentially conclude relevant changes in these distributions. Nevertheless, these results point to the direction of age- and genotype-related differences in the distribution of active and non-active NSCs along the lateral wall of the vSVZ, which should be addressed by future studies.

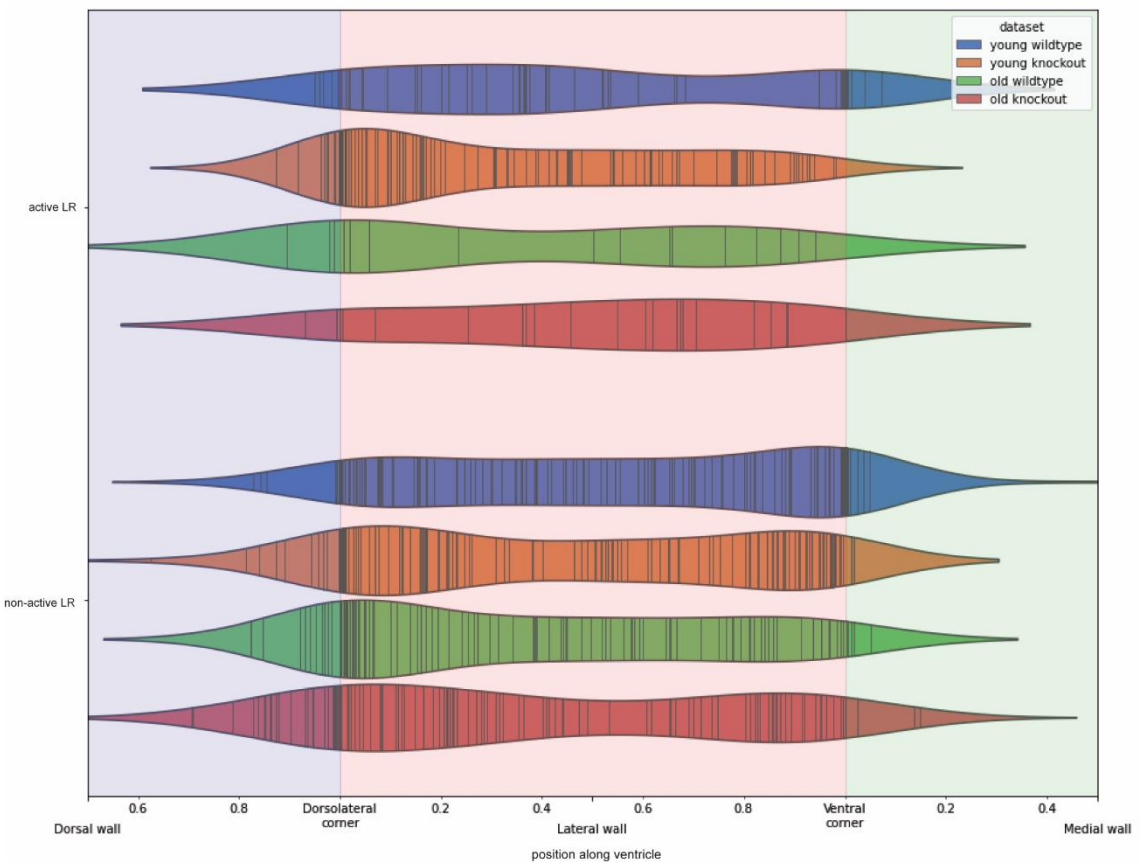

Figure 3.29: Distribution of active and non-active LRCs along the vSVZ walls in aging

Violin plots summarizing the vSVZ distribution of active and non-active LRCs across young (2 months-old) and old (22 months-old) IFIT1^{WT} and IFIT1^{KO} animals. Biological replicates were not taken into consideration, all manually-annotated LRCs are aggregated together.

3.5.3 IFIT1 seems to safeguard NSCs in the Dentate Gyrus from activation in the aged animals

Given the dramatic changes in NSC numbers and neurogenic output in the vSVZ, I also assessed the effect of IFIT1 in the dentate gyrus (DG) (Figure 3.30A). The DG is the second largest neurogenic niche in the adult brain having a crucial role in learning and memory (Bond *et al*, 2015). Due to the morphological complexity of the DG, the analysis by FACS of NSCs and their offspring is generally not employed in this neurogenic niche. Thus, I performed immunofluorescence (IF) staining of the DG of IFIT1^{WT} and IFIT1^{KO} mice of 2-3 and 22 months of age. I then imaged and quantified our cells of interest in the subgranular zone (SGZ) of the DG, and normalized their abundance to the area of

the analyzed tissue. I identified NSCs ($Sox2^{+}GLAST^{+}S100\beta^{-}$), aNSCs ($Sox2^{+}GLAST^{+}S100\beta^{-}KI\text{-}67^{+}$), and astrocytes ($Sox2^{+}GLAST^{+}S100\beta^{+}$).

At young ages, $IFIT1^{KO}$ animals showed a higher NSC pool with a similar number of aNSCs (Figure 3.30A). This unveils an effect on the global NSC numbers in the DG opposite from that observed in the vSVZ. This increase in total NSCs in $IFIT1^{KO}$ mice, without a change in the pool of aNSC, could indicate a higher degree of self-renewal without compromising NSC activation (Figure 3.30B-C).

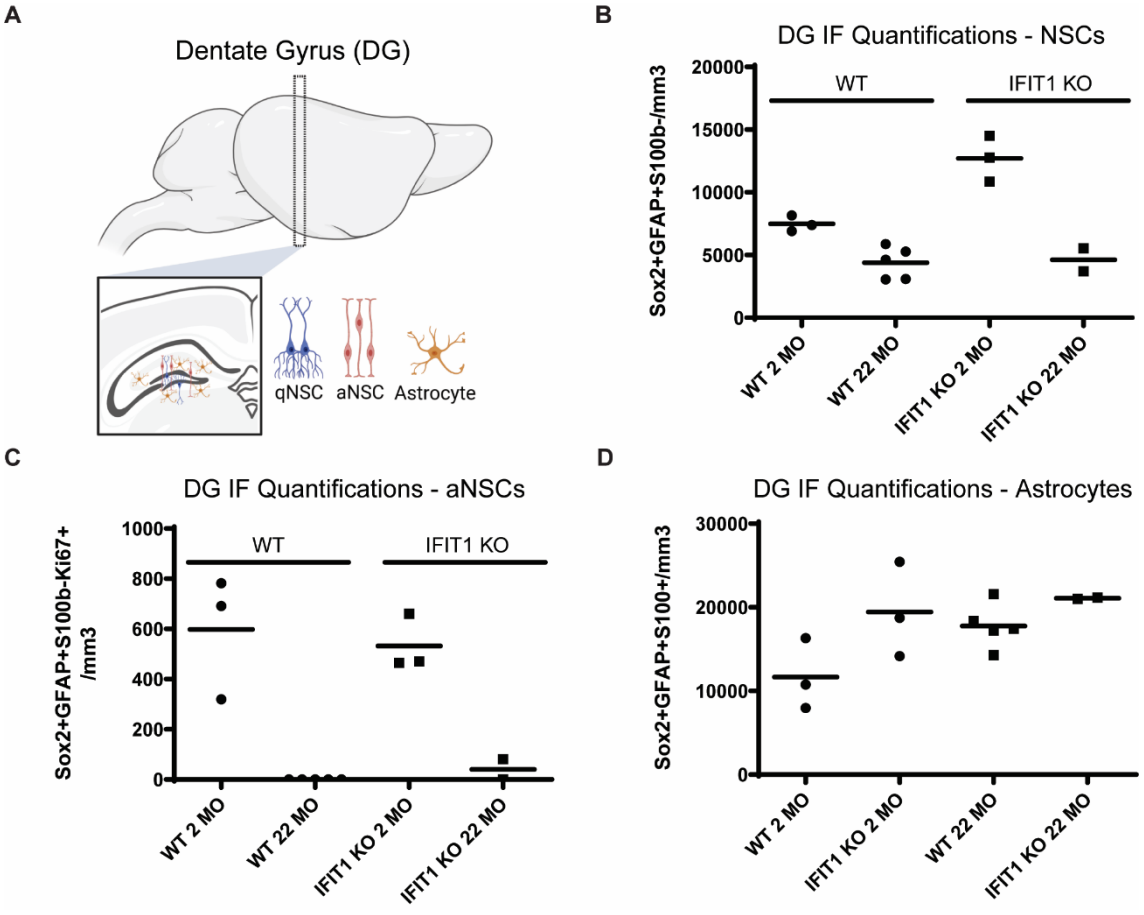

Figure 3. 30: NSC dynamics in the DG assessed by IF

(**A**) Schematic simplification of the neuronal lineage of the Dentate Gyrus (DG) from quiescent neural stem cells (qNSC), active NSCs (aNSC), and the non-lineage astrocytes. Immunofluorescence (IF) quantifications of NSCs (**B**), aNSCs (**C**), and astrocytes (**D**) of the hippocampal dentate gyrus (DG) per brain of WT or IFIT1 KO animals at different ages. n = 2-5 biological replicates per age and genotype. MO = Months old.

At old ages, both $IFIT1^{KO}$ and $IFIT1^{WT}$ animals display the same amount of NSCs, albeit aNSCs are only found in one of the $IFIT1^{KO}$ old animals and none of the $IFIT1^{WT}$ samples (Figure 3.30B-C). The complete absence of aNSCs in IF sections in the old DG is not surprising as aNSC are relatively sparse compared to the tissue in the young brain and proliferation of NSCs drops to 80% with aging in the DG (Encinas *et al*, 2011).

Surprisingly, IFIT1 seems to also prevent the early astrocyte differentiation of NSCs, as young IFIT1^{KO} animals display a higher density of astrocytes in the DG (Figure 3.30D). This higher propensity of astrocytes is a hallmark of aging in the DG (Bonaguidi *et al*, 2011), which would speak in favor of accelerated aging in the absence of IFIT1.

Overall, due to time and mice limitations, these results have a low sample size and I can therefore only claim preliminary tendencies that would require further confirmation.

3.5.4 The absence of IFIT1 impairs social behaviour and spatial memory acquisition in mice

To validate the large effects of the absence of IFIT1 in the dynamics of NSCs in the vSVZ and the DG, Dr. Santiago Cerrizuela and I performed behavioural studies to validate the functional relevance of IFIT1 in the adult brain. Dr. Santiago Cerrizuela performed the below-described behavioural studies in the young (2-3 MO) cohort and I performed the experiments on the old (30 MO) cohort, both comprising IFIT1^{KO} and FIT1^{WT} animals. These experiments were performed with the assistance of Sonja Anslinger and the supervision of Dr. Claudia Pitzer. Overall, the animals were subjected to three behavioral tests: 1) Elevated Plus Maze, 2) Active Place Avoidance Test, and 3) Three-Chamber Sociability and Social Novelty Test.

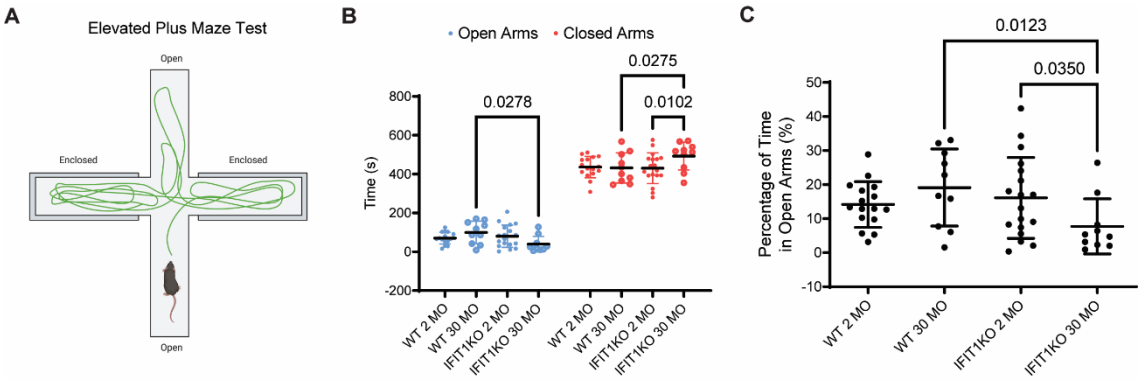

Figure 3.31: IFIT1^{KO} animals display no anxiety-related behaviour except in old ages

(**A**) Schematic representation of the Elevated Plus Maze (EPM) test. (**B**) Quantification of the time (seconds) spent by the subject animals in the open (blue) or the closed (red) arms of the EPM. Two-way RM ANOVA with multiple comparison test (p-values specified). (**C**) Quantification of the percentage of time spent by the subject animals in the open arms of the EPM. One-way ANOVA (p-values specified). n = 16 (2MO IFIT1^{WT}); 18 (2MO IFIT1^{KO}); 10 (30MO IFIT1^{WT}); 10 (30MO IFIT1^{KO}) biological replicates. MO = months old.

I first employed the Elevated Plus Maze Test (EPM) to assess anxiety-related behavior (Figure 3.31A). In the EPM test, the movement of the subject mice was tracked to record the time spent in the open vs. the closed arms of the Plus Maze. In young animals, the

absence of IFIT1 did not cause any anxiety-related behavior. However, old IFIT1^{KO} animals spent significantly more time in closed arms, indicative of anxiety in these animals (Figure 3.31B-C).

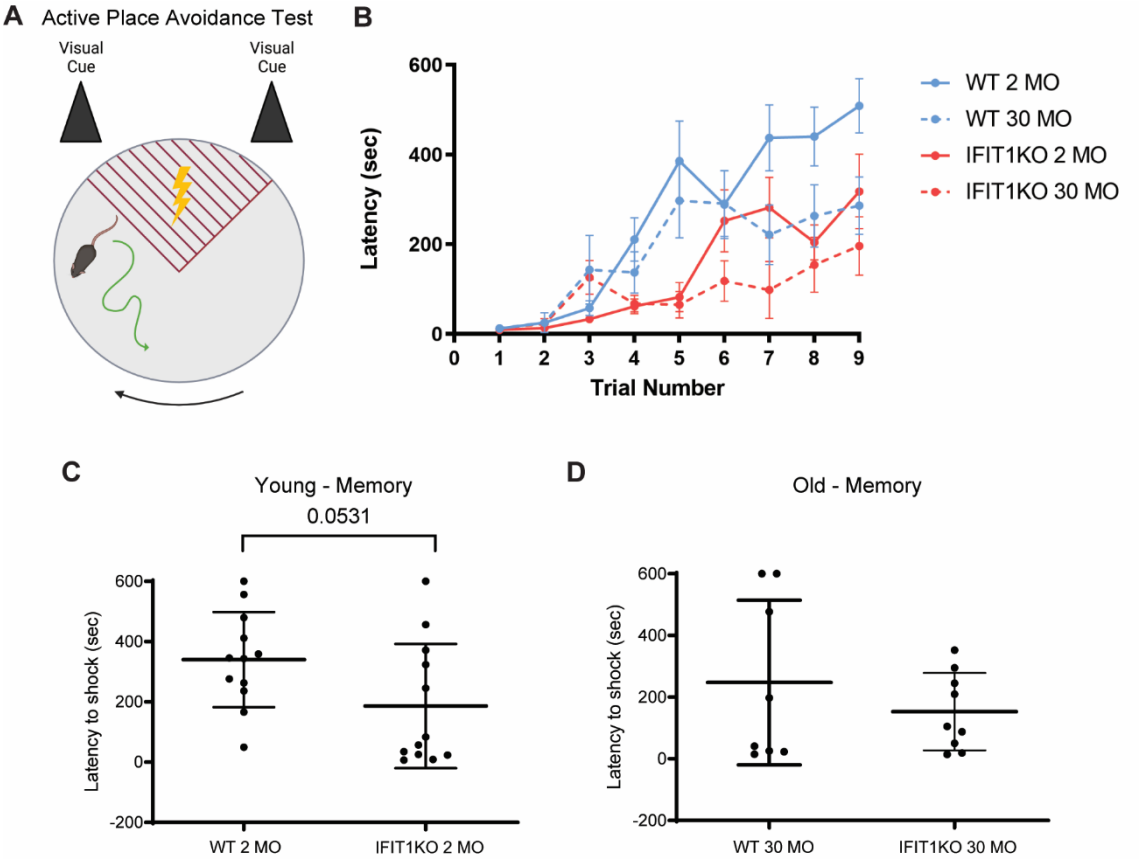

Figure 3.32: IFIT1^{KO} animals display lower spatial memory in young ages and worse learning traits at all ages

(**A**) Schematic representation of the Active Place Avoidance (APA) Test arena. Arrow indicates the direction of active rotation of the platform; the red triangle with thunder represents the shock area. (**B**) Quantification of the latency to first (time in seconds to the first entry in the shock zone) in the subject mice across the learning period (trials 1-9). Simple linear regression indicates all slopes to be significantly different ($P < 0.0001$). Quantification of the latency to first (time in seconds to the first entry in the shock zone) in the subject mice in the memory consolidation trial (trial 10) in young (**C**) and old (**D**) animals. Panels C and D are separated as these two cohorts were tested with different instruments (see Materials and Methods). Mann-Whitney test (p-values specified). n = 8 (2MO IFIT1^{WT}); 8 (2MO IFIT1^{KO}); 8 (30MO IFIT1^{WT}); 9 (30MO IFIT1^{KO}) biological replicates. MO = months old.

Second, I employed the Active Place Avoidance Test (APA) to assess the learning and spatial memory of the mice (Figure 3.32A). In the APA test, the subject mice learn to actively avoid entering a specific area, marked by visual cues. During 9 consecutive trials, mice learn to stay away from the marked area to avoid receiving an electric shock (Figure 3.32B). Then, 24 hours after the learning dynamic, spatial cognition is measured

by tracking the time until the animal falls in the designated area (Figure 3.32C-D). Surprisingly, the absence of IFIT1 strongly impacts the learning curve of IFIT1^{KO} animals both at young and old ages. Regarding memory consolidation, IFIT1^{KO} animals show slightly deficient cognition, on the verge of statistical significance (Figure 3.32C). Despite the increased size of the DG-NSC pool in young IFIT1^{KO} animals, these results indicate that young IFIT1^{KO} animals display defects in their spatial memory (see discussion in section 4.5.4). In aging, the spatial memory is similar in both genotypes. Altogether, while IFIT1^{WT} animals show an age-related decrease in spatial memory, as previously described (Seib *et al*, 2013), IFIT1^{KO} animals show a reduced memory in young individuals with an absence of an aging-related effect in memory acquisition.

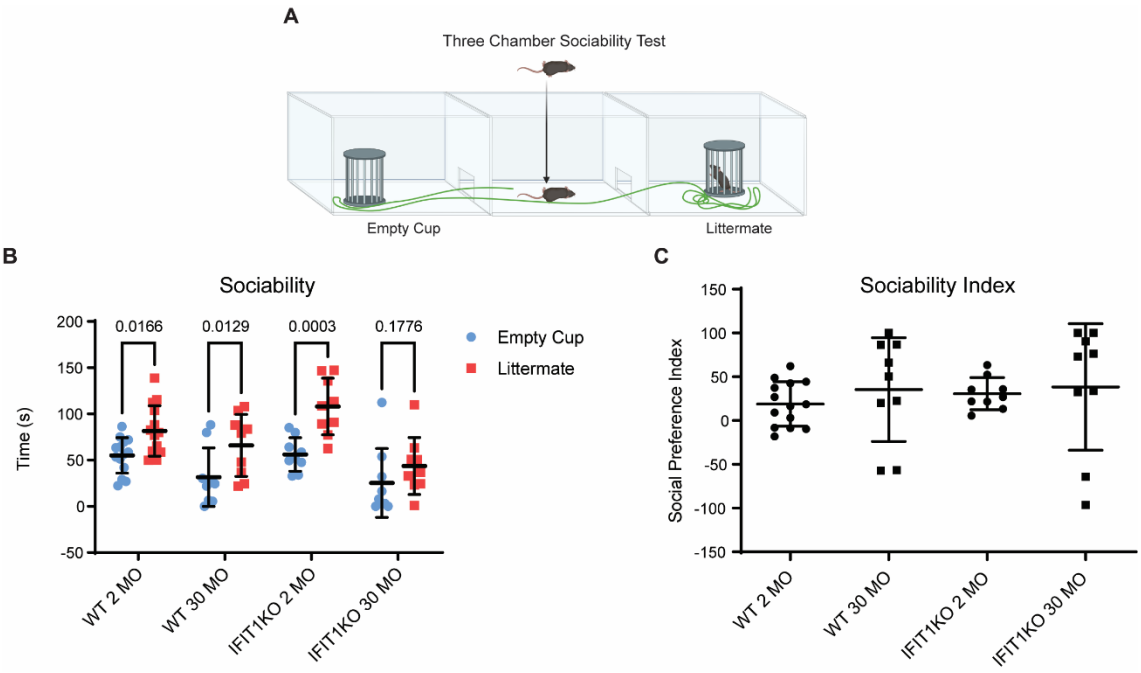

Figure 3.33: Assessment of sociability traits in IFIT1^{KO} animals

(**A**) Schematic representation of the Three Chamber Sociability Test. (**B**) Quantification of the time spent by the subject animals with the empty cup (blue) or the littermate animal (red). Bars display mean ± SD. Two-way RM ANOVA with multiple comparison test (p-values specified). (**C**) Quantification of the Social Preference Index (see Materials and Methods) as the preference of visiting the littermate vs. the empty cup. Kruskal-Wallis test with Dunn's multiple comparison test (p-values specified). n = 14 (2MO IFIT1^{WT}); 9 (2MO IFIT1^{KO}); 9 (30MO IFIT1^{WT}); 9 (30MO IFIT1^{KO}) biological replicates. MO = months old.

Last, I employed the Three-Chamber Sociability and Social Novelty Test to assess deficits in sociability or social/novelty traits. In this test, subject mice are introduced in the middle section of a three-chamber set. The motion of the mice is tracked to calculate the ratio of time spent in which of the two lateral chambers. These lateral chambers contain different caged mice to test for different behavioural traits. The "Sociability test"

measures the time spent with a littermate vs. an empty chamber (Figure 3.33A). No sociability impairment was found in neither young nor old IFIT1^{KO} animals (Figure 3.33B-C).

The “Social Novelty Test” measures the time spent with an intruder versus a littermate mouse (Figure 3.34A). Interestingly, IFIT1^{KO} animals displayed an impaired social novelty preference, as compared with IFIT1^{WT} animals. While young IFIT1^{KO} animals were less curious towards social novelty -a trait typical of aged mice-, old IFIT1^{KO} animals reverted this phenotype and regain the curiosity to explore the intruder animal (Figure 3.34B-C). The addition of additional old IFIT1^{KO} animals to the sample size would be desirable given the high dispersion of these individuals.

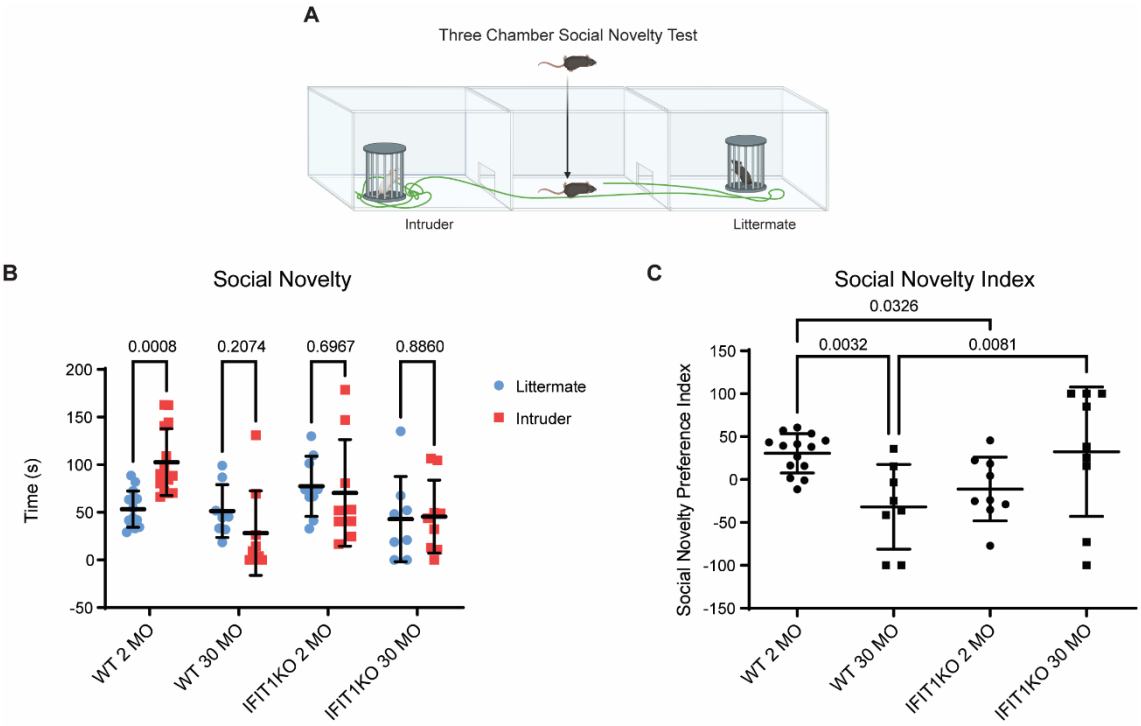

Figure 3. 34: Assessment of social novelty traits in IFIT1^{KO} animals

(**A**) Schematic representation of the Three Chamber Social Novelty Test. The white intruder mouse represents a CD1-background mouse. (**B**) Quantification of the time spent by the subject animals with the littermate (blue) or the intruder animal (red). Bars display mean ± SD. Two-way RM ANOVA with multiple comparison test (p-values specified). (**C**) Quantification of the Social Novelty Preference Index (see Materials and Methods) as the preference of visiting the intruder vs. the littermate. Kruskal-Wallis test with Dunn’s multiple comparison test (p-values specified). n = 14 (2MO IFIT1^{WT}); 9 (2MO IFIT1^{KO}); 9 (30MO IFIT1^{WT}); 9 (30MO IFIT1^{KO}) biological replicates. MO = months old.

4. Discussion

4.1 Interferon modulates stem cell activation in the young and the old brain

Previous studies unveiled interferons as regulators of stem cell quiescence and drivers of the decline of adult neurogenesis in the chronically-inflamed aging brain (Kalamakis *et al*, 2019; Dulken *et al*, 2019; Baruch *et al*, 2014). However, these studies did not address the potential role of interferon in controlling neurogenesis in the healthy adult brain. In this study, I, together with Dr. Cerrizuela and Jooa Hooli, confirm that neural stem cells are targeted by interferons at all ages, as revealed by scRNA-Seq of the vSVZ of young and old $IFNAGR^{WT}$ and $IFNAGR^{KO}$ mice. While previous scRNA-Seq studies were underpowered to sensibly account for basal interferon responses, I now treated NSCs with IFN-β to create the "NSC type-I IFN Response" signature. This new signature, which proves to be sensitive, confirms the presence of interferon response in NSCs in the young brain. Of note, the "NSC Type-I Interferon Response" is not only specific for NSCs, as it maintains the highest score for microglia and endothelial cells in the niche, consistent with previous reports (Kalamakis *et al*, 2019).

4.1.1 Neural Stem Cells selectively respond to interferons: Intrinsic vs extrinsic response

Our scRNA-Seq data reveals that NSCs display an interferon response at all ages, yet their downstream neural progenitors -TAPs and NBs- remain refractory to interferons. Intriguingly, it was previously proposed that stem cells display an intrinsic interferon response that differentiates them from their differentiated progeny (Wu *et al*, 2018). This raises the question of whether the observed interferon response in NSCs is cell-intrinsic or extrinsic.

Based on my results, I can conclude that the interferon response of these NSCs is not exclusively cell-intrinsic. First, in the young brain, NSCs selectively display an intrinsic interferon response in the absence of interferon sensing ($IFNAGR^{KO}$), consistent with the reported intrinsic signature of stem cells (Wu *et al*, 2018). However, the basal interferon response in $IFNAGR^{KO}$ NSCs is slightly dysregulated compared to $IFNAGR^{WT}$ NSCs. This indicates that even in the young brain, external interferons modulate the interferon signature of NSCs and fine-tune their intrinsic response. Second, external interferons are responsible for the age-related increase in interferon signature of NSCs, as $IFNAGR^{KO}$ NSCs fail to upregulate their basal interferon response even in aging.

Of note, the study led by Charles Rice and colleagues proposed not only that stem cells display an intrinsic interferon response but also that stem cells are refractory to external interferons (Wu *et al*, 2018). While my findings support the presence of the intrinsic response in NSCs, they do not agree with the proposed inability of stem cells to react to interferons. Importantly, the claim by Wu *et al*. that stem cells are refractory to interferons is solely based on the response of human embryonic stem cells (hESCs) and on similar previous reports also employing hESCs (Wu *et al*, 2018; Burke *et al*, 1978; Muckenhuber *et al*, 2023). Conversely, substantial proof has been shown that adult stem cells across different tissues effectively respond to interferons (Essers *et al*, 2009; Baldridge *et al*, 2010; Baruch *et al*, 2014; Takashima *et al*, 2019; Carvajal Ibañez *et al*, 2023), suggesting that such refractory trait might be a signature of hESCs rather than stem cells.

This unresponsiveness to interferons is reflected in our dataset rather by neural progenitors -TAPs and NBs- than by the mother NSCs. Notably, my results reveal that TAPs and NBs remain refractory to interferons even in the aging brain. Why and how neural progenitors remain refractory to interferons remains unknown. Interestingly, in the hematopoietic system, hematopoietic progenitors do not only respond to interferon but also are responsible for the infection-driven differentiation of cells (Fanti *et al*, 2023). This selective response to interferons of NSCs but not TAPs and NBs might have novel implications in the regenerative capacity of these cells as well as their ability to respond to viral infections (further discussed in section 4.3.2).

4.1.2 Heterogeneity of the interferon response in NSCs

The advent of single-cell technologies allows the possibility to discern the heterogeneity in the response of a given population to a certain stimulus. Although poorly explored, our dataset reveals a heterogenous score of interferon signature among NSCs in the vSVZ. How this heterogeneity in the response occurs and its potential role in influencing the fate of NSCs remains to be explored.

By employing the ISRE-based type-I interferon reporter mouse model, I can confirm that the interferon response in NSCs is heterogeneous and dynamically changing in aging. Interestingly, the higher prevalence of interferon-positive NSCs in aging seems to result from a faster depletion of the interferon-negative NSCs, rather than an amplification of the interferon-positive NSC pool. The dynamics of these two populations, their spatial distribution along the ventricle, and their fate should be addressed by future studies.

Of note, the heterogeneity of the interferon and inflammatory responses in stem cells has recently been reported in the hematopoietic niche (Bogeska *et al*, 2022; preprint Bouman *et al*, 2023). Interestingly, recent reports have also proposed that stem cells can

stably “memorize” sensing of interferon or pathogens (Naik *et al*, 2018), as well as the long-lasting detrimental effects of repeated inflammation in the niche (Bogeska *et al*, 2022). This underscores the importance of harnessing the potential of scRNA-Seq technologies to address open questions such as: do interferon-positive and -negative NSCs comprise two different lineages? Can they transition from an interferon-negative into a positive state reversibly? Is the onset of interferon-positive and -negative NSCs dictated by their spatial distribution in the vSVZ?

4.2 Interferon induces a novel bi-phasic control of mTOR to modulate the exit of the activation state

Despite the relevant role of interferons in inducing quiescence in the aging vSVZ, the molecular underpinnings of the interferon response are yet poorly studied. Here, I describe how type-I interferon drives a dynamic control of mTOR consisting of a transient upregulation, followed up by a late strong downregulation of mTORC1 activity. Notably, the biphasic regulation of mTOR leads to a biphasic control of protein synthesis in NSCs. Interferons are reported to regulate mTOR activity unidirectionally via non-canonical signaling (Mazewski *et al*, 2020; Su *et al*, 2015). However, to the best of my knowledge, there is no reported biphasic control of mTOR by interferons to date. Thus, I aimed to profile the mechanistic effectors driving this response.

4.2.1 The biphasic control of protein synthesis: mTORC1 and eIF2α

I first confirmed the exclusive role of mTORC1 in the biphasic regulation of mTOR activity by the specific regulation of p-S6K^{Thr389} (Ma & Blenis, 2009) and p-4E-BP1^{Ser65} (Qin *et al*, 2016; Gingras *et al*, 2001) and the absence of regulation of the mTORC2-dependent p-Akt^{Ser473} (Breuleux *et al*, 2009). I also validated the selective role of mTORC1 over mTORC2 in the interferon response in NSCs by using Torin1 and Rapamycin -inhibitors of mTORC1/2 or mTORC1, respectively (Thoreen *et al*, 2009, 2012)-. Additionally, CRISPR-mediated knockdown of TSC2 -regulator of mTORC1- confirmed the causal role of mTORC1 in the biphasic regulation of mTOR. Then, I aimed to profile the different effectors involved in the early and late response of the biphasic regulation.

In the transient upregulation of mTOR, the IFNAR-PI3K-Akt signaling crosstalk induces the activation of mTORC1, responsible for the transient increase of protein synthesis, as revealed by OPP incorporation. Interestingly, during this early time point, the regulation of mRNA translation by interferon relies on p-S6$^{S235/236\ \&\ S240/244}$ rather than on p-4E-BP1^{S65}. The lack of early modulation of E4-BP1 can explain why the increase of protein synthesis is very mild, as 4E-BP1 has a more prominent role in cap-dependent mRNA translation, including TOP-mRNAs (Thoreen *et al*, 2012; Pende *et al*, 2004).

In the late downregulation of mTOR, levels of both p-S6$^{S235/236\ \&\ S240/244}$ and p-4E-BP1^{S65} are reduced, causing a more prominent shutdown of mRNA translation. This late downregulation of mTOR relies on a shutdown of the IFNAR-PI3K-Akt crosstalk. How, in the continuous presence of interferon, the activated IFNAR-PI3K-Akt shifts to downregulation of p-Akt^{T308} remains elusive. Previous reports have pointed out the relevance of inhibitory feedback loops acting on IRS1 via Grb10 or mTORC2 (Hsu *et al*, 2011). Based on my results, I can rule out the implication of mTORC2 in these feedback loops, but the implications of other reported effectors have not been addressed in NSCs.

Strikingly, although the causal role of mTORC1 in the late downregulation of mTOR was confirmed in TSC2^{mut} NSCs, it revealed that additional mechanisms independent of mTOR activity also contribute to the late protein synthesis shutdown induced by interferon β. As interferon elicits a relevant upregulation of ISGs, I hypothesized that some of those could be contributing to the late downregulation of protein synthesis. Indeed, extended incubation of NSCs to interferon increased the expression of PKR and levels of p-eIF2α^{S51}. I further confirmed the causal role of p-eIF2α^{S51} in shutting-down protein synthesis in NSCs upon interferon treatment by selectively inhibiting the effect of increased p-eIF2α^{S51} with the ISRIB inhibitor (Sidrauski *et al*, 2015). The additional contribution of other ISGs such as *ifit* members to this late downregulation of mRNA translation was not explicitly assessed.

4.2.2 Interferon uncouples mTOR activity and cell cycle to repress translation of *Sox2*

Our group recently discovered that a coordinated inhibition of mTOR and cell cycle is necessary to effectively induce the downregulation of *Sox2* in NSCs (Baser *et al*, 2019). However, the upstream regulators driving this dual control were missing.

Here, I show that interferon β transiently uncouples mTORC1 activity and cell cycle to late orchestrate a dual inhibition of both processes to efficiently represses the translation of *Sox2* in NSCs. Notably, the repression of *Sox2* translation by interferon β is more prominent than that resulting in the chemical inhibition of mTORC1 and cell cycle (Baser *et al*, 2019). Also, interferon β slightly repressed *Sox2* translation already during the early response, when mTORC1 was upregulated and cell cycle downregulated. Strikingly, I here show the relevant role of this transient upregulation of mTORC1 in the selective repression of *Sox2* in NSCs, irrespective of the translation efficiency of other TOP-mRNAs.

In addition, *Sox2* holds a 5' UTR pyrimidine-rich motif (PRM) located a few bases downstream of its 5'-termini. This PRM motif was previously suggested to be responsible

for the post-transcriptional downregulation of *Sox2*, yet its relevance was never tested (Baser *et al*, 2019). By using 5' UTRs containing WT or mutant versions of the PRM motif of *Sox2*, created by Dr. Baser and Dr. Skabkin, I now show that it is indeed the presence of PRM that dictates the repression of *Sox2* translation upon interferon treatment, irrespective of the translation efficiency of TOP-mRNAs.

I propose that interferon β, with its transient upregulation of protein synthesis, might translate mediators involved in the late translation repression of *Sox2* potentially by recognizing or promoting the recognition of the PRM motif. This hypothesis cannot explain however the slight downregulation of *Sox2* already in the early interferon β incubation. This early downregulation of *Sox2*, however, could also result from the sudden translocation of the ribosomes to mRNAs selectively controlled by mTOR, such as TOP-mRNAs. Last, as the highest repression of *Sox2* is observed when mTOR is shutdown, it would be interesting to assess the translation efficiency of *Sox2* in a continuous mTOR activation scenario (i.e. with PIP_3) in NSCs.

4.2.3 Interferon induces exit of activation in NSCs: Quiescence or differentiation?

As discussed in the previous section, the downregulation of *Sox2* is a necessary step at the onset of differentiation in NSCs (Baser *et al*, 2019). However, qNSCs also downregulate *Sox2* to prevent replicative stress (Marqués-Torrejón *et al*, 2013). In line with the decrease of SOX2 in quiescent cells, SOX2 levels decrease in the old brain, correlating with the age-related increase in quiescence (Carrasco-Garcia *et al*, 2019). Therefore, the reduction of SOX2 levels drives the exit of the activation state in NSCs, albeit whether interferon drives differentiation or quiescence -states where both mTOR and cell cycle are repressed- remains unknown (Figure 4.1).

Interestingly, preliminary crosschecking of different omics datasets in our laboratory does not shed light on the fate directionality of the interferon treatment in NSCs. While most of the post-transcriptionally repressed genes at the NSC-to-NB transition (Baser *et al*, 2019) correlate with the changes observed in NSCs treated with interferon β (Ribo-Seq), so do correlate the differentially-expressed proteins in the proteome of NSCs induced for quiescence by BMP4 treatment (Mira *et al*, 2010) (results not provided). Of note, the Ribo-Seq data is produced in bulk NSCs, and therefore the similarities of these changes both with quiescence and differentiation might underscore a heterogeneity of NSCs in the response to interferon β. Future studies should investigate whether interferon induces quiescence or differentiation in NSCs with single-cell resolution.

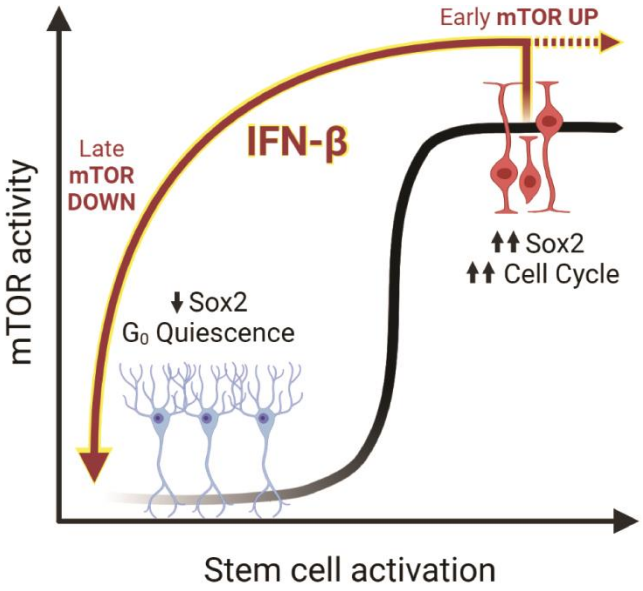

Figure 4.1: The biphasic regulation of mTORC1 by interferon β induces exit of the activation state in NSCs

Figure adapted from Carvajal Ibañez *et al*, 2023

Interestingly, while mTORC1 hyperactivation biases stem cells to a glial-fate, inhibition of mTORC1 promotes neurogenesis (Blair *et al*, 2018). It would be worth-investigating whether interferons can bias the fate of NSCs, independently of inducing quiescence or differentiation. In addition, recent reports have also highlighted the relevance of *Sox2* levels in leveraging interferon signaling and self-renewal in NSCs. *Sox2* upregulates the expression of *Socs3*, an inhibitor of JAK/STAT signaling that favors long-term self-renewal in NSCs (Bertolini *et al*, 2019). Although I find that interferon reduces *Sox2* levels in NSCs, my results do not reveal any changes in the abundance of *Socs3* mRNA or footprints.

4.2.4 Additional implications of interferons in stem cells: ISGs, senescence, and uORFs

Intriguingly, the uncoupling of mTOR and cell cycle does not only repress translation of *Sox2* but has also potential implications in other features of stem cell biology.

First, despite the late downregulation of mRNA translation, ISGs maintain and even increase their translation efficiency in NSCs. Translation of ISGs has always been linked to mTOR activity (Mazewski *et al*, 2020). A recent report however shows that the translation of ISGs is homeostatically mTOR-insensitive and interferons elicit changes in the transcription start site (TSS) of ISGs that drive their mTOR-sensitivity (Livingstone *et al*, 2015). Unfortunately, our Ribo-Seq data lacks the power to identify differential

transcription initiation sites, as it does not consist of full-length mRNA sequencing. Whether interferons fail to shift the TSS of ISGs in stem cells to disconnect mTOR activity to ISG translation is a hypothesis to be addressed by future studies. In addition, whether the increase in translation efficiency of ISGs is relevant for stemness or it occurs as a collateral consequence of a higher availability of ternary complex in the cell also remains unaddressed.

Second, the early upregulation of mTORC1 induced by interferon β transiently uncouples mTOR activity to cell cycle in stem cells. This uncoupling has, to the best of my knowledge, not been described before in stem cells and it only resembles the induction of senescence, where cells hyperactivate mTOR while halting cell cycle progression (Payea *et al*, 2021). Differently to senescence, NSCs re-couple mTOR activity to cell cycle in the late response to interferon β, coupling both processes. Interestingly, interferons are key inducers of senescence in somatic cells (Glück & Ablasser, 2019). I hypothesize that this selective late re-coupling of mTOR and cell cycle in response to interferons might be promoting quiescence in stem cells to prevent the induction of senescence. This can be the missing mechanism explaining why despite the age-related increase of senescent cells in the brain (Molofsky *et al*, 2006; Fernández-Fernández *et al*, 2012; Ogrodnik *et al*, 2019; Jin *et al*, 2021) stem cells remain protected. In addition, I also show that interferon treatment gradually inhibits the activity of the Cdk4/6 complex, potentially via Cyclin D1, leading to cell cycle exit (G_0) rather than cell-cycle lengthening, as previously proposed (Daynac *et al*, 2016). Although the relevance of CyclinD1-Cdk4/6 in regulating the activation of NSCs is already reported (Lange *et al*, 2009; Artegiani *et al*, 2011), upstream regulators of these effectors were still missing.

Third, interferon also increased the levels of p-eIF2α^{S51} in NSCs, which has also been associated with the induction of quiescence in muscle stem cells (Zismanov *et al*, 2016a). In NSCs, the increased levels of p-eIF2α^{S51} also correlated with an enhanced density of ribosomes in the 5’ UTRs of genes. The increase in 5’UTR footprints denotes an enhanced use of uORFs, yet no changes in footprint abundance in CDS of these mRNAs were observed. In addition, typically upregulated uORF genes under the effect of the integrated stress response (IRS) such as *Atf4*, *Chop,* or *Gadd34*, are not increased in NSCs despite the increase of p-eIF2α^{S51} (data not shown). This suggests that the uORF usage in NSCs upon interferon β differs from the canonical IRS response. Interestingly, uORF usage in NSCs resembles that previously-described in cells with impaired tRNAs methylation, where the translation of the CDS was also not altered (Blanco *et al*, 2016). However, this thesis does not address either the differential methylation of tRNAs or the causal role of p-eIF2α^{S51} in changing uORFs usage in NSCs.

4.3 The therapeutic potential of interferons and stem cells in aging and disease in the brain

4.3.1 Interferon is beneficial in the young but detrimental in the old brain

The blockage of interferons or interferon signaling has proved to be effective to revert aging in the adult brain, increasing the activation of NSCs and their neurogenic output (Kalamakis *et al*, 2019; Baruch *et al*, 2014). As I now conclude that interferons also modulate NSCs in the young brain, it remained unanswered whether the blockage of interferon signaling would also promote neurogenesis in young individuals. Recently, my colleague Jooa Hooli computed the dynamics of $IFNAGR^{WT}$ and $IFNAGR^{KO}$ vSVZ-NSCs at different ages combining new data acquired by my colleagues Dr. Santiago Cerrizuela and published data at Kalamakis *et al*, 2019 (Carvajal Ibañez *et al*, 2023). This data concluded that opposite to aging, the absence of interferons in the young brain leads to a significant reduction of the neurogenic output of NSCs, being detrimental to neurogenesis. Conversely, the absence of interferons in the aged brain has beneficial effects and rescues the age-related decrease in neurogenic output (Carvajal Ibañez *et al*, 2023), in agreement with previous reports (Kalamakis *et al*, 2019; Baruch *et al*, 2014). This indicates that despite the beneficial effects of blocking interferons in the late stages of life to increase neurogenesis, an early-in-life intervention is detrimental to the neurogenic output and potentially also to the olfactory and cognitive abilities of these individuals (Figure 4.2).

This duality of the beneficial or detrimental effects of the interferon response in the young and old brain raises the question of what is driving the switch. I hypothesize that the extrinsic factors driving inflammation might be responsible, as NSCs are intrinsically-fit to activate at all ages (Kalamakis *et al*, 2019). Of note, the employed transgenic models were KO for both type-I and -II interferon receptors. While type-I IFNs increase in aging and induce quiescence (Kalamakis *et al*, 2019; Baruch *et al*, 2014), type-II IFNs are also present at young ages in the choroid plexus and even promote neurogenesis during brain injury (Llorens-Bobadilla *et al*, 2015; Deczkowska *et al*, 2016). It is plausible that a basal and balanced presence of type-I and -II IFNs are promoting the activation of NSCs in young individuals, while a chronic increase of type-I IFNs in aging induces quiescence to maintain the NSC pool during the whole mouse lifespan. In addition, given the full-knockout nature of the mouse models, it is possible that the defective sensing of interferons by local immune cells, astrocytes, or endothelial cells might also be affecting the shift of the response by paracrine signals or cell-to-cell control of NSCs. Future

studies should use conditional knockouts of interferon that are timely-controlled and specific for the NSC compartment.

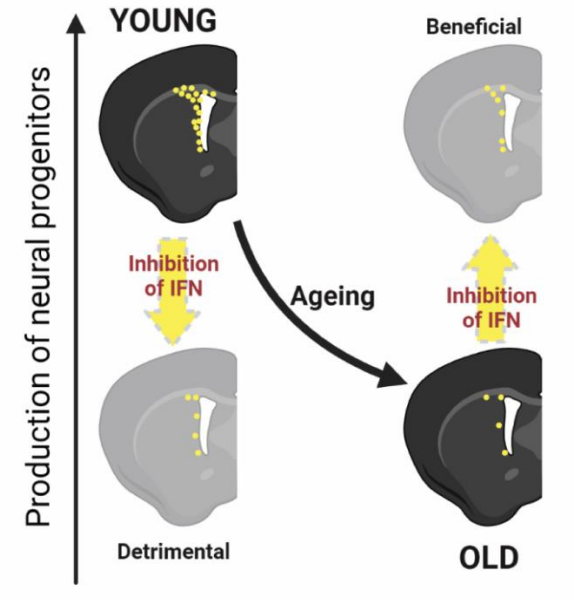

Figure 4.2: Blockage of IFN is detrimental in the young but beneficial in the old brain
Figure adapted from Carvajal Ibañez *et al*, 2023

Interestingly, intervening in aging to increase neurogenesis could potentially lead to increased cognition. Supporting this hypothesis, blocking type-I IFN response in mice increased memory recognition in aging (Baruch *et al*, 2014). Paradoxically, the integration of new neurons in the DG enhances new memory consolidation, yet weakens existing memories, as revealed by recent studies (Epp *et al*, 2016; Temprana *et al*, 2015; McHugh *et al*, 2022). Artificially promoting neurogenesis in the DG after stroke leads to enhanced memory impairment in mice (Cuartero *et al*, 2019). This raises the almost philosophical concern of whether quiescence of NSCs might be induced in aging to maintain the existing memories, at the expense of detrimental learning in old mice. To the best of my knowledge, whether blocking interferons in aging would also promote the weakening of existing memories has not yet been addressed. Similarly, it remains unknown whether the rescued cognition by blocking interferons in aged individuals (Baruch *et al*, 2014) is a long-term phenotype or rather a transient event.

4.3.2 Medical use of interferons in cancer, brain infections, and Alzheimer's disease

In addition to aging, interferons and neurogenesis are related to the pathophysiology of certain conditions in the adult brain. My findings on how 1) interferons control NSCs in the young brain, 2) their selective action on stem cells over neural progenitors, and 3) its

effects on mTOR and cell cycle, reveal novel implications of interferons relevant for brain disorders.

As interferons exert cytostatic effects in somatic cells, interferon β has historically been clinically used to reduce the proliferation of tumor glioblastoma cells (Yoshida *et al*, 1987). Later studies underscored the beneficial effect of interferons in treating glioblastoma beyond its cytostatic effects, as interferon improved tumor regression in combination with temozolomide *in-vitro* (Natsume *et al*, 2005) and more recently in a phase-III trial (Guo *et al*, 2023). Interestingly, NSCs can act as the cell of origin of glioblastoma (Lee *et al*, 2018). In fact, it was recently reported that increased fatty-acid oxidation in mutation-bearing NSCs keeps them quiescent and prevents the onset of glioblastoma (Amodeo *et al*, 2023). Of note, interferon β has also been reported recently to induce cell death in glioblastoma stem cells, supporting its therapeutic relevance in glioblastoma (Khan *et al*, 2021). All these findings underscore the relevance of the shared mechanisms between NSC activation and glioblastoma tumor initiation. The selective response of interferon in NSCs over neural progenitors that I hereby present, suggests that interferon treatment in glioblastoma patients is potentially targeting only the stem-like tumor cells and not the progenitor-like tumor cells, as these cells are refractory to interferons. Future studies should address the mechanisms preventing the interferon response in these progenitors and their potential application in a combination treatment with interferon β for glioblastoma tumors.

Similarly, the unresponsiveness to interferons of neural progenitor cells might have implications for brain developmental pathologies. Viral infections in the brain such as the Zyka virus are more prevalent and have more severe consequences in developmental or infant stages of life (reviewed in Jash & Sharma, 2022). I hypothesize that the lack of interferon response in the abundant neural progenitors of an infected developing brain might be detrimental to the antiviral response. Future studies should investigate the mechanism that prevents interferon signaling in neural progenitors and the therapeutic potential of triggering IFN signaling in these progenitor cells in the context of pathogenic infections during pregnancy or early infancy.

Last, human adult neurogenesis is reduced in the brains of patients suffering from neurodegenerative disorders such as Alzheimer's disease (AD) (reviewed in Salta *et al*, 2023). AD is the most prevalent cause of age-related dementia characterized by a progressive impairment of cognition in aging patients. AD is caused by a disbalance of proteostasis in neurons and neighboring cells leading to the accumulation of extracellular amyloid plaques and intracellular neurofibrillary tangles, driving cell death and chronic

inflammation (Salta *et al*, 2023). Yet, a specific role of interferons in the inflammatory context of AD has only recently been proposed (Roy *et al*, 2020) but not in the context of adult neurogenesis. The consistent correlation between the presence of AD and reduced adult neurogenesis encouraged researchers to study the causality of reduced adult neurogenesis in developing AD. Interestingly, mouse models of AD display reduced adult neurogenesis as early as 2 months and cognitive defects at 4 months, long before the onset of the first pathological hallmarks of the disease (Billings *et al*, 2005). Strikingly, AAV-mediated expression of IL10 in neurons of AD mice models ameliorates the decline in adult neurogenesis and cognitive function (Kiyota *et al*, 2012). IL10 exerts an anti-inflammatory role by upregulating the expression of SOCS3, which antagonizes type-I interferon signaling (Williams *et al*, 2004). Whether a disbalanced interferon signature is present in the neurogenic niches of AD patients remains elusive. However, several mechanisms involved in the interferon response in NSCs including regulation of mTOR (An *et al*, 2003; Pei *et al*, 2008), Pkr, and eIF2α (Chang *et al*, 2002; Peel & Bredesen, 2003) are also shared in AD. Future studies should investigate the potential of downregulating type-I interferon response not only in neurons (Kiyota *et al*, 2012) but also in astrocytes or NSCs in the DG, implementing new approaches of non-invasive brain delivery of AAVs (Blesa *et al*, 2023).

4.4 Limitations of the presented results studying the role of interferons in NSCs

In this section, I discuss the most relevant limitations of my results, as future experiments should aim to tackle those to continue unveiling the role of interferons in NSCs in a more specific and informative manner.

First, the assessed translatome of NSCs (Ribo-Seq) and their signaling phospho-dynamics were assessed in bulk samples of NSCs *ex-vivo*. Especially for the Ribo-Seq, the experiment was performed in bulk NSCs due to the RNA limitation of this technique, which restrains the possibility to investigate the heterogeneity of the interferon response in NSCs. Recent studies developed more sensitive scRibo-Seq techniques (VanInsberghe *et al*, 2021), yet they are limited to the footprint fractions and fail to control for mRNA expression changes.

Second, regarding the *ex-vivo* nature of some of the acquired datasets. Although NSCs were used in low passages and were checked for neurosphere formation, the response of these NSCs *ex-vivo* might differ from that *in-vivo*. In addition, the dosage of interferon might also alter the protein synthesis and cell-cycle regulation in NSCs, as acute or chronic interferon exposure elicits different responses in NSCs (Llorens-Bobadilla *et al*,

2015; Kalamakis *et al*, 2019). In addition, future studies should validate the biphasic response of mTOR in response to interferon as well as the repression of translation of *Sox2 in-vivo*. These validations are however more technically and biologically challenging than they might seem. When treating animals with IFN, the dosage, mode of administration, and timing of the response would need to be assessed and adapted accordingly. Especially in the context of aging, the number of cells showing high levels of p-S6 in the vSVZ decreases dramatically with age (Paliouras *et al*, 2012), indicative of reduced mTORC1 activity in the old brain. This decrease in mTORC1 activity correlate with the increase in type-I interferon signature but also with the decrease in cycling cells in the aged vSVZ (Kalamakis *et al*, 2019). Given that mTORC1 activity is also low in non-cycling NSCs in the vSVZ (Romero-Pozuelo *et al*, 2020), it is yet not possible to discriminate the selective role of increased interferon or reduced cell cycle separately in downregulating mTORC1 *in-vivo* in the aging brain.

Third, the employed mouse models of research are based on full knock-out models for type-I and -II interferon receptors. This full IFNAGR^{KO} mouse model 1) limits the possibility of studying the selective effect of type-I or -II interferons, 2) hampers the assessment of the causal role of NSCs over the collateral role of interferon on other cells, and 3) might affect stem cells during development resulting in permanent effects that are not the direct result of perturbed neurogenesis only in the adult. To tackle these limitations, in the course of my PhD I have also worked on establishing and expanding different interferon-related mouse models including flox-driven knockouts for type-I interferon, the ISRE-eGFP reporter, as well as combinations of those, to be employed in future studies.

4.5 IFIT1: Antiviral defense meets stem cell biology

IFIT1 is a key ISG in the interferon response, restricting the translation of certain viral RNAs upon infection (Fensterl & Sen, 2015). Despite the historically-defined role of IFIT1 in restricting viral infections, my results conclude that IFIT1 plays also a role in modulating eukaryotic mRNAs in NSCs. This unveils a novel function of IFIT1 and underscores the relevance of interferons in stem cell biology.

4.5.1 How does IFIT1 bind eukaryotic mRNAs?

The unpublished work of Dr. Skabkin in our group revealed that immunoprecipitated fractions of IFIT1 were enriched in neurogenesis-related eukaryotic mRNAs. The nature of this binding is however unclear, as current literature cannot explain how IFIT1 is targeting eukaryotic mRNAs involved in neurogenesis.

Typically, IFIT1 binds capped 5'-end 2′-O-unmethylated viral RNAs (cap0), and with a lower affinity, uncapped 5'-end triphosphate (5'-ppp) viral RNAs (Fensterl & Sen, 2015; Abbas *et al*, 2017). In eukaryotes, mRNAs are co-transcriptionally capped and 2′-O-methylated to conform to the cap1 structure in the nucleus, before being exported to the cytoplasm (Ramanathan *et al*, 2016). Consequently, in eukaryotes, capped 2′-O-unmethylated mRNAs are not present in the cytoplasm, and uncapped mRNAs appear as unstable degradation by-products. More recently, the presence of cytoplasmic mRNA decapping and recapping has been proposed as a mechanism to quickly and effectively adapt to stress stimuli (Trotman *et al*, 2017; revied in Trotman & Schoenberg, 2019). I hypothesize that interferons might influence the epitranscriptome of the cap of certain mRNAs in NSCs to rapidly modify their translation efficiency (i.e. to induce quiescence) while protecting these mRNAs from fast degradation. The selective decapping of neurogenic mRNAs would lead to partial degradation of their 5'UTR sequence, which would remove the 2′-O-methylated nucleotides. Consequently, cytoplasmic recapping of these 5'end 2′-O-unmethylated mRNAs would lead to the generation of cap0 mRNAs, which would be targeted by IFIT1 (Figure 4.3).

To prove this hypothesis, I designed a method to capture the phospho- and cap- mRNA fractions in the cell combining the optimizations of scRNA-Seq techniques (Hagemann-Jensen *et al*, 2020) with previously defined methods for cap- and phospho-RNA sequencing (Ibrahim & Mourelatos, 2019; Pelechano *et al*, 2016; Hagemann-Jensen *et al*, 2018). This method has been further developed and applied in our group by Alena Laier. Our joint efforts have so far focussed on the technical validation of the technique (not shown), which will in the future test the presented hypothesis (Figure 4.3). Furthermore, the recent advent of a novel method to discriminate between cap0, cap1, and cap2 structures should be implemented both in this cap-phospho-Seq as well as in the RNA-IP fractions of IFIT1 (Despic & Jaffrey, 2023). In addition, following my hypothesis that cytoplasmic decapping and recapping license mRNAs for IFIT1 binding, these target mRNAs should undergo a shortening on their 5'UTR. To validate such shortening, I performed 5'UTR 10x scRNA-Seq of the neural lineage cells in 2- and 22-months old WT and IFIT1^{KO} animals during my PhD (see Materials and Methods). Analysis of this experiment has not been included in this thesis given the time limitations but will shed light on the 5'UTRome of the neural lineage in aging and its potential relation to IFIT1.

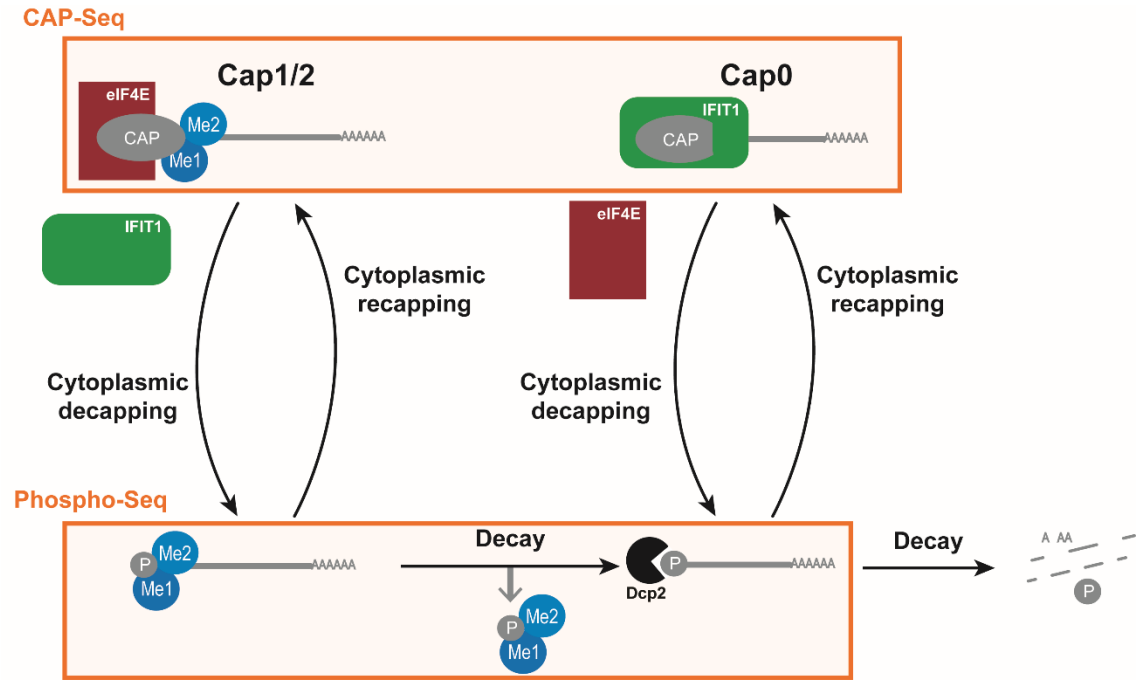

Figure 4.3: Proposed model of cytoplasmic decapping-recapping to license mRNA binding by IFIT1

Last, in support of my hypothesis, recent literature supports the interaction between interferons and the modulation of the cap epitranscriptome. The cap methyltransferase 1 (CMTR1) -responsible for cap1 methylation- is a key ISG to establish the antiviral response in the cell, contributing to higher ISG translation and self-mRNA recognition (Williams *et al*, 2020). In addition, preliminary scouting of changes in NSCs treated with interferon β in our dataset shows an upregulation of phospho Dcp1a^{S335} (data not provided), involved in the regulation of the decapping enzyme, Dcp2 (Chiang *et al*, 2013). Future studies should clarify the mechanisms allowing the binding of IFIT1 to eukaryotic mRNAs, to which the cap-phospho-Seq technology will be highly valuable.

4.5.2 IFIT1 binding affects translation but also the abundance of target mRNAs

Despite the discovery that IFIT1 binds mRNAs relevant for neurogenesis in NSCs, the functional consequences of this binding remain elusive.

Here, together with Dr. Maxim Skabkin, I find that the translational regulation of two key IFIT1 binders, *Gadd45g,* and *Smad6*, might be exerted in opposite directions. While IFIT1 represses translation of *Gadd45g*, it simultaneously seems to show a tendency of increased translation of *Smad6*, although not significant. These observations are based

on qRT-PCR analysis of polysome fractions, as the preliminary evaluation of the Ribo-Seq data of interferon-β-treated IFIT1^{WT} and IFIT1^{KO} NSCs did not show striking differences transcriptome-wide. However, it is worth-discussing the fact that most of the observed change in translation efficiency of *Gadd45g* relies on a drastic change in total RNA levels, as the expression of *Gadd45g* is enhanced by interferon in IFIT1^{WT} NSCs. The presence or absence of transcriptome-wide changes of mRNAs upon interferon treatment in IFIT1^{WT} and IFIT1^{KO} NSCs should be thoroughly validated in the Ribo-Seq dataset in future analyses. In addition, the footprint levels of *Gadd45g* are found to increase both in IFIT1^{WT} and IFIT1^{KO} NSCs. Regardless of the reduced translation efficiency in IFIT1^{KO}. Thus, whether the absence of IFIT1 affects the protein levels of GADD45G remains to be confirmed.

Regardless of the translation efficiency, how the presence of IFIT1 is selectively upregulating the abundance of *Gadd45g* mRNA remains unclear. Future experiments should elucidate whether the differential abundance of Gadd45g results from increased *de-novo* transcription or IFIT1 capturing and stabilizing the *Gadd45g* mRNA upon interferon treatment. Interestingly, as I also found that interferon is increasing p-eIF2α^{S51} as well as shutting down global protein synthesis, it is plausible that the presence of stress granules (SGs) might be relevant for the interferon response in NSCs. Although the role of IFIT1 in SGs is not yet reported, recent reports have highlighted the correlative relation between the expression of the G3BP Stress Granule Assembly Factor 1 (G3BP1) and IFIT1 (Manivannan *et al*, 2020). Whether IFIT1 translocates neurogenesis-relevant mRNAs into SGs to prevent degradation and promote their delayed translation upregulation should be addressed by future studies.

4.5.3 Loss of IFIT1 impairs adult neurogenesis

Here, I show how IFIT1 influences the neurogenic activity and composition of the vSVZ and the DG, highlighting the role of IFIT1 in regulating adult neurogenesis.

In the vSVZ, IFIT1^{KO} mice display a lower number of total NSCs in 2 young individuals. Yet, higher activation of IFIT1^{KO} NSCs leads to increased levels of neural progenitors (TAPs and NBs) in middle and old 6 – 22 months old individuals. This increased prevalence of neural progenitors despite the lower initial NSCs suggests that the rounds of amplifications by TAPs might be increased in the absence of IFIT1. Taking into consideration my previous finding that neural progenitors are refractory to interferons, I hypothesize that IFIT1 might imprint an effect in the stem cells, that might influence the activity of TAPs, despite the potential absence of IFIT1 upregulation in these progenitors. Strikingly, IFIT1^{KO} individuals display a no-aging phenotype in the pool of NSCs, which

largely recapitulates that observed in NSCs in IFNAGR^{KO} mice (Kalamakis *et al*, 2019). This underscores the relevance of IFIT1 as a main effector of interferon in the dynamics of the vSVZ.

Strikingly, my results show discrepancies between the vSVZ and the DG niches. While young IFIT1^{KO} animals display a lower number of NSCs in the vSVZ, the NSC pool in young animals is slightly increased in the DG of these same animals. However, as IFIT1^{KO} animals present the same number of aNSCs, it remains unclear whether the total neurogenic output differs between the two genotypes. Since neurogenic output in the DG controls memory consolidation, the potential implication of these changes in the cognition of IFIT1^{KO} animals is discussed in the next section.

Last, the spatial analysis of actively-cycling or non-active BrdU-retaining NSCs in the vSVZ shows a preferential of active NSCs to cluster together, irrespective of the genotype. These preliminary results are however underpowered to elucidate the mechanisms driving the clustering of active NSCs. As only cell-to-cell distances were computed in my analysis, further definitions of clusters of cells should also give an estimation of the composition of neurogenic clusters in the vSVZ. However, given the time and sample limitations on these animals, the conclusions driven from the spatial analysis can only be taken as preliminary and further assessment should be carried out.

4.5.4 Loss of IFIT1 impairs behavioural traits in mice

Given the strong impact of the absence of IFIT1 in the dynamic of NSCs in the adult brain, I decided to investigate the potential impact of the absence of IFIT1 in the behavioural traits of young and old IFIT1^{KO} mice.

The absence of IFIT1 in young mice indicates a tendency towards deficient memory consolidation, which was maintained in aged IFIT1^{KO} mice. Conversely, young IFIT1^{KO} mice showed a bigger pool of NSCs in the DG with no striking difference in aNSCs. I hypothesize that despite a similar activation rate of NSCs in the DG, IFIT1^{KO} mice display a bigger pool of NSCs given a potential bias in their NSCs to self-renew or differentiate into astrocytes, reducing their neurogenic output and therefore their memory consolidation. In agreement with this hypothesis, I find a higher prevalence of astrocytes in young IFIT1^{KO} mice, as compared to IFIT1^{WT}. This would also explain why despite the slightly higher activation in the DG of old IFIT1^{KO} mice, memory consolidation is not improved. Importantly, learning (and not just memory) is strongly affected at all ages in IFIT1^{KO} mice. Rather than an indication of impaired neurogenesis, this learning defect might underscore a deficient hippocampal function in IFIT1^{KO} mice. Of note, to the best of my knowledge, no functional defects have been reported on IFIT1^{KO} mice, except for

a defective innate immune response in these animals (Fensterl & Sen, 2015). However, interestingly, IFIT1 is enriched over other *ifit* members in the CA1 and CA2 pyramidal neuron layers of the hippocampus in the course of viral infections (Wacher *et al*, 2007). As my results indicate that interferons are present in the neurogenic niches and also in the young brain, it is plausible that basal IFIT1 is also involved in the homeostatic functioning of the hippocampal circuitries.

In terms of social interactions, young IFIT1^{KO} mice showed asocial traits, with a lack of social preference for an intruder versus a littermate mouse. Although this phenotype cannot be related to defects in adult neurogenesis, it again highlights the relevance of IFIT1 in the homeostatic function of the brain. Strikingly, old IFIT1^{KO} mice reversed this trait and regained social novelty preference. Nevertheless, the dispersion of the evaluated individuals is extremely high. Thus, the sample size should be increased to identify possible outliers in the current dataset.

5. References

Abbas YM, Laudenbach BT, Martínez-Montero S, Cencic R, Habjan M, Pichlmair A, Damha MJ, Pelletier J & Nagar B (2017) Structure of human IFIT1 with capped RNA reveals adaptable mRNA binding and mechanisms for sensing N1 and N2 ribose 2′-O methylations. *Proc Natl Acad Sci* 114: E2106–E2115

Del Águila Á, Adam M, Ullom K, Shaw N, Qin S, Ehrman J, Nardini D, Salomone J, Gebelein B, Lu QR, *et al* (2022) Olig2 defines a subset of neural stem cells that produce specific olfactory bulb interneuron subtypes in the subventricular zone of adult mice. *Development* 149: 1–13

Akunuru S & Geiger H (2016) Aging, Clonality, and Rejuvenation of Hematopoietic Stem Cells. *Trends Mol Med* 22: 701–712

Alsayed Y, Uddin S, Ahmad S, Majchrzak B, Druker BJ, Fish EN & Platanias LC (2000) IFN-γ Activates the C3G/Rap1 Signaling Pathway1. *J Immunol* 164: 1800–1806

Alspach E, Lussier DM & Schreiber RD (2019) Interferon γ and its important roles in promoting and inhibiting spontaneous and therapeutic cancer immunity. *Cold Spring Harb Perspect Biol* 11: 1–22

Altman J (1962) Are New Neurons Formed in the Brains of Adult Mammals? *Science (80-)* 135: 1127–1128

Alvarez-Buylla A, Theelen M & Nottebohm F (1990) Proliferation 'hot spots' in adult avian ventricular zone reveal radial cell division. *Neuron* 5: 101–109

Amodeo V, Davies T, Martinez-segura A, Gould AP, Marguerat S, Amodeo V, Davies T, Martinez-segura A, Clements MP & Ragdale HS (2023) Diet suppresses glioblastoma initiation in mice by maintaining quiescence of mutation-bearing neural stem cells Short article Diet suppresses glioblastoma initiation in mice by maintaining quiescence of mutation-bearing neural stem cells. *Dev Cell* 58: 1–11

An WL, Cowburn RF, Li L, Braak H, Alafuzoff I, Iqbal K, Iqbal IG, Winblad B & Pei JJ (2003) Up-regulation of phosphorylated/activated p70 S6 kinase and its relationship to neurofibrillary pathology in Alzheimer's disease. *Am J Pathol* 163: 591–607

Artegiani B, Lindemann D & Calegari F (2011) Overexpression of cdk4 and cyclinD1 triggers greater expansion of neural stem cells in the adult mouse brain. *J Exp Med* 208: 937–948

Artegiani B, Lyubimova A, Muraro M, van Es JH, van Oudenaarden A & Clevers H (2017)

A Single-Cell RNA Sequencing Study Reveals Cellular and Molecular Dynamics of the Hippocampal Neurogenic Niche. *Cell Rep* 21: 3271–3284

Asselineau D, Benlhassan K, Arosio B, Mari D, Ferri E, Casati M, Gussago C, Tedone E, Annoni G, Mazzola P, *et al* (2015) Interleukin-10 Production in Response to Amyloid-β Differs between Slow and Fast Decliners in Patients with Alzheimer's Disease. *J Alzheimer's Dis* 46: 837–842

Averous J, Fonseca BD & Proud CG (2008) Regulation of cyclin D1 expression by mTORC1 signaling requires eukaryotic initiation factor 4E-binding protein 1. 1106–1113

Avni D, Biberman Y & Meyuhas O (1996) The 5′ Terminal Oligopyrimidine Tract Confers Translational Control on Top Mrnas in a Cell Type-and Sequence Context-Dependent Manner. *Nucleic Acids Res* 25: 995–1001

Baldridge MT, King KY, Boles NC, Weksberg DC & Goodell MA (2010) Quiescent haematopoietic stem cells are activated by IFN-γ in response to chronic infection. *Nature* 465: 793–797

Baron R, Nemirovsky A, Harpaz I, Cohen H, Owens T & Monsonego A (2008) IFN-γ enhances neurogenesis in wild-type mice and in a mouse model of Alzheimer's disease. *FASEB J* 22: 2843–2852

Baruch K, Deczkowska A, David E, Castellano JM, Miller O, Kertser A, Berkutzki T, Barnett-Itzhaki Z, Bezalel D, Wyss-Coray T, *et al* (2014) Aging-induced type I interferon response at the choroid plexus negatively affects brain function. *Science (80-)* 346: 89 LP – 93

Basak O, Krieger TG, Muraro MJ, Wiebrands K, Stange DE, Frias-Aldeguer J, Rivron NC, van de Wetering M, van Es JH, van Oudenaarden A, *et al* (2018) Troy+ brain stem cells cycle through quiescence and regulate their number by sensing niche occupancy. *Proc Natl Acad Sci* 115: E610–E619

Baser A, Skabkin M, Kleber S, Dang Y, Gülcüler Balta GS, Kalamakis G, Göpferich M, Carvajal Ibañez D, Schefzik R, Lopez AS, *et al* (2019) Onset of differentiation is post-transcriptionally controlled in adult neural stem cells. *Nature* 566: 100–104

Bate C, Kempster S, Last V & Williams A (2006) Interferon-γ increases neuronal death in response to amyloid-β1-42. *J Neuroinflammation* 3: 1–7

Beane OS, Fonseca VC, Cooper LL, Koren G & Darling EM (2014) Impact of aging on the regenerative properties of bone marrow-, muscle-, and adipose-derived

mesenchymal stem/stromal cells. *PLoS One* 9: 1–22

Bergmann O, Liebl J, Bernard S, Alkass K, Yeung MSY, Steier P, Kutschera W, Johnson L, Landén M, Druid H, *et al* (2012) The Age of Olfactory Bulb Neurons in Humans. *Neuron* 74: 634–639

Bergmann O, Spalding KL & Frisén J (2015) Adult neurogenesis in humans. *Cold Spring Harb Perspect Med* 5: 1–13

Bertolini JA, Favaro R, Zhu Y, Pagin M, Ngan CY, Wong CH, Tjong H, Vermunt MW, Martynoga B, Barone C, *et al* (2019) Mapping the Global Chromatin Connectivity Network for Sox2 Function in Neural Stem Cell Maintenance. *Cell Stem Cell* 24: 462-476.e6

Billings LM, Oddo S, Green KN, McGaugh JL & LaFerla FM (2005) Intraneuronal Aβ causes the onset of early Alzheimer's disease-related cognitive deficits in transgenic mice. *Neuron* 45: 675–688

Bizen N, Inoue T, Shimizu T, Tabu K & Kagawa T A Growth-Promoting Signaling Component Cyclin D1 in Neural Stem Cells Has Antiastrogliogenic Function to Execute Self-Renewal T ISSUE - SPECIFIC S TEM C ELLS A Growth-Promoting Signaling Component Cyclin D1 in Neural Stem Cells Has Antiastrogliogenic Func.

Blair JD, Hockemeyer D & Bateup HS (2018) Genetically engineered human cortical spheroid models of tuberous sclerosis. *Nat Med* 24: 1568–1578

Blanco S, Bandiera R, Popis M, Hussain S, Lombard P, Aleksic J, Sajini A, Tanna H, Cortés-Garrido R, Gkatza N, *et al* (2016) Stem cell function and stress response are controlled by protein synthesis. *Nature* 534: 335–340

Blank T, Detje CN, Spieß A, Hagemeyer N, Brendecke SM, Wolfart J, Staszewski O, Zöller T, Papageorgiou I, Schneider J, *et al* (2016) Brain Endothelial- and Epithelial-Specific Interferon Receptor Chain 1 Drives Virus-Induced Sickness Behavior and Cognitive Impairment. *Immunity* 44: 901–912

Blank T & Prinz M (2017) Type I interferon pathway in CNS homeostasis and neurological disorders. *Glia* 65: 1397–1406

Blasko I, Veerhuis R, Stampfer-Kountchev M, Saurwein-Teissl M, Eikelenboom P & Grubeck-Loebenstein B (2000) Costimulatory Effects of Interferon-γ and Interleukin-1β or Tumor Necrosis Factor α on the Synthesis of Aβ1-40 and Aβ1-42 by Human Astrocytes. *Neurobiol Dis* 7: 682–689

Blesa J, Pineda-Pardo JA, Inoue KI, Gasca-Salas C, Balzano T, Del Rey NLG, Reinares-Sebastián A, Esteban-García N, Rodríguez-Rojas R, Márquez R, *et al* (2023) BBB opening with focused ultrasound in nonhuman primates and Parkinson's disease patients: Targeted AAV vector delivery and PET imaging. *Sci Adv* 9: eadf4888

Blomfield IM, Rocamonde B, del Mar Masdeu M, Mulugeta E, Vaga S, van den Berg DLC, Huillard E, Guillemot F & Urbán N (2019) Id4 promotes the elimination of the pro-activation factor ascl1 to maintain quiescence of adult hippocampal stem cells. *Elife* 8: 1–26

Bogeska R, Mikecin AM, Kaschutnig P, Fawaz M, Büchler-Schäff M, Le D, Ganuza M, Vollmer A, Paffenholz S V., Asada N, *et al* (2022) Inflammatory exposure drives long-lived impairment of hematopoietic stem cell self-renewal activity and accelerated aging. *Cell Stem Cell* 29: 1273-1284.e8

Boldrini M, Fulmore CA, Tartt AN, Simeon LR, Pavlova I, Poposka V, Rosoklija GB, Stankov A, Arango V, Dwork AJ, *et al* (2018) Human Hippocampal Neurogenesis Persists throughout Aging. *Cell Stem Cell* 22: 589-599.e5

Bonaguidi MA, Wheeler MA, Shapiro JS, Stadel RP, Sun GJ, Ming GL & Song H (2011) In vivo clonal analysis reveals self-renewing and multipotent adult neural stem cell characteristics. *Cell* 145: 1142–1155

Bond AM, Ming GL & Song H (2015) Adult Mammalian Neural Stem Cells and Neurogenesis: Five Decades Later. *Cell Stem Cell* 17: 385–395

Bouman BJ, Demerdash Y, Sood S, Grünschläger F, Pilz F, Itani AR, Kuck A, Haas S, Haghverdi L & Essers MAG (2023) Single-cell time series analysis reveals the dynamics of in vivo HSPC responses to inflammation. *bioRxiv*

Brack AS, Conboy MJ, Roy S, Lee M, Kuo CJ, Keller C & Rando TA (2007) Increased Wnt signaling during aging alters muscle stem cell fate and increases fibrosis. *Science (80-)* 317: 807–810

Breuleux M, Klopfenstein M, Stephan C, Doughty CA, Barys L, Maira SM, Kwiatkowski D & Lane HA (2009) Increased AKT S473 phosphorylation after mTORC1 inhibition is rictor dependent and does not predict tumor cell response to PI3K/mTOR inhibition. *Mol Cancer Ther* 8: 742–753

de Bruin AM, Demirel Ö, Hooibrink B, Brandts CH & Nolte MA (2013) Interferon-γ impairs proliferation of hematopoietic stem cells in mice. *Blood* 121: 3578–3585

Burke DC, Graham CF & Lehman JM (1978) Appearance of interferon inducibility and

sensitivity during differentiation of murine teratocarcinoma cells in vitro. *Cell* 13: 243–248

Carlson ME, Hsu M & Conboy IM (2008) Imbalance between pSmad3 and Notch induces CDK inhibitors in old muscle stem cells. *Nature* 454: 528–532

Carrasco-Garcia E, Moreno-Cugnon L, Garcia I, Borras C, Revuelta M, Izeta A, Lopez-Lluch G, de Pancorbo MM, Vergara I, Vina J, *et al* (2019) SOX2 expression diminishes with ageing in several tissues in mice and humans. *Mech Ageing Dev* 177: 30–36

Carvajal Ibañez D, Skabkin M, Hooli J, Cerrizuela S, Göpferich M, Jolly A, Volk K, Zumwinkel M, Bertolini M, Figlia G, *et al* (2023) Interferon regulates neural stem cell function at all ages by orchestrating mTOR and cell cycle . *EMBO Mol Med*: 1–18

Cebrian-Silla A, Nascimento MA, Redmond SA, Mansky B, Wu D, Obernier K, Rodriguez RR, Gonzalez-Granero S, Garcia-Verdugo JM, Lim DA, *et al* (2021) Single-cell analysis of the ventricular-subventricular zone reveals signatures of dorsal and ventral adult neurogenic lineages. *Elife* 10: 1–34

De Cecco M, Ito T, Petrashen AP, Elias AE, Skvir NJ, Criscione SW, Caligiana A, Brocculi G, Adney EM, Boeke JD, *et al* (2019) L1 drives IFN in senescent cells and promotes age-associated inflammation. *Nature* 566: 73–78

Chaker Z, Codega P & Doetsch F (2016) A mosaic world: puzzles revealed by adult neural stem cell heterogeneity. *Wiley Interdiscip Rev Dev Biol* 5: 640–658

Chaker Z, Segalada C & Doetsch F (2021) Spatio-Temporal Recruitment of Adult Neural Stem Cells for Transient Neurogenesis During Pregnancy. *bioRxiv*

Chang RCC, Wong AKY, Ng H-K & Hugon J (2002) Phosphorylation of eukaryotic initiation factor-2α (eIF2α) is associated with neuronal degeneration in Alzheimer's disease. *Neuroreport* 13

Chauvin C, Koka V, Nouschi A, Mieulet V, Dreazen A, Cagnard N, Carpentier W, Kiss T & Meyuhas O (2014) Ribosomal protein S6 kinase activity controls the ribosome biogenesis transcriptional program. 474–483

Cheng M, Nguyen MH, Fantuzzi G & Koh TJ (2008) Endogenous interferon-γ is required for efficient skeletal muscle regeneration. *Am J Physiol - Cell Physiol* 294: 1183–1191

Cheung TH & Rando TA (2013) Molecular regulation of stem cell quiescence. *Nat Rev Mol Cell Biol* 14: 329–340

Chiang PY, Shen YF, Su YL, Kao CH, Lin NY, Hsu PH, Tsai MD, Wang SC, Chang GD, Lee SC, *et al* (2013) Phosphorylation of mRNA Decapping Protein Dcp1a by the ERK Signaling Pathway during Early Differentiation of 3T3-L1 Preadipocytes. *PLoS One* 8

Costa V, Aigner S, Vukcevic M, Sauter E, Behr K, Ebeling M, Dunkley T, Friedlein A, Zoffmann S, Meyer CA, *et al* (2016) MTORC1 Inhibition Corrects Neurodevelopmental and Synaptic Alterations in a Human Stem Cell Model of Tuberous Sclerosis. *Cell Rep* 15: 86–95

Cuartero MI, Parra J de la, Pérez-Ruiz A, Bravo-Ferrer I, Durán-Laforet V, García-Culebras A, García-Segura JM, Dhaliwal J, Frankland PW, Lizasoain I, *et al* (2019) Abolition of aberrant neurogenesis ameliorates cognitive impairment after stroke in mice. *J Clin Invest* 129: 1536–1550

Daffis S, Szretter KJ, Schriewer J, Li J, Youn S, Errett J, Lin TY, Schneller S, Zust R, Dong H, *et al* (2010) 2′-O methylation of the viral mRNA cap evades host restriction by IFIT family members. *Nature* 468: 452–456

Daugherty MD, Schaller AM, Geballe AP & Malik HS (2016) Evolution-guided functional analyses reveal diverse antiviral specificities encoded by ifit1 genes in mammals. *Elife* 5: 1–22

Daynac M, Morizur L, Chicheportiche A, Mouthon MA & Boussin FD (2016) Age-related neurogenesis decline in the subventricular zone is associated with specific cell cycle regulation changes in activated neural stem cells. *Sci Rep* 6: 1–10

Deana M. Apple, Swetha Mahesula, Rene Solano Fonseca, Chang Zhu & Erzsebet Kokovay (2019) Calorie restriction protects neural stem cells from age-related deficits in the subventricular zone. *Aging (Albany NY)* 11: 115–126

Deczkowska A, Baruch K & Schwartz M (2016) Type I/II Interferon Balance in the Regulation of Brain Physiology and Pathology. *Trends Immunol* 37: 181–192

Delgado AC, Maldonado-Soto AR, Silva-Vargas V, Mizrak D, von Känel T, Tan KR, Paul A, Madar A, Cuervo H, Kitajewski J, *et al* (2021) Release of stem cells from quiescence reveals gliogenic domains in the adult mouse brain. *Science (80-)* 372: 1205–1209

Demerdash Y, Kain B, Essers MAG & King KY (2021) Yin and Yang: The dual effects of

interferons on hematopoiesis. *Exp Hematol* 96: 1–12

Demidenko ZN, Zubova SG, Bukreeva EI, Pospelov VA, Pospelova T V. & Blagosklonny M V. (2009) Rapamycin decelerates cellular senescence. *Cell Cycle* 8: 1888–1895

Deng W, Saxe MD, Gallina IS & Gage FH (2009) Adult-Born Hippocampal Dentate Granule Cells Undergoing Maturation Modulate Learning and Memory in the Brain. 29: 13532–13542

Despic V & Jaffrey SR (2023) mRNA ageing shapes the Cap2 methylome in mammalian mRNA. *Nature* 614: 358–366

Dettke M, Scheidt P, Prange H & Kirchner H (1997) Correlation between interferon production and clinical disease activity in patients with multiple sclerosis. *J Clin Immunol* 17: 293–300

Doetsch F & Alvarez-Buylla A (1996) Network of tangential pathways for neuronal migration in adult mammalian brain. *Proc Natl Acad Sci U S A* 93: 14895–14900

Doetsch F, Caille I, Lim DA, Garcı JM & Alvarez-buylla A (1999) Subventricular Zone Astrocytes Are Neural Stem Cells in the Adult Mammalian Brain. 97: 703–716

Dulken BW, Buckley MT, Navarro Negredo P, Saligrama N, Cayrol R, Leeman DS, George BM, Boutet SC, Hebestreit K, Pluvinage J V., *et al* (2019) Single-cell analysis reveals T cell infiltration in old neurogenic niches. *Nature*

Dulken BW, Leeman DS, Boutet SC, Hebestreit K & Brunet A (2017) Single-Cell Transcriptomic Analysis Defines Heterogeneity and Transcriptional Dynamics in the Adult Neural Stem Cell Lineage. *Cell Rep* 18: 777–790

Eiermann N, Haneke K, Sun Z, Stoecklin G & Ruggieri A (2020) Dance with the Devil: Stress Granules and Signaling in Antiviral Responses. *Viruses* 12: 1–47

Ejlerskov P, Hultberg JG, Wang JY, Carlsson R, Ambjørn M, Kuss M, Liu Y, Porcu G, Kolkova K, Friis Rundsten C, *et al* (2015) Lack of Neuronal IFN-β-IFNAR Causes Lewy Body- and Parkinson's Disease-like Dementia. *Cell* 163: 324–339

Eltokhi A, Kurpiers B & Pitzer C (2020) Behavioral tests assessing neuropsychiatric phenotypes in adolescent mice reveal strain- and sex-specific effects. *Sci Rep* 10: 1–15

Encinas JM, Michurina T V., Peunova N, Park JH, Tordo J, Peterson DA, Fishell G, Koulakov A & Enikolopov G (2011) Division-coupled astrocytic differentiation and age-related depletion of neural stem cells in the adult hippocampus. *Cell Stem Cell*

8: 566–579

Epp JR, Mera RS, Köhler S, Josselyn SA & Frankland PW (2016) Neurogenesis-mediated forgetting minimizes proactive interference. *Nat Commun* 7: 5–12

Eriksson PS, Perfilieva E, Bjork-Eriksson T, Alborn AM, Nordborg C, Peterson DA, Gage FH, Björk-Eriksson T, Alborn AM, Nordborg C, *et al* (1998) Neurogenesis in the adult human hippocampus. *Nat Med* 4: 1313–1317

Ernst A, Alkass K, Bernard S, Salehpour M, Perl S, Tisdale J, Possnert G, Druid H & Frisén J (2014) Neurogenesis in the striatum of the adult human brain. *Cell* 156: 1072–1083

Essers MAG, Offner S, Blanco-Bose WE, Waibler Z, Kalinke U, Duchosal MA & Trumpp A (2009) IFNα activates dormant haematopoietic stem cells in vivo. *Nature* 458: 904–908

Fanti AK, Busch K, Greco A, Wang X, Cirovic B, Shang F, Nizharadze T, Frank L, Barile M, Feyerabend TB, *et al* (2023) Flt3- and Tie2-Cre tracing identifies regeneration in sepsis from multipotent progenitors but not hematopoietic stem cells. *Cell Stem Cell* 30: 207-218.e7

Faye MD, Graber TE & Holcik M (2014) Assessment of selective mRNA translation in mammalian cells by polysome profiling. *J Vis Exp*: 1–8

Feierstein CE, Wagner S, Gabellec M, Lledo P & Gheusi G (2010) Disruption of adult neurogenesis in the olfactory bulb affects social interaction but not maternal behavior. 4: 1–17

Fensterl V & Sen GC (2011) The ISG56/IFIT1 Gene Family. *J Interf \& Cytokine Res* 31: 71–78

Fensterl V & Sen GC (2015) Interferon-Induced Ifit Proteins: Their Role in Viral Pathogenesis. *J Virol* 89: 2462–2468

Fensterl V, Wetzel JL, Ramachandran S, Ogino T, Stohlman SA, Bergmann CC, Diamond MS, Virgin HW & Sen GC (2012) Interferon-induced Ifit2/ISG54 protects mice from lethal VSV neuropathogenesis. *PLoS Pathog* 8

Fernández-Fernández L, Comes G, Bolea I, Valente T, Ruiz J, Murtra P, Ramirez B, Anglés N, Reguant J, Morelló JR, *et al* (2012) LMN diet, rich in polyphenols and polyunsaturated fatty acids, improves mouse cognitive decline associated with aging and Alzheimer's disease. *Behav Brain Res* 228: 261–271

Florez MA, Matatall KA, Jeong Y, Ortinau L, Shafer PW, Lynch AM, Jaksik R, Kimmel M, Park D & King KY (2020) Interferon Gamma Mediates Hematopoietic Stem Cell Activation and Niche Relocalization through BST2. *Cell Rep* 33: 108530

Franjic D, Skarica M, Ma S, Arellano JI, Tebbenkamp ATN, Choi J, Xu C, Li Q, Morozov YM, Andrijevic D, *et al* (2022) Transcriptomic taxonomy and neurogenic trajectories of adult human, macaque, and pig hippocampal and entorhinal cells. *Neuron* 110: 452-469.e14

Frisch SM & MacFawn IP (2020) Type I interferons and related pathways in cell senescence. *Aging Cell* 19: 1–12

Frye M & Blanco S (2016) Post-transcriptional modifications in development and stem cells. *Development* 143: 3871–3881

Fuentealba LC, Rompani SB, Parraguez JI, Obernier K, Romero R, Cepko CL & Alvarez-Buylla A (2015) Embryonic Origin of Postnatal Neural Stem Cells. *Cell* 161: 1644–1655

Funk MC, Gleixner JG, Heigwer F, Valentini E, Aydin Z, Tonin E, Hetzer J, Heide D, Stegle O, Heikenwalder M, *et al* (2021) Epithelial cells of the intestine acquire cell-intrinsic inflammation signatures during ageing. *bioRxiv*: 2021.12.19.473357

Furutachi S, Miya H, Watanabe T, Kawai H, Yamasaki N, Harada Y, Imayoshi I, Nelson M, Nakayama KI, Hirabayashi Y, *et al* (2015) Slowly dividing neural progenitors are an embryonic origin of adult neural stem cells. *Nat Neurosci* 18: 657–665

G R Klimpel, W R Fleischmann J and KDK (1982) Gamma interferon (IFN gamma) and IFN alpha/beta suppress murine myeloid colony formation (CFU-C)N: magnitude of suppression is dependent upon level of colony-stimulating factor (CSF). *J Immunol* 129: 76–80

Gal-Ben-Ari S, Barrera I, Ehrlich M & Rosenblum K (2019) PKR: A kinase to remember. *Front Mol Neurosci* 11: 1–20

Gallay L, Fermon C, Lessard L, Weiss-Gayet M, Viel S, Streichenberger N, Corpet A, Mounier R, Gitiaux C, Mouchiroud G, *et al* (2022) Involvement of Type I Interferon Signaling in Muscle Stem Cell Proliferation During Dermatomyositis. *Neurology* 98: e2108--e2119

Gheusi G, Cremer H, McLean H, Chazal G, Vincent JD & Lledo PM (2000) Importance of newly generated neurons in the adult olfactory bulb for odor discrimination. *Proc Natl Acad Sci U S A* 97: 1823–1828

Gingras AC, Raught B & Sonenberg N (2001) Regulation of translation initiation by FRAP/mTOR. *Genes Dev* 15: 807–826

Glück S & Ablasser A (2019) Innate immunosensing of DNA in cellular senescence. *Curr Opin Immunol* 56: 31–36

Götz M, Stoykova A & Gruss P (1998) Pax6 controls radial glia differentiation in the cerebral cortex. *Neuron* 21: 1031–1044

Grabole N, Zhang JD, Aigner S, Ruderisch N, Costa V, Weber FC, Theron M, Berntenis N, Spleiss O, Ebeling M, *et al* (2016) Genomic analysis of the molecular neuropathology of tuberous sclerosis using a human stem cell model. *Genome Med* 8: 1–14

Grow EJ, Flynn RA, Chavez SL, Bayless NL, Wossidlo M, Wesche DJ, Martin L, Ware CB, Blish CA, Chang HY, *et al* (2015) Intrinsic retroviral reactivation in human preimplantation embryos and pluripotent cells. *Nature* 522: 221–246

Guan Q, Ezzati P, Spicer V, Krokhin O, Wall D & Wilkins JA (2017) Interferon γ induced compositional changes in human bone marrow derived mesenchymal stem/stromal cells. *Clin Proteomics* 14: 1–14

Guo C, Yang Q, Xu P, Deng M, Jiang T, Cai L, Li J, Sai K, Xi S, Ouyang H, *et al* (2023) Adjuvant Temozolomide Chemotherapy with or Without Interferon Alfa among Patients with Newly Diagnosed High-grade Gliomas: A Randomized Clinical Trial. *JAMA Netw Open* 6: E2253285

Guo J, Hui DJ, Merrick WC & Sen GC (2000) A new pathway of translational regulation mediated by eukaryotic initiation factor 3. *EMBO J* 19: 6891–6899

Guo Y, Yang K, Harwalkar J, Nye JM, Mason DR, Garrett MD, Hitomi M & Stacey DW (2005) Phosphorylation of cyclin D1 at Thr 286 during S phase leads to its proteasomal degradation and allows efficient DNA synthesis. *Oncogene* 24: 2599–2612

Haas S, Hirche C, Schnell A, Sönmezer C, Langstein J, Wurzer S, Thier M, Blaszkiewicz S, Pilz F, Milsom MD, *et al* (2017) A Stem Cell-Based Epigenetic Memory Mediates Interferon Response-Heterogeneity within the Hematopoietic System. *Blood* 130: 634–634

Habjan M, Hubel P, Lacerda L, Benda C, Holze C, Eberl CH, Mann A, Kindler E, Gil-Cruz C, Ziebuhr J, *et al* (2013) Sequestration by IFIT1 Impairs Translation of 2′O-unmethylated Capped RNA. *PLoS Pathog* 9

Hagemann-Jensen M, Abdullayev I, Sandberg R & Faridani OR (2018) Small-seq for single-cell small-RNA sequencing. *Nat Protoc* 13: 2407–2424

Hagemann-Jensen M, Ziegenhain C, Chen P, Ramsköld D, Hendriks GJ, Larsson AJM, Faridani OR & Sandberg R (2020) Single-cell RNA counting at allele and isoform resolution using Smart-seq3. *Nat Biotechnol* 38: 708–714

Hara K, Yonezawa K, Kozlowski MT, Sugimoto T, Andrabi K, Weng QP, Kasuga M, Nishimoto I & Avruch J (1997) Regulation of eIF-4E BP1 phosphorylation by mTOR. *J Biol Chem* 272: 26457–26463

He F, Ge W, Martinowich K, Becker-Catania S, Coskun V, Zhu W, Wu H, Castro D, Guillemot F, Fan G, *et al* (2005) A positive autoregulatory loop of Jak-STAT signaling controls the onset of astrogliogenesis. *Nat Neurosci* 8: 616–625

Herculano-Houzel S (2009) The human brain in numbers: A linearly scaled-up primate brain. *Front Hum Neurosci* 3: 1–11

Hochgerner H, Zeisel A, Lönnerberg P & Linnarsson S (2018) Conserved properties of dentate gyrus neurogenesis across postnatal development revealed by single-cell RNA sequencing. *Nat Neurosci* 21: 290–299

Hong HS, Hwang EM, Sim HJ, Cho HJ, Boo JH, Oh SS, Kim SU & Mook-Jung I (2003) Interferon γ stimulates β-secretase expression and sAPPβ production in astrocytes. *Biochem Biophys Res Commun* 307: 922–927

Hou Q, Huang J, Ayansola H, Masatoshi H & Zhang B (2021) Intestinal Stem Cells and Immune Cell Relationships: Potential Therapeutic Targets for Inflammatory Bowel Diseases. *Front Immunol* 11: 1–14

Hsu PP, Kang SA, Rameseder J, Zhang Y, Ottina KA, Lim D, Peterson TR, Choi Y, Gray NS, Yaffe MB, *et al* (2011) The mTOR-regulated phosphoproteome reveals a mechanism of mTORC1-mediated inhibition of growth factor signaling. *Science (80-)* 332: 1317–1322

Huang S, Hendriks W, Althage A, Hemmi S, Bluethmann H, Kamijo R, Vilček J, Zinkernagel RM & Aguet M (1993) Immune response in mice that lack the interferon-γ receptor. *Science (80-)* 259: 1742–1745

Huberman M, Shalit F, Roth-Deri I, Gutman B, Brodie C, Kott E & Sredni B (1994) Correlation of cytokine secretion by mononuclear cells of Alzheimer patients and their disease stage. *J Neuroimmunol* 52: 147–152

Hyde JL, Gardner CL, Kimura T, White JP, Liu G, Trobaugh DW, Huang C, Tonelli M, Paessler S, Takeda K, *et al* (2014) A Viral RNA Structural Element Alters Host Recognition of Nonself RNA. *Science (80-)* 343: 783–787

Ibrahim F & Mourelatos Z (2019) Capturing 5' and 3' native ends of mRNAs concurrently with Akron sequencing. *Nat Protoc* 14: 1578–1602

Imayoshi I, Sakamoto M, Ohtsuka T, Takao K, Miyakawa T, Yamaguchi M, Mori K, Ikeda T, Itohara S & Kageyama R (2008) Roles of continuous neurogenesis in the structural and functional integrity of the adult forebrain. *Nat Neurosci* 11: 1153–1161

Isaacs A, Lindenmann J & Andrewes CH (1957a) Virus interference. I. The interferon. *Proc R Soc London Ser B - Biol Sci* 147: 258–267

Isaacs A, Lindenmann J, Valentine RC & Andrewes CH (1957b) Virus interference. II. Some properties of interferon. *Proc R Soc London Ser B - Biol Sci* 147: 268–273

Ivashkiv LB (2018) IFNγ: signalling, epigenetics and roles in immunity, metabolism, disease and cancer immunotherapy. *Nat Rev Immunol* 18: 545–558

Ivashkiv LB & Donlin LT (2014) Regulation of type i interferon responses. *Nat Rev Immunol* 14: 36–49

Jash S & Sharma S (2022) Pathogenic Infections during Pregnancy and the Consequences for Fetal Brain Development. *Pathogens* 11

Jasper H (2020) Intestinal Stem Cell Aging: Origins and Interventions. *Annu Rev Physiol* 82: 203–226

Jean S & Kiger AA (2014) Classes of phosphoinositide 3-kinases at a glance. *J Cell Sci* 127: 923–928

Jejurikar SS, Henkelman EA, Cederna PS, Marcelo CL, Urbanchek MG & Kuzon WM (2006) Aging increases the susceptibility of skeletal muscle derived satellite cells to apoptosis. *Exp Gerontol* 41: 828–836

Jia JJ, Lahr RM, Solgaard MT, Moraes BJ, Pointet R, Yang AD, Celucci G, Graber TE, Hoang HD, Niklaus MR, *et al* (2021) MTORC1 promotes TOP mRNA translation through site-specific phosphorylation of LARP1. *Nucleic Acids Res* 49: 3461–3489

Jin WN, Shi K, He W, Sun JH, Van Kaer L, Shi FD & Liu Q (2021) Neuroblast senescence in the aged brain augments natural killer cell cytotoxicity leading to impaired neurogenesis and cognition. *Nat Neurosci* 24: 61–73

John SP, Sun J, Carlson RJ, Cao B, Bradfield CJ, Song J, Smelkinson M & Fraser IDC (2018) IFIT1 Exerts Opposing Regulatory Effects on the Inflammatory and Interferon Gene Programs in LPS-Activated Human Macrophages. *Cell Rep* 25: 95-106.e6

Johnson B, VanBlargan LA, Xu W, White JP, Shan C, Shi PY, Zhang R, Adhikari J, Gross ML, Leung DW, *et al* (2018) Human IFIT3 Modulates IFIT1 RNA Binding Specificity and Protein Stability. *Immunity* 48: 487-499.e5

Jolly A, Fanti AK, Kongsaysak-Lengyel C, Claudino N, Gräßer I, Becker NB & Höfer T (2022) CycleFlow simultaneously quantifies cell-cycle phase lengths and quiescence in vivo. *Cell Reports Methods* 2

Kalamakis G, Brüne D, Ravichandran S, Bolz J, Ziebell F, Stiehl T, Catalá-Martinez F, Kupke J, Zhao S, Llorens-Bobadilla E, *et al* (2019) Quiescence Modulates Stem Cell Maintenance and Regenerative Capacity in the Aging Brain Article Quiescence Modulates Stem Cell Maintenance and Regenerative Capacity in the Aging Brain.

Katsimpardi L, Litterman NK, Schein PA, Miller CM, Loffredo FS, Wojtkiewicz GR, Chen JW, Lee RT, Wagers AJ & Rubin LL (2014) Vascular and Neurogenic Rejuvenation of the Aging Mouse Brain by Young Systemic Factors. *Science (80-)* 344: 630–634

Kempermann G (2022) What Is Adult Hippocampal Neurogenesis Good for? *Front Neurosci* 16: 1–8

Kempermann G, Gage FH, Aigner L, Song H, Curtis MA, Thuret S, Kuhn HG, Jessberger S, Frankland PW, Cameron HA, *et al* (2018) Human Adult Neurogenesis: Evidence and Remaining Questions. *Cell Stem Cell* 23: 25–30

Khan S, Mahalingam R, Sen S, Martinez-Ledesma E, Khan A, Gandy K, Lang FF, Sulman EP, Alfaro-Munoz KD, Majd NK, *et al* (2021) Intrinsic interferon signaling regulates the cell death and mesenchymal phenotype of glioblastoma stem cells. *Cancers (Basel)* 13

Kim PG, Canver MC, Rhee C, Ross SJ, Harriss J V., Tu HC, Orkin SH, Tucker HO & Daley GQ (2016) Interferon-α signaling promotes embryonic HSC maturation. *Blood* 128: 204–216

Kiyota T, Ingraham KL, Swan RJ, Jacobsen MT, Andrews SJ & Ikezu T (2012) AAV serotype 2/1-mediated gene delivery of anti-inflammatory interleukin-10 enhances neurogenesis and cognitive function in APP+PS1 mice. *Gene Ther* 19: 724–733

Knobloch M, Pilz GA, Ghesquière B, Kovacs WJ, Wegleiter T, Moore DL, Hruzova M,

Zamboni N, Carmeliet P & Jessberger S (2017) A Fatty Acid Oxidation-Dependent Metabolic Shift Regulates Adult Neural Stem Cell Activity. *Cell Rep* 20: 2144–2155

Kopel H, Schechtman E, Groysman M, Mizrahi A, Campus EJS & Ram G (2012) Enhanced Synaptic Integration of Adult-Born Neurons in the Olfactory Bulb of Lactating Mothers. 32: 7519–7527

Kremer LP, Cerrizuela S, Eid M, Shukairi A, Ellinger T, Straub J, Dehler S, Korkmaz A, Weichenhan D, Plass C, *et al* (2022) Single-cell triple-omics uncovers DNA methylation as key feature of stemness in the healthy and ischemic adult brain. *bioRxiv*: 2022.07.13.499860

Kremer LPM, Cerrizuela S, Dehler S, Stiehl T, Weinmann J, Abendroth H, Kleber S, Laure A, El Andari J, Anders S, *et al* (2021) High throughput screening of novel AAV capsids identifies variants for transduction of adult NSCs within the subventricular zone. *Mol Ther - Methods Clin Dev* 23: 33–50

Krieger M, Both M, Kranig SA, Pitzer C, Klugmann M, Vogt G, Draguhn A & Schneider A (2012) The hematopoietic cytokine granulocyte-macrophage colony stimulating factor is important for cognitive functions. *Sci Rep* 2: 1–10

Kriegstein A & Alvarez-Buylla A (2009) The Glial Nature of Embryonic and Adult Neural Stem Cells. *Annu Rev Neurosci* 32: 149–184

Kulkarni A, Ganesan P & O'Donnell LA (2016) Interferon gamma: Influence on neural stem cell function in neurodegenerative and neuroinflammatory disease. *Clin Med Insights Pathol* 2016: 9–19

Kumar P, Sweeney TR, Skabkin MA, Skabkina O V, Hellen CUT & Pestova T V (2014) Inhibition of translation by IFIT family members is determined by their ability to interact selectively with the 5′-terminal regions of cap0-, cap1- and 5′ppp- mRNAs. *Nucleic Acids Res* 42: 3228–3245

Kunis G, Baruch K, Rosenzweig N, Kertser A, Miller O, Berkutzki T & Schwartz M (2013) IFN-γ-dependent activation of the brain's choroid plexus for CNS immune surveillance and repair. *Brain* 136: 3427–3440

Lange C, Huttner WB & Calegari F (2009) Cdk4/CyclinD1 Overexpression in Neural Stem Cells Shortens G1, Delays Neurogenesis, and Promotes the Generation and Expansion of Basal Progenitors. *Cell Stem Cell* 5: 320–331

Lee AJ & Ashkar AA (2018) The dual nature of type I and type II interferons. *Front Immunol* 9: 1–10

Lee JH, Lee JE, Kahng JY, Kim SH, Park JS, Yoon SJ, Um JY, Kim WK, Lee JK, Park J, *et al* (2018) Human glioblastoma arises from subventricular zone cells with low-level driver mutations. *Nature* 560: 243–247

Leeman DS, Hebestreit K, Ruetz T, Webb AE, McKay A, Pollina EA, Dulken BW, Zhao X, Yeo RW, Ho TT, *et al* (2018) Lysosome activation clears aggregates and enhances quiescent neural stem cell activation during aging. *Science (80-)* 359: 1277–1283

Lekmine F, Sassano A, Uddin S, Smith J, Majchrzak B, Brachmann SM, Hay N, Fish EN & Platanias LC (2004) Interferon-γ engages the p70 S6 kinase to regulate phosphorylation of the 40S S6 ribosomal protein. *Exp Cell Res* 295: 173–182

Lekmine F, Uddin S, Sassano A, Parmar S, Brachmann SM, Majchrzak B, Sonenberg N, Hay N, Fish EN & Platanias LC (2003) Activation of the p70 S6 kinase and phosphorylation of the 4E-BP1 repressor of mRNA translation by type I interferons. *J Biol Chem* 278: 27772–27780

Li Y, Li C, Xue P, Zhong B, Mao AP, Ran Y, Chen H, Wang YY, Yang F & Shu HB (2009) ISG56 is a negative-feedback regulator of virus-triggered signaling and cellular antiviral response. *Proc Natl Acad Sci U S A* 106: 7945–7950

Lim D & Alvarez-Buylla A (2016) The Adult Ventricular – Subventricular Zone and Olfactory bulb Neurogenesis. *Cold Spring Harb Perspect Biol* 8: a018820

Liu GY & Sabatini DM (2020) mTOR at the nexus of nutrition, growth, ageing and disease. *Nat Rev Mol Cell Biol* 21: 183–203

Liu HK, Belz T, Bock D, Takacs A, Wu H, Lichter P, Chai M & Schütz G (2008) The nuclear receptor tailless is required for neurogenesis in the adult subventricular zone. *Genes Dev* 22: 2473–2478

Livingstone M, Sikström K, Robert PA, Uzé G, Larsson O & Pellegrini SP (2015) Assessment of mTOR-Dependent translational regulation of interferon stimulated genes. *PLoS One* 10: 1–20

Llorens-Bobadilla E, Zhao S, Baser A, Saiz-Castro G, Zwadlo K & Martin-Villalba A (2015) Single-Cell Transcriptomics Reveals a Population of Dormant Neural Stem Cells that Become Activated upon Brain Injury. *Cell Stem Cell* 17: 329–340

Ma J, Yu Z & Qu W (2010) Proliferation and Differentiation of Neural Stem Cells Are Selectively Regulated by Knockout of Cyclin D1. 35–43

Ma XM & Blenis J (2009) Molecular mechanisms of mTOR-mediated translational control. *Nat Rev Mol Cell Biol* 10: 307–318

Maiwald T, Schneider A, Busch H, Sahle S, Gretz N, Weiss TS, Kummer U & Klingmüller U (2010) Combining theoretical analysis and experimental data generation reveals IRF9 as a crucial factor for accelerating interferon-α induced early antiviral signalling. *FEBS J* 277: 4741–4754

Mak GK, Enwere EK, Gregg C, Pakarainen T, Poutanen M, Huhtaniemi I & Weiss S (2008) Male pheromone – stimulated neurogenesis in the adult female brain : possible role in mating behavior. 10: 1003–1012

Mak GK & Weiss S (2010) Paternal recognition of adult offspring mediated by newly generated CNS neurons. *Nat Publ Gr* 13

Manivannan P, Siddiqui MA & Malathi K (2020) RNase L Amplifies Interferon Signaling by Inducing Protein Kinase R-Mediated Antiviral Stress Granules. *J Virol* 94

Marqués-Torrejón MÁ, Porlan E, Banito A, Gómez-Ibarlucea E, Lopez-Contreras AJ, Fernández-Capetillo Ó, Vidal A, Gil J, Torres J & Fariñas I (2013) Cyclin-dependent kinase inhibitor p21 controls adult neural stem cell expansion by regulating Sox2 gene expression. *Cell Stem Cell* 12: 88–100

Matatall KA, Jeong M, Chen S, Sun D, Chen F, Mo Q, Kimmel M & King KY (2016) Chronic Infection Depletes Hematopoietic Stem Cells through Stress-Induced Terminal Differentiation. *Cell Rep* 17: 2584–2595

Matatall KA, Shen C-C, Challen GA & King KY (2014) Type II Interferon Promotes Differentiation of Myeloid-Biased Hematopoietic Stem Cells. *Stem Cells* 32: 3023–3030

Mazewski C, Perez RE, Fish EN & Platanias LC (2020) Type I Interferon (IFN)-Regulated Activation of Canonical and Non-Canonical Signaling Pathways. *Front Immunol* 11: 1–13

McCabe A, Zhang Y, Thai V, Jones M, Jordan MB & MacNamara KC (2015) Macrophage-lineage cells negatively regulate the hematopoietic stem cell pool in response to interferon gamma at steady state and during infection. *Stem Cells* 33: 2294–2305

McGlincy NJ & Ingolia NT (2017) Transcriptome-wide measurement of translation by ribosome profiling. *Methods* 126: 112–129

McHugh SB, Lopes-dos-Santos V, Gava GP, Hartwich K, Tam SKE, Bannerman DM & Dupret D (2022) Adult-born dentate granule cells promote hippocampal population sparsity. *Nat Neurosci* 25: 1481–1491

Mejia-Ramirez E & Florian MC (2020) Understanding intrinsic hematopoietic stem cell aging. *Haematologica* 105: 22–37

Mercado N, Schutzius G, Kolter C, Estoppey D, Bergling S, Roma G, Gubser Keller C, Nigsch F, Salathe A, Terranova R, *et al* (2019) IRF2 is a master regulator of human keratinocyte stem cell fate. *Nat Commun* 10

Mesquita SD, Ferreira AC, Gao F, Coppola G, Geschwind DH, Sousa JC, Correia-Neves M, Sousa N, Palha JA & Marques F (2015) The choroid plexus transcriptome reveals changes in type I and II interferon responses in a mouse model of Alzheimer's disease. *Brain Behav Immun* 49: 280–292

Di Micco R, Krizhanovsky V, Baker D & d'Adda di Fagagna F (2021) Cellular senescence in ageing: from mechanisms to therapeutic opportunities. *Nat Rev Mol Cell Biol* 22: 75–95

Michalska A, Blaszczyk K, Wesoly J & Bluyssen HAR (2018) A positive feedback amplifier circuit that regulates interferon (IFN)-stimulated gene expression and controls type I and type II IFN responses. *Front Immunol* 9: 1–17

Micheli L, D'Andrea G, Ceccarelli M, Ferri A, Scardigli R & Tirone F (2019) P16Ink4a prevents the activation of aged quiescent dentate gyrus stem cells by physical exercise. *Front Cell Neurosci* 13: 1–14

Miloslavski R, Cohen E, Avraham A, Iluz Y, Hayouka Z, Kasir J, Mudhasani R, Jones SN, Cybulski N, Rüegg MA, *et al* (2014) Oxygen sufficiency controls TOP mRNA translation via the TSC-Rheb-mTOR pathway in a 4E-BP-independent manner. *J Mol Cell Biol* 6: 255–266

Minter MR, Moore Z, Zhang M, Brody KM, Jones NC, Shultz SR, Taylor JM & Crack PJ (2016) Deletion of the type-1 interferon receptor in APPSWE/PS1ΔE9 mice preserves cognitive function and alters glial phenotype. *Acta Neuropathol Commun* 4: 72

Mira H, Andreu Z, Suh H, Chichung Lie D, Jessberger S, Consiglio A, Emeterio JS, Hortigüela R, Marqués-Torrejón MÁ, Nakashima K, *et al* (2010) Signaling through BMPR-IA regulates quiescence and long-term activity of neural stem cells in the adult hippocampus. *Cell Stem Cell* 7: 78–89

Miranda CJ, Braun L, Jiang Y, Mark E, Zhang L, Riolo M, Wang H, Rao M, Altura RA & Kaspar BK (2012) Aging brain microenvironment decreases hippocampal neurogenesis through Wnt-mediated survivin signaling. *Aging Cell* 11: 542–552

Mirzadeh Z, Doetsch F, Sawamoto K, Wichterle H & Alvarez-Buylla A (2010) The subventricular zone en-face: Wholemount staining and ependymal flow. *J Vis Exp*: 1–8

Mirzadeh Z, Merkle FT, Soriano-Navarro M, Garcia-Verdugo JM & Alvarez-Buylla A (2008) Neural Stem Cells Confer Unique Pinwheel Architecture to the Ventricular Surface in Neurogenic Regions of the Adult Brain. *Cell Stem Cell* 3: 265–278

Molofsky A V., Slutsky SG, Joseph NM, He S, Pardal R, Krishnamurthy J, Sharpless NE & Morrison SJ (2006) Increasing p16INK4a expression decreases forebrain progenitors and neurogenesis during ageing. *Nature* 443: 448–452

Moore DL, Pilz GA, Araúzo-Bravo MJ, Barral Y & Jessberger S (2015) A mechanism for the segregation of age in mammalian neural stem cells. *Science (80-)* 349: 1334–1338

Moreno-Jiménez EP, Flor-García M, Terreros-Roncal J, Rábano A, Cafini F, Pallas-Bazarra N, Ávila J & Llorens-Martín M (2019) Adult hippocampal neurogenesis is abundant in neurologically healthy subjects and drops sharply in patients with Alzheimer's disease. *Nat Med* 25: 554–560

Moss J, Gebara E, Bushong EA, Sánchez-Pascual I, O'Laoi R, El M'Gharia I, Kocher-Braissant J, Ellisman MH & Toni N (2016) Fine processes of Nestin-GFP-positive radial glia-like stem cells in the adult dentate gyrus ensheathe local synapses and vasculature. *Proc Natl Acad Sci U S A* 113: E2536–E2545

Muckenhuber M, Seufert I, Müller-Ott K, Mallm JP, Klett LC, Knotz C, Hechler J, Kepper N, Erdel F & Rippe K (2023) Epigenetic signals that direct cell type-specific interferon beta response in mouse cells. *Life Sci alliance* 6: 1–18

Müller U, Steinhoff U, Reis LFL, Hemmi S, Pavlovic J, Zinkernagel RM & Aguet M (1994) Functional role of type I and type II interferons in antiviral defense. *Science (80-)* 264: 1918–1921

Murao N, Noguchi H & Nakashima K (2016) Epigenetic regulation of neural stem cell property from embryo to adult. *Neuroepigenetics* 5: 1–10

Naik S, Larsen SB, Cowley CJ & Fuchs E (2018) Two to Tango: Dialog between Immunity and Stem Cells in Health and Disease. *Cell* 175: 908–920

Nandagopal N & Roux PP (2015) Regulation of global and specific mRNA translation by the mTOR signaling pathway. *Translation* 3: e983402

Natsume A, Ishii D, Wakabayashi T, Tsuno T, Hatano H, Mizuno M & Yoshida J (2005) IFN-β down-regulates the expression of DNA repair gene MGMT and sensitizes resistant glioma cells to temozolomide. *Cancer Res* 65: 7573–7579

Negrotto S, De Giusti CJ, Lapponi MJ, Etulain J, Rivadeneyra L, Pozner RG, Gomez RM & Schattner M (2011) Expression and functionality of type I interferon receptor in the megakaryocytic lineage. *J Thromb Haemost* 9: 2477–2485

Nicaise AM, Willis CM, Crocker SJ & Pluchino S (2020) Stem Cells of the Aging Brain. *Front Aging Neurosci* 12: 1–23

Obernier K & Alvarez-Buylla A (2019) Neural stem cells: Origin, heterogeneity and regulation in the adult mammalian brain. *Dev* 146

Obernier K, Cebrian-Silla A, Thomson M, Parraguez JI, Anderson R, Guinto C, Rodas Rodriguez J, Garcia-Verdugo JM & Alvarez-Buylla A (2018) Adult Neurogenesis Is Sustained by Symmetric Self-Renewal and Differentiation. *Cell Stem Cell* 22: 221-234.e8

Ogrodnik M, Zhu Y, Langhi LGP, Tchkonia T, Krüger P, Fielder E, Victorelli S, Ruswhandi RA, Giorgadze N, Pirtskhalava T, *et al* (2019) Obesity-Induced Cellular Senescence Drives Anxiety and Impairs Neurogenesis. *Cell Metab* 29: 1061-1077.e8

Orvain C, Lin YL, Jean-Louis F, Hocini H, Hersant B, Bennasser Y, Ortonne N, Hotz C, Wolkenstein P, Boniotto M, *et al* (2020) Hair follicle stem cell replication stress drives IFI16/STING-dependent inflammation in hidradenitis suppurativa. *J Clin Invest* 130: 3777–3790

Paliouras GN, Hamilton LK, Aumont A, Joppé SE, Barnaб́-Heider F & Fernandes KJL (2012) Mammalian target of rapamycin signaling is a key regulator of the transit-amplifying progenitor pool in the adult and aging forebrain. *J Neurosci* 32: 15012–15026

Palmer TD, Willhoite AR & Gage FH (2000) Vascular niche for adult hippocampal neurogenesis. *J Comp Neurol* 425: 479–494

Pang WW, Price EA, Sahoo D, Beerman I, Maloney WJ, Rossi DJ, Schrier SL & Weissman IL (2011) Human bone marrow hematopoietic stem cells are increased in frequency and myeloid-biased with age. *Proc Natl Acad Sci U S A* 108: 20012–20017

Paredes MF, James D, Gil-Perotin S, Kim H, Cotter JA, Ng C, Sandoval K, Rowitch DH, Xu D, McQuillen PS, *et al* (2016) Extensive migration of young neurons into the infant human frontal lobe. *Science (80-)* 354

Paredes MF, Sorrells SF, Cebrian-Silla A, Sandoval K, Qi D, Kelley KW, James D, Mayer S, Chang J, Auguste KI, *et al* (2018) Does Adult Neurogenesis Persist in the Human Hippocampus? *Cell Stem Cell* 23: 780–781

Pavitt GD (2018) Regulation of translation initiation factor eIF2B at the hub of the integrated stress response. *WIREs RNA* 9

Payea MJ, Anerillas C, Tharakan R & Gorospe M (2021) Translational Control during Cellular Senescence. *Mol Cell Biol* 41: 1–14

Peel AL & Bredesen DE (2003) Activation of the cell stress kinase PKR in Alzheimer's disease and human amyloid precursor protein transgenic mice. *Neurobiol Dis* 14: 52–62

Pei J-J, Björkdahl C, Zhang H, Zhou X & Winblad B (2008) p70 S6 Kinase and Tau in Alzheimer's Disease. *J Alzheimer's Dis* 14: 385–392

Pelechano V, Wei W & Steinmetz LM (2016) Genome-wide quantification of 5′-phosphorylated mRNA degradation intermediates for analysis of ribosome dynamics. *Nat Protoc* 11: 359–376

Pende M, Um SH, Mieulet V, Sticker M, Goss VL, Mestan J, Mueller M, Fumagalli S, Kozma SC & Thomas G (2004) S6K1−/−/S6K2−/− Mice Exhibit Perinatal Lethality and Rapamycin-Sensitive 5′-Terminal Oligopyrimidine mRNA Translation and Reveal a Mitogen-Activated Protein Kinase-Dependent S6 Kinase Pathway. *Mol Cell Biol* 24: 3112–3124

Pereira L, Medina R, Baena M, Planas AM & Pozas E (2015) IFN gamma regulates proliferation and neuronal differentiation by STAT1 in adult SVZ niche. *Front Cell Neurosci* 9: 1–10

Pestka S, Krause CD & Walter MR (2004) Interferons, interferon-like cytokines, and their receptors. *Immunological Reviews* 202: 8-32

Pichlmair A, Lassnig C, Eberle CA, Górna MW, Baumann CL, Burkard TR, Búrckstúmmer T, Stefanovic A, Krieger S, Bennett KL, *et al* (2011) IFIT1 is an antiviral protein that recognizes 5′-triphosphate RNA. *Nat Immunol* 12: 624–630

Pidugu VK, Wu M-M, Yen A-H, Pidugu HB, Chang K-W, Liu C-J & Lee T-C (2019) IFIT1

and IFIT3 promote oral squamous cell carcinoma metastasis and contribute to the anti-tumor effect of gefitinib via enhancing p-EGFR recycling. *Oncogene* 38: 3232–3247

Pietras EM, Lakshminarasimhan R, Techner JM, Fong S, Flach J, Binnewies M & Passegué E (2014) Re-entry into quiescence protects hematopoietic stem cells from the killing effect of chronic exposure to type I interferons. *J Exp Med* 211: 245–262

Pinto AK, Williams GD, Szretter KJ, White JP, Proença-Módena JL, Liu G, Olejnik J, Brien JD, Ebihara H, Mühlberger E, *et al* (2015) Human and Murine IFIT1 Proteins Do Not Restrict Infection of Negative-Sense RNA Viruses of the Orthomyxoviridae, Bunyaviridae, and Filoviridae Families. *J Virol* 89: 9465–9476

Platanias LC (2005) Mechanisms of type-I- and type-II-interferon-mediated signalling. *Nat Rev Immunol* 5: 375–386

Ponti GP, Obernier K & Alvarez-Buylla A (2013) Lineage progression from stem cells to new neurons in the adult brain ventricularsubventricular zone. *Cell Cycle* 12: 1649–1650

Potel CM, Lin MH, Heck AJR & Lemeer S (2018) Defeating major contaminants in Fe3-immobilized metal ion affinity chromatography (IMAC) phosphopeptide enrichment. *Mol Cell Proteomics* 17: 1028–1034

Prendergast ÁM, Kuck A, van Essen M, Haas S, Blaszkiewicz S & Essers MAG (2017) IFN α -mediated remodeling of endothelial cells in the bone marrow niche. *Haematologica* 102: 445–453

Qin X, Jiang B & Zhang Y (2016) 4E-BP1, a multifactor regulated multifunctional protein. *Cell Cycle* 15: 781–786

Ramanathan A, Robb GB & Chan SH (2016) mRNA capping: Biological functions and applications. *Nucleic Acids Res* 44: 7511–7526

Ran FA, Hsu PD, Wright J, Agarwala V, Scott DA & Zhang F (2013) Genome engineering using the CRISPR-Cas9 system. *Nat Protoc* 8: 2281–2308

Rand U, Rinas M, Werk JS, Nöhren G, Linnes M, Kröger A, Flossdort M, Kály-Kullai K, Hauser H, Höfer T, *et al* (2012) Multi-layered stochasticity and paracrine signal propagation shape the type-I interferon response. *Mol Syst Biol* 8: 1–13

Raychoudhuri A, Shrivastava S, Steele R, Kim H, Ray R & Ray RB (2011) ISG56 and

IFITM1 Proteins Inhibit Hepatitis C Virus Replication. *J Virol* 85: 12881–12889

Romero-Pozuelo J, Figlia G, Kaya O, Martin-Villalba A & Teleman AA (2020) Cdk4 and Cdk6 Couple the Cell-Cycle Machinery to Cell Growth via mTORC1. *Cell Rep* 31

Romine J, Gao X, Xu XM, So KF & Chen J (2015) The proliferation of amplifying neural progenitor cells is impaired in the aging brain and restored by the mTOR pathway activation. *Neurobiol Aging* 36: 1716–1726

Rothhammer V, Mascanfroni ID, Bunse L, Takenaka MC, Kenison JE, Mayo L, Chao CC, Patel B, Yan R, Blain M, *et al* (2016) Type i interferons and microbial metabolites of tryptophan modulate astrocyte activity and central nervous system inflammation via the aryl hydrocarbon receptor. *Nat Med* 22: 586–597

Roy ER, Wang B, Wan YW, Chiu G, Cole A, Yin Z, Propson NE, Xu Y, Jankowsky JL, Liu Z, *et al* (2020) Type I interferon response drives neuroinflammation and synapse loss in Alzheimer disease. *J Clin Invest* 130: 1912–1930

Ruvinsky I, Sharon N, Lerer T, Cohen H, Stolovich-rain M, Nir T, Dor Y, Zisman P & Meyuhas O (2005) Ribosomal protein S6 phosphorylation is a determinant of cell size and glucose homeostasis. 2199–2211

Sakamoto M, Imayoshi I, Ohtsuka T, Yamaguchi M & Mori K (2011) Continuous neurogenesis in the adult forebrain is required for innate olfactory responses. 108: 8479–8484

Saleiro D & Platanias LC (2019) Interferon signaling in cancer. Non-canonical pathways and control of intracellular immune checkpoints. *Semin Immunol* 43: 101299

Salta E, Lazarov O, Fitzsimons CP, Tanzi R, Lucassen PJ & Choi SH (2023) Adult hippocampal neurogenesis in Alzheimer's disease: A roadmap to clinical relevance. *Cell Stem Cell* 30: 120–136

Sanai N, Nguyen T, Ihrie RA, Mirzadeh Z, Tsai HH, Wong M, Gupta N, Berger MS, Huang E, Garcia-Verdugo JM, *et al* (2011) Corridors of migrating neurons in the human brain and their decline during infancy. *Nature* 478: 382–386

Sato T, Ishikawa S, Asano J, Yamamoto H, Fujii M, Sato T, Yamamoto K, Kitagaki K, Akashi T, Okamoto R, *et al* (2020) Regulated IFN signalling preserves the stemness of intestinal stem cells by restricting differentiation into secretory-cell lineages. *Nat Cell Biol* 22: 919–926

Sawamiphak S, Kontarakis Z & Stainier DYR (2014) Interferon Gamma Signaling

Positively Regulates Hematopoietic Stem Cell Emergence. *Dev Cell* 31: 640–653

Schmeisser H, Mejido J, Balinsky CA, Morrow AN, Clark CR, Zhao T & Zoon KC (2010) Identification of Alpha Interferon-Induced Genes Associated with Antiviral Activity in Daudi Cells and Characterization of IFIT3 as a Novel Antiviral Gene. *J Virol* 84: 10671–10680

Schreiber G (2017) The molecular basis for differential type i interferon signaling. *J Biol Chem* 292: 7285–7294

Schürch CM, Riether C & Ochsenbein AF (2014) Cytotoxic CD8+ T cells stimulate hematopoietic progenitors by promoting cytokine release from bone marrow mesenchymal stromal cells. *Cell Stem Cell* 14: 460–472

Segel M, Neumann B, Hill MFE, Weber IP, Viscomi C, Zhao C, Young A, Agley CC, Thompson AJ, Gonzalez GA, *et al* (2019) Niche stiffness underlies the ageing of central nervous system progenitor cells. *Nature* 573: 130–134

Seib DRM, Corsini NS, Ellwanger K, Plaas C, Mateos A, Pitzer C, Niehrs C, Celikel T, Martin-Villalba A & Decline CC (2013) Loss of dickkopf-1 restores neurogenesis in old age and counteracts cognitive decline. *Cell Stem Cell* 12: 204–214

Seib DRM & Martin-Villalba A (2014) Neurogenesis in the Normal Ageing Hippocampus: A Mini-Review. *Gerontology* 61: 327–335

Sendoel A, Dunn JG, Rodriguez EH, Naik S, Gomez NC, Hurwitz B, Levorse J, Dill BD, Schramek D, Molina H, *et al* (2017) Translation from unconventional 5′ start sites drives tumour initiation. *Nature* 541: 494–499

Serrano P, Friedman EL, Kenney J, Taubenfeld SM, Zimmerman JM, Hanna J, Alberini C, Kelley AE, Maren S, Rudy JW, *et al* (2008) PKMζ maintains spatial, instrumental, and classically conditioned long-term memories. *PLoS Biol* 6: 2698–2706

Shetty AK, Hattiangady B & Shetty GA (2005) Stem / Progenitor Cell Proliferation Factors FGF-2 , IGF-1 , and VEGF Exhibit Early Decline During the Course of Aging in the Hippocampus : Role of Astrocytes. 186: 173–186

Shin JJY, Berg DA, Zhu Y, Shin JJY, Song J, Bonaguidi MA, Enikolopov G, Nauen DW, Christian KM, Ming GL, *et al* (2015) Single-Cell RNA-Seq with Waterfall Reveals Molecular Cascades underlying Adult Neurogenesis. *Cell Stem Cell* 17: 360–372

Shingo T, Gregg C, Enwere E, Fujikawa H, Hassam R, Geary C, Cross JC & Weiss S (2003) Pregnancy-Stimulated Neurogenesis in the Adult Female Forebrain

Mediated by Prolactin. 299: 117–121

Sidrauski C, McGeachy AM, Ingolia NT & Walter P (2015) The small molecule ISRIB reverses the effects of eIF2α phosphorylation on translation and stress granule assembly. *Elife* 2015: 1–16

Signer RAJJ, Magee JA, Salic A & Morrison SJ (2014) Haematopoietic stem cells require a highly regulated protein synthesis rate. *Nature* 508: 49–54

Silva-Vargas V, Maldonado-Soto AR, Mizrak D, Codega P & Doetsch F (2016) Age-Dependent Niche Signals from the Choroid Plexus Regulate Adult Neural Stem Cells. *Cell Stem Cell* 19: 643–652

Silva-vargas V, Maldonado-soto AR, Mizrak D, Codega P, Silva-vargas V, Maldonado-soto AR, Mizrak D, Codega P & Doetsch F (2016) Short Article Age-Dependent Niche Signals from the Choroid Plexus Regulate Adult Neural Stem Cells Short Article Age-Dependent Niche Signals from the Choroid Plexus Regulate Adult Neural Stem Cells. *Stem Cell* 19: 643–652

Song L, Tian X & Schekman R (2021) Extracellular vesicles from neurons promote neural induction of stem cells through cyclin D1. 220

Sorrells SF, Paredes MF, Cebrian-Silla A, Sandoval K, Qi D, Kelley KW, James D, Mayer S, Chang J, Auguste KI, *et al* (2018) Human hippocampal neurogenesis drops sharply in children to undetectable levels in adults. *Nature* 555: 377–381

Sousa-Victor P, Gutarra S, García-Prat L, Rodriguez-Ubreva J, Ortet L, Ruiz-Bonilla V, Jardí M, Ballestar E, González S, Serrano AL, *et al* (2014) Geriatric muscle stem cells switch reversible quiescence into senescence. *Nature* 506: 316–321

Spalding KL, Bergmann O, Alkass K, Bernard S, Salehpour M, Huttner HB, Boström E, Westerlund I, Vial C, Buchholz BA, *et al* (2013) Dynamics of hippocampal neurogenesis in adult humans. *Cell* 153: 1219

Spalding KL, Bhardwaj RD, Buchholz BA, Druid H & Frisén J (2005) Retrospective birth dating of cells in humans. *Cell* 122: 133–143

Stanifer ML, Guo C, Doldan P & Boulant S (2020) Importance of Type I and III Interferons at Respiratory and Intestinal Barrier Surfaces. *Front Immunol* 11: 1–14

Stemmer M, Thumberger T, Del Sol Keyer M, Wittbrodt J & Mateo JL (2015) CCTop: An intuitive, flexible and reliable CRISPR/Cas9 target prediction tool. *PLoS One* 10: 1–11

Stewart MD, Choi Y, Johnson GA, Yu-Lee LY, Bazer FW & Spencer TE (2002) Roles of Stat1, Stat2, and interferon regulatory factor-9 (IRF-9) in interferon tau regulation of IRF-1. *Biol Reprod* 66: 393–400

Su X, Yu Y, Zhong Y, Giannopoulou EG, Hu X, Liu H, Cross JR, Rätsch G, Rice CM & Ivashkiv LB (2015) Interferon-γ regulates cellular metabolism and mRNA translation to potentiate macrophage activation. *Nat Immunol* 16: 838–849

Sun GJ, Zhou Y, Stadel RP, Moss J, Yong JHA, Ito S, Kawasaki NK, Phan AT, Oh JH, Modak N, *et al* (2015) Tangential migration of neuronal precursors of glutamatergic neurons in the adult mammalian brain. *Proc Natl Acad Sci U S A* 112: 9484–9489

Sun L, Tian Z & Wang J (2010) A direct cross-talk between interferon-γ and sonic hedgehog signaling that leads to the proliferation of neuronal precursor cells. *Brain Behav Immun* 24: 220–228

Syedbasha M, Bonfiglio F, Linnik J, Stuehler C, Wüthrich D & Egli A (2020) Interferon-λ Enhances the Differentiation of Naive B Cells into Plasmablasts via the mTORC1 Pathway. *Cell Rep* 33

Tahmasebi S, Amiri M & Sonenberg N (2019) Translational control in stem cells. *Front Genet* 10: 1–9

Takashima S, Martin ML, Jansen SA, Fu Y, Bos J, Chandra D, O'Connor MH, Mertelsmann AM, Vinci P, Kuttiyara J, *et al* (2019) T cell-derived interferon-γ programs stem cell death in immune-mediated intestinal damage. *Sci Immunol* 4: 1–15

Tartt AN, Fulmore CA, Liu Y, Rosoklija GB, Dwork AJ, Arango V, Hen R, Mann JJ & Boldrini M (2018) Considerations for Assessing the Extent of Hippocampal Neurogenesis in the Adult and Aging Human Brain. *Cell Stem Cell* 23: 782–783

Tcherkezian J, Cargnello M, Romeo Y, Huttlin EL, Lavoie G, Gygi SP & Roux PP (2014) Proteomic analysis of cap-dependent translation identifies LARP1 as a key regulator of 5′TOP mRNA translation. *Genes Dev* 28: 357–371

Teige I, Treschow A, Teige A, Mattsson R, Navikas V, Leanderson T, Holmdahl R & Issazadeh-Navikas S (2003) IFN-β Gene Deletion Leads to Augmented and Chronic Demyelinating Experimental Autoimmune Encephalomyelitis. *J Immunol* 170: 4776–4784

Temprana SG, Mongiat LA, Yang SM, Trinchero MF, Alvarez DD, Kropff E, Giacomini D, Beltramone N, Lanuza GM & Schinder AF (2015) Delayed Coupling to Feedback

Inhibition during a Critical Period for the Integration of Adult-Born Granule Cells. *Neuron* 85: 116–130

Terenzi F, Pal S & Sen GC (2005) Induction and mode of action of the viral stress-inducible murine proteins, P56 and P54. *Virology* 340: 116–124

Terenzi F, Saikia P & Sen GC (2008) Interferon-inducible protein, P56, inhibits HPV DNA replication by binding to the viral protein E1. *EMBO J* 27: 3311–3321

Terreros-Roncal J, Moreno-Jiménez EP, Flor-García M, Rodríguez-Moreno CB, Trinchero MF, Cafini F, Rábano A, Llorens-Martín M, Arellano JI, Duque A, *et al* (2021) Impact of neurodegenerative diseases on human adult hippocampal neurogenesis. *Science (80-)* 374: 1106–1113

Thoreen CC, Chantranupong L, Keys HR, Wang T, Gray NS & Sabatini DM (2012) A unifying model for mTORC1-mediated regulation of mRNA translation. *Nature* 485: 109–113

Thoreen CC, Kang SA, Chang JW, Liu Q, Zhang J, Gao Y, Reichling LJ, Sim T, Sabatini DM & Gray NS (2009) An ATP-competitive mammalian target of rapamycin inhibitor reveals rapamycin-resistant functions of mTORC1. *J Biol Chem* 284: 8023–8032

Toda T & Gage FH (2018) Review: adult neurogenesis contributes to hippocampal plasticity. *Cell Tissue Res* 373: 693–709

Topacio BR, Zatulovskiy E, Cristea S, Xie S, Tambo CS, Rubin SM, Sage J, Kõivomägi M & Skotheim JM (2019) Cyclin D-Cdk4,6 Drives Cell-Cycle Progression via the Retinoblastoma Protein's C-Terminal Helix. *Mol Cell* 74: 758-770.e4

Tosoni G, Ayyildiz D, Bryois J, Macnair W, Fitzsimons CP, Lucassen PJ & Salta E (2023) Mapping human adult hippocampal neurogenesis with single-cell transcriptomics: Reconciling controversy or fueling the debate? *Neuron*: 1–18

Tovey MG, Lallemand C, Meritet JF & Maury C (2006) Adjuvant activity of interferon alpha: Mechanism(s) of action. *Vaccine* 24: S46–S47

Trotman JB, Giltmier AJ, Mukherjee C & Schoenberg DR (2017) RNA guanine-7 methyltransferase catalyzes the methylation of cytoplasmically recapped RNAs. *Nucleic Acids Res* 45: 10726–10739

Trotman JB & Schoenberg DR (2019) A recap of RNA recapping. *WIREs RNA* 10: e1504

Uckelmann H, Blaszkiewicz S, Nicolae C, Haas S, Schnell A, Wurzer S, Wagener R, Aszodi A & Essers MAG (2016) Extracellular matrix protein Matrilin-4 regulates

stressinduced HSC proliferation via CXCR4. *J Exp Med* 213: 1961–1971

Uddin S, Yenush L, Sun XJ, Sweet ME, White MF & Platanias LC (1995) Interferon-α engages the insulin receptor substrate-1 to associate with the phosphatidylinositol 3'-kinase. *J Biol Chem* 270: 15938–15941

Umemoto T, Matsuzaki Y, Shiratsuchi Y, Hashimoto M, Yoshimoto T, Nakamura-Ishizu A, Petrich B, Yamato M & Suda T (2017) Integrin αvβ3 enhances the suppressive effect of interferon-γ on hematopoietic stem cells. *EMBO J* 36: 2390–2403

Urbaìn N, Cheung TH, Urbán N & Cheung TH (2021) Stem cell quiescence: The challenging path to activation. *Dev* 148

Urbán N, Van Den Berg DLC, Forget A, Andersen J, Demmers JAA, Hunt C, Ayrault O & Guillemot F (2016) Return to Quiescence of mouse neural stem cells by degradation of a proactivation protein. *Science (80-)* 353: 292–295

Urbán N, Blomfield IM & Guillemot F (2019) Quiescence of Adult Mammalian Neural Stem Cells: A Highly Regulated Rest. *Neuron* 104: 834–848

VanInsberghe M, van den Berg J, Andersson-Rolf A, Clevers H & van Oudenaarden A (2021) Single-cell Ribo-seq reveals cell cycle-dependent translational pausing. *Nature* 597: 561–565

Vigo T, La Rocca C, Faicchia D, Procaccini C, Ruggieri M, Salvetti M, Centonze D, Matarese G & Uccelli A (2019) IFNβ enhances mesenchymal stromal (Stem) cells immunomodulatory function through STAT1-3 activation and mTOR-associated promotion of glucose metabolism. *Cell Death Dis* 10

Villeda SA, Luo J, Mosher KI, Zou B, Britschgi M, Bieri G, Stan TM, Fainberg N, Ding Z, Eggel A, *et al* (2011) The ageing systemic milieu negatively regulates neurogenesis and cognitive function. *Nature* 477: 90–94

Vincent EE, Elder DJE, Thomas EC, Phillips L, Morgan C, Pawade J, Sohail M, May MT, Hetzel MR & Tavaré JM (2011) Akt phosphorylation on Thr308 but not on Ser473 correlates with Akt protein kinase activity in human non-small cell lung cancer. *Br J Cancer* 104: 1755–1761

Wacher C, Müller M, Hofer MJ, Getts DR, Zabaras R, Ousman SS, Terenzi F, Sen GC, King NJC & Campbell IL (2007) Coordinated Regulation and Widespread Cellular Expression of Interferon-Stimulated Genes (ISG) ISG-49, ISG-54, and ISG-56 in the Central Nervous System after Infection with Distinct Viruses. *J Virol* 81: 860–

871

Wack A, Terczyńska-Dyla E & Hartmann R (2015) Guarding the frontiers: The biology of type III interferons. *Nat Immunol* 16: 802–809

Wang C, Pflugheber J, Sumpter R, Sodora DL, Hui D, Sen GC & Gale M (2003) Alpha Interferon Induces Distinct Translational Control Programs To Suppress Hepatitis C Virus RNA Replication. *J Virol* 77: 3898–3912

Wang W, Wang M, Yang M, Zeng B, Qiu W, Ma Q, Jing X, Zhang Q, Wang B, Yin C, *et al* (2022) Transcriptome dynamics of hippocampal neurogenesis in macaques across the lifespan and aged humans. *Cell Res* 32: 729–743

Williams GD, Gokhale NS, Snider DL & Horner SM (2020) The mRNA Cap 2=-O-Methyltransferase CMTR1 Regulates the Expression of Certain Interferon-Stimulated Genes. *mSphere* 5

Williams L, Bradley L, Smith A & Foxwell B (2004) Signal Transducer and Activator of Transcription 3 Is the Dominant Mediator of the Anti-Inflammatory Effects of IL-10 in Human Macrophages. *J Immunol* 172: 567–576

Wu H, Coskun V, Tao J, Xie W, Ge W, Yoshikawa K, Li E, Zhang Y & Sun YE (2010) Dnmt3a-dependent nonpromoter DNA methylation facilitates transcription of neurogenic genes. *Science (80-)* 329: 444–447

Wu X, Dao Thi VL, Huang Y, Billerbeck E, Saha D, Hoffmann HH, Wang Y, Silva LAV, Sarbanes S, Sun T, *et al* (2018) Intrinsic Immunity Shapes Viral Resistance of Stem Cells. *Cell* 172: 423-438.e25

Wu Y, Bottes S, Fisch R, Zehnder C, Cole JD, Pilz G, Helmchen F, Simons BD & Jessberger S (2023) Chronic in vivo imaging defines age- dependent alterations of neurogenesis in the mouse hippocampus.

Xia P, Wang S, Ye B, Du Y, Li C, Xiong Z, Qu Y & Fan Z (2018) A Circular RNA Protects Dormant Hematopoietic Stem Cells from DNA Sensor cGAS-Mediated Exhaustion. *Immunity* 48: 688-701.e7

Yamakawa H, Kusumoto D, Hashimoto H & Yuasa S (2020) Stem Cell Aging in Skeletal Muscle Regeneration and Disease. *Int J Mol Sci* 21

Yang H, Jiang X, Li B, Yang HJ, Miller M, Yang A, Dhar A & Nikola P (2017) Mechanisms of mTORC1 activation by RHEB and inhibition by PRAS40. *Nat Publ Gr*

Yang K, Wang J, Wu M, Li M, Wang Y & Huang X (2015) Mesenchymal stem cells detect

and defend against gammaherpesvirus infection via the cGAS-STING pathway. *Sci Rep* 5: 1–9

Yang L, Dybedal I, Bryder D, Nilsson L, Sitnicka E, Sasaki Y & Jacobsen SEW (2005) IFN-γ Negatively Modulates Self-Renewal of Repopulating Human Hemopoietic Stem Cells. *J Immunol* 174: 752–757

Yang Z, Liang H, Zhou Q, Li Y, Chen H, Ye W, Chen D, Fleming J, Shu H & Liu Y (2012) Crystal structure of ISG54 reveals a novel RNA binding structure and potential functional mechanisms. *Cell Res* 22: 1328–1338

Yoshida J, Kato K, Wakabayashi T, Enomoto H, Inoue I & Kageyama N (1987) Antitumor Activity of Interferon-$β$ Against Malignant Glioma in Combination with Chemotherapeutic Agent of Nitrosourea(ACNU). In *The Biology of the Interferon System 1986: Proceedings of the 1986 ISIR-TNO meeting on the interferon system, 7--12 September 1986, Dipoli Congress Center, Espoo, Finland*, Cantell K & Schellekens H (eds) pp 399–406. Dordrecht: Springer Netherlands

Young SK & Wek RC (2016) Upstream open reading frames differentially regulate genespecific translation in the integrated stress response. *J Biol Chem* 291: 16927–16935

Yousef H, Czupalla CJ, Lee D, Chen MB, Burke AN, Zera KA, Zandstra J, Berber E, Lehallier B, Mathur V, *et al* (2019) Aged blood impairs hippocampal neural precursor activity and activates microglia via brain endothelial cell VCAM1. *Nat Med* 25: 988–1000

Yousef H, Morgenthaler A, Schlesinger C, Bugaj L, Irina M & Schaffer D V (2015) Age-Associated Increase in BMP Signaling Inhibits Hippocampal Neurogenesis. *Stem Cells* 33: 1577–1588

Zhang C, Cheng N, Qiao B, Zhang F, Wu J, Liu C, Li Y & Du J (2020) Age-related decline of interferon-gamma responses in macrophage impairs satellite cell proliferation and regeneration. *J Cachexia Sarcopenia Muscle* 11: 1291–1305

Zhang X, Li Y, Ji J, Wang XX, Zhang M, Li X, Zhang Y, Zhu Z, Ye SD & Wang XX (2021) Gadd45g initiates embryonic stem cell differentiation and inhibits breast cell carcinogenesis. *Cell Death Discov* 7

Zheng LS, Kaneko N & Sawamoto K (2015) Minocycline treatment ameliorates interferon-alpha-induced neurogenic defects and depression-like behaviors in mice. *Front Cell Neurosci* 9: 1–10

Zhou Y, Su Y, Li S, Kennedy BC, Zhang DY, Bond AM, Sun Y, Jacob F, Lu L, Hu P, *et al* (2022) Molecular landscapes of human hippocampal immature neurons across lifespan. *Nature* 607: 527–533

Zhu X, Chen Z, Shen W, Huang G, Sedivy JM, Wang H & Ju Z (2021) Inflammation, epigenetics, and metabolism converge to cell senescence and ageing: the regulation and intervention. *Signal Transduct Target Ther* 6: 1–29

Zismanov V, Chichkov V, Colangelo V, Jamet S, Wang S, Syme A, Koromilas AE & Crist C (2016a) Phosphorylation of eIF2α is a Translational Control Mechanism Regulating Muscle Stem Cell Quiescence and Self-Renewal. *Cell Stem Cell* 18: 79–90

Zismanov V, Chichkov V, Colangelo V, Syme A, Koromilas AE & Crist C (2016b) Phosphorylation of eIF2 a Is a Translational Control Mechanism Regulating Muscle Stem Cell Article Phosphorylation of eIF2 a Is a Translational Control Mechanism Regulating Muscle Stem Cell Quiescence and Self-Renewal. 79–90

6. Appendix

6.1 Supplementary figures and tables

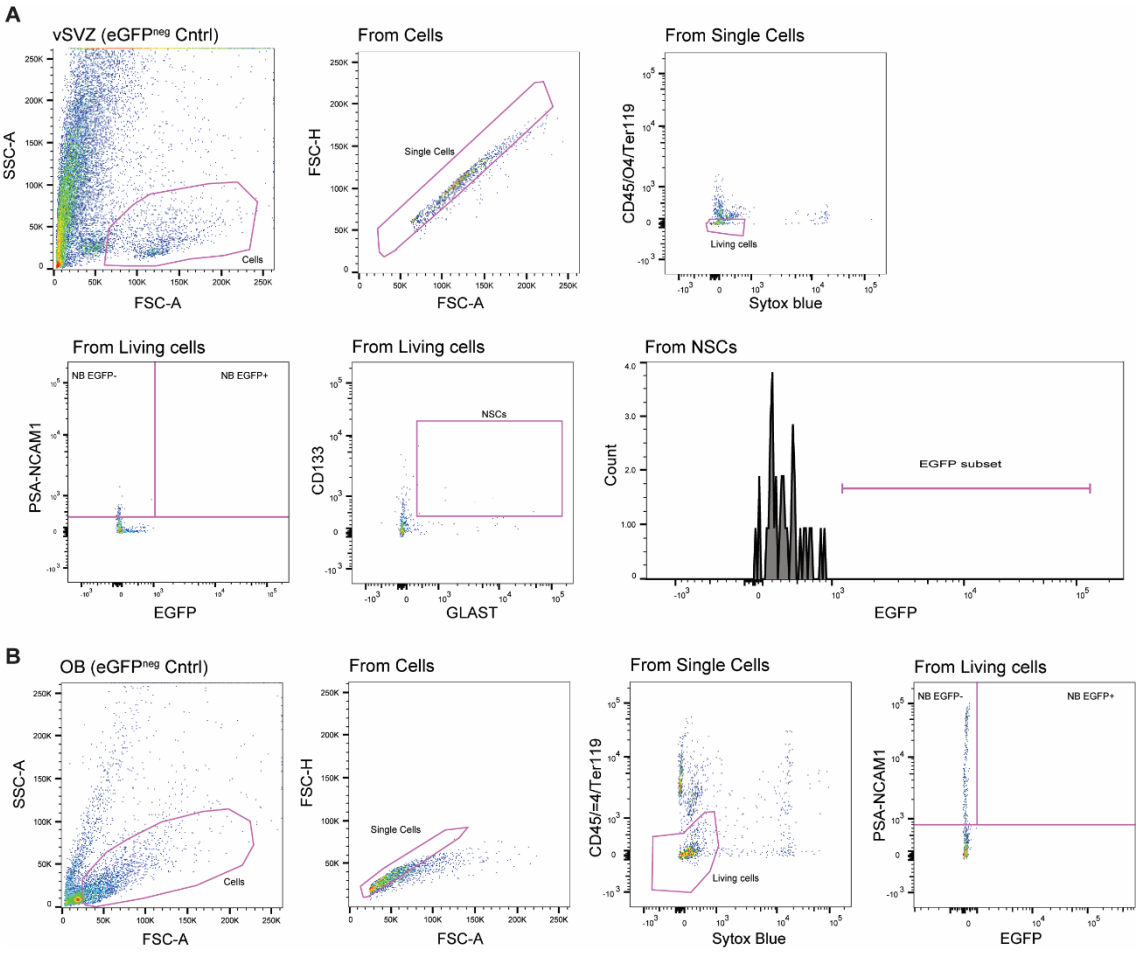

Figure Supl. 1: Interferon reporter EGFP gating strategy

Gating strategy for FACS Quantification of ISRE-eGFP mouse in the vSVZ (**A**) and the OB (**B**).

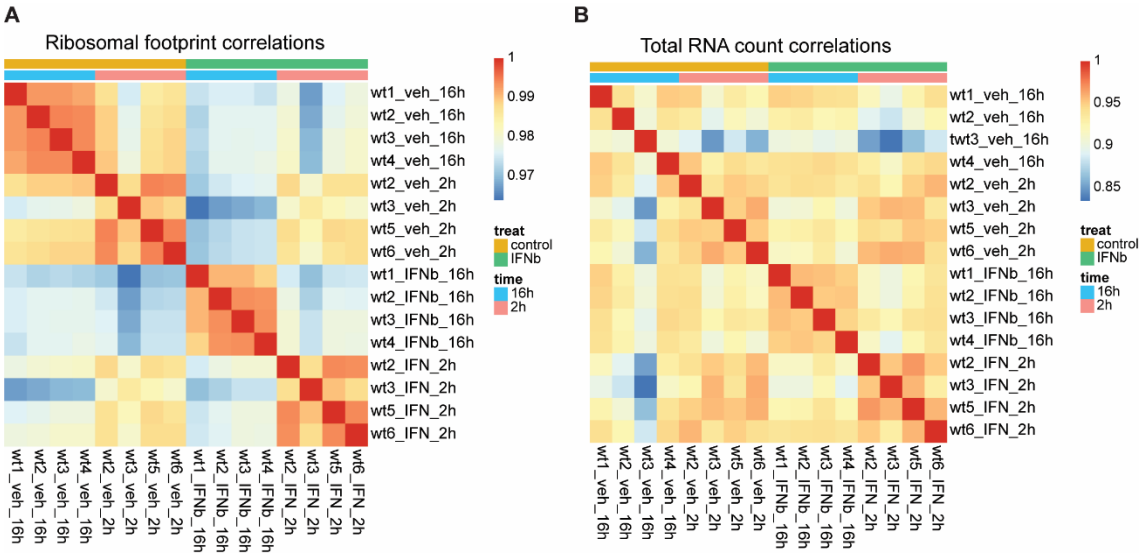

Figure Supl. 2: Quality control of ribosomal sequencing (Ribo-Seq) in NSCs

Figure and caption adapted from Carvajal Ibañez *et al*, 2023, as: "(**A**) Correlation matrix for ribosomal footprint libraries depicting pearson correlation coefficients for all samples. n = 4 biological replicates. (**B**) Correlation matrix for total RNA libraries depicting pearson correlation coefficients for all samples. N = 4 biological replicates."

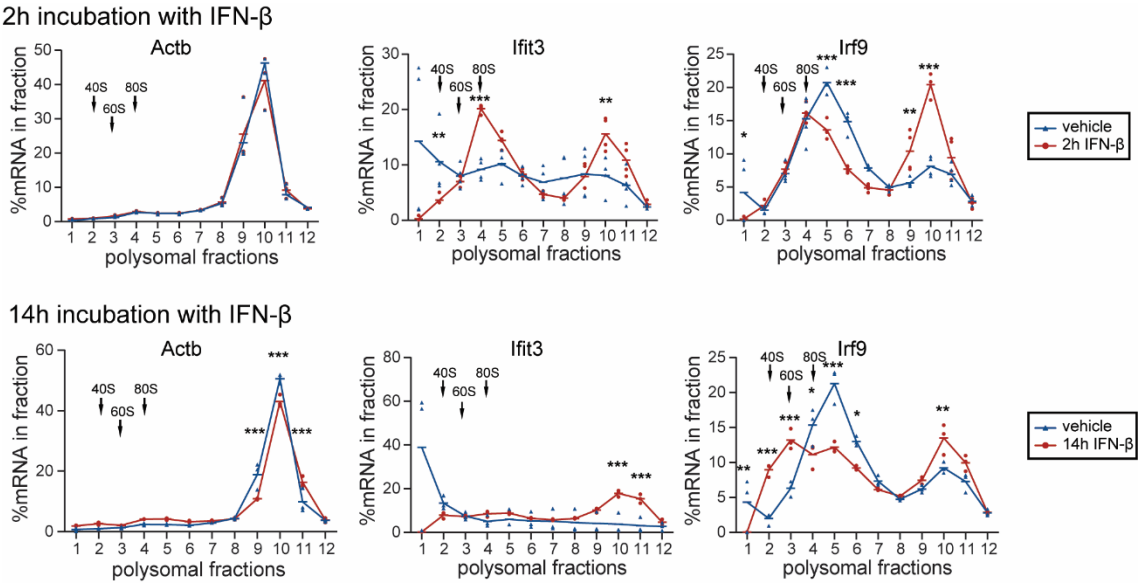

Figure Supl. 3: Interferon consistently upregulates translation of ISGs in NSCs

Figure and caption adapted from Carvajal Ibañez *et al*, 2023, as: “Polysome profiling (RT-qPCR) of *Actb*, *Ifit3,* and *Irf9* upon 2 and 14 h IFN-β. Hyphens represent mean of biological replicates. Arrows indicate the 40S, 60S, and 80S subunits of the ribosome. Two-way ANOVA with Šídák's multiple comparison test was computed. 2h *Ifit3*: fraction 4 ***(P < 0.0001), fraction 10 **(P = 0.0024); 2h *Irf9*: fractions 5, 6, 10 ***(P < 0.0001), fraction 9 **(P = 0.0091). 14h *Actb*: fractions 9, 10 ***(P < 0.0001), fraction 11 ***(P = 0.0002); 14h *Ifit3*: fraction 10 ***(P < 0.0001), fraction 11 ***(P = 0.0003); 14h *Irf9*: fraction 1 *(P = 0.0093), fractions 2, 3, 5 ***(P < 0.0001), fraction 4 *(P = 0.0104), fraction 6 *(P = 0.0263), fraction 10 **(P = 0.0092). n = 3–4 biological replicates. Outliers of *Ifit3* fraction 1 were excluded from the statistical analysis.”

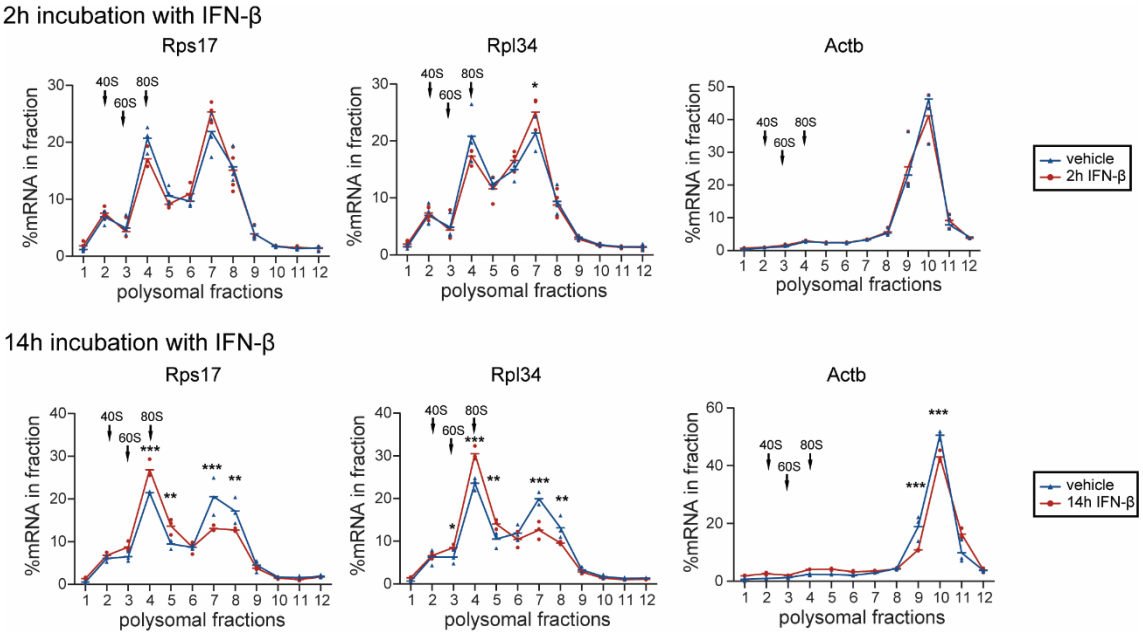

Figure Supl. 4: Interferon biphasically control distribution of TOP-mRNAs in the polysome profiles of NSCs

Figure and caption adapted from Carvajal Ibañez *et al*, 2023, as: “Polysome profiling (RT-qPCR) of *Actb*, *Rps17,* and *Rpl34* upon 2 and 14 h IFN-β. Hyphens represent mean of biological replicates. Arrows indicate the 40S, 60S, and 80S subunits of the ribosome. Two-way ANOVA with Šídák's multiple comparison test was computed. 2h *Rpl34* fraction 7 *(P = 0.037). 14h *Rps17*: fraction 4 ***(P = 0.0002), fraction 5 **(P = 0.003), fraction 7 ***(P < 0.0001), fraction 8 **(P = 0.0018); 14h *Rpl34* :fractions 4, 7 ***(P < 0.0001), fraction 5 (P = 0.0047), fraction 8 **(P = 0.0042); 14h *Actb*: fractions 9, 10 ***(P < 0.0001), fraction 11 ***(P = 0.0002). n = 3–4 biological replicates.”

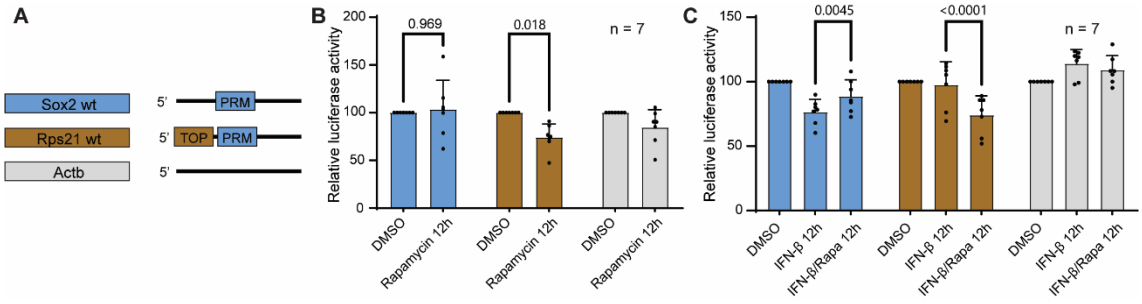

Figure Supl. 5: Repression of *Sox2* translation by interferon is mTORC1-dependent

Figure and caption adapted from Carvajal Ibañez *et al*, 2023, as: "(**A**) 5'UTR constructs priming renilla luciferase controlled by the upstream 5'UTR fragment from *Sox2*, *Rps21*, and *Actb*. TOP = 5'Terminal Oligopyrimidine motif; PRM = 5' Pyrimidine Rich Motif. (**B**) Luciferase activity assay in NSCs treated with Rapamycin. Data are normalized to vehicle and are represented as mean ± SD. n = 7 biological replicates. Two-way ANOVA test with Ŝídák's multiple comparison test (P-values specified). (**C**) Luciferase activity assay in NSCs treated with Rapamycin (Rapa) and IFN-β. Data are normalized to vehicle and are represented as mean ± SD. n = 7 biological replicates. Two-way ANOVA test with Ŝídák's multiple comparison test (P-value specified)."

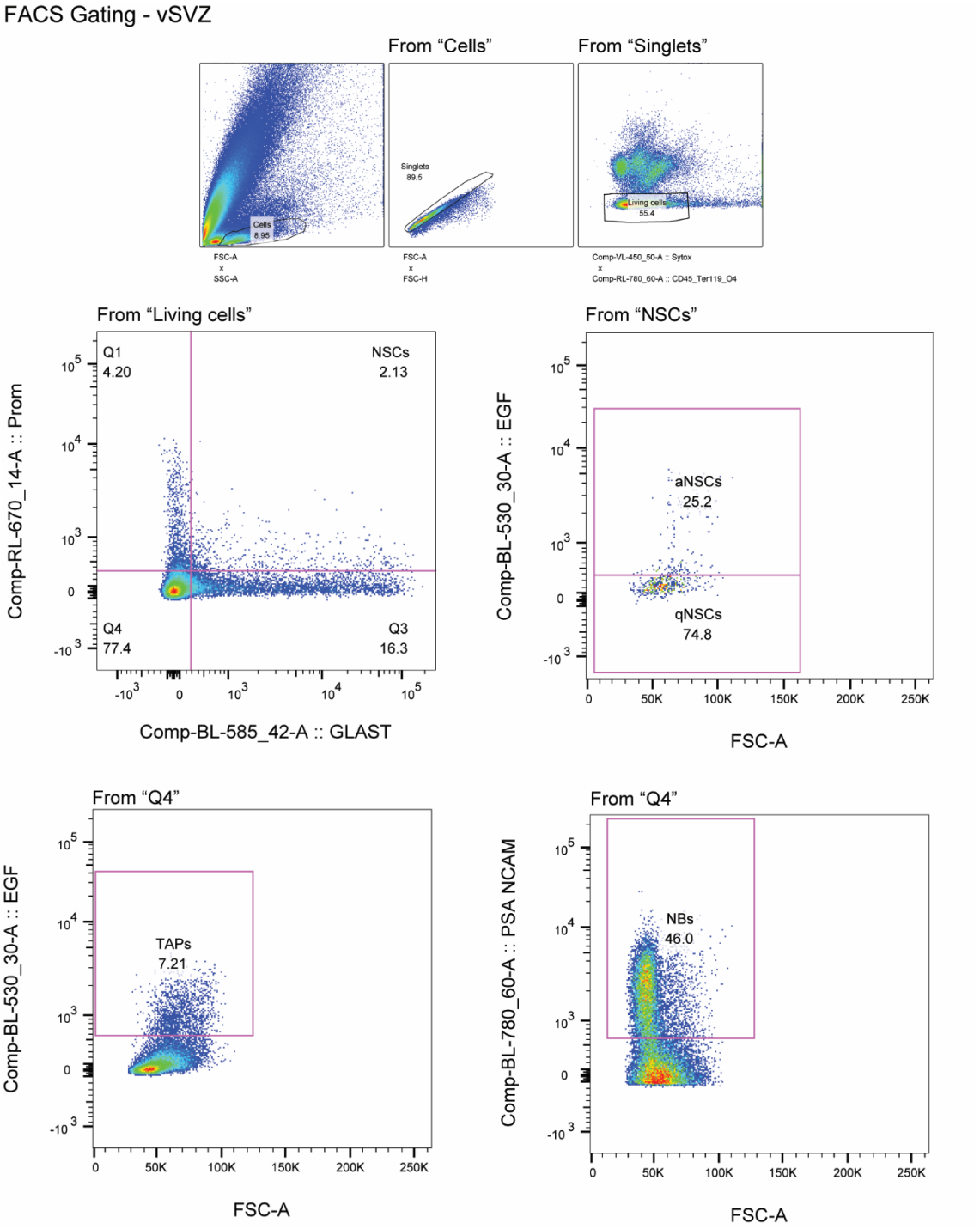

Figure Supl. 6: FACS gating strategy for vSVZ quantifications

Gating strategy for FACS of the vSVZ.

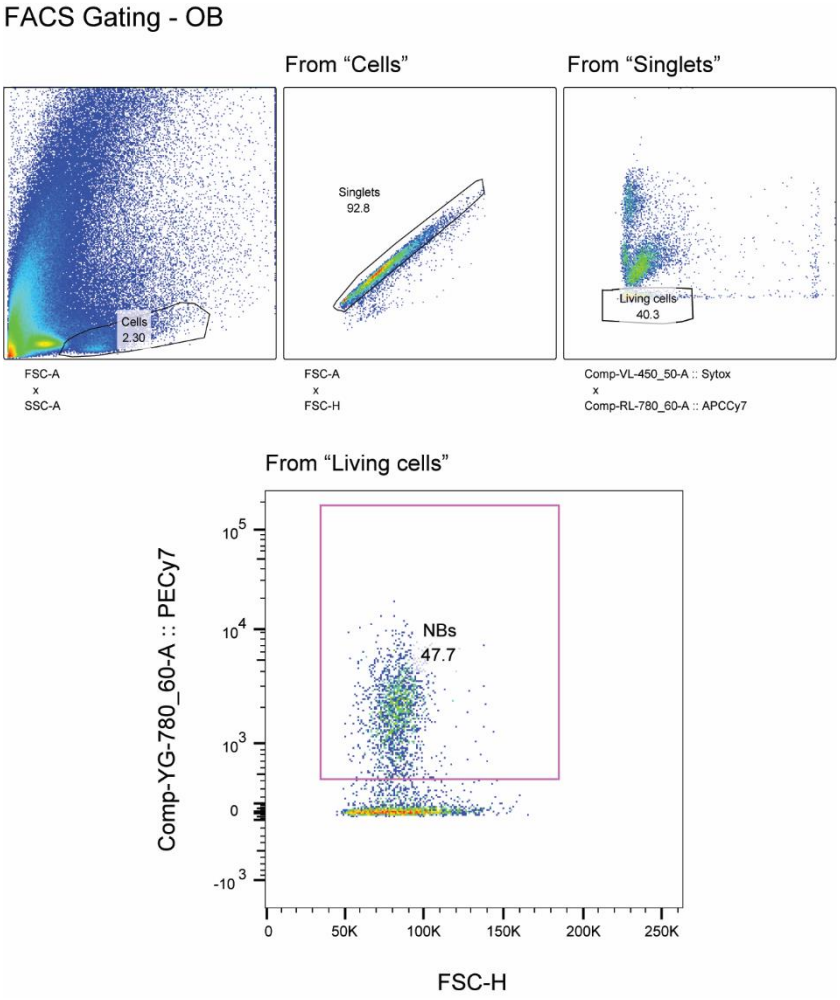

Figure Supl. 7: FACS gating strategy for OB quantifications

Gating strategy for FACS of the OB.

Table Supl. 1: NSC Type I Interferon response gene list

4933412E12Rik	Gbp4	Lynx1	Samhd1
9330175E14Rik	Gbp6	Mitd1	Scarb2
9530053A07Rik	Gbp7	Mlkl	Scarf1
9530082P21Rik	Gbp8	Mmp28	Sdc3
A230050P20Rik	Gbp9	Mocos	Serpina3n
A930037H05Rik	Gfap	Mov10	Serping1
Abca1	Gm11131	Mpeg1	Sfxn2
Ace	Gm12185	Mvp	Shisa5
Acsl5	Gm12216	Mx1	Slc12a7
Adamts4	Gm12250	Mx2	Slc25a22
Adar	Gm17334	Myd88	Slc2a12
Adgrd1	Gm20559	Myh7	Slfn2
Ankfy1	Gm26797	Myo16	Slfn5
Apobec1	Gm4841	Nampt	Slfn8
Apobec3	Gm4951	Ncoa7	Slfn9
Apod	Gm6548	Nlrc5	Socs1
Apol9a	Gm9869	Nmi	Sp100
Apol9b	Gper1	Nmnat2	Spats2l
Asah2	Gprin2	Nod1	Spsb1
Asap3	Grn	Nrp2	Sqstm1
Asb13	Gsdmd	Nudt13	Stard5
Ascc3	H2-D1	Oas1a	Stat1
Atp10a	H2-K1	Oas1b	Stat2
AW011738	H2-M3	Oas1c	Stk32c
Axl	H2-Q4	Oas1g	Tap1
B2m	H2-Q6	Oas2	Tap2
Batf2	H2-Q7	Oas3	Tapbp
BC023105	H2-T10	Oasl1	Tapbpl
Bfsp2	H2-T22	Oasl2	Tcirg1
Bst2	H2-T23	Ogfr	Tdrd7
C1ra	Hap1	Olfm1	Tgm2
C2	Hdc	Olfml2b	Tgtp1
C4b	Helz2	P2rx6	Tgtp2
Cacng5	Herc6	Pacsin1	Thbs1
Capn5	Hfe	Parp10	Thrsp
Card10	Hspb8	Parp11	Timp1
Casp12	Idnk	Parp12	Tlr3
Cbs	Ifi204	Parp14	Tmco4
Ccdc80	Ifi206	Parp3	Tmem106a
Ccdc88b	Ifi27l2a	Parp9	Tmem151a
Cd274	Ifi35	Pdlim4	Tmem176b
Cd47	Ifi44	Perm1	Tmem40
Cds1	Ifi47	Phactr1	Tnfsf10
Cerk	Ifih1	Phf11b	Tor1aip1
Chga	Ifit1	Phf11d	Tor3a

Chmp4b	Ifit2	Pik3ip1	Trafd1
Clec2d	Ifit3	Pla1a	Trim12a
Cmpk2	Ifit3b	Plac8	Trim12c
Cnih2	Ifitm3	Plekha4	Trim14
Cnp	Igtp	Plod3	Trim21
Cox18	Iigp1	Plscr2	Trim25
Crybg1	Il17rc	Pml	Trim26
Csf1	Il18	Pnpt1	Trim30a
Csrnp1	Il18bp	Ppp1r1a	Trim30d
Cxcl10	Insc	Psmb10	Trim34a
Dapp1	Irf1	Psmb8	Trim56
Daxx	Irf7	Psmb9	Tspo
Ddit3	Irf9	Psme1	Tuba8
Ddx24	Irgm1	Psme2	Tulp3
Ddx58	Irgm2	Pttg1	Uaca
Ddx60	Isg15	Rarres2	Uba7
Dhx58	Isg20	Rbm43	Ube2l6
Dtx3l	Islr	Rbms2	Unc93b1
Dusp28	Itm2b	Rd3	Upp1
Eif2ak2	Jade2	Rec8	Usp18
Emp2	Klc2	Rgs14	Usp35
Erap1	Klhdc7a	Rgs2	Vamp5
F830016B08Rik	Lck	Rnf114	Vcam1
Fam46a	Lgals3bp	Rnf135	Vwa5a
Foxf1	Lgals8	Rnf213	Xaf1
Gadd45g	Lgals9	Rnf31	Zbp1
Gbp10	Lmo2	Rsad2	Zc3hav1
Gbp11	Ly6a	Rtp4	Zcchc6
Gbp2	Ly6c1	Rxrg	Zfp521
Gbp3	Ly6e	Samd9l	Znfx1

Table adapted from Carvajal Ibañez *et al*, 2023.

Table Supl. 2: Relevant differentially-phopshorylated phosphosites

Protein	Site (*mus musculus*)	log2FC (2h IFN-β)	Student's T-test p-value 2h	log2FC (16h IFN-β)	Student's T-test p-value 16h
Akt1	S473	0,1	0,88895	-1	0,01947
Irs1	Y608	1,2	0,23201	0,3	0,77939
Irs1	S1134	0,9	0,04265	-2,3	0,15171
Irs1	S1137	0,2	0,87699	-1,7	0,39230
Eif2ak2	S32	0,1	0,81752	4,2	0,00012
Eif2ak2	S110	0,4	0,56152	3,3	0,00094
Eif2ak2	S163	-0,2	0,63997	2,4	0,00003
Eif2ak2	S223	0,5	0,29608	2,1	0,00091
Eif2ak2	S240	-1	0,14584	3,1	0,02378
Ccnd1	T286	1,9	0,09878	0,3	0,67907
Larp1	S498	1	0,13790	3,2	0,00043
Larp1	T492	-0,1	1,00000	2,6	0,02198

Table adapted from Carvajal Ibañez *et al*, 2023.

Table Supl. 3: Top 100 IFIT1 mRNA-binding targets in NSCs

Symbol	Gene	log2FC	stat	pvalue	padj
Catsperg2	ENSMUSG00000049123	4,468	5,074	0,000	0,001
Prss32	ENSMUSG00000048992	4,114	5,009	0,000	0,001
Upk3bl	ENSMUSG00000006143	3,897	3,793	0,000	0,015
Nkx6-1	ENSMUSG00000035187	3,786	4,346	0,000	0,005
Hist4h4	ENSMUSG00000096010	3,301	3,805	0,000	0,015
BC107364	ENSMUSG00000046317	3,208	3,450	0,001	0,028
Lmx1b	ENSMUSG00000038765	3,202	5,244	0,000	0,001
Runx3	ENSMUSG00000070691	2,944	3,402	0,001	0,031
Hist2h3b	ENSMUSG00000074403	2,782	3,591	0,000	0,022
Npc1l1	ENSMUSG00000020447	2,580	3,140	0,002	0,050
Pou4f1	ENSMUSG00000048349	2,454	3,187	0,001	0,045
Tmem28	ENSMUSG00000071719	2,431	2,835	0,005	0,078
Rgs8	ENSMUSG00000042671	2,406	2,675	0,007	0,098
Foxq1	ENSMUSG00000038415	2,373	2,829	0,005	0,079
NA	ENSMUSG00000090863	2,359	2,928	0,003	0,069
Trappc3l	ENSMUSG00000071340	2,343	3,187	0,001	0,045
Pax2	ENSMUSG00000004231	2,329	2,909	0,004	0,070
Hist1h2bp	ENSMUSG00000069308	2,301	3,004	0,003	0,061
Slc16a8	ENSMUSG00000032988	2,290	3,757	0,000	0,016
Syne3	ENSMUSG00000054150	2,285	3,312	0,001	0,036
Cldn19	ENSMUSG00000066058	2,274	2,666	0,008	0,099
Hes5	ENSMUSG00000048001	2,214	3,917	0,000	0,012
E130012A19Rik	ENSMUSG00000043439	2,176	4,348	0,000	0,005
Tbc1d16	ENSMUSG00000039976	2,176	2,876	0,004	0,073
Hist1h4n	ENSMUSG00000069305	2,174	3,401	0,001	0,031
Gata2	ENSMUSG00000015053	2,160	2,703	0,007	0,094
Rims4	ENSMUSG00000035226	2,156	3,902	0,000	0,013
Pklr	ENSMUSG00000041237	2,125	3,488	0,000	0,027
Cyp27b1	ENSMUSG00000006724	2,114	4,434	0,000	0,005
Gbx1	ENSMUSG00000067724	2,106	5,280	0,000	0,001
Lhx1	ENSMUSG00000018698	2,057	3,552	0,000	0,024
Gys2	ENSMUSG00000030244	2,045	2,793	0,005	0,083
Cd74	ENSMUSG00000024610	2,029	2,884	0,004	0,073
Tmem235	ENSMUSG00000070330	2,023	3,107	0,002	0,053
Ahnak	ENSMUSG00000069833	2,014	2,762	0,006	0,087
Tal1	ENSMUSG00000028717	1,991	3,824	0,000	0,014
Pax7	ENSMUSG00000028736	1,977	2,698	0,007	0,095
Gadd45g	ENSMUSG00000021453	1,963	4,907	0,000	0,001
Acoxl	ENSMUSG00000027380	1,961	3,422	0,001	0,030
Odf3	ENSMUSG00000025482	1,959	3,000	0,003	0,061
Myo1h	ENSMUSG00000066952	1,923	3,456	0,001	0,028
Kcng1	ENSMUSG00000074575	1,917	3,601	0,000	0,021
Irx2	ENSMUSG00000001504	1,911	2,744	0,006	0,089
Kcnq4	ENSMUSG00000028631	1,906	4,359	0,000	0,005
Gnao1	ENSMUSG00000031748	1,897	3,459	0,001	0,028
Dpf1	ENSMUSG00000030584	1,893	3,616	0,000	0,021
Tcf23	ENSMUSG00000006642	1,893	3,257	0,001	0,040
Fbxo41	ENSMUSG00000047013	1,874	3,080	0,002	0,055
Kctd15	ENSMUSG00000030499	1,867	3,451	0,001	0,028
Gp1bb	ENSMUSG00000050761	1,852	3,622	0,000	0,020
Six3	ENSMUSG00000038805	1,851	3,323	0,001	0,036

Marveld3	ENSMUSG00000001672	1,849	2,899	0,004	0,072
Tssk2	ENSMUSG00000045521	1,844	2,709	0,007	0,094
En2	ENSMUSG00000039095	1,843	4,503	0,000	0,004
Fam167a	ENSMUSG00000035095	1,839	2,874	0,004	0,073
Phf24	ENSMUSG00000036062	1,836	2,701	0,007	0,094
Gpr161	ENSMUSG00000040836	1,808	3,580	0,000	0,022
Chst3	ENSMUSG00000057337	1,796	4,005	0,000	0,010
Mmp23	ENSMUSG00000029061	1,788	4,024	0,000	0,010
Spns3	ENSMUSG00000020798	1,778	2,739	0,006	0,089
Polr3e	ENSMUSG00000030880	1,759	2,938	0,003	0,067
Arrb1	ENSMUSG00000018909	1,758	2,813	0,005	0,081
Pdzrn3	ENSMUSG00000035357	1,744	3,441	0,001	0,029
Scgb1c1	ENSMUSG00000038801	1,744	2,875	0,004	0,073
Mybl2	ENSMUSG00000017861	1,728	5,301	0,000	0,001
Pitpnm2	ENSMUSG00000029406	1,724	3,028	0,002	0,059
Foxd2	ENSMUSG00000055210	1,723	4,305	0,000	0,006
Tmcc2	ENSMUSG00000042066	1,720	3,190	0,001	0,045
Prelp	ENSMUSG00000041577	1,720	3,711	0,000	0,018
Tub	ENSMUSG00000031028	1,720	3,453	0,001	0,028
Col11a2	ENSMUSG00000024330	1,713	3,028	0,002	0,059
Nkd2	ENSMUSG00000021567	1,711	2,859	0,004	0,075
Chrm4	ENSMUSG00000040495	1,680	3,048	0,002	0,057
Zfp423	ENSMUSG00000045333	1,671	4,686	0,000	0,003
C030006K11Rik	ENSMUSG00000033707	1,669	2,662	0,008	0,100
Ltbp4	ENSMUSG00000040488	1,668	3,102	0,002	0,053
NA	ENSMUSG00000055271	1,667	2,812	0,005	0,081
Lmod1	ENSMUSG00000048096	1,662	3,653	0,000	0,019
Trim71	ENSMUSG00000079259	1,660	2,958	0,003	0,066
Wnt7b	ENSMUSG00000022382	1,659	3,093	0,002	0,054
Mdga1	ENSMUSG00000043557	1,654	2,727	0,006	0,091
Smad6	ENSMUSG00000036867	1,647	3,834	0,000	0,014
Inhbb	ENSMUSG00000037035	1,641	4,910	0,000	0,001
Zfp703	ENSMUSG00000085795	1,638	2,911	0,004	0,070
Pmepa1	ENSMUSG00000038400	1,636	4,168	0,000	0,007
Begain	ENSMUSG00000040867	1,630	3,287	0,001	0,039
Dlx1	ENSMUSG00000041911	1,625	3,173	0,002	0,047
Vwa5b2	ENSMUSG00000046613	1,625	2,958	0,003	0,066
Syndig1l	ENSMUSG00000071234	1,622	3,074	0,002	0,056
Tns1	ENSMUSG00000055322	1,616	3,117	0,002	0,052
Igsf3	ENSMUSG00000042035	1,602	4,183	0,000	0,007
Scx	ENSMUSG00000034161	1,598	2,716	0,007	0,093
D430019H16Rik	ENSMUSG00000094910	1,597	5,524	0,000	0,001
Apcdd1	ENSMUSG00000071847	1,596	4,433	0,000	0,005
Kcnab2	ENSMUSG00000028931	1,592	2,731	0,006	0,090
Adgra2	ENSMUSG00000031486	1,587	3,079	0,002	0,055
Lingo4	ENSMUSG00000044505	1,587	2,681	0,007	0,097
Kif21b	ENSMUSG00000041642	1,584	2,767	0,006	0,086
E2f2	ENSMUSG00000018983	1,583	3,600	0,000	0,021
Stab2	ENSMUSG00000035459	1,574	3,592	0,000	0,022

Table adapted from Carvajal Ibañez *et al*, 2023.

Table Supl. 4: Intersection of IFIT1 binders with differentially-translated mRNAs from Ribo-Seq

Gene	Symbol	RiboSeq Log2FC	RiboSeq_pvalue	RIP_log2FC	RIP_pvalue
ENSMUSG00000032611	1700102P08Rik	5,5505	0,1199	0,8253	0,0868
ENSMUSG00000027460	Angpt4	4,7820	0,1090	1,0296	0,0294
ENSMUSG00000036867	**Smad6**	**4,0250**	**0,2194**	**1,4670**	**0,0001**
ENSMUSG00000042510	AA986860	3,9422	0,1035	0,6732	0,0545
ENSMUSG00000058743	Kcnj14	3,8765	0,3884	1,1510	0,0109
ENSMUSG00000049608	Gpr55	3,7014	0,3437	1,2800	0,0085
ENSMUSG00000022702	Hira	3,5510	0,1461	0,8562	0,0165
ENSMUSG00000056947	Mab21l1	3,2025	0,1073	1,3928	0,0148
ENSMUSG00000038276	Asic3	3,1343	0,2325	1,1922	0,0164
ENSMUSG00000037660	Gdf7	3,1168	0,0053	0,7924	0,1755
ENSMUSG00000039512	Uhrf1bp1	3,0429	0,0275	0,9671	0,0526
ENSMUSG00000054206	Gzmm	3,0020	0,1251	0,9043	0,0562
ENSMUSG00000035403	Crb2	2,7652	0,0046	1,0569	0,0230
ENSMUSG00000018405	Mrm1	2,6309	0,0301	0,9211	0,0242
ENSMUSG00000047030	Spata2	2,5711	0,1440	1,0973	0,0108
ENSMUSG00000044361	BC024139	2,4167	0,1077	1,0163	0,0186
ENSMUSG00000044505	Lingo4	2,4023	0,2235	1,3098	0,0070
ENSMUSG00000036160	Surf6	2,1674	0,0673	0,7217	0,0271
ENSMUSG00000032860	P2ry2	2,1584	0,0604	1,3506	0,0074
ENSMUSG00000006678	Pola1	2,0690	0,0073	0,7375	0,0915
ENSMUSG00000041165	Spem1	1,9587	0,2180	1,3010	0,0273
ENSMUSG00000021253	Tgfb3	1,9176	0,0033	0,9058	0,0065
ENSMUSG00000090231	Cfb	1,7295	0,0157	1,2515	0,0310
ENSMUSG00000021453	**Gadd45g**	**1,5499**	**0,0000**	**1,7766**	**0,0000**
ENSMUSG00000033257	Ttll4	1,4552	0,0086	1,0587	0,0060
ENSMUSG00000038765	Lmx1b	1,2614	0,3458	2,6132	0,0000
ENSMUSG00000079259	Trim71	1,2261	0,0161	1,3201	0,0049
ENSMUSG00000024501	Dpysl3	1,0648	0,0104	0,9728	0,0344
ENSMUSG00000028631	Kcnq4	0,7042	0,3225	1,7185	0,0000
ENSMUSG00000028840	Zfp593	0,6930	0,0002	0,6690	0,0234
ENSMUSG00000055210	Foxd2	-0,3468	0,0324	1,5484	0,0000
ENSMUSG00000074575	Kcng1	-0,3779	0,0261	1,6321	0,0003
ENSMUSG00000062115	Rai1	-0,4179	0,0000	1,0195	0,0419
ENSMUSG00000063317	Usp31	-0,4455	0,0012	0,9630	0,0008
ENSMUSG00000045817	Zfp36l2	-0,4556	0,0011	0,9860	0,0104
ENSMUSG00000022521	Crebbp	-0,4722	0,0000	0,8195	0,0346
ENSMUSG00000028051	Hcn3	-0,4863	0,0006	1,0376	0,0088
ENSMUSG00000048385	Scrt1	-0,5105	0,0028	1,4073	0,0106
ENSMUSG00000037331	Larp1	-0,5227	0,0037	1,1367	0,0046
ENSMUSG00000037885	Stk35	-0,5564	0,0026	1,0452	0,0098
ENSMUSG00000038319	Kcnh2	-0,5735	0,0024	1,3104	0,0035
ENSMUSG00000038866	Zcchc2	-0,5792	0,0000	0,9697	0,0013
ENSMUSG00000037253	Mex3c	-0,6387	0,0002	0,6256	0,0122
ENSMUSG00000085795	Zfp703	-0,6463	0,0343	1,3646	0,0037

ENSMUSG00000041115	Iqsec2	-0,6517	0,0000	0,8740	0,1137
ENSMUSG00000028799	Zfp362	-0,6551	0,0000	0,7882	0,1047
ENSMUSG00000036863	Syde2	-0,6694	0,0353	0,9775	0,0003
ENSMUSG00000033396	Spg11	-0,8274	0,0000	0,6160	0,0614
ENSMUSG00000096010	Hist4h4	-0,8746	0,2977	2,2574	0,0001
ENSMUSG00000018412	Kansl1	-0,9035	0,0008	0,6390	0,0133
ENSMUSG00000024371	C2	-0,9051	0,0130	1,1344	0,0180
ENSMUSG00000072494	Ppp1r3e	-0,9265	0,0091	0,8494	0,0248
ENSMUSG00000030411	Nova2	-0,9344	0,0000	0,8470	0,0800
ENSMUSG00000024042	Sik1	-0,9395	0,1360	1,4171	0,0001
ENSMUSG00000041642	Kif21b	-0,9402	0,1009	1,3173	0,0056
ENSMUSG00000097061	9330151L19Rik	-1,2630	0,0009	0,6958	0,0994
ENSMUSG00000031706	Rfx1	-1,2633	0,0000	0,6066	0,1987
ENSMUSG00000038658	Ric1	-1,2714	0,0044	0,7920	0,0237
ENSMUSG00000051323	Pcdh19	-1,3332	0,0000	0,5926	0,1378
ENSMUSG00000041482	Piezo2	-1,4154	0,0646	0,9166	0,0082
ENSMUSG00000037791	Phf12	-1,4651	0,0064	0,7064	0,0360
ENSMUSG00000048271	Rbm33	-1,5376	0,0105	0,6655	0,0527
ENSMUSG00000021318	Gli3	-1,5834	0,0719	1,0301	0,0156
ENSMUSG00000034282	Evpl	-1,7364	0,3467	1,3395	0,0002
ENSMUSG00000091393	NA	-1,7684	0,0339	1,5489	0,0001
ENSMUSG00000047013	Fbxo41	-1,7992	0,0109	1,5308	0,0020
ENSMUSG00000050199	Lgr4	-1,8461	0,0053	0,6437	0,0814
ENSMUSG00000031983	2310022B05Rik	-1,9891	0,0276	0,9940	0,0251
ENSMUSG00000014786	Slc9a5	-2,0311	0,1098	1,2366	0,0129
ENSMUSG00000041911	Dlx1	-2,1091	0,2313	1,4013	0,0015
ENSMUSG00000036545	Adamts2	-2,1609	0,1640	1,0717	0,0134
ENSMUSG00000097025	NA	-2,1699	0,4402	1,1246	0,0006
ENSMUSG00000026974	Zmynd19	-2,1777	0,1581	0,9320	0,0058
ENSMUSG00000038331	Satb2	-2,2609	0,0000	0,8805	0,0066
ENSMUSG00000055799	Tcf7l1	-2,3721	0,0013	0,6411	0,1161
ENSMUSG00000053835	H2-T24	-2,3857	0,0000	0,5485	0,1439
ENSMUSG00000070331	Qrich2	-2,5710	0,0240	1,0039	0,0416
ENSMUSG00000025216	Lbx1	-2,6450	0,0889	1,3720	0,0220
ENSMUSG00000032968	Inha	-2,7223	0,0489	0,8650	0,0830
ENSMUSG00000020475	Pgam2	-2,7757	0,0001	0,7670	0,0985
ENSMUSG00000068270	Shroom4	-2,8435	0,0374	0,8517	0,0558
ENSMUSG00000066800	Rnasel	-2,8466	0,0397	0,8380	0,1110
ENSMUSG00000058665	En1	-2,8749	0,0000	0,4421	0,3825
ENSMUSG00000053081	NA	-3,1801	0,1290	1,4408	0,0011
ENSMUSG00000078485	Plekhn1	-3,3299	0,0600	0,6746	0,0880
ENSMUSG00000022032	Scara5	-3,4620	0,3656	1,0098	0,0019
ENSMUSG00000035298	Klhl35	-3,5733	0,1469	0,7917	0,0659
ENSMUSG00000008496	Pou2f2	-3,5744	0,5303	1,1146	0,0026
ENSMUSG00000078302	Foxd1	-4,0705	0,0089	0,7505	0,2312
ENSMUSG00000073741	NA	-4,2526	0,2694	0,9925	0,0157
ENSMUSG00000035184	Fam124a	-4,3892	0,0442	1,0715	0,0016
ENSMUSG00000032812	Arap1	-4,4531	0,0041	0,6841	0,1726

ENSMUSG00000046607	Hrk	-4,7582	0,3251	1,1147	0,0126
ENSMUSG00000004798	Ulk2	-5,1755	0,0111	0,6216	0,1001
ENSMUSG00000031441	Atp11a	-5,3135	0,0029	0,4529	0,2398
ENSMUSG00000066406	Akap13	-5,3316	0,0204	0,6408	0,1104
ENSMUSG00000078591	Hs3st4	-5,5837	0,0007	0,7161	0,2528
ENSMUSG00000085584	Rgag1	-6,6345	0,0096	0,6976	0,1670
ENSMUSG00000034459	Ifit1	-10,6202	0,0060	1,1889	0,0094

Table adapted from Carvajal Ibañez *et al*, 2023. Gadd45g and Smad6 are highlighted.

6.2 List of figures

Figures related to section 1. Introduction

Figures related to section 3. Results

Figures related to section 4. Discussion

Figures related to section 6. Appendix

6.3 List of tables

Tables related to section 2. Materials and Methods

Tables related to section 3. Results

Tables related to section 6. Appendix

Acknowledgments

First, I would like to sincerely thank by mentor and supervisor Ana Martin-Villalba for believing in and granting a PhD position to a naive 5-years younger me in this lab full of passionate science, excellent professionals, and incredible humans. Thank you, Ana, for your relentless interest in discussing my projects and for bringing to every meeting the best of your creativity. Thank you for promoting such an interdisciplinary and collaborative atmosphere. Also, thank you for passionately caring about my scientific and professional careers: for supporting me with conferences I attended, non-scientific projects I embraced, and for polishing my soft skills with your advice. Gracias.

I would like to express my gratitude to the members of my Thesis Advisory Committee: Prof. Dr. Aurelio Teleman and Prof. Dr. Bernd Bukau for their pivotal feedback and support. I would like to also thank Dr. Michael Milsom and Dr. Alessia Ruggieri for evaluating my dissertation and for the previous discussions at SFB retreats and translation clubs where we coincided. Huge thanks also to our great collaborators: Prof. Dr. Anna Marciniak-Czochra, Prof. Dr. Aurelio Teleman, Prof. Dr. Fred Hamprecht, Prof. Dr. Thomas Höfer, Dr. Günter Kramer, and Dr. Simon Anders. Especially to the members of their laboratories Adrien Jolly, Matilde Bertolini, Roman Remme, Dr. Gianluca Figlia, and Diana Danciu.

Working in Ana's lab was an exceptional experience and I would like to express my immense gratitude to every member of the lab that I have worked with. Thank you for the scientific input, advices, and the great support. Especially, thank you Santi and Andrés for being the beating heart of the lab, your energy, your scientific feedback, and your power to boost Plashcudo smiles. Thank you, Maxim, my former supervisor, for your patience, support and for sharing your expertise and passion for science with me. Thank you Jooa, your analysis and support were indispensable for the projects. Thank you, Alena, for being the most brilliant master student, your robust dedication and limitless resilience. Thank you Oğuzhan for your continuous help and feedback as well as for making every celebration memorable. Thank you, Leo, Lukas, André, Nikhil, Irene, Masha, Andrea, Jan and many others for your eagerness to share not only your best scientific feedback but also a warm smile over lunch/coffee/beer. Heads-up to Masha for reminding me to keep pushing with the sweetest rewards, and to Leo's walking rounds on Fridays at 5 pm. Thank you also Marc for your contribution to my work and for sharing your passion with us all, as well as other amazing students in the lab Ruth, Daniel, Noelia, Kevin, Lucrezia, Veronika, Srijita, Ana, Marta... Thanks to the seniors Georgios, Sascha, and Gülce for your initial support, it was a pleasure building up on your achievements.

A very special thank you is reserved for the invaluable contribution of the technicians: Katrin, Heike, Kathrin, Sonja, Aylin, Mohammad, and Steffi. Especially, Katrin for your extraordinary passion and work to keep my experiments alive, and Heike for keeping our mice (and students) under control. Vielen Dank auch an Irmgard und Susanne, die stillen Helden unserer Gruppe. Danke, dass ihr das Labor im Hintergrund am Laufen haltet, dass ihr immer bereit seid zu helfen und uns das Leben unendlich viel leichter macht.

I would like to thank all DKFZ employees that have helped during my Ph.D., especially those from the Genomics and Proteomics Core Facility, the Flow Cytometry Core Facility, the scOpenLab, the Centre for Preclinical Research, the Microscopy Facility, as well as the PhD Graduate Office from DKFZ.

A massive thank to my family: Mum, Dad, Raquel and Mar, they are the true last author of this thesis, supporting my life and work economically and emotionally since 1995. Dos mil kilómetros son un paseo sabiendo que os tengo siempre a mi lado. Estéis donde estéis, esté donde esté, sois hogar. Gracias por construir mi mejor yo, dándome siempre vuestra mejor versión. Os quiero.

The heartiest and greatest thanks to my Spanish second family that, outside the lab, made Heidelberg a living home: Alberto, Ali, Dani, Maria, Mírian, Nuria, and Paula. Mil gracias por estar en lo mejor y lo peor. Gracias por deshacer las nubes de mi PhD con vuestra mejor sonrisa. Sois el mejor sol que Heidelberg pudiera tener.

Thanks also to all friends whose smiles and laughs filled my evenings and weekends: Catarina, Alessa, André, Laura G., Karo, Josh, Julianne, Jeyan, Shub, Mike, Eirini, and many others. Also, to my TMR partners-in-crime, Mírian, and Sara, trial is over! Herzlich Dank auch an Fabi, Kyra, Anne und Laura B., ihr habt mich an die reale Welt da draußen erinnert und am Boden -der besten WG- gehalten.

Last, I would like to thank my High School chemistry and biology teachers Yolanda and Margarita for seeding the passion for science on me. Also, to those excellent professionals that patiently watered and took care of it including Cristina Madrid, Carlos Balsalobre, Magdalena Griffols, David Bueno, Muwan Chen, and Mark Denham.

PS: To you, for reading until the end, thank you.